

**University of Sheffield  
Department of Civil and Structural Engineering**

---

**Finite Element Analysis of Embankments  
on Soft Ground  
Incorporating Reinforcement and Drains**

---

**by  
Darren Russell  
MSc, BSc**

**Thesis Submitted to the University of Sheffield  
for the Degree of Doctor of Philosophy**

**June, 1992**

## Summary

The objectives of the research were threefold. Firstly, to improve the numerical modelling capability for reinforced embankments constructed over soft compressible soils containing vertical drains. Secondly, to demonstrate the ability to model accurately such embankments. Finally, to develop simplified procedures to be used in the design of embankments over soft soils.

The modifications to the finite element program, CRISP, included the incorporation of three additional elements; modelling the reinforcement, the soil/reinforcement interface and the vertical drains. The facility to vary permeability with stress level was also implemented. A technique for modelling the consolidation of soil containing vertical drains in plane strain finite element analyses was developed and validated.

The modified program was validated in three ways. Firstly, each element was used to analyse simple problems so that the correct formulation was ensured. Secondly, a series of analyses was carried out of problems for which analytical solutions were available; these problems involved collapse of undrained subsoils and consolidation around a single vertical drain. Thirdly, an analysis of a case history of an embankment constructed over a normally consolidated clay, improved with vertical drains, was performed.

Based on the results of the previous finite element analyses, and an additional analysis of an idealized two-stage constructed embankment, simple design procedures have been proposed. Firstly, a method for the design of single stage embankments and, secondly, a method for the calculation of subsoil strength increases in multi-stage construction, which can be used in conjunction with limit equilibrium analyses.

It is concluded that the finite element method is a useful technique for the analysis of reinforced embankments over soft soils containing vertical drains.

## Acknowledgement

The research presented in this Thesis was carried out under the supervision of Dr. C.C. Hird and Dr. I.C. Pyrah, as part of a SERC funded project.

The Author would very much like to thank his supervisors for their invaluable help and encouragement with all aspects of the research project. Their numerous comments during the preparation of this Thesis are gratefully acknowledged.

Dr. R.A. Jewell was involved with the SERC contract and participated in several discussions during the project, his comments were both timely and useful.

The Author would like to express his gratitude to all members of the geotechnics group at the University of Sheffield who always found time to discuss the work. The staff at the University's Computer Services department provided advice and facilities whenever necessary.

# Table of Contents

<b>1. Introduction</b>	<b>1</b>
<b>1.1. Embankments Over Soft Soils</b>	<b>1</b>
<b>1.2. Methods of Analysis</b>	<b>2</b>
1.2.1. Stability analysis	4
1.2.2. deformation analysis	5
1.2.3. summary of traditional analysis methods	6
<b>1.3. Numerical Analysis</b>	<b>7</b>
1.3.1. Constitutive modelling	8
1.3.2. material parameters	9
<b>1.4. Aims of the Research</b>	<b>9</b>
<b>2. Literature Review: Embankment Finite Element Analysis</b>	<b>11</b>
<b>2.1. Undrained Analyses</b>	<b>11</b>
2.1.1. Unreinforced Embankments	12
2.1.2. Reinforced Embankments	14
<b>2.2. Multi-Stage Construction</b>	<b>17</b>
2.2.1. Consolidation analyses without Drains	18
2.2.2. subsoils containing vertical Drains	21
<b>2.3. Discussion</b>	<b>23</b>
2.3.1. Summary of embankment Finite Element Analyses	23
2.3.2. Validation and Accuracy of Modelling	25
<b>2.4. The Need for Further Finite Element Research</b>	<b>27</b>
<b>3. The Finite Element Program CRISP and Modifications</b>	<b>29</b>
<b>3.1. Crisp</b>	<b>29</b>
3.1.1. The History of CRISP	29
3.1.2. Types of Analysis	30
3.1.3. Additional Features of CRISP	31

<b>3.2. Reinforcement Element</b>	<b>33</b>
3.2.1. Constitutive Relationship	34
3.2.2. Reinforcement Element Stiffness Matrix Formulation	35
3.2.3. Equivalent Nodal Forces	38
3.2.4. Analyses Using the Reinforcement Element	39
<b>3.3. Interface Element</b>	<b>39</b>
3.3.1. Interface Element Stiffness Matrix Formulation	39
3.3.2. Transformation to Global Coordinate System	41
3.3.3. Interface Element Constitutive Relationship and Modes of Behaviour	42
3.3.4. Equivalent Nodal Forces	44
3.3.5. Analyses Using the Interface Element	45
<b>3.4. Drainage Element</b>	<b>46</b>
3.4.1. Element Formulation	46
3.4.2. Transformation to Two-Dimensions	47
3.4.3. Incorporation of the Drainage Element in a Two-Dimensional Mesh	48
3.4.4. Analyses Using the Drainage Element	49
<b>3.5. Variation of Permeability with Stress Level</b>	<b>49</b>
<b>3.6. Summary</b>	<b>51</b>
<b>4. Collapse of Undrained Subsoils</b>	<b>52</b>
<b>4.1. Introduction</b>	<b>52</b>
4.1.1. Plasticity Theory	52
4.1.2. reinforced embankments	54
4.1.3. Application of Plasticity Theory to Reinforced Embankment Problems	55
<b>4.2. Finite Element Analysis of Plasticity Problems</b>	<b>58</b>
4.2.1. Meshes for Equivalent Loading Problems	58
4.2.2. Material Properties	60
4.2.3. Results	61
4.2.4. Effect of the interface element	64
4.2.5. predicted displacements for a rough footing on a uniform strength/limited depth subsoil	69
4.2.6. further analysis using modified cam-clay	73

<b>4.3. Embankments with Constant Side Slope</b>	<b>77</b>
4.3.1. Finite Element Analyses of Constant Side Slope Loading	80
4.3.2. Results	81
4.3.3. A comparison of limit equilibrium and finite element analysis for embankments with constant side slope	83
<b>4.4. Summary</b>	<b>86</b>
<b>5. Consolidation Around a Single Vertical Drain</b>	<b>90</b>
5.1. Introduction	90
5.2. Comparison of Finite Element Analysis with a Closed Form Solution	93
5.3. Matching Procedure for Plane Strain Analyses	104
5.3.1. Validation of the matching procedure	107
5.3.2. pore pressure variation across unit cells	114
5.3.3. Effect of vertical permeability on matching procedure	117
5.4. Summary	120
<b>6. Case History: Porto Tolle</b>	<b>121</b>
6.1. Introduction	121
6.2. Porto Tolle	122
6.2.1. subsurface conditions	122
6.2.2. Construction of the trial embankment	122
6.2.3. Vertical drains	124
6.2.4. Instrumentation	126
6.3. Unit Cell Analyses	126
6.3.1. Finite element mesh and material parameters	126
6.3.2. in situ stresses	129
6.3.3. undrained analyses to assess shear strength	129
6.3.4. Axisymmetric unit cell consolidation analyses	129
6.3.5. comparison of finite element and observed behaviour	131
6.3.6. plane strain unit cell consolidation analyses	135
6.4. Full Plane Strain Analysis	138

6.4.1. finite element mesh and boundary conditions	138
6.4.2. material parameters	139
6.4.3. comparison of observed and predicted behaviour	140
<b>6.5. Summary</b>	<b>145</b>
<b>7. Multi-Stage Embankment Construction</b>	<b>147</b>
7.1. Introduction	147
7.2. Idealized Two-Stage Construction	148
7.2.1. Finite element Analysis of Idealized Two-Stage Construction	149
7.2.2. Finite Element Results	154
7.3. Subsoil Strength Increase	172
7.3.1. Simple Calculation Methods	172
7.3.2. Factors Influencing the Strength Increase of Soft Clays	179
7.3.3. comparison of the strength increases predicted by finite element and simple methods	183
7.3.4. Strength Increases Calculated from Simple Methods	184
7.4. Porto Tolle	189
7.5. Summary	198
<b>8. Conclusions and Further Work</b>	<b>200</b>
8.1. Objectives and Completed Work	200
8.2. Conclusions	201
8.2.1. undrained collapse of cohesive soils	201
8.2.2. consolidation of soil around single vertical drains	202
8.2.3. Porto tolle case history analysis	203
8.2.4. idealized two-stage construction	204
8.3. Suggestions for Further Work	205
8.3.1. further modifications to CRISP	205
8.3.2. matching procedure	206
8.3.3. simplified design procedures	206

<b>Appendix A - Strength of Modified Cam-clay</b>	<b>207</b>
<b>Appendix B- Consolidation of a Plane Strain Unit Cell</b>	<b>218</b>
<b>Appendix C - Development of Pore Pressures Due to Ramp Loading</b>	<b>224</b>
<b>References</b>	<b>226</b>

## List of Symbols

<b>a</b>	Vector of displacement at any point in a finite element
<b>a<sub>o</sub></b>	Vector of nodal displacement for a finite element
<b>b</b>	Bishop stress parameter
<b>b*</b>	Modified Bishop stress parameter
<b>B</b>	Footing half width
<b>B</b>	Width of a plane strain unit cell
<b>B</b>	Strain matrix
<b>c'</b>	Cohesion intercept
<b>c<sub>a</sub></b>	Coefficient of secondary compression
<b>C<sub>c</sub></b>	Compression index
<b>c<sub>h</sub></b>	Coefficient of consolidation
<b>C<sub>k</sub></b>	Permeability change index
<b>D</b>	Depth of a constant depth soil
<b>D</b>	Finite element constitutive matrix
<b>e</b>	Void ratio
<b>e<sub>o</sub></b>	Initial void ratio
<b>E</b>	Youngs modulus
<b>E</b>	First derivative of drainage element flow shape function matrix
<b>F<sub>o</sub></b>	Nodal force matrix
<b>FS</b>	Factor of safety
<b>G</b>	Elastic shear modulus
<b>G<sub>i</sub></b>	Initial shear modulus
<b>H</b>	Embankment height
<b>H<sub>o</sub></b>	Embankment design height
<b>i</b>	Hydraulic gradient
<b>J</b>	Reinforcement stiffness per unit strain
<b>k</b>	Permeability
<b>k<sub>h</sub></b>	Horizontal permeability

## List of Symbols

$k_n$	Interface element normal stiffness
$k_{nt}$	Interface element normal stiffness after separation
$k_s$	Interface element shear stiffness
$k_s$	Soil permeability in smeared zone
$k_v$	Vertical permeability
$k_w$	Drain permeability
$k_0$	Initial permeability
$K_e$	Finite element stiffness matrix in local coordinate system
$K_{eg}$	Finite element stiffness matrix in global coordinate system
$K_w$	Bulk modulus of water
$K_0$	Coefficient of earth pressure at rest
$K_{0NC}$	Coefficient of earth pressure at rest for normally consolidated soil
<b>KS</b>	Drainage element force stiffness matrix
$l$	length of drain
$L$	Length of a one-dimensional finite element
$L$	Well resistance dimensionless parameter
$L$	Link matrix
$LL$	Liquid limit
$m_v$	Coefficient of volume change
$n$	$R/r_w$
$N$	Displacement shape function matrix
$N^p$	Drainage element pore pressure shape function matrix
$N_r$	Relative displacement shape function matrix
<b>OCR</b>	Over-consolidation ratio in terms of vertical effective stress
$p$	Mean stress invariant
<b>PI</b>	Plasticity index
$q$	Deviatoric stress invariant
$q$	Load applied during ramp loading
$q_w$	Axisymmetric vertical drain discharge capacity
$Q_w$	Plane strain vertical drain discharge capacity
$r_s$	Radius of smeared zone

$r_w$	Radius of vertical drain
$R$	Radius of axisymmetric unit cell
$R$	Over-consolidation ratio in terms of mean effective stress
$s$	$r_s/r_w$
$s_u$	Undrained shear strength
$s_{u0}$	Undrained shear strength at surface
$t$	Thickness of finite element
$t$	Time
$T$	Transformation matrix
$T_h$	Time factor for horizontal drainage
$T_{h90}$	Time factor for horizontal drainage causing 90% consolidation
$u$	Pore pressure
$\bar{U}_h$	Average degree of consolidation based on pore pressure at a given depth
$\bar{U}$	Overall average degree of consolidation
$v$	Specific volume
$v$	Rate of pore water flow
$V$	Volume
$w_r$	Relative displacement matrix for interface element
$w_n$	Natural water content
$w_e$	Relative nodal displacement matrix for interface element
$(x,y)$	Global coordinate system
$x_d$	Width of embankment side slope
$x'$	Cartesian local coordinate system for one-dimensional finite element
$z$	Depth below surface
$\alpha$	Orientation of one-dimensional element in global coordinate system
$\alpha$	Characteristic line associated with plasticity theory
$\alpha$	Rate of loading for a ramp loading embankment
$\beta$	Characteristic line associated with plasticity theory
$\delta$	Interface element cohesion
$\Delta$	Large increment

$\varepsilon$	Strain
$\eta$	$q/p'$
$\kappa$	Gradient of swelling line in critical state frame work
$\phi$	Angle of shearing resistance
$\Phi$	Drainage element flow stiffness matrix
$\gamma$	Bulk unit weight
$\gamma_w$	Unit weight of water
$\Gamma$	Specific volume of soil at critical state with $p=1 \text{ kN/m}^2$
$\lambda$	Gradient of compression line in critical state frame work
$\Lambda$	$(\lambda-\kappa)/\lambda$
$M$	Gradient of critical state line
$\mu$	Coefficient for unit cell consolidation
$\nu$	Poissons ratio
$\rho$	Rate of undrained shear strength increase with depth
$\sigma$	Stress
$\sigma_y$	Yield stress for reinforcement element
$\sigma_n$	Normal stress
$\sigma_v$	Vertical stress
$\sigma_2$	Out of plane stress in plane strain analysis
$\sigma_1$	Maximum principal stress
$\sigma_3$	Minimum principal stress
$\tau$	Shear stress
$(\xi,\eta)$	Local coordinate system

### **Superscripts**

'	Effective stress
*	Virtual displacement
T	Transformed matrix

**Subscripts**

ax    Axisymmetric conditions

pl    Plane strain conditions

## List of Figures

### **Chapter 3 - The Finite Element Program CRISP and Modifications**

- 3.1 (a) Reinforcement element; (b) bilinear constitutive model.
- 3.2 Calculation of one-dimensional element length and orientation.
- 3.3 (a) Interface element; (b) constitutive relationship.
- 3.4 Interface element shear stress sign convention and stress regimes.
- 3.5 Drainage element.

### **Chapter 4 - Collapse of Undrained Subsoils**

- 4.1 Definition of stress characteristics for undrained loading.
- 4.2 Reinforced embankment configuration.
- 4.3 Idealized soil profiles for plasticity analyses: (a) uniform strength/limited depth; (b) strength increasing linearly with depth.
- 4.4 Ideal load distributions on an idealized profile of: (a) uniform strength/limited depth; (b) strength increasing linearly with depth.
- 4.5 Finite element mesh used for uniform strength/limited depth analyses (mesh shown for smooth case).
- 4.6 Finite element mesh used for strength increasing with depth analyses (mesh shown for smooth case).
- 4.7 Finite element approximation for strength increasing linearly with depth.
- 4.8 Load displacement curves for displacement controlled analyses: (a) smooth footing on a uniform strength/limited depth subsoil; (b) rough footing on a uniform strength/limited depth subsoil; (c) smooth footing on a strength increasing with depth subsoil; (d) rough footing on a strength increasing with depth subsoil.
- 4.9 Comparison of vertical stress distributions at failure predicted by plasticity and finite element analysis for a uniform strength/limited depth idealized subsoil.
- 4.10 Comparison of vertical stress distributions at failure predicted by plasticity and finite element analysis for a strength increasing linearly with depth idealized subsoil.

- 4.11 Load displacement curves for load controlled analyses: (a) subsoil of uniform strength/limited depth; (b) subsoil with strength increasing linearly with depth.
- 4.12 Surface settlement profiles for load controlled analyses: (a) subsoil of uniform strength/limited depth ; (b) subsoil with strength increasing linearly with depth.
- 4.13 Vertical stress distribution at failure predicted using three different finite element meshes compared with plasticity theory.
- 4.14 Plasticity analysis of a rough rigid footing on a subsoil of uniform strength/limited depth: (a) slip line mesh; (b) hodograph.
- 4.15 Comparison of the lateral displacements predicted by finite element and plasticity analyses: (a) 2D; (b) 4D; (c) 6D; (d) 8D from toe.
- 4.16 Stress and strength profiles used for the modified Cam-clay analysis.
- 4.17 Load settlement curves for a displacement controlled analysis using modified Cam-clay to model a subsoil with strength increasing linearly with depth.
- 4.18 Comparison of finite element and plasticity predicted vertical stress distributions at failure beneath a rough footing on a subsoil with strength increasing linearly with depth modelled using modified Cam-clay.
- 4.19 Error in the undrained shear strength profile used for the modified Cam-clay analysis (after Potts and Ganendra, 1991).
- 4.20 Proposed practical embankment shape to approximate ideal loading predicted by plasticity theory (after Jewell, 1988) and a proposed simplified constant side slope design profile.
- 4.21 Typical load displacement curves for a constant side slope analysis. Curves shown for a uniform strength/limited depth analysis with  $x_q/D=5$ .
- 4.22 Comparison of the finite element predicted collapse load of a constant side slope embankment with plasticity theory for a subsoil with uniform strength/limited depth.
- 4.23 Comparison of the finite element predicted collapse load of a constant side slope embankment with plasticity theory for a subsoil with strength increasing linearly with depth.
- 4.24 Displacement vectors at failure for embankments with constant side slopes on a subsoil of uniform strength/limited depth: (a)  $x_q/D=1$ ; (b)  $x_q/D=3$ ; (c)  $x_q/D=5$ .

- 4.25 Displacement vectors at failure for embankments with constant side slopes on a subsoil with strength increasing linearly with depth: (a)  $\rho x_d/s_{u0}=1.6$ ; (b)  $\rho x_d/s_{u0}=4.8$ ; (c)  $\rho x_d/s_{u0}=8.0$ .
- 4.26 Maximum shear strain contours at failure for a constant side slope embankment on a subsoil of uniform strength and limited depth ( $x_d/D=5$ ).
- 4.27 Maximum shear strain contours at failure for a constant side slope embankment on a subsoil with strength increasing linearly with depth ( $\rho x_d/s_{u0}=4.8$ ).

## **Chapter 5 - Consolidation Around a Single Vertical Drain**

- 5.1 Unit cells and direction of flow: (a) axisymmetric conditions; (b) plane strain conditions.
- 5.2 Unit cell adopted for analytical solution (after: Hansbo, 1981).
- 5.3 Finite element mesh used for unit cell analysis comparison with Hansbo (1981).
- 5.4 Comparison of finite element *and analytical results for consolidation* of a unit cell: (a)  $L=0.0$ ; (b)  $L=0.5$ ; (c)  $L=3.0$ ; (d)  $L=5.0$ .
- 5.5 Finite element mesh used for unit cell analyses: comparison with Jamiolkowski et al (1983).
- 5.6 Effect of well resistance on rate of consolidation.
- 5.7 Effect of drain length on rate of consolidation.
- 5.8 Effect of smear on rate of consolidation.
- 5.9 Development of surface settlement profiles in finite element analyses: (a) without smear or well resistance; (b) without smear but with well resistance; (c) with smear but without well resistance.
- 5.10 Variation of vertical strain with depth at unit cell periphery in finite element analysis with well resistance ( $q_w/k=150m^2$ ).
- 5.11 Comparison of average surface settlement for axisymmetric and plane strain analyses: (a) without smear or well resistance; (b) with smear but without well resistance; (c) without smear but with well resistance; (d) with smear and well resistance.
- 5.12 Comparison of average excess pore pressure at mid-depth for axisymmetric and plane strain analyses: (a) without smear or well resistance; (b) with smear but without well resistance; (c) without smear but with well resistance; (d) with smear and well resistance.

- 5.13 Errors in geometry matched plane strain analyses: (a) based on settlements; (b) based on pore pressure.
- 5.14 Development of surface settlement profile in geometry matched plane strain analysis: (a) without smear or well resistance; (b) without smear but with well resistance.
- 5.15 Comparison of pore pressure distribution from axisymmetric and geometry matched plane strain analyses without smear or well resistance (degree of consolidation=65%).
- 5.16 Excess pore pressure distribution after the first consolidation increment from the axisymmetric finite element analysis without smear or well resistance.
- 5.17 Comparative results for axisymmetric and matched plane strain analyses with vertical flow ( $k_v=k_h$ ), degree of consolidation based on excess pore pressure: (a) without smear or well resistance; (b) without smear but with well resistance.
- 5.18 Errors in geometry matched plane strain analyses for unit cells with vertical permeability ( $k_v=k_h$ ), based on excess pore pressure.

## **Chapter 6 - Case History: Porto Tolle**

- 6.1 Soil profile (after Jamiolkowski and Lancellotta, 1984).
- 6.2 Stress history and maximum overburden from one-dimensional consolidation tests according to Casagrande's procedure (after Jamiolkowski and Lancellotta, 1984).
- 6.3 Porto Tolle Trial embankment: (a) Plan view, (b) cross section; (c) construction schedule.
- 6.4 Mesh used for axisymmetric finite element analyses.
- 6.5 Undrained shear strength in: (a) plane strain; (b) axisymmetry.
- 6.6 Axisymmetric unit cell consolidation based on average surface settlement.
- 6.7 Excess pore pressure on centreline of the embankment: (a) 19.7m below ground level; (b) 12.6m below ground level.
- 6.8 Rate of surface settlement at centreline of the embankment.
- 6.9 Unit cell rate of consolidation based on the average excess pore pressure at mid-depth.
- 6.10 Unit cell rate of consolidation based on the average surface settlement.
- 6.11 Unit cell rate of consolidation matching errors.

- 6.12 Mesh used for plane strain analysis.
- 6.13 Surface settlement at centreline.
- 6.14 Maximum horizontal displacement.
- 6.15 Lateral movement profiles at the inclinometer position: (a) at the end of the construction stage; (b) at the end of the consolidation stage.
- 6.16 Excess pore pressure on centreline of the embankment (full plane strain): (a) 19.7m below ground level; (b) 12.6m below ground level.

## **Chapter 7 - Multi-Stage Embankment Construction**

- 7.1 Idealized two-stage embankment geometry.
- 7.2 Idealized soil: (a) stress; (b) over-consolidation ratio; (c) initial undrained shear strength.
- 7.3 Lower interface shear strength after the consolidation stage.
- 7.4 Finite element mesh and boundary conditions.
- 7.5 Settlement at of points at the subsoil surface against embankment height.
- 7.6 Surface settlement profiles.
- 7.7 Lateral movement of a section through the toe.
- 7.8 Maximum surface settlement against maximum lateral movement beneath the toe.
- 7.9 Ratio of maximum settlement to maximum lateral movement plotted against embankment height.
- 7.10 Displacement vectors at failure.
- 7.11 Stress paths: (a) beneath the slope; (b) beneath the crest.
- 7.12 Principal stress rotations: (a) beneath the slope; (b) beneath the crest.
- 7.13 Modified Bishop stress parameter: (a) beneath the slope; (b) beneath the crest.
- 7.14 Variation of  $s_v/\sigma_v'$ : (a) beneath the slope; (b) beneath the crest.
- 7.15 Variation of  $s_v/\sigma_1$ : (a) beneath the slope; (b) beneath the crest.
- 7.16 Reinforcement strain.
- 7.17 Shear stress on: (a) reinforcement/fill interface; (b) reinforcement/clay interface.
- 7.18 Stress state on a potential failure surface in a soil near failure subjected to embankment loading.

- 7.19 Undrained shear strength anisotropy of normally consolidated clays.
- 7.20 Estimation of vertical stress increase in a soil due to embankment loading: (a) one-dimensional; (b) Gray (1936).
- 7.21 Predicted strength increase near centreline.
- 7.22 Predicted absolute strength near centreline.
- 7.23 Contours at the end of the consolidation stage predicted by the finite element analysis: (a) strength increase; (b) absolute strength.
- 7.24 Contours of strength increase at the end of the consolidation stage: (a) predicted by Method G; (b) predicted by Method H.
- 7.25 Contours of absolute strength at the end of the consolidation stage: (a) predicted by Method G; (b) predicted by Method H.
- 7.26 Contours of strength difference at the end of the consolidation stage: (a) between Method G and finite element; (b) between Method H and finite element.
- 7.27 Porto Tolle predicted: (a) degree of consolidation; (b) total vertical stress.
- 7.28 Porto Tolle predicted: (a) undrained shear strength increase; (b) absolute undrained shear strength..
- 7.29 Contours of strength increase at the end of the consolidation stage at Porto Tolle predicted by: (a) the finite element analysis; (b) the simplified method.
- 7.30 Contours of the strength difference predicted by finite element analysis and the simplified method at the end of the consolidation stage at Porto Tolle.

**Appendix A - Undrained Shear Strength of Modified Cam-clay**

- A1 Definition of Mohr-Coulomb yield surface for a cohesive material.
- A2 Undrained stress path for a normally consolidated modified Cam-clay sample.
- A3 Undrained stress path for a normally consolidated and over-consolidated modified Cam-clay sample.

**Appendix B - Consolidation of a Plane Strain Unit Cell**

- B1 Plane strain unit cell.

**Appendix C - Development of Pore Pressures Due to Ramp Loading**

**C1 Ramp loading scheme.**

## List of Tables

### **Chapter 6 - Case History: Porto Tolle**

- 6.1 Summary of Porto Tolle soft clay material properties.
- 6.2 Summary of parameters used to model Porto Tolle clay.

### **Chapter 7 - Multi-Stage Embankment Construction**

- 7.1 Summary of assumptions in the simple methods used to predict strength increases.

# 1. Introduction

## 1.1. Embankments Over Soft Soils

Recent social and economic development around the world has brought about an increase in the construction of embankments used in highway and railway systems, flood and irrigation projects and harbour and airport installations. This coupled with increasing urbanisation has required the geotechnical engineer to design and construct embankments over increasingly weak and compressible soils.

Often the soil is sufficiently weak that the embankment cannot be constructed in a single lift, in the area available; in such situations it is necessary to improve the soil on which the embankment is to be placed. This improvement can take several forms depending on the soil conditions encountered.

Where settlement is the major consideration the rate at which settlement occurs can be increased with the installation of vertical drains (Barron, 1948; Hansbo, 1981; Holtz et al, 1987; Holtz et al, 1991) and the post-construction settlements therefore reduced. Preloading the compressible soils with a surcharge is a technique used with both embankments and settlement sensitive structures (Johnson, 1970a) and is often used in conjunction with vertical drains (Johnson, 1970b).

Other techniques may have to be considered to ensure stability of the embankment during construction. Stage construction can be used to construct embankments with relatively steep side slopes (Jardine and Hight, 1987; Ladd, 1991; Leroueil et al, 1991). This method relies on the increase in the undrained shear strength of the subsoil during consolidation and is therefore most beneficial when used with vertical drains. An

Increasingly popular technique is the use of tensile reinforcing material, such as geogrids, geotextiles or steel reinforcement, placed at the base of the embankment fill (Bonaparte and Christopher, 1987). The reinforcement provides lateral restraint and effectively increases the bearing capacity of the subsoil.

Other less common expedients include the use of light-weight fills, drainage trenches, stone columns, lime columns, piles, replacement of the subsoil, electro-osmosis, electro-injection, dynamic compaction or a combination of the above (brief descriptions and further references for these techniques can be obtained from: Pilot et al, 1987; Delmas et al, 1987, Lerouiel et al, 1991).

In this research three of the more popular embankment construction techniques have been examined: 1) reinforcement at the base of the fill material, 2) vertical drains in the subsoil and 3) multi-stage construction with vertical drains.

## **1.2. Methods of Analysis**

Traditionally the analysis of embankments has been divided into two parts: firstly, stability, in which a factor of safety is calculated and, secondly, deformation, in which displacements are calculated. However, before either stability or deformation analysis are carried out it is necessary to decide on the drainage conditions in the subsoil as these will influence the type of analysis performed.

### **Undrained, Drained or Consolidating Behaviour**

For an embankment constructed in a single lift, failure would be most likely to occur during construction, before the excess pore pressures have had time to dissipate and the subsoil to gain strength. If the loading period is relatively short it is often realistically conservative to assume that the subsoil

is undrained and a stability analysis based on total stresses could be performed. However, care must be taken that this approach is not overly conservative as measurement of pore pressures beneath embankments on soft cohesive deposits (Tavenas and Leroueil, 1980) has shown that partial drainage may still occur even during short construction periods.

For multi-stage construction, total stress analyses have the obvious limitation that the increase in the subsoil strength due to consolidation is not taken into account. An alternative analysis procedure proposed by Bishop and Bjerrum (1960) is an effective stress analysis. The effective stress analysis allows for strength increases in the subsoil but requires knowledge of the excess pore pressures. The excess pore pressures are difficult to calculate reliably and for major works Bishop and Bjerrum advocated that insitu pore pressures should be measured.

Effective stress analyses also implicitly assume the complete dissipation of shear induced excess pore pressures during failure. This implies that the effective stress at failure in an effective stress analysis will be higher than in a total stress analysis. This results in a higher calculated factor of safety from an effective stress analysis than from a total stress analysis (Ladd, 1991).

A third analysis procedure for the design of multi-stage embankments (Hight and Jardine, 1987; Leroueil et al, 1990; Ladd, 1991) has been proposed and termed an undrained strength analysis (Ladd, 1991). In such an analysis the failure mechanism is assumed to be undrained and the analysis is based on total stresses, but the increase in subsoil undrained shear strength due to consolidation is taken into account. The undrained strength analysis of each loading stage is carried out in two parts; firstly, the distribution of undrained shear strength in the subsoil, immediately before loading commences, is calculated and, secondly, these strengths are used in a conventional total stress analysis to assess the factor of safety. Ladd

(1991) examined three case histories and demonstrated that the factor of safety calculated using an effective stress analysis was approximately twice as high as that calculated using an undrained strength analysis.

In this Thesis, where appropriate, the philosophy of an undrained strength analysis has been used for multi-stage embankment construction (Chapter 7). Undrained analysis based on the initial undrained shear strength has been used as a conservative method of analysis for quickly constructed single stage embankments (Chapter 4).

### **1.2.1. Stability Analysis**

After consideration of the subsoil drainage conditions the analysis of stability can be performed. Two methods that have been frequently used in design are based on limit equilibrium and plasticity theory.

#### **Limit Equilibrium**

The most commonly used method of analysis in current design practice is that of limit equilibrium. In this analysis a failure mechanism is postulated and a factor of safety is defined in terms of the disturbing and resisting forces. This method is often computerised with the failing mass divided into slices; several assumptions have been postulated for the distribution of the inter slice forces (e.g: Fellenius, 1927; Bishop, 1955; Morgenstern and Price, 1965).

The limit equilibrium method has several significant disadvantages. The method requires the postulation of a failure mechanism; if an incorrect mechanism is postulated then the predicted factor of safety is in error. The method also does not take account of the complex stress distribution which will develop in the subsoil beneath an embankment nor for the possibility of a progressive failure.

Limit equilibrium analysis has been extended to the analysis of embankments with reinforcement at the base of the fill (Fowler, 1982; Jewell, 1982). The reinforcement provides an additional resisting force, the magnitude of which is dependent on both the fill material and the surface undrained shear strength of the subsoil.

### **Plasticity Theory**

Often an accurate estimation of the collapse load of a geotechnical structure can be made using plasticity theory. Jewell (1988) has suggested that the plasticity solutions for two idealized soil profiles (Mandel and Saleçon, 1972; Davis and Booker, 1973) have direct relevance to the stability analysis of embankments constructed on soft soils. These plasticity solutions predict the collapse loads for rigid strip footings on idealized subsoils. The solutions can also model the shear stress distribution on the underside of the footing. This shear stress can be interpreted as the action of an infinitely stiff reinforcement; the varying roughness factors define the bond between the soil and the reinforcement (Houlsby and Jewell, 1988).

The plasticity solutions have been shown to match well limit equilibrium analysis for the idealized conditions (Jewell, 1988) but further research is required before the method can be directly applied to embankment design.

### **1.2.2. Deformation Analysis**

Traditionally the deformation of the embankment and the subsoil has been calculated without consideration of stability. The immediate or undrained displacement and the long term consolidation settlement are analysed separately.

Analytical solutions for the undrained displacements based on elastic conditions are available (Poulos and Davis, 1974). These solutions have the obvious disadvantage that the subsoil is often not elastic. This is especially true with the soft, often normally consolidated, soils encountered.

The consolidation settlements are calculated assuming one dimensional consolidation theory and using parameters obtained from oedometer and/or field tests. The stress in the subsoil can be estimated from elastic theory (e.g: Newmark, 1942; Gray, 1936). The rate at which the settlement occurs can be found by calculating the rate of consolidation using Terzaghi's one dimensional consolidation theory (Terzaghi and Peck, 1967) or in the case of subsoils containing vertical drains, using one of the available analytical solutions (e.g. Barron, 1948; Hansbo, 1981).

Secondary compression can also be a significant factor. The estimation of it's magnitude may be made based on laboratory test data. However, several aspects of the secondary compression phenomenon are still the subject of debate (Leroueil et al, 1990).

The prediction of the lateral displacement is also important, especially in reinforced embankments where it's magnitude can significantly affect the reinforcement forces developed. There are no analytical solutions available for the calculation of lateral displacement. Tavenas and Leroueil (1980) proposed empirical relationships. However, the application of these relationships is uncertain for clays not included in their study.

### **1.2.3. Summary of Traditional Analysis Methods**

The analysis of embankments has traditionally been separated into stability and deformation calculations. However, displacement and stability are interrelated and an accurate analysis requires the consideration of both aspects. Analytical solutions are not available for such an analysis and in order to obtain accurate predictions it is often necessary to use a numerical analysis technique.

## 1.3. Numerical Analysis

With the increased availability of computers the application of numerical techniques for the solution of geotechnical problems has expanded. These techniques rely on the solution of the partial differential equations which describe the behaviour of the soil for the particular boundary conditions considered. Although an exact solution cannot be achieved, an approximate solution can be found by using an appropriate numerical technique. The degree of approximation is a function of the complexity of the analysis and the material model, the amount of computational effort used and the experience of the analyst.

The numerical technique used in this research is the finite element method (e.g. Zienkiewicz, 1977). The finite element analysis of geotechnical problems relies on the discretization of a continuum into a number of elements which are connected at nodal points. The displacement response of each element, when subjected to loading, is defined by the element shape, the variation of displacement within the element and the stress-strain relationship (constitutive model) used to represent the material. The result of the discretization process is a set of simultaneous equations which must be solved to yield nodal displacements. The nodal displacements can then be used to calculate the strains and stresses within each element. For analysis of consolidation problems the excess pore pressure can be coupled with displacements and additional nodal information is obtained.

The finite element method has the advantage over traditional analysis techniques that the displacements and stresses within the soil are coupled and, depending on the constitutive model, more realistic soil behaviour can be represented. However, with this increased potential for accurate analysis there is a corresponding increased complexity in the constitutive modelling of the soil and therefore the input parameters required. The approximate nature of the solution procedure results in the possibility of different

solutions to the same problem if incorrect discretization or solution techniques are used.

### **1.3.1. Constitutive Modelling**

Increasingly complex constitutive models have been developed to represent geotechnical materials. It is essential that the appropriate model be used for each problem. The adopted solution technique should also be appropriate to that model.

#### **Linear Elastic Model**

The majority of traditional deformation analyses assume a linear elastic material. This is a gross approximation of soil behaviour if the major displacements occur when the soil yields and becomes plastic. This is particularly true of soft clays which are usually normally or lightly over-consolidated. However, if the purpose of the finite element analysis is to perform numerical comparisons with an analytical solution it may be appropriate to use an elastic model. Also, if the information available describing the soil is insufficient then a more complex analysis may not be justifiable.

#### **Elastic-Perfectly Plastic Model**

Elastic-perfectly plastic models are used widely and various yield criteria can be implemented to define when the material response changes from elastic to plastic. Collapse occurs when a mechanism is produced. For undrained behaviour, yield criteria which predict a constant undrained shear strength produce theoretically correct collapse loads. However, for drained or consolidation conditions both displacement and collapse may be incorrectly predicted as the model does not allow for volumetric strain hardening or softening.

In drained conditions the Mohr-Colomb yield criterion is often used and for mathematical convenience the flow rule is usually associated (Smith, 1982). Such models produce excessive dilatancy and may predict an incorrect response.

### **Critical State Models**

Critical state theory (Schofield and Wroth, 1968; Roscoe and Burland, 1968; Atkinson and Bransby, 1978) provides a realistic framework for the prediction of the behaviour of normally and lightly over-consolidated clays. These models can predict strain hardening for such soils and have been used widely in numerical analyses to provide accurate predictions of displacements and stresses. The increased complexity of these models produces increasing difficulty in the analysis in which the equilibrium condition is more difficult to enforce. This requires a larger number of loading iterations or a more complex solution procedure.

#### **1.3.2. Material Parameters**

With more complex constitutive models more input parameters are required. Often the site investigation data is not sufficiently accurate to justify the use of these models for prediction. However, the more complex models may still be useful in a parametric study.

### **1.4. Aims of the Research**

The use of reinforcement, vertical drains and multi-stage construction is increasing in the construction of embankments overlying soft soils. The analysis of these problems is far from straightforward and traditional techniques are not always sufficiently accurate to be a reliable method for design. Numerical analysis using the finite element method overcomes several of the disadvantages of the traditional methods and produces coupled predictions for displacements, stresses and pore pressures. The

finite element method is therefore an excellent tool with which to study the behaviour of embankments constructed over soft ground.

However, accurate numerical predictions require careful analysis and it is often necessary to conduct a study in which material parameters, boundary conditions and solution techniques are varied. Therefore, It may be unrealistic to perform a finite element analysis at an initial stage of the design process, instead simple design procedures may be used for preliminary analysis.

The aims of the present research were:

1. To modify an existing finite element program, CRISP (Gunn and Britto, 1984), to better model reinforced embankments over soft soils containing vertical drains (Chapter 3).
2. To benchmark the modified program against analytical solutions for both the undrained collapse of idealized soils and the consolidation behaviour of soil surrounding a single vertical drain (Chapters 4 and 5).
3. To develop procedures so that soil systems containing vertical drains can be analysed accurately using the finite element method (Chapter 5).
4. To compare finite element predictions with observed behaviour for an embankment constructed over soft soil incorporating vertical drains (Chapter 6).
5. To develop simple procedures which aid routine design of embankments on soft soils containing vertical drains, reinforcement and stage constructed embankments (Chapters 4 and 7).

## **2. Literature Review: Embankment Finite Element Analysis**

Published finite element analyses of embankments constructed over soft ground can be divided into two categories. Firstly, undrained analyses of embankments which are constructed sufficiently quickly that consolidation of the subsoil is negligible. Secondly, analyses of embankments which are constructed in more than one lift or slowly enough that consolidation effects are significant. This literature review is divided into these two sections with particular attention being given to analyses in which reinforcement or vertical drains have been modelled. All analyses reviewed have been carried out in plane strain.

The review is a selective account of the significant contributions to the area of finite element analysis of embankments, mainly constructed over soft ground. Each author's work is described and, where relevant to the present research, the main findings stated. There then follows a discussion of difficulties which have been encountered and areas in which the analysis may be improved.

### **2.1. Undrained Analyses**

Undrained analyses were first conducted using elastic constitutive models considering unreinforced embankments. Subsequent studies considered increasingly sophisticated constitutive models and, as the use of reinforcement became more widespread, analysts included idealizations of reinforcement and soil/reinforcement interface behaviour.

### **2.1.1. Unreinforced Embankments**

#### **Brown and King**

Brown and King (1966) performed one of the first finite element studies of an embankment problem. They analysed built up and cut down embankments using an elastic model to represent the soil. The authors speculated on possible failure mechanisms and compared the factors of safety calculated from the finite element predicted stress distributions with Taylor's (1948) stability parameters.

#### **Clough and Woodward**

Clough and Woodward (1967) compared elastic embankments, over rigid subsoils, constructed in a single increment with those constructed in several increments. The authors concluded that it is essential to model the construction sequence to produce accurate embankment displacement predictions.

Further research included a parametric study of the stiffness of a subsoil of finite depth. The authors concluded that the vertical stress was relatively insensitive but horizontal and shear stresses were strongly dependent on subsoil stiffness.

Clough and Woodward also performed a non-linear elastic analysis of the Otter Brook Dam. The elastic properties of the soil were modified at the end of each of 14 lifts using data obtained from a series of triaxial tests. The finite element predicted and observed displacements, for two positions, were in good agreement.

#### **Kulhawy and Duncan**

Kulhawy and Duncan (1972) analysed the Oroville Dam. The embankment fill was represented using a hyperbolic model (Duncan and Chang, 1970) and the subsoil was assumed to be rigid. The predicted displacements were

in good agreement with the observed values. Embankment stresses did not compare favourably with those measured but the authors expressed concern over the measured values. The finite element predicted tension zones agreed closely with visible tension cracks.

### **Smith and Hobbs**

Smith and Hobbs (1974) compared finite element analyses with centrifuge model tests. The subsoil was represented with an undrained elastic-perfectly plastic soil model. The effect of the elastic parameters and the distance of the mesh boundaries were studied. The authors showed that, for their analyses, the finite element method predicted collapse loads agreed well with limit equilibrium calculations.

### **Wroth and Simpson**

Wroth and Simpson (1972) analysed a test embankment constructed at King's Lynn, UK. The subsoil was modelled using Cam-clay (Schofield and Wroth, 1968) and the embankment loading by equivalent vertical loads applied over a number of increments. Undrained analyses were carried out representing the short term conditions. The predicted vertical and horizontal displacements were in good agreement with those observed. However, the predicted pore pressures were not in such good agreement. The authors suggested that the disagreement may have been caused by consolidation near the drained boundaries during construction.

The authors also carried out drained analyses to simulate long term conditions. The predicted displacements were again in good agreement with those observed.

## **2.1.2. Reinforced Embankments**

### **Boutrop and Holtz**

Boutrop and Holtz (1983) performed finite element analyses of reinforced and unreinforced embankments constructed over a soft clay. The embankment fill was modelled as an elasto-plastic material with a Drucker-Prager failure criterion. The authors compared reinforced and unreinforced analyses and observed that the reinforcement reduced the shear stresses in the subsoil and the differential settlement of the top of the embankment.

### **Rowe**

Rowe and his co-researchers performed several finite element studies of the behaviour of reinforced embankments. Their research included both back analyses and analyses of idealized problems. The subsoil was modelled as an elasto-plastic material with a Mohr-Coulomb failure criterion and a non-associated flow rule. In order to better represent granular materials the embankment was idealized using the same model but with the stiffness varying with stress level. The geotextile was modelled as a membrane with axial stiffness but no flexural rigidity. Slip could occur between the reinforcement and soil. All studies reviewed consider single stage construction in which the subsoil was modelled as undrained.

The first of these analyses, Rowe (1982), consisted of a parametric study of a reinforced embankment constructed at Pinto Pass, USA. The analysis used a large deformation finite element formulation. Rowe et al (1984) and Rowe (1984) analysed a second reinforced embankment, at Bloomington Road, Ontario, USA, using the same finite element program. These two studies confirmed the beneficial effects of reinforcement on stability and deformations.

Rowe and Soderman (1985) proposed an extended limit equilibrium procedure in which reinforcement strain level was considered. The procedure was developed using results from a finite element parametric study of an idealized embankment. The method can be used to assess the likely increase in the factor of safety when using reinforcement.

Rowe and Soderman (1987) reviewed their finite element procedure and used plasticity solutions to predict failure for an idealized embankment. The authors found that the finite element results were within 7% of the predicted plasticity failure heights for highly reinforced embankments.

Rowe and Mylleville (1988) analysed steel reinforced embankments and showed that the failure mechanism was dependent on the amount of reinforcement used. Yielding of the reinforcement occurred well before a subsoil failure mechanism developed.

Rowe and Mylleville (1989) presented results from several finite element analyses in which they showed that the subsoil shear strains exceeded the reinforcement strain significantly at working loads. An increase in the reinforcement modulus was shown to increase the failure height and also the subsoil shear strain. The authors pointed out that these increased shear strains would have important consequences for strain softening soils. Mylleville and Rowe (1991) presented further evidence of the subsoil shear strains exceeding the reinforcement strain and discussed the implications for practical design.

Rowe and Mylleville (1990) showed that the subsoil shear strains corresponding to only modest reinforcement strains were large enough to cause concern, particularly when considering strain softening soils. Analyses were also carried out with a higher strength surface crust. The authors showed that the crust, a) increased the failure height, b) reduced reinforcement strains and c) reduced the maximum shear strains in the subsoil. The authors compared finite element analyses with one and two

layers of reinforcement and concluded that an embankment constructed using two layers of reinforcement of a given modulus behaved in essentially the same way as one constructed with a single layer of twice the modulus.

### **Basset and Guest**

Basset and Guest (1990) compared results from model tests and finite element analyses, using a version of the finite element program CRISP, with plasticity predicted failure loads and displacement fields for a clay subsoil of limited depth. The finite element analysis seriously over-predicted failure loads and under-predicted displacements. This discrepancy was a result of discretization errors at the rough boundaries where, as shown by the plasticity solution, discontinuities develop. The use of interface elements to model such discontinuities has been discussed by Hird et al (1990) and Van Langen and Vermeer (1991). Basset and Guest showed that the slip line field (e.g: Atkinson, 1981) inferred from finite element and model tests was similar to that predicted by plasticity theory.

### **Kwok, Hird and Pyrah**

Kwok (1987) implemented a reinforcement element and an interface element in the finite element program CRISP81. Analyses of both real and idealized embankments were carried out. The modified version of CRISP81 was used in a parametric study to investigate the effect of the reinforcement stiffness, the subsoil conditions, the geometry and the embankment constitutive model. An analysis of a trial embankment constructed at Stanstead Abbots, UK, (Basset, 1987) was also performed. Kwok concluded that in the short term considerable reductions of deformations may be achieved by the insertion of reinforcement, provided that the reinforcement is sufficiently stiff and strong. Examination of the embankment model showed that an elastic-perfectly plastic model produced realistic behaviour. However, care must be taken that unrealistic tensile stresses do not develop.

Hird and Kwok (1990a) presented results from two embankment analyses using the modified version of CRISP. Interface elements were used to model the soil/reinforcement interfaces and it was shown that useful information regarding the transmission of shear stresses from the soil to the reinforcement could be extracted.

Hird and Kwok (1990b) carried out a parametric study of an idealized embankment considering the effect of the reinforcement stiffness and the subsoil depth. The authors concluded that provided the reinforcement was sufficiently stiff and strong: 1) subsoil deformations would be significantly reduced, 2) the development of tension in the reinforcement would be in accordance with the principles suggested by Jewell (1988) and 3) very stiff reinforcement may cause arching in the embankment fill. Study of the effect of subsoil depth showed that for a subsoil of constant strength the effect of reinforcement reduced with increasing depth.

Hird and Pyrah (1990) performed a parametric study of a second trial embankment constructed at Stanstead Abbots, UK. The embankment was modelled with both elements and equivalent vertical loads. The finite element predicted vertical displacements compared well with those observed. The horizontal displacements agreed less well and according to the authors may have been attributed to the relatively coarse mesh. The analyses modelling the embankment using equivalent vertical loads produced unrealistic reinforcement stress and strain profiles, this may have been due to the large deformations which occurred in a highly compressible peat layer.

## **2.2. Multi-Stage Construction**

Analyses of stage constructed embankments must allow for the dissipation of the excess pore pressures which develop during construction. Numerically this can be achieved in several ways. Firstly, a partially drained

situation can be simulated by specifying a reduced value for the bulk modulus of water. Secondly, the excess pore pressure profile within the subsoil can be fixed to some assumed value. Thirdly, a fully coupled consolidation approach can be used.

The analysis is further complicated by the frequent inclusion of vertical drains which make the assumption of plane strain conditions invalid. In order to analyse accurately an embankment constructed on a subsoil in which vertical drains have been installed a rational approach to the modelling of the drains must be developed. Finite element analyses in which modelling of vertical drains has been attempted are reviewed in Section 2.2.2.

### **2.2.1. Consolidation Analyses Without Drains**

#### **Smith and Hobbs**

Smith and Hobbs (1976) presented one of the first coupled consolidation finite element analyses of embankments constructed over a soft clay. The stage construction of two embankments was analysed. In both cases the rate of centreline settlement was predicted accurately. The excess pore pressures were in close agreement with observed values for one embankment but less favourable agreement was achieved for the second. The authors stated that the poor agreement in the second analysis may have been due to anomalies in the field records.

#### **Wroth**

Wroth (1977) analysed the MIT test embankment. The embankment was built quickly and then allowed to consolidate for five years after which it was loaded as quickly as possible to failure. Predictions of the amount of fill required to produce failure were invited. Wroth represented the subsoil using a critical state soil model. The five year wait period was simulated by using a reduced bulk modulus for water to estimate the in-situ conditions

before the final loading stage which was then modelled as completely undrained. The finite element analysis could not correctly predict failure as the clay subsoil exhibited strain softening behaviour. However, the predicted displacements and excess pore pressures due to the additional fill agreed favourably with the observed values.

### **Imperial College**

Several finite element studies have been carried out at Imperial College. Bond (1984) compared different drainage conditions and illustrated the strengthening effects of a surface crust for a 'typical' soft clay using an extended modified Cam-clay constitutive model to represent the subsoil.

The same set of soil parameters were used by Smith (1984) to investigate some effects of stage constructed embankments. The embankment was constructed in 1m lifts with partial dissipation of excess pore pressure specified after each increment. Smith observed large principal stress rotations during the first undrained loading stage and that these rotations were greatest below the toe of the embankment. Interestingly no rotations greater than  $5^\circ$  were observed during subsequent loading or consolidation stages. Smith also plotted the variation of the undrained shear strength ratio with the maximum principal effective stress and the vertical effective stress ( $s_u/\sigma_1'$  and  $s_u/\sigma_v'$ ) against embankment height and observed that neither of these ratios fell below the normally consolidated value.

Further details of these analyses can be found in Jardine and Hight (1987).

### **Schafer**

Schafer (1987) carried out fully coupled consolidation analyses of reinforced embankments using a finite element program which included an extended version of modified Cam-clay, used to model the soil, and bar elements, used to model the reinforcement.

The program was used to analyse the Mohicanville Dike (Schafer, 1987; Duncan et al, 1988). The subsoil consisted of peat and soft clay on which a previous embankment had failed. Steel reinforcement was used to allow the construction of the dike to the design height. The finite element analysis of these highly complex subsoil conditions showed good agreement for reinforcement stresses and subsoil displacements. However, the predicted excess pore pressures were less good. The discrepancies were explained as being due to creep occurring in the subsoil and ageing of the fill material.

Schafer (1987) also analysed the test embankments at St Alban, Canada, constructed on Champlain Clay. The author found that the initial results were not in good agreement with the observed behaviour. A reinterpretation of preconsolidation pressures improved the quality of the analysis with respect to predicted failure, displacements and excess pore pressures. The author suggested that the lack of agreement, when using the measured soil properties, occurred because of the inability of the constitutive model to reproduce the brittle behaviour of Champlain Clay.

#### **Almeida**

Almeida (1984) used a version of CRISP to compare finite element analyses with centrifuge tests (Almeida et al 1985; Almeida et al, 1986). The finite element analyses did not accurately predict failure, but this may have been due to the embankment being modelled as elastic. Subsoil stress paths predicted by Almeida were similar to those predicted by Smith (1984).

Almeida (1984) implemented a variation of permeability with stress level relationship and presented results indicating improved pore pressure prediction when using this algorithm. The predictions of excess pore pressure using fully coupled consolidation were, generally, encouraging.

### **Dluzewski and Termaat**

Dluzewski and Termaat (1990) used a novel method to analyse stage constructed embankments. The procedure consisted of an undrained elasto-plastic analysis of loading stages followed by an elastic consolidation analysis for the wait stages. This method of analysis simplified the calculations and reduced the computer time required for solution.

## **2.2.2. Subsoils Containing Vertical Drains**

### **Zeng, Xie and Shi**

Zeng et al (1987) conducted *fully coupled consolidation analyses to assess* the effectiveness of two methods for representing vertical drains. The first method, developed by Shinsha et al (1982), calculated an equivalent horizontal permeability for a plane strain analysis in which the vertical drains were represented as sheets. The second method analysed *the same* cross-section but was converted into a three dimensional problem by modelling half a unit cell (Chapter 5) width into the plane using three-dimensional elements.

The authors showed an improvement when using the three dimensional analysis but acknowledged the large increase in computation cost.

### **Hird and Kwok**

Hird and Kwok (1986) performed a parametric study of a test embankment constructed at Stanstead Abbots, UK. The subsoil consisted of clay and peat into which vertical drains were installed.

The effect of the vertical drains was allowed for by globally increasing the subsoil permeability by an estimated factor. The observed displacements and reinforcement strains were within the predicted range, although the predictions of pore pressure were not good. The error in the excess pore pressure prediction were most likely caused by an under-estimation of the

global permeability. The peat showed marked variation of permeability with stress level and the authors indicated that this should be allowed for in future analysis.

### **Poran**

Poran (1986) analysed the Stanstead Abbots trial embankment. The soil was represented using a 'Bounding Surface Plasticity' model and the reinforcement as a linear viscoelastic material.

An attempt was made to represent the vertical drains installed in the subsoil. An axisymmetric analysis of a cylindrical unit cell, with drainage occurring both horizontally, inwards, and vertically, upwards, was compared with a plane strain unit cell with drainage towards the upper boundary only. An 'equivalent' vertical permeability for the plane strain analysis was interpolated to produce a similar average degree of consolidation at two points in time. This equivalent vertical permeability was then used in a full plane strain analysis.

The authors stated that it was difficult to compare the predicted pore pressures with the observed values as several major assumptions had to be made due to a lack of input information. This led to a wide range of predictions and the accuracy of the procedure for modelling the vertical drains could not be assessed.

### **Sanchez and Sagaseta**

Sanchez and Sagaseta (1990) used a version of the finite element program CRISP to carry out a back analysis of an embankment built over a soft clay subsoil in which vertical drains were installed to reduce the required construction time. The authors developed a method of equating the drain spacing in a plane strain finite element analysis with the field drain spacing by manipulating the horizontal subsoil permeability. However, using this

method the derived plane strain vertical drain spacing is only applicable for one degree of consolidation.

A consolidation analysis of the embankment was compared with a partially drained analysis in which the bulk compressibility of the pore water was manipulated. The agreement of the finite element analyses with the observed behaviour was not good but the consolidation and partially drained analyses produced similar results.

## **2.3. Discussion**

### **2.3.1. Summary of Embankment Finite Element Analyses**

The finite element analyses reviewed above have been divided into two categories: firstly, undrained analyses (which have been used to assess the short term behaviour of a single stage constructed embankment) and, secondly, analyses which have considered the dissipation of the excess pore pressures due to the consolidation of the subsoil. Particular attention has been placed on analyses which have modelled reinforcement and/or vertical drains.

The development of the constitutive models used to represent the subsoil has been an important aspect of the analysis of embankments constructed over soft soils. The earliest analyses used an elastic subsoil model (Brown and King, 1966) but quickly developed with a non-linear elastic model (Clough and Woodward, 1967), an elastic-perfectly plastic model (Smith and Hobbs, 1974) and a critical state model (Wroth and Simpson, 1972).

Improvements of the constitutive modelling for the embankment material have also been made and several authors have indicated that accurate modelling of the embankment is essential to ensure realistic predictions. Kwok (1987) performed a parametric study of embankment models. Hird and Pyrah (1990) compared the use of finite elements, using an

elastic-perfectly plastic constitutive model with a Mohr-Coulomb yield criterion, with equivalent vertical loads and found the equivalent vertical loading produced unrealistic results. Almeida et al (1985) indicated that the use of an elastic embankment model produced unrealistic failure predictions.

Over the last decade with the availability of faster computers with larger data storage, it has become possible to perform finite element analyses of increasingly complex problems involving larger numbers of elements. This has allowed the analysis of reinforced embankments in which the reinforcement has been modelled using bar elements and the interface with interface or slip elements (Rowe, 1982; Boutrup and Holtz, 1983; Kwok, 1987; Schafer, 1987, Hird and Kwok, 1990a). The use of the finite element method for reinforced embankment analysis has provided evidence which has allowed a better understanding of the action of the reinforcing material and facilitated the development of methods for their design (Rowe and Soderman, 1982). The use of parametric studies of back analyses and idealized reinforced embankments has also provided insight into the possible improvements provided by reinforcement.

In order to model accurately embankments in which strengthening of the subsoil occurs due to consolidation, it is necessary to model the dissipation of excess pore water pressures with time. Coupled consolidation finite element analyses have been shown to be capable of predicting the pore pressure response in the field and in centrifuge tests (Smith and Hobbs, 1976; Wroth, 1977; Schafer, 1987; Almeida, 1984).

An area which has been less widely researched is the modelling of vertical drains in a subsoil subjected to embankment loading. Several authors have proposed approximate procedures for the modelling of vertical drains. Hird and Kwok (1986) and Poran (1986) allowed for the effect of the vertical drains by increasing the vertical permeability of the subsoil in plane strain

analyses. This approach increases the rate of consolidation but fails to model the localized consolidation around individual drains. The permeability increase factor is also difficult to define. Shinsha et al (1982) and Sanchez and Sagaseta (1990) developed methods in which an equivalent drain spacing in a plain strain finite element analysis could be calculated. These methods produce an equivalent average degree of consolidation at only one stage of the analysis and the methods cannot account for the effects of well resistance or smear which have been shown to be significant in certain situations (Jamiolkowski et al, 1983).

### **2.3.2. Validation and Accuracy of Modelling**

It is necessary to validate a finite element program before sufficient confidence in the ability to model real situations is achieved. The validation can be approached in two ways. Firstly, by analysing relevant idealized problems for which analytical solutions are available. If satisfactory agreement is obtained then finite element analyses can be performed to examine more complex problems for which analytical solutions are not available. Secondly, the back analysis of case histories enables the finite element predictions to be compared against actual behaviour. Differences between observed and predicted behaviour must be assessed carefully in order to highlight deficiencies in the analysis as opposed to inaccuracies in input parameters or observed results.

Several authors have compared undrained plane strain finite element analyses with limit equilibrium solutions (Brown and King, 1966; Smith and Hobbs, 1974; Rowe and Soderman, 1985) and with plasticity solutions for strip footings (Rowe and Soderman, 1987; Basset and Guest, 1990; Hird et al, 1990). Comparisons of analytical and finite element analyses for consolidation of soil using vertical drains are rare, and the Author is not aware of any comparison made between strength increases beneath

embankments predicted by finite element analyses and those predicted by simple design methods.

The improvement in constitutive modelling and the refinement of analysis techniques have resulted in the potential to model embankment problems more accurately. However, these improvements must be shown to reproduce observed behaviour. This can only be achieved by the back analysis of embankments or model tests.

Back analysis requires high quality case histories which provide sufficient soil data, detailed construction information, accurate instrumentation and the extended recording of observed behaviour. The definition of the subsoil conditions is very difficult and parameters such as mass permeability can be unreliable. During and after construction it is necessary to monitor pore water pressure and settlement at several positions and to record lateral movements, particularly near the toe.

Several authors have attempted back analyses and with the refinement of input parameters it is possible to produce good agreement between observed and finite element predicted pore pressures and displacements. However, it is not possible to assess the accuracy of the finite element analysis until sufficient confidence in the input material parameters and observed results is achieved.

Centrifuge testing can provide data which can be used as an alternative to full scale embankments. Several authors have used centrifuge tests for comparison with finite element analyses (Almeida, 1984; Basset and Guest, 1990). Centrifuge tests have the advantage, over full scale embankments, that they are relatively cheap and provide reproducible results under controlled laboratory conditions.

## **2.4. The Need for Further Finite Element Research**

A large amount of research into the finite element analysis of embankments constructed over soft clays has been carried out over the last few decades. Advances in the constitutive modelling of the subsoil and fill and the representation of reinforcing materials and their interface with the soils have been made. However, there are several areas that have been less well researched, and further analyses are presented in this Thesis, as outlined below:

- 1. Plasticity solutions are available for the collapse loads of rigid strip footing over various subsoils. Jewell (1988) has suggested that these solutions are relevant to the design of single stage reinforced embankments. In order to assess the validity of these solutions finite element analyses have been compared with plasticity theory for undrained loading of two idealized subsoils. Further analyses have been performed and a simplified design method which is based on plasticity theory has been proposed (Chapter 4).**
- 2. Vertical drains have become increasingly popular in embankment construction. Few attempts have been made to develop a rational approach to their inclusion in plane strain finite element analyses and these methods have significant limitations. In Chapter 5 the consolidation behaviour of single drains is investigated by comparison of finite element analyses with an analytical solution. A new procedure for modelling vertical drains in plane strain finite element analyses is developed and validated.**
- 3. Few authors have carried out analyses of stage constructed embankments and the Author is not aware of any comparisons of**

simple design methods with finite element analyses. In Chapter 7 an idealized two stage constructed embankment is analysed and the strength increases predicted in a fully coupled analysis are compared with a simple design procedure. The procedure is then used to analyse the Porto Tolle trial embankment (analysed in Chapter 6) and again comparisons of strength increases predicted by finite element analysis and the simple design procedure are compared.

## **3. The Finite Element Program**

### **CRISP and Modifications**

CRISP is a finite element program for the analysis of geotechnical problems; the program has been modified and used in all analyses presented. Details of the use of the modified program are given in Russell (1992). In this Chapter the 1984 version of CRISP (Gunn and Britto, 1984) is described and then the modifications to the program, to enable the efficient analysis of reinforced embankments on soft ground incorporating vertical drains, are presented.

#### **3.1. Crisp**

##### **3.1.1. The History of Crisp**

The computer programs known as CRISP were developed at Cambridge University. Work started in 1975 when the program was originally called MZOL but in 1976, after additional work, it was renamed CRISTINA. The program was developed further and in 1982 given the name CRISP (CRITICAL STATE PROGRAM). The 1982 version of the program (Gunn and Britto, 1982), referred to as CRISP82, has been used in previous research of reinforced embankments at the University of Sheffield (Kwok, 1987).

In 1984 a new version of the program was produced (CRISP84). The double precision version of the 1984 program has been modified, by the Author, and used in this research. In the Thesis this version of the program will be referred to as CRISP.

Other versions of the program are available. In 1987 a reduced program was made available to coincide with the publication of Britto and Gunn

(1987). In 1990 the program was extensively rewritten for use on personal computers (CRISP90).

### **3.1.2. Types of Analysis**

Analyses can be carried out in plane strain, axisymmetry (with axisymmetric loading) or three dimensions. The soil can be modelled as drained, undrained or as undergoing fully-coupled consolidation.

The method by which the program allows for drained or undrained conditions is by the specification of an appropriate value for the bulk modulus of water ( $K_w$ ). The bulk modulus of water is then included in the formulation of the element stiffness matrices.

#### **Types of Constitutive Model Available**

The five constitutive models available are: anisotropic elastic, inhomogenous elastic (Young's modulus varying with depth), Cam-clay, modified Cam-clay and elastic-perfectly plastic.

The elastic-perfectly plastic model can be used with four yield criteria: Von Mises, Tresca, Drucker-Prager and Mohr-Coulomb.

#### **Types of Finite Element Available**

Eight elements are available. The basic four elements are the linear strain triangle, the linear strain quadrilateral, the cubic strain triangle and the linear strain brick. Each of these elements have nodal displacements as unknowns and each element is also available with pore pressure nodes for consolidation analysis. All elements are formulated using full integration.

Theoretical limitations on the use of linear strain elements have been identified. For example, when using full integration Sloan and Randolph (1982) has shown that failure loads for undrained analyses using elastic-perfectly plastic constitutive models are overestimated in certain circumstances. The linear strain triangle and linear strain quadrilateral

over-estimate axisymmetric failure loads. This over-prediction can be avoided by using the higher order cubic strain elements or reduced integration.

When analysing an embankment in plane strain, due to the complex geometry and soil conditions, it is often necessary to use a large number of elements. This is particularly the case when considering reinforcement and/or vertical drains. Cubic strain elements cannot be used economically for such problems, and so for the present research linear strain elements have been used to model the soil.

A subsoil containing vertical drains forms a three-dimensional problem. However, the three-dimensional analysis of an embankment would be impractical, even when using modern super computers, due to the large number of elements required for accurate modelling. The present embankment analyses have been carried out in plane strain and a procedure has been developed for modelling accurately the three-dimensional rate of consolidation around a single vertical drain in a two-dimensional plane strain analysis (Chapter 5).

### **3.1.3. Additional Features of Crisp**

#### **Material Non-Linearity**

An incremental tangent stiffness solution procedure is used by CRISP for analyses including non-linear constitutive models. The result is that for any increment in which an element's stiffness changes an error in equilibrium is generated as the change in stiffness of the element is ignored.

For the elastic-perfectly plastic constitutive models it is possible to correct the stress state back to the yield surface by calculating 'out of balance' loads which are applied in the next increment. CRISP corrects the stresses back along a line normal to the yield surface (Owen and Hinton, 1980). This

is an arbitrary assumption so that even though the yield criterion is not violated a large number of increments must still be used to ensure that the stress state never passes beyond the yield surface by a large amount.

Tangent stiffness parameters are also used for the critical state constitutive models; 'out of balance loads' are not calculated as the correct position on the yield surface is unknown. In order to reduce these errors it is essential that a large number of increments are used. CRISP produces information on the rate of change in the size of the yield locus and recommended values are discussed by Britto and Gunn (1987).

An alternative solution technique is the use of iterations to ensure that displacements and forces are consistent at the end of each increment. CRISP has been compared with a finite element program using an iterative solution technique (Potts et al, 1990) and was shown to produce a correct solution provided sufficient increments were used.

To ensure that the CRISP analyses are accurate it is necessary to perform several analyses with increasing numbers of increments until a further increase in the number of increments produces no change in the final increment displacements. Where practical this procedure has been adopted in the analyses presented.

### **Geometric Non-Linearity**

In analyses using non-linear constitutive models the specified changes in load or displacement conditions are applied over a number of increments. The result of each increment is a set of nodal displacements and as these displacements become large the equilibrium equations based on the undeformed geometry may no longer be accurate.

This geometric non-linearity can be approximated in CRISP by updating the nodal coordinates at the end of each increment. The updated nodal coordinates are then used to calculate the new element stiffness matrices. This coordinate updating is only a first approximation to a large strain theory

(Cook, 1981). If excessively large strains occur the solution may no longer be reliable.

### **Embankment Construction**

CRISP allows for the simulation of the construction of an embankment by specifying an initial mesh containing elements which represent the fill material. CRISP then allows these elements to be added as the analysis proceeds. To avoid using a large number of thin elements the self weight of the added elements is applied over a number of increments. Excavation can be simulated by removing elements.

### **Restarted Analyses**

The original CRISP program outputted information at the end of each increment so that an analysis could be restarted from some earlier point. The file produced became extremely large for any reasonable number of increments. In order to reduce its size the program has been modified so that restart information is only saved for specified increments. The analysis can then be restarted from any one of these increments.

## **3.2. Reinforcement Element**

To analyse accurately reinforced embankments it is necessary to model the reinforcing material. This could be achieved using thin quadrilateral elements. Whilst this method has the advantage that no new elements need be added to CRISP, the aspect ratio of the elements modelling the reinforcement may become large enough to cause numerical problems. A second approach, which overcomes this problem, is to model the reinforcement using one-dimensional bar elements, Figure 3.1a. This method has the additional advantage that no extra degrees of freedom are added to the mesh.

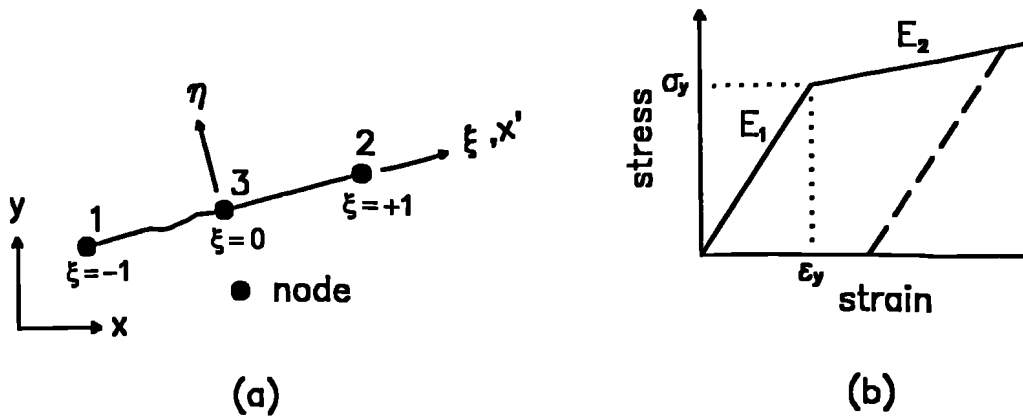


Figure 3.1 - a) Reinforcement element; b) bi-linear constitutive model.

Following a preliminary study (Russell, 1988) it was decided that a bar element of the type developed by Kwok (1987) should be added to CRISP. The element was implemented for plane strain analyses only.

### 3.2.1. Constitutive Relationship

The reinforcement is usually a polymer material with high tensile strength and little bending resistance. Therefore, in the element formulation the flexural stiffness has been ignored. To maintain a simple constitutive relationship the reinforcement is modelled as bi-linear elastic, Figure 3.1b. Four parameters are required, the elastic Young's modulus ( $E_1$ ), the Young's modulus after yielding ( $E_2$ ), the yield stress ( $\sigma_y$ ) and the reinforcement thickness ( $t$ ). The element thickness is required as an input parameter, even though the element is formulated as one dimensional, and is used to calculate the reinforcement element stiffness matrix.

It should be noted that the axial stiffness of a geotextile or geogrid is usually expressed as force per unit width per unit strain (kN/m). This is commonly

referred to as the 'reinforcement modulus' (J) and is equal to the Young's modulus (E) multiplied by the thickness (t) (for plane strain conditions).

When a bi-linear relationship is assumed the material behaves elastically with a Young's modulus  $E_1$  until the yield stress is reached after which the modulus is changed to  $E_2$ . If unloading occurs the original modulus is restored.

### 3.2.2. Reinforcement Element Stiffness Matrix Formulation

The reinforcement element, Figure 3.1a, has three displacement nodes so as to be compatible with the linear strain elements which are used to model the soil.

The displacement at any point along the element,  $a$ , can be related to the nodal displacements,  $a_n$ , by the element shape functions,  $N$ , as

$$a = Na_n \dots\dots\dots(3.1)$$

For the element shown in Figure 3.1a the shape functions,  $N$ , in the local coordinate system,  $(\xi)$ , are

$$N = \left[ \begin{array}{ccc} 0.5\xi(\xi-1) & 0.5\xi(\xi+1) & (1-\xi^2) \end{array} \right] \dots\dots\dots(3.2)$$

The element strains,  $\epsilon$ , are expressed in terms of the nodal displacements as

$$\epsilon = Ba_n \dots\dots\dots(3.3)$$

where

$$B = \frac{\partial N}{\partial x'} \dots\dots\dots(3.4)$$

In which  $x'$  is the coordinate system defining the element length, i.e.  $x'=0$  at node 1 and  $x'=L$  at node 2, where  $L$  is the length of the element.

However, the shape functions are in terms of the element local coordinate system,  $(\xi)$ . Using the chain rule for differentiation it can be shown that

$$\frac{\partial N}{\partial x'} = \frac{\partial N}{\partial \xi} \frac{d\xi}{dx'} \dots\dots\dots(3.5)$$

By consideration of the element geometry, Figure 3.1a

$$\frac{d\xi}{dx'} = \frac{2}{L} \dots\dots\dots(3.6)$$

Differentiating the shape functions, Equation 3.2 and using the chain rule

$$B = \frac{2}{L} \left[ (0.5 - \xi) \quad -(0.5 + \xi) \quad 2\xi \right] \dots\dots\dots(3.7)$$

The element stiffness matrix for a displacement finite element (Eg. Zienkiewicz, 1977) is

$$K_e = \int^v B^T D B d(vol) \dots\dots\dots(3.8)$$

where D is the constitutive matrix relating stresses to strains as  $\sigma = D\epsilon$ .

The cross sectional area for a unit width of the element in a plane strain analysis is constant and equal to the element thickness, t, therefore Equation 3.8 becomes

$$(K_e)_\xi = t \int_{-1}^1 B^T D B d\xi \dots\dots\dots(3.9)$$

To transform Equation 3.9 into the x' coordinate system it must be multiplied by  $\frac{dx'}{d\xi}$ , which from Equation 3.6 is L/2. Thus

$$(K_e)_{x'} = \frac{tL}{2} \int_{-1}^1 B^T D B d\xi \dots\dots\dots(3.10)$$

Numerical integration is used to calculate the element stiffness matrix for each reinforcement element. Two point Gaussian integration would produce an exact solution, but three Gauss points have been used to provide extra data.

### **Incorporation of the Reinforcement Element in a Two-Dimensional Mesh**

In general the reinforcement element will be at an angle  $\alpha$  to the global (x) axis. A transformation matrix T is used to convert the element stiffness

matrix,  $(K_e)_x$ , to the global element stiffness matrix  $K_{eg}$  in global coordinate system  $(x,y)$ .

$$K_{eg} = T^T (K_e)_{x'} T \dots\dots\dots(3.11)$$

where

$$T = \begin{bmatrix} c & s & 0 & 0 & 0 & 0 \\ 0 & 0 & c & s & 0 & 0 \\ 0 & 0 & 0 & 0 & c & s \end{bmatrix} \dots\dots\dots(3.12)$$

in which  $c = \cos\alpha$  and  $s = \sin\alpha$ .

**Calculation of the Reinforcement Length and Angle of Orientation**

In analyses in which the option to update the nodal coordinates has been used it is desirable for the length and angle of orientation of the reinforcement element to be calculated at the start of each increment. These coordinates are then used in the calculation of the new element stiffness matrices.

The continuum elements have an isoparametric formulation, therefore, the element sides may be curved. The reinforcement element is approximated by two straight lines connecting the three nodes, Figure 3.2, and the length is calculated as

$$L = L_1 + L_2 \dots\dots\dots(3.13)$$

and the angle of orientation as

$$\alpha = 0.5(\alpha_1 + \alpha_2) \dots\dots\dots(3.14)$$

The error introduced by this approximation, for relatively coarse meshes, is less than 1% (Kwok, 1987) and becomes smaller as the mesh is refined.

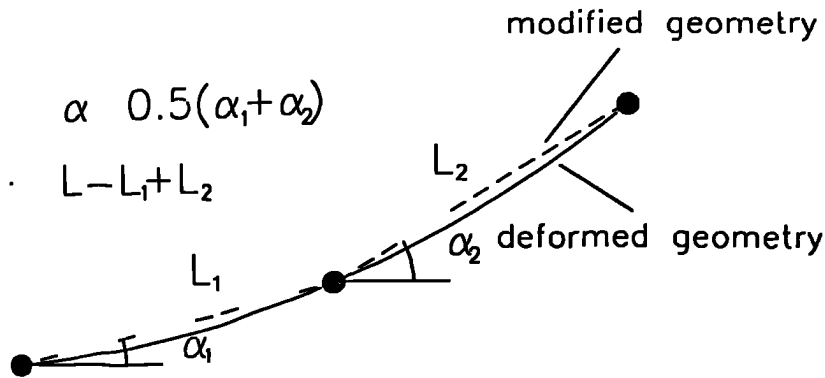


**Figure 3.2 - Calculation of one-dimensional element length and orientation.**

### 3.2.3. Equivalent Nodal Forces

It is necessary to convert the element stresses into equivalent nodal forces,  $F_e$ . These forces are found by integrating the stresses over the volume of the element

$$F_e = \int^v B^T \sigma d(vol) \dots\dots\dots(3.15)$$

The element is used in plane strain analyses; therefore, consider a unit width of constant thickness,  $t$ . Using the local coordinate system ( $\xi$ ), Equation 3.15 becomes

$$\left( F_e \right)_\xi = t \int_{-1}^1 B^T \sigma d(\xi) \dots\dots\dots(3.16)$$

Converting to the coordinate system ( $x'$ )

$$\left( F_e \right)_{x'} = \frac{2t}{L} \int_{-1}^1 B^T \sigma d(\xi) \dots\dots\dots(3.17)$$

Again a three point Gaussian integration scheme is used to evaluate Equation 3.17 and the nodal forces are resolved into the global coordinate system ( $x,y$ ).

### **3.2.4. Analyses Using the Reinforcement Element**

To check the correct implementation of the reinforcement element two problems were analysed. These test problems were analysed previously by Kwok (1987).

The first analysis involved a single reinforcement element with a bi-linear constitutive relationship. The element was restrained at one end and a load applied at the other. The load displacement response predicted by the finite element analysis was as defined by the constitutive model.

The second analysis involved a three bar structure for which the displacements could be calculated analytically. The finite element analysis produced the expected displacements.

## **3.3. Interface Element**

An interface element has been implemented for plane strain analyses and can be used to model slip between the reinforcement and soil or at a rough boundary. The element also allows interface shear and normal stress to be retrieved easily. The element is similar to the Goodman (1968) relative displacement element and was implemented previously in CRISP82 by Kwok (1987).

### **3.3.1. Interface Element Stiffness Matrix Formulation**

The interface element, Figure 3.3a, has a quadratic displacement variation so as to be compatible with the linear strain elements used to model the soil.

If a set of nodal forces,  $F_n$ , are acting on the interface element such that nodal displacements,  $a_n$ , occur then it is possible to define a set of relative local displacements at any position along the element,  $w$ , such that

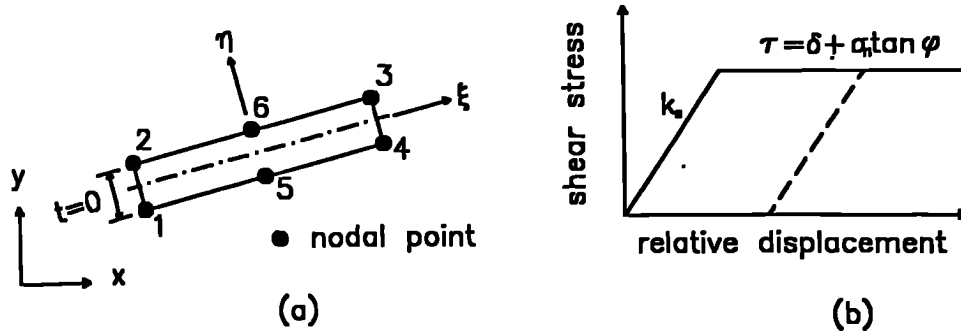


Figure 3.3 - a) Interface element; b) constitutive relationship.

$$W = \begin{bmatrix} a_{\xi}^{top} - a_{\xi}^{bottom} \\ a_{\eta}^{top} - a_{\eta}^{bottom} \end{bmatrix} \dots\dots\dots(3.18)$$

The shape functions for the interface element are defined in Equation 3.2 and can be rewritten

$$N = [ N_1 \ N_2 \ N_3 ] \dots\dots\dots(3.19)$$

The relative nodal displacements in terms of the actual nodal displacements,  $a_e$ , and the shape functions are

$$w_e = N_r a_e \dots\dots\dots(3.20)$$

where

$$N_r = \begin{bmatrix} -N_1 & 0 & -N_2 & 0 & N_2 & 0 & N_1 & 0 & -N_3 & 0 & N_3 & 0 \\ 0 & -N_1 & 0 & -N_2 & 0 & N_2 & 0 & N_1 & 0 & -N_3 & 0 & N_3 \end{bmatrix} \dots\dots(3.21)$$

The stresses can then be related to the relative displacements by a constitutive matrix,  $D$ , as

$$\sigma = D w_e \dots\dots\dots(3.22)$$

The vector of stresses,  $\sigma$ , has components of normal stress,  $\sigma_n$ , and shear stress,  $\tau$ . The constitutive matrix has components of shear stiffness,  $k_s$ , and normal stiffness,  $k_n$ .

$$D = \begin{bmatrix} k_s & 0 \\ 0 & k_n \end{bmatrix} \dots\dots\dots(3.23)$$

Equation 3.23 implies that there is no coupling of the shear and normal stiffnesses of the interface.

The principal of virtual work can now be used to define a set of nodal forces which are in equilibrium with the state of internal stress. It is assumed that a set of virtual nodal displacements,  $\mathbf{a}_e^*$ , cause a set of virtual nodal relative displacements,  $\mathbf{w}_e^*$ , where

$$\mathbf{w}_e^* = \mathbf{N}_r \mathbf{a}_e^* \dots\dots\dots(3.24)$$

and from the principal of virtual work

$$\mathbf{a}_e^{*T} \mathbf{F}_e = \int_{-1}^1 \mathbf{w}_e^{*T} \sigma d(\xi) \dots\dots\dots(3.25)$$

Substituting for  $\sigma$  and  $\mathbf{w}_e^*$  in Equation 3.25 and dividing both sides by  $\mathbf{a}_e^{*T}$

$$\mathbf{F}_e = \int_{-1}^1 \mathbf{N}_r^T \mathbf{D} \mathbf{N}_r d(\xi) \mathbf{a}_e \dots\dots\dots(3.26)$$

The element stiffness matrix for the interface element is therefore

$$(\mathbf{K}_e)_\zeta = \int_{-1}^1 \mathbf{N}_r^T \mathbf{D} \mathbf{N}_r d(\xi) \dots\dots\dots(3.27)$$

Transforming to the  $x'$  coordinate system

$$(\mathbf{K}_e)_{x'} = \frac{L}{2} \int_{-1}^1 \mathbf{N}_r^T \mathbf{D} \mathbf{N}_r d(\xi) \dots\dots\dots(3.28)$$

### 3.3.2. Transformation to Global Coordinate System

The element stiffness matrix from Equation 3.28 has been defined in the  $x'$  coordinate system and must be transformed into the global coordinate system  $(x,y)$ . This is achieved using a transformation matrix, such that,  $\mathbf{K}_{eg} = \mathbf{T}^T (\mathbf{K}_e)_{x'} \mathbf{T}$ , where

$$T = \begin{bmatrix} t & 0 & 0 & 0 & 0 & 0 \\ 0 & t & 0 & 0 & 0 & 0 \\ 0 & 0 & t & 0 & 0 & 0 \\ 0 & 0 & 0 & t & 0 & 0 \\ 0 & 0 & 0 & 0 & t & 0 \\ 0 & 0 & 0 & 0 & 0 & t \end{bmatrix} \dots\dots\dots(3.29)$$

in which

$$t = \begin{bmatrix} \cos\alpha & \sin\alpha \\ -\sin\alpha & \cos\alpha \end{bmatrix} \dots\dots\dots(3.30)$$

To calculate the orientation of the element in the two-dimensional global coordinate system,  $\alpha$ , and the element length,  $L$ , a reference plane through the centre of the element is defined by averaging the positions of the pairs of nodes. The orientation angle and element length are calculated according to Equations 3.13 and 3.14.

### 3.3.3. Interface Element Constitutive Relationship and Modes of Behaviour

The interface element has been implemented as elastic-perfectly plastic with a Mohr-Coulomb yield criterion, Figure 3.3b. The elastic shear stiffness,  $k_s$ , is set to zero when the soil yields. The normal stiffness,  $k_n$ , is not changed when yielding occurs but can be set to a modified value,  $k_{nt}$ , if the normal stress becomes tensile. Kwok (1987) showed that the interface element is insensitive to the value of shear and normal stiffness except when very low values are used.

Five modes of behaviour can be represented:

- 1 Non-slip - the element is behaving elastically with a normal stiffness,  $k_n$ , and shear stiffness,  $k_s$ .
- 2 Slip - when the shear stress reaches the bond strength, governed by the Mohr-Colomb relationship, slip occurs; the shear stiffness,  $k_s$ , is then set to zero.

- 3 Unloading - if unloading occurs then the original shear stiffness is restored.
- 4 Separation - if the normal stress becomes tensile then the shear stiffness is set to zero and the normal stiffness is allowed to change to a specified value,  $k_n$ .
- 5 Rebonding - if separation has occurred and during some later increment the interface normal stress becomes compressive then the original shear and normal stiffnesses are restored.

The mode of behaviour is identified at each of the three integration points and the appropriate shear and normal stiffnesses are used to calculate the element stiffness matrix.

Oscillation of stresses has often been observed when using interface elements. To try to minimise this problem Kwok (1987) carried out a study in which two methods of smoothing the value of the normal stress were evaluated. The first method was a local stress smoothing technique (Hinton and Campbell, 1974) and the second was a simple averaging of the normal stress calculated at integration points along the element. Kwok showed that the stress averaging technique was almost as efficient as the local smoothing method. The interface element has been implemented using the stress averaging technique so as to minimize oscillations of shear stresses efficiently.

The stress averaging technique involves calculating an average normal stress and using this value to calculate the Mohr-Coulomb shear strength. Improved performance may be achieved by using a more complicated integration rule (Hohberg, 1990).

The interface shear stress sign convention is defined in Figure 3.4. Compressive normal stresses are positive. This Figure also identifies four

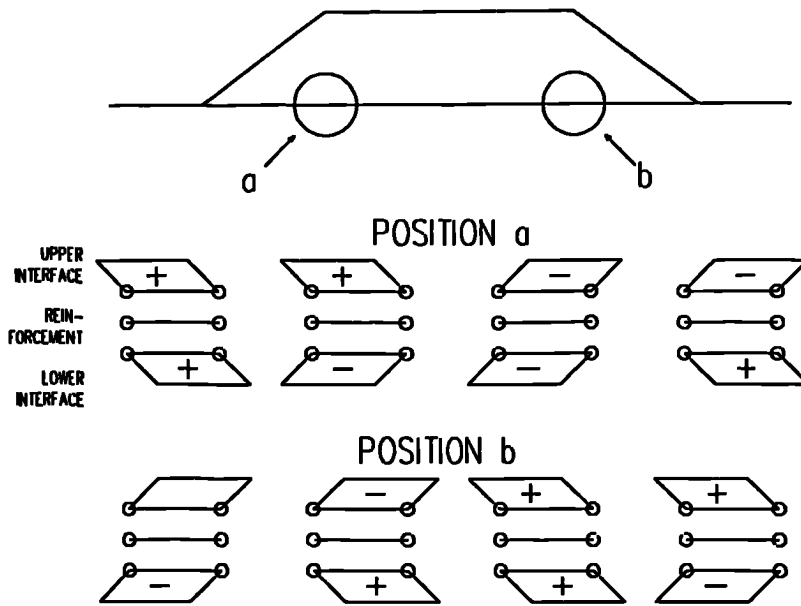


**Figure 3.4 - Interface element shear stress sign convention and shear stress regimes.**

shear stress regimes which may develop, by differential movement of the fill and subsoil, in a reinforced embankment.

### 3.3.4. Equivalent Nodal Forces

The equivalent nodal forces, which are in equilibrium with the internal stresses, are calculated for the interface element at the end of each increment. Stresses ( $\tau$ ,  $\sigma_n$ ), which act on a plane through the centre of the interface element, are used to calculate the nodal forces  $F$ .

Consider an infinitesimally small section of the element. The forces which are in equilibrium with the stresses are

$$dF_x = (\tau \cos \alpha - \sigma_n \sin \alpha) d\xi \quad \dots\dots\dots(3.31a)$$

$$dF_y = (\tau \sin \alpha + \sigma_n \cos \alpha) d\xi \quad \dots\dots\dots(3.31b)$$

where  $\alpha$  defines the orientation of the interface element central reference plane in the global (x,y) coordinate system, Section 3.3.2.

If a set of virtual displacements,  $a^*$ , are applied to the element then the virtual displacements at any position along the element can be related to the nodal virtual displacements by the element shape functions

$$a^* = Na_g^* \dots\dots\dots(3.32)$$

The work done by the nodal forces due to the virtual displacements is equivalent to the work done by the internal stresses

$$\left(dF_\theta\right)_x = \int_{-1}^1 N(\tau \cos \alpha - \sigma_n \sin \alpha) d\xi \dots\dots\dots(3.33a)$$

$$\left(dF_\theta\right)_y = \int_{-1}^1 N(\tau \sin \alpha + \sigma_n \cos \alpha) d\xi \dots\dots\dots(3.33b)$$

The equivalent nodal forces are then evaluated by numerical integration. These forces are acting on both faces of the interface element but in opposite senses.

### 3.3.5. Analyses Using the Interface Element

A finite element analysis was carried out to ensure that the Mohr-Coulomb yield criterion had been implemented correctly. The test involved a single element to which a shear displacement was applied. The shear stress response was compared with that defined by the constitutive relationship and found to be acceptable. Further details of this analysis can be found in Kwok (1987).

Results from an analytical solution developed by Hird and Russell (1990) were used to compare with a second finite element analysis. The analytical solution allows the calculation of the shear stress distribution along a rough boundary of a block which is loaded in compression. Results from the finite element analysis were in excellent agreement with those predicted using

the analytical solution; comparisons are presented by Hird and Russell (1990).

### 3.4. Drainage Element

In consolidation finite element analyses of subsoil containing vertical drains it is often adequate to represent the drain as a boundary with zero excess pore pressure. However, this approximation is in error if well resistance, due to the drain's finite permeability, restricts the flow along the drain.

To model the well resistance accurately an element, termed a drainage element, has been developed for use in plane strain and axisymmetric consolidation analyses (Russell, 1990). The drainage element can be used to represent a thin layer of relatively high permeability in consolidation analyses, for example a sand lamination in a clay soil or, as for the present research, to model a vertical drain in a clay soil.

#### 3.4.1. Element Formulation

The drainage element is compatible with linear strain elements having three displacements nodes and two pore pressure nodes, Figure 3.5.

Discretising the continuity and equilibrium equations (Biot, 1941) and using a fully implicit approximation over time, the element stiffness matrix is

$$K_e = \begin{bmatrix} KS & L \\ L & -\Delta\Phi \end{bmatrix} \dots\dots\dots(3.34)$$

where

$$KS = \int^v B^T DB d(vol) \quad \text{stiffness matrix}$$

$$L = \int^v B^T m N^p d(vol) \quad \text{link matrix}$$

$$\Phi = \frac{1}{\gamma_w} \int^v E^T k E d(vol) \quad \text{permeability matrix}$$

in which  $\Delta t$  is an increment of time,  $N$  are the displacement shape functions,  $B$  are the first derivative of the displacement shape functions,  $N^p$  are the

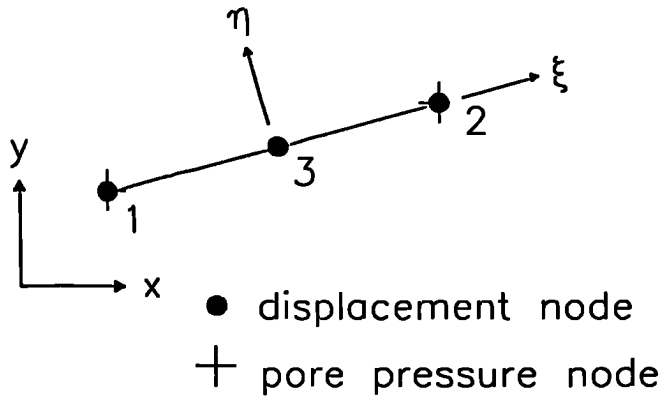


**Figure 3.5 - Drainage element.**

pore pressure shape functions,  $E$  are the first derivative of the pore pressure shape functions,  $k$  is the permeability matrix,  $D$  is the constitutive matrix,  $m=[1\ 1\ 0]^T$  and  $\gamma_w$  is the unit weight of water.

### 3.4.2. Transformation to Two-Dimensions

The element stiffness matrix, Equation 3.34, is in the  $x'$  coordinate system and must be transformed to the global coordinate system  $(x,y)$  using a transformation matrix

$$K_{eg} = T^T(K_e)_{x'} T \dots\dots\dots(3.35)$$

where

$$T = \begin{bmatrix} \cos\alpha & \sin\alpha & 0 & 0 & 0 & 0 & 0 & 0 \\ 0 & 0 & \cos\alpha & \sin\alpha & 0 & 0 & 0 & 0 \\ 0 & 0 & 0 & 0 & \cos\alpha & \sin\alpha & 0 & 0 \\ 0 & 0 & 0 & 0 & 0 & 0 & 1 & 0 \\ 0 & 0 & 0 & 0 & 0 & 0 & 0 & 1 \end{bmatrix} \dots\dots\dots(3.36)$$

The element length,  $L$ , and angle of orientation,  $\alpha$ , are defined as for the reinforcement element, Figure 3.2.

### 3.4.3. Incorporation of the Drainage Element in a Two-Dimensional Mesh

The drainage element has been transformed so that it can be used as a two-dimensional element, but before it is included in a two-dimensional mesh the significance of each of the terms in the element stiffness matrix, Equation 3.34, must be considered.

A fully coupled Biot consolidation analysis with a fully implicit approximation over the time increment (Booker and Small, 1975) is used in CRISP. For an increment of time,  $\Delta t$ , the discretized form of the continuity and equilibrium equations are:

$$\text{equilibrium} \quad \mathbf{KS}\Delta\mathbf{d} + \mathbf{L}\Delta\mathbf{u} = \Delta\mathbf{F}_1$$

$$\text{continuity} \quad \mathbf{L}^T\Delta\mathbf{d} - \Delta t\Phi\Delta\mathbf{u} = \Delta\mathbf{F}_2$$

where  $\Delta\mathbf{d}$ ,  $\Delta\mathbf{u}$ ,  $\Delta\mathbf{F}_1$  and  $\Delta\mathbf{F}_2$  are increments of nodal displacement, pore pressure, nodal force and nodal flow respectively.

Considering each term separately:

- 1  $\mathbf{KS}\Delta\mathbf{d}$  - is the change of nodal displacement,  $\Delta\mathbf{d}$ , caused by an increment of nodal force  $\Delta\mathbf{F}_1$ .
- 2  $\mathbf{L}\Delta\mathbf{u}$  - is the change of nodal pore pressure,  $\Delta\mathbf{u}$ , caused by an increment of nodal force  $\Delta\mathbf{F}_1$ .
- 3  $\mathbf{L}^T\Delta\mathbf{d}$  - is the change of nodal displacement,  $\Delta\mathbf{d}$ , caused by an increment of flow,  $\Delta\mathbf{F}_2$ .
- 4  $\Delta t\Phi\Delta\mathbf{u}$  - is the change of nodal pore pressure,  $\Delta\mathbf{u}$ , caused by an increment of flow,  $\Delta\mathbf{F}_2$ .

Terms 1 and 4 are relatively easy to understand, in that they have the usual finite element meaning.  $\mathbf{KS}$  is the force stiffness ascribed to the element multiplied by the defined area; similarly,  $\Phi$  can be considered as the flow

stiffness of the element which is related to the drain's permeability and defined area. However, the element itself is one-dimensional and whilst it does have force and flow stiffnesses, it does not have a real cross sectional area when included in a two-dimensional mesh. The linkage terms 2 and 3, are therefore zero.

Expressed another way, the element is not a simple one-dimensional consolidation element of unit cross sectional area (where terms  $L$  and  $L^T$  would be non zero) but a bar element with force and flow stiffness but no real thickness. The element stiffness matrix, Equation 3.34, is reduced to

$$K_e = \begin{bmatrix} KS & 0 \\ 0 & -\Delta t \Phi \end{bmatrix} \dots\dots\dots(3.37)$$

### 3.4.4. Analyses Using the Drainage Element

The correct implementation of the drainage element has been checked in two series of analyses. Firstly, comparing plane strain analyses using drainage elements, to represent relatively permeable laminations within a less permeable soil, with previous research using a different finite element program (Abid, 1986; Abid and Pyrah, 1990). Secondly, axisymmetric analyses of inward drainage to a vertical drain were compared with an analytical solution (Hansbo, 1981). The latter analyses are fully documented in Chapter 5.

## 3.5. Variation of Permeability with Stress Level

The modified Cam-clay constitutive model provides a realistic framework for the analysis of soft clay soils. However, an observed behaviour of soft clay, not implemented in the critical state models in CRISP, is the reduction of permeability with increasing stress level (Tavenas et al, 1983). In order to assess the influence of this effect modifications to the program have been made.

Tavenas et al (1983) reviewed several permeability/void ratio relationships. They compared each relationship with carefully derived experimental results from intact soil samples taken from 14 different sites in Canada, USA and Sweden. They concluded that Taylor's (1948) relationship, Equation 3.38, was the most representative for soils of initial void ratio less than 2.5 at volumetric strain levels normally encountered.

Taylor (1948) suggested an empirical linear relationship between the logarithm of the permeability,  $k$ , and the void ratio,  $e$

$$\log k = \log k_0 - \left( \frac{e_0 - e}{C_k} \right) \dots\dots\dots(3.38)$$

Where  $k_0$  and  $e_0$  are the initial values of the permeability and void ratio respectively and  $C_k$  is the permeability change index. Tavenas et al (1983) showed that the permeability change index can be reasonably approximated as  $C_k=0.5e_0$ .

The permeability stress level relationship, Equation 3.38 (with  $C_k=0.5e_0$ ), has been implemented in CRISP. The option is available when using modified Cam-clay and if the option is selected the program calculates a new horizontal and vertical permeability at the end of each increment.

Analyses, of an idealized triaxial test, were carried out in which the permeability and void ratio were monitored and found to agree with calculated values using Taylor's relationship. The variation of permeability with stress level was used in an analysis of the Porto Tolle case history (Chapter 6). A comparison of analyses of this case history showed negligible difference with and without varying the permeability with stress level.

Two aspects of the selection of permeability parameters which have been found to be more significant are the initial values of both vertical and horizontal permeabilities and ensuring that the coefficient of consolidation throughout the clay depth has been modelled correctly (Section 7.3.2).

Results of analyses using the permeability variation algorithm are not presented, but this aspect of soft clay behaviour will become more important as the soil becomes more compressible and this algorithm may be of use in future analyses.

### **3.6. Summary**

The finite element program CRISP is a versatile program which can be used to model geotechnical problems. However, in order to model accurately reinforced embankments over soft soils incorporating vertical drains several modifications were necessary:

- 1 The implementation of a bi-linear elastic one-dimensional element to model the reinforcing material in plane strain analyses.
- 2 The implementation of an elastic-perfectly plastic relative displacement interface element to model the soil/reinforcement interface in plane strain analyses.
- 3 The implementation of a one-dimensional bar element which can be used to model vertical drains in axisymmetric or plane strain analyses.
- 4 The implementation of an algorithm which allows the permeability to be varied with stress level when using the modified Cam-clay constitutive model.

The modified version of the program has been used in all analyses presented in the remaining Chapters.

# 4. Collapse of Undrained Subsoils

## 4.1. Introduction

Plasticity theory (Eg. Atkinson, 1981) is a method frequently used for the prediction of the collapse of geotechnical structures. It has been suggested (Jewell, 1988) that plasticity solutions for the collapse of strip footings on undrained soils can be used to predict the short term stability of reinforced embankments built over soft cohesive deposits.

Plasticity theory is of limited use in that it can only predict collapse loads and displacement patterns for specific problems. The finite element method is a more flexible analysis technique which can reproduce plasticity solutions as well as providing additional information for more complex boundary conditions.

In this Chapter relevant plasticity theory is briefly discussed with reference to two idealized soil profiles. Finite element solutions for rigid strip footings are then presented which approximate closely to the plasticity theory. Finally, finite element analyses of embankment loading are carried out to verify a simple design procedure.

### 4.1.1. Plasticity Theory

The application of the theory of plasticity allows upper and lower bounds of the collapse loads for a geotechnical structure to be calculated. If yield and compatibility conditions are satisfied, but equilibrium conditions are ignored, the solution is an upper bound of the collapse load. If equilibrium and yield conditions are satisfied, but compatibility conditions are ignored, the solution is a lower bound. If the upper and lower bounds coincide then the true collapse load has been obtained.

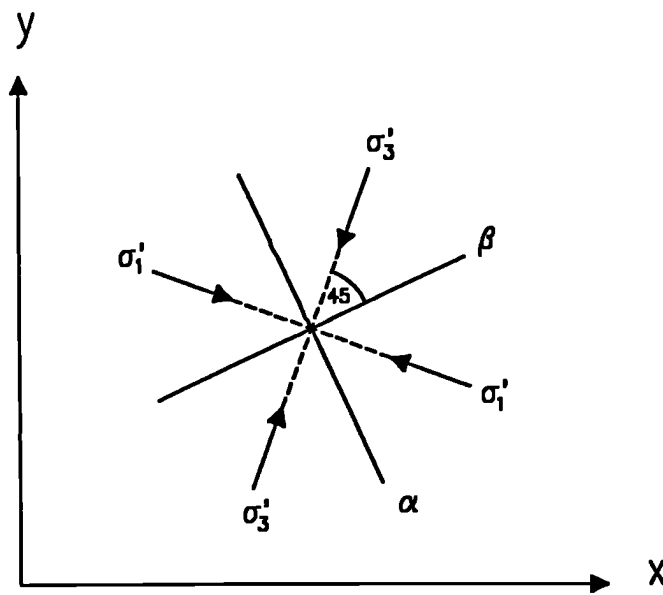


**Figure 4.1 - Definition of stress characteristics for undrained loading.**

Coincident upper and lower bound solutions can be found using methods which depend on the solution of hyperbolic partial differential equations. One such solution technique is the method of characteristics (Eg. Atkinson, 1981). This method involves the extension of two sets of slip lines from known boundaries, the directions of the slip lines being defined by the boundary conditions. At the intersection of two slip lines the state of stress can be calculated. The slip lines are referred to as  $\alpha$  and  $\beta$ , or stress, characteristics and are associated with positive and negative shear stresses respectively, Figure 4.1. For undrained soil the  $\alpha$  and  $\beta$  characteristics intersect at  $90^\circ$ .

From the slip line field it is possible to construct a vector displacement diagram which defines the relative displacement of areas bounded by slip lines. The displacement diagram is referred to as a hodograph.

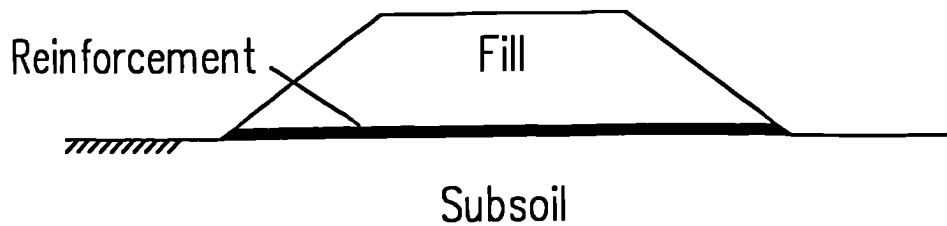


**Figure 4.2 - Reinforced embankment configuration.**

Plasticity theory assumes that the soil is perfectly plastic satisfying the normality condition and that the flow rule is associated. It is also assumed that the coaxiality condition, which states that the directions of principal stress and principal strain increment coincide, is valid.

A set of strain increment characteristics, also referred to as velocity characteristics or zero extension lines, can be defined in a similar way to the stress characteristics shown in Figure 4.1. For an undrained soil which is undergoing purely plastic deformations and has an associated flow rule, characteristics of stress and strain increment coincide.

#### **4.1.2. Reinforced Embankments**

(Embankments overlying soft clay soils often make use of geotextile reinforcement, placed at the surface of the subsoil (Figure 4.2), to allow construction to the design height within the area available (Bonaparte and Christopher, 1987). The stability of the embankment is most critical at the end of a loading stage, after which the subsoil consolidates and gains strength. The reinforcement is only required to maintain the factor of safety

above unity until the subsoil has consolidated sufficiently to maintain stability without the assistance of the reinforcement.

The reinforcement can improve stability in two ways. Firstly by resisting the shear stresses developed due to the lateral thrust in the embankment. Secondly, if sufficiently strong, the reinforcement may provide restraint to the surface of the subsoil.

The force in the reinforcement due to the lateral thrust of the embankment has been termed  $P_m$  and the force in the reinforcement due to the spreading of the subsoil as  $P_{m\text{dn}}$  (Jewell, 1988).

The stability of an embankment reinforced at its base has been discussed by Hird and Jewell (1990). Three classes of failure can be identified: internal stability of the embankment, instability of the subsoil and overall instability involving the embankment and the subsoil. The second of these has been selected for investigation; comparisons of finite element analyses and plasticity theory are made for relevant subsoil conditions.

#### **4.1.3. Application of Plasticity Theory to Reinforced Embankment Problems**

The loading due to an embankment is similar to that of a rigid strip footing. A heavily reinforced embankment is analogous to a rough footing in which the soil surface shear strength,  $s_{u0}$ , is fully mobilised. A smooth footing can be thought of as an embankment in which the reinforcement is sufficiently strong to resist the shear stress generated by the embankment but unable to provide any restraint at the subsoil surface.

Plasticity solutions have been developed for two idealized soil profiles. Firstly, a subsoil of uniform strength over a limited depth with a rough rigid layer beneath, Figure 4.3a (Mandel and Salençon, 1972) and secondly, a

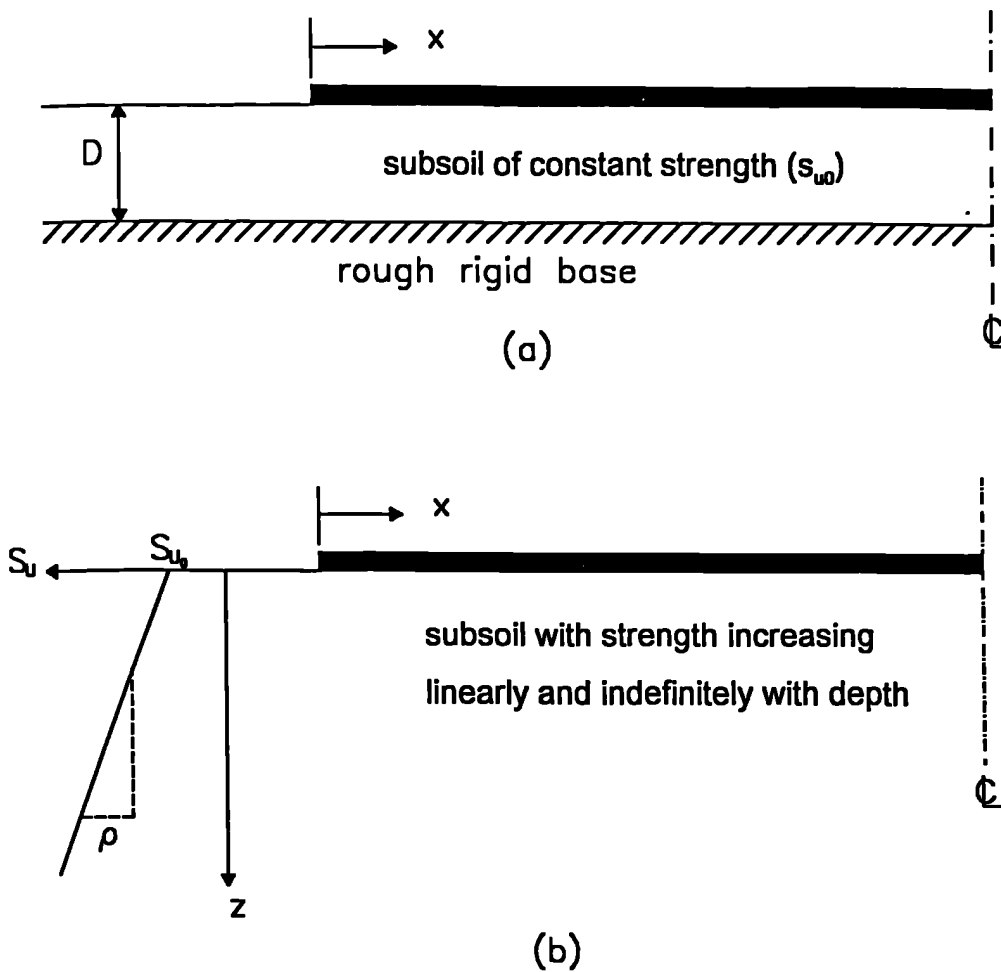


**Figure 4.3 - Idealized soil profiles for plasticity analyses: (a) uniform strength/limited depth; (b) strength increasing linearly with depth.**

subsoil with strength increasing linearly and indefinitely with depth, Figure 4.3b (Davis and Booker, 1973).

Plasticity theory gives the distribution of vertical stress on the underside of the rigid footing, shown in a non-dimensional form in Figure 4.4. These are ideal distributions which make the best possible use of the available subsoil strength and provide a meaningful comparison for finite element analyses.

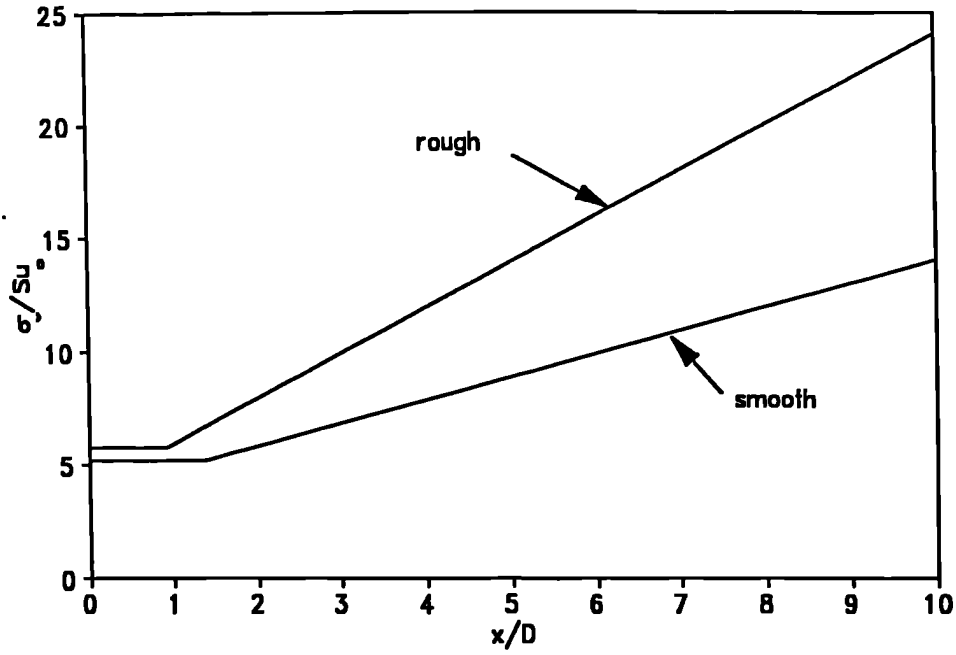


**Figure 4.4a - Ideal load distribution on an idealized soil profile of uniform strength/limited depth (Mandel and Salençon, 1972).**

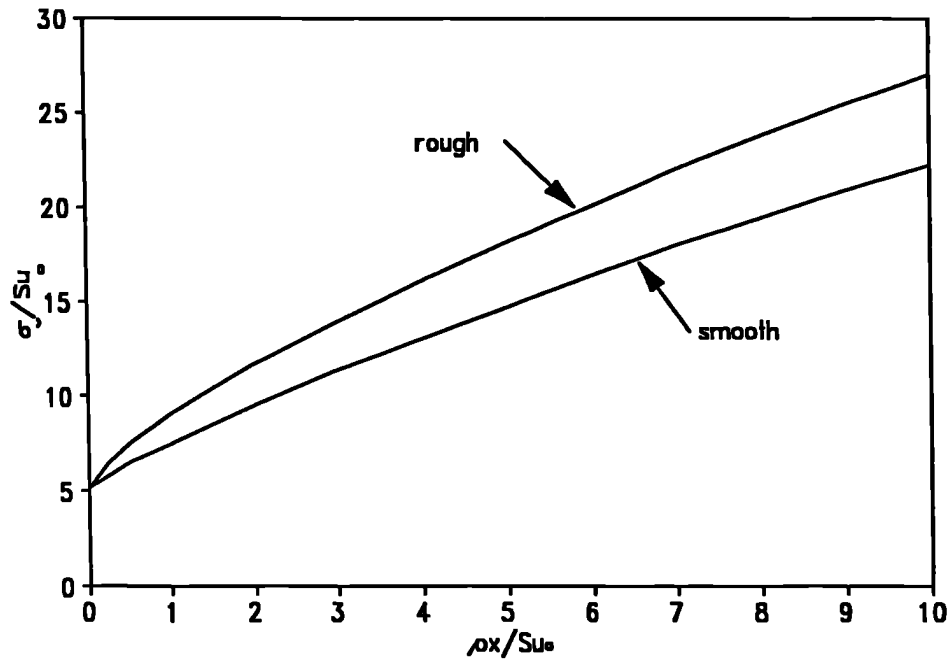


**Figure 4.4b - Ideal load distribution on an idealized soil profile of strength increasing linearly with depth (Davis and Booker, 1973).**

## 4.2. Finite Element Analysis of Plasticity

### Problems

CRISP has been used to perform plane strain undrained analyses of the plasticity problems defined in Figure 4.3. Both rough and smooth footings were modelled so that four situations were examined. Linear strain triangles using an elastic-perfectly plastic constitutive model, with a Tresca yield criterion, were used to model the soil; this is equivalent to the yield criteria used for the plasticity solutions. Interface elements have been used to model all rough boundaries, the interface strength is taken as equal to that of the soil adjacent to the element and is assumed to be purely cohesive.

#### 4.2.1. Meshes for Equivalent Loading Problems

In all cases advantage was taken of symmetry and only half of the loaded width was modelled.

For the soil of uniform strength and limited depth ( $D$ ), the mesh for the smooth loading case is shown in Figure 4.5. The width of the loading was relatively large ( $20D$ ). Sufficient distance was allowed beyond the edge of the loading that the conditions at the left-hand boundary of the mesh had no significant effect on the solution. It was assumed that the soil rests on a perfectly rough, perfectly rigid surface, modelled using a row of interface elements. In the rough case, the same mesh was used except that a row of interface elements was also included along the loaded surface, which was restrained horizontally.

For the soil with strength increasing linearly with depth, the mesh for the smooth loading case is shown in Figure 4.6. As the soil is of unlimited depth, the mesh had to be sufficiently extensive to ensure that none of the boundaries affected the solution significantly. The extent of the failure zone was initially estimated from charts produced by Houlsby and Jewell (1988).

287 linear strain triangles  
 39 interface elements  
 1488 degrees of freedom

$D=4.0\text{m}$

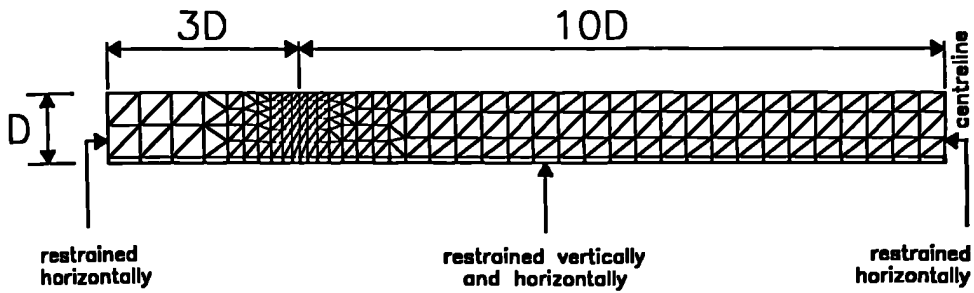


**Figure 4.5 - Finite element mesh used for uniform strength/limited depth analyses (mesh shown for smooth case).**

243 linear strain triangles  
 1096 degrees of freedom

$B=12.0\text{m}$

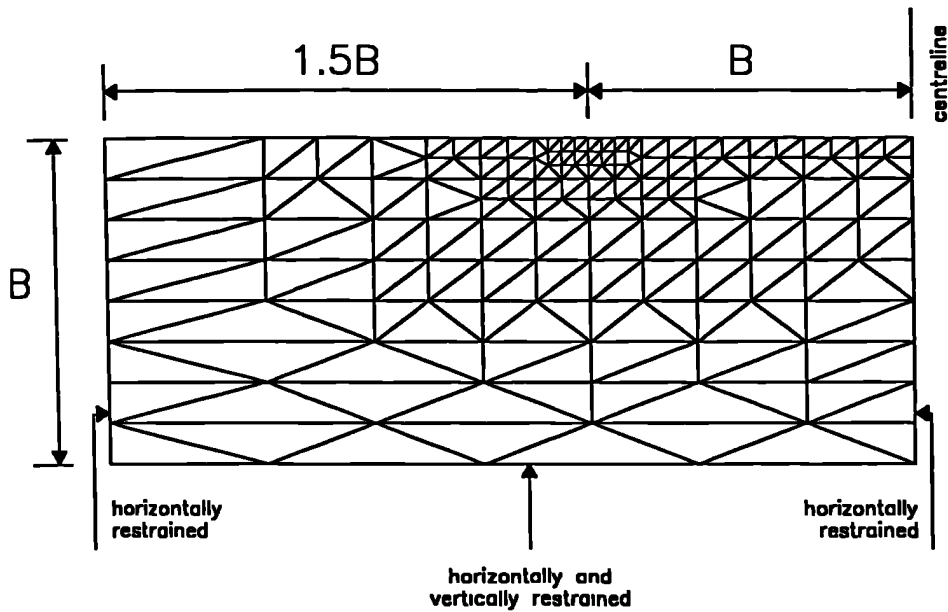


**Figure 4.6 - Finite element mesh used for strength increasing linearly with depth analyses (mesh shown for smooth case).**

For the rough loading analysis a row of interface elements was included along the surface and no horizontal movement was allowed.

#### **4.2.2. Material Properties**

In working with an elastic-perfectly plastic material to obtain comparisons with the plasticity solutions, it was important to restrict elastic strains as much as possible. A high value of shear modulus was therefore used ( $G=6000\text{kPa}$ ). Undrained conditions can be modelled by specifying a large bulk modulus for water, but if this parameter is too large, numerical problems may occur (Griffiths, 1985). A bulk modulus for water  $K_w=5 \times 10^5 \text{kPa}$  (equal to a total stress Poissons ratio  $\nu=0.4925$ ) was found to be satisfactory.

The soil yielded according to a Tresca yield criterion when the shear stress equalled either a constant value,  $s_u=30\text{kPa}$  (limited depth case), or a value which increased with depth from the subsoil surface,  $s_{u0}=2.5\text{kPa}$ , at a constant rate of  $\rho=2\text{kPa/m}$  (strength increasing with depth case). For the case of strength increasing linearly with depth the strength profile could not be modelled exactly, but it was possible to divide the mesh into several horizontal layers and to specify a different strength for each layer, Figure 4.7. The resulting stepped distribution was found to give sufficiently accurate results.

When interface elements were used their strength was set equal to the strength of the adjacent idealized soil. To limit the relative displacements prior to slip the shear and normal stiffness parameters were set to high values,  $k_s=6 \times 10^3 \text{kN/m}^2$  and  $k_n=5 \times 10^5 \text{kN/m}^2$ .

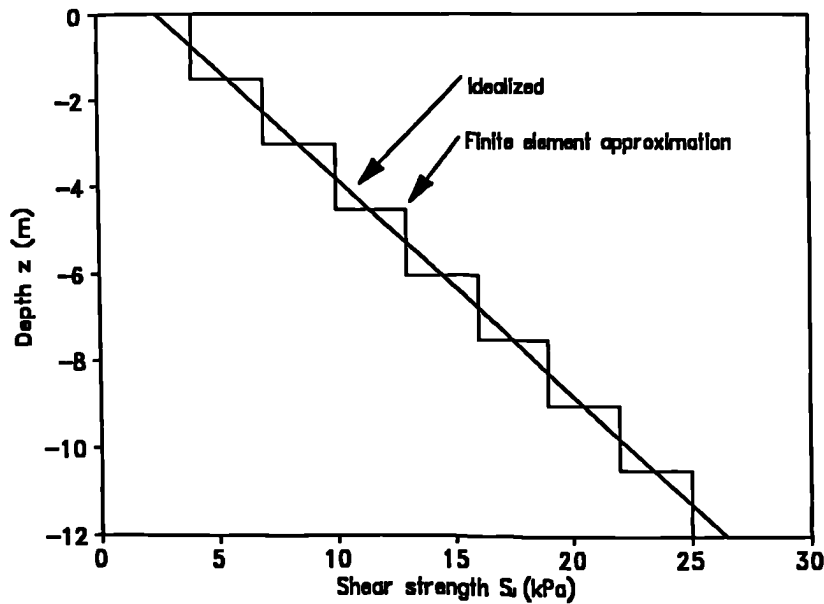
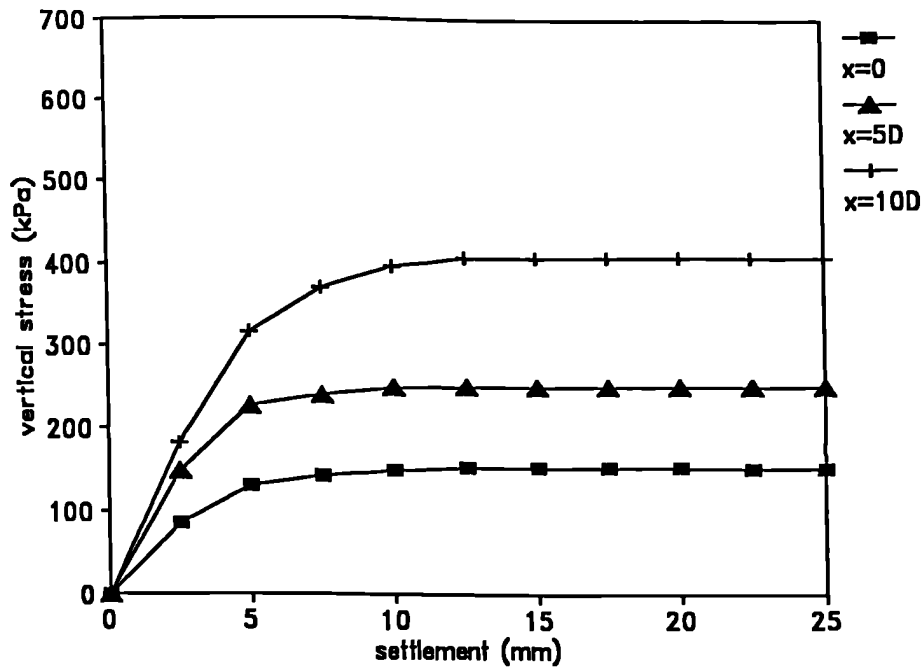


Figure 4.7 - Finite element approximation for strength increasing linearly with depth.

### 4.2.3. Results

#### Displacement Controlled Analyses

In order to model the rigid strip footing assumed by the plasticity solutions, plane strain finite element analyses were carried out by applying increments of uniform vertical displacement along the loaded surface. Failure was deemed to have occurred when a further increase in vertical displacement caused no significant increase in vertical stress at any point on the displaced boundary. Failure was reached in approximately 100 increments. The normal stresses in the upper interface elements (equivalent to the vertical stress distributions at the subsoil surface) were compared with the vertical stress distribution predicted by plasticity theory. The load-settlement curves for three points on the subsoil surface beneath the footing, for each of the four cases, are shown in Figure 4.8.



**Figure 4.8a - Load displacement curves from displacement controlled analyses for a smooth footing on a limited uniform strength/depth subsoil.**

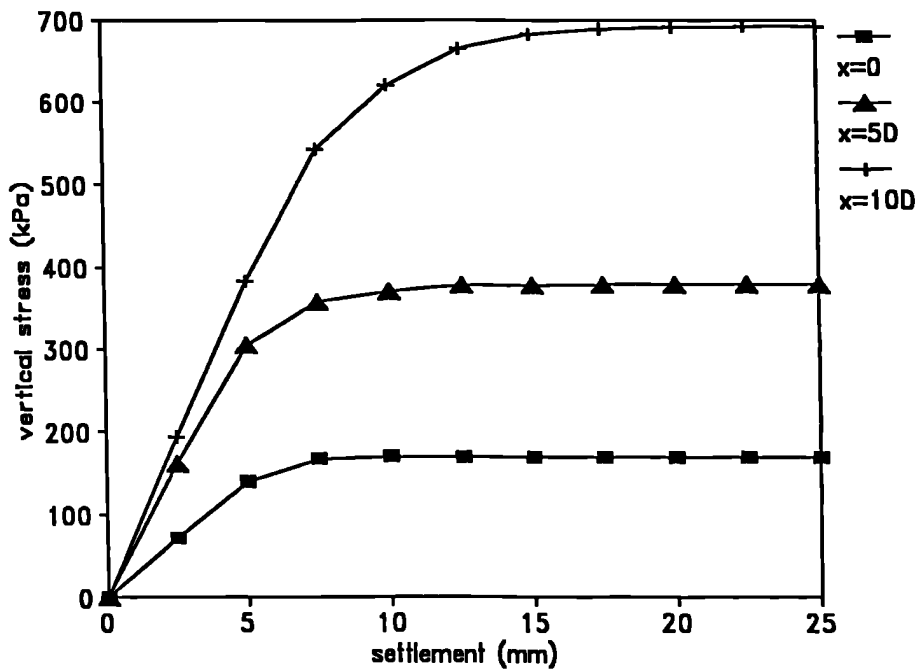


**Figure 4.8b - Load displacement curves from displacement controlled analyses for a rough footing on a uniform strength/limited depth subsoil.**

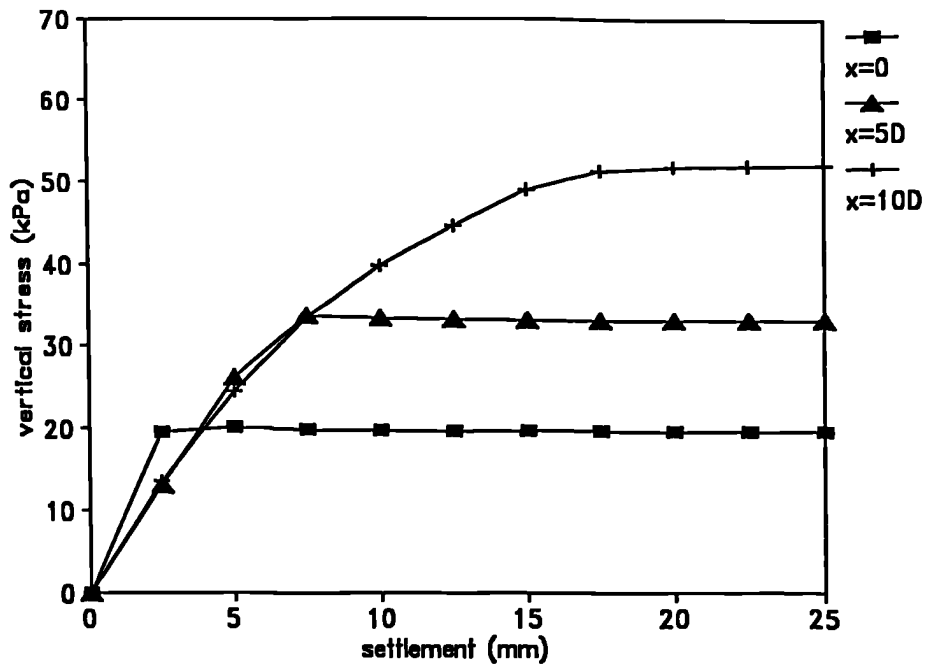


**Figure 4.8c - Load displacement curves from displacement controlled analyses for a smooth footing on a strength increasing with depth subsoil.**

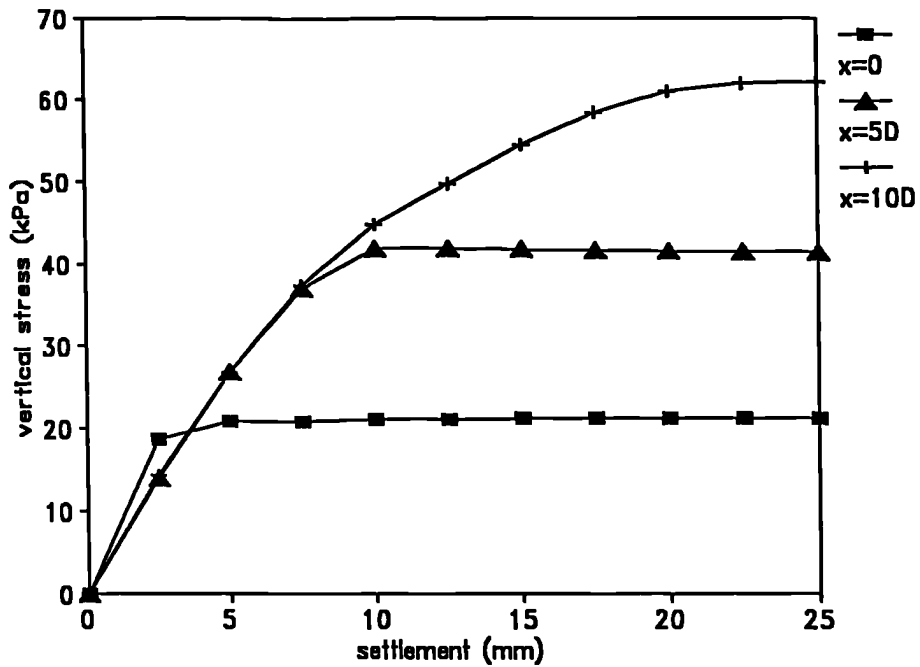


**Figure 4.8d - Load displacement curves from displacement controlled analyses for a rough footing on a strength increasing with depth subsoil.**

For soil of uniform strength and limited depth the distribution of total vertical stress for both the rough and the smooth footings are shown in non-dimensional form, together with the distribution predicted by plasticity theory, Figure 4.9. The corresponding distributions for the case of strength increasing linearly with depth is shown in Figure 4.10.

### **Load Controlled Analyses**

In addition to the displacement controlled analyses, load controlled analyses were performed in which the ideal plasticity distributions were applied in increments at the ground surface. The load was applied in 100 equal increments, i.e. 1% of the failure load predicted by plasticity theory was applied in each increment. Only rough cases were examined.

As the applied load reached the plasticity load, the incremental displacements increased rapidly, Figure 4.11. An attempt was made to increase the load above that predicted by the plasticity solution by 5% applied over 50 increments, but the analyses failed due to numerical problems. The settlements profiles under full plasticity load are shown in Figure 4.12 for soils of uniform strength and limited depth and soil of increasing strength with depth.

#### **4.2.4. Effect of the Interface Element**

Plasticity theory predicts a displacement discontinuity at the rough boundaries. At a discontinuity an infinite strain gradient may develop when the soil yields. In the analyses presented interface elements have been used at all rough boundaries to model the infinite gradient which develops; this is achieved when the, zero thickness, interface element reaches its yield stress and slip of the interface occurs. In order to assess the effect of the interface element a series of analyses was carried out in which different meshes were used to analyse the rough footing resting on the idealized soil of uniform strength over a limited depth, described previously.

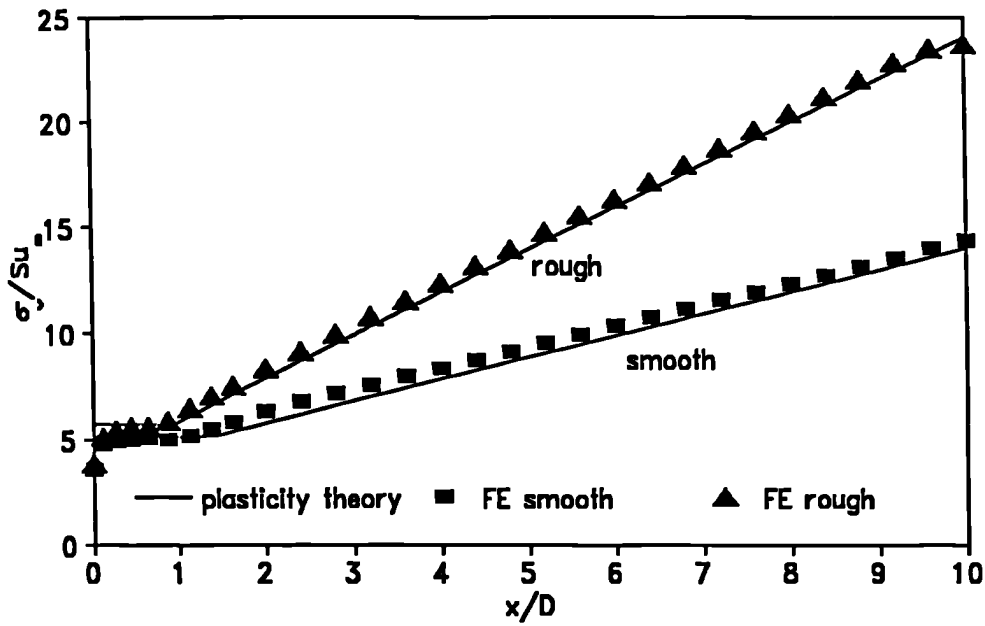


**Figure 4.9 - Comparison of the vertical stress distribution at failure predicted by plasticity theory and finite element analysis for the uniform strength/limited depth idealized subsoil (values interpolated to nodes from adjacent elements).**

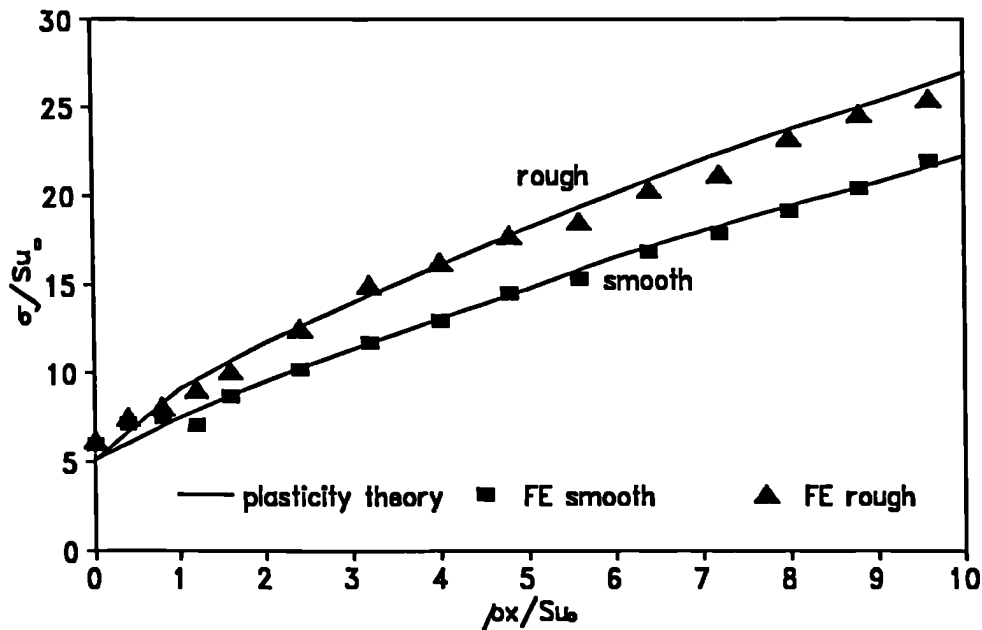


**Figure 4.10 - Comparison of the vertical stress distribution at failure predicted by plasticity theory and finite element analysis for the strength increasing linearly with depth idealized subsoil (values interpolated to nodes from adjacent elements).**

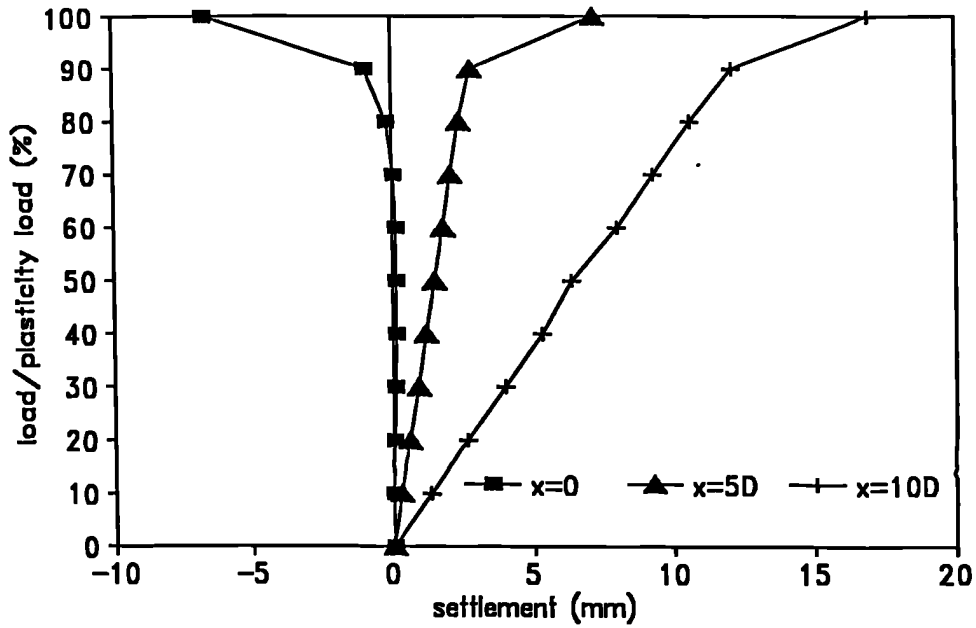


**Figure 4.11a - Load displacement curve for a load controlled analysis on a subsoil of uniform strength/limited depth .**

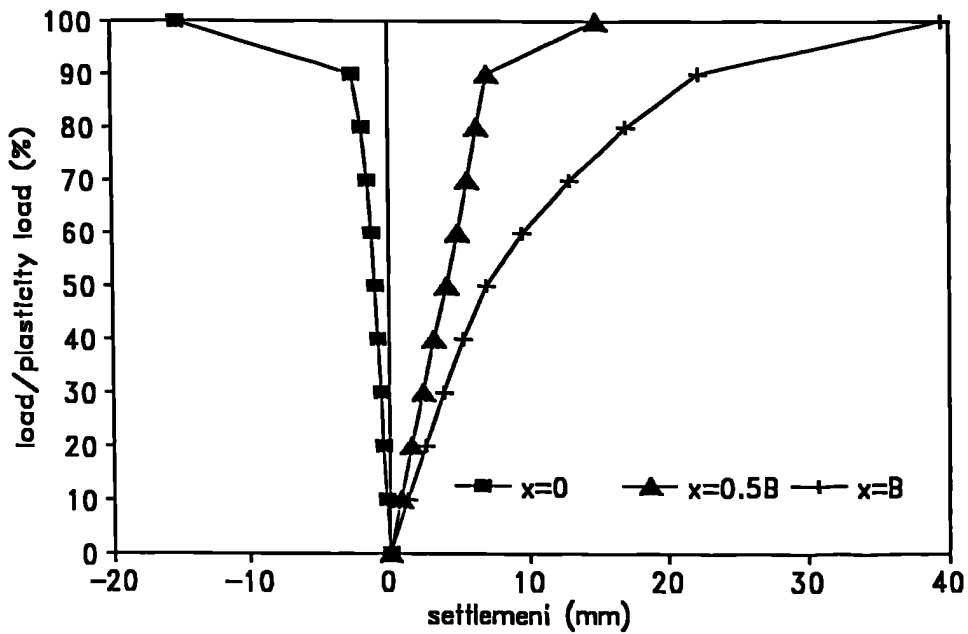


**Figure 4.11b - Load displacement curve for a load controlled analysis on a subsoil with strength increasing linearly with depth.**

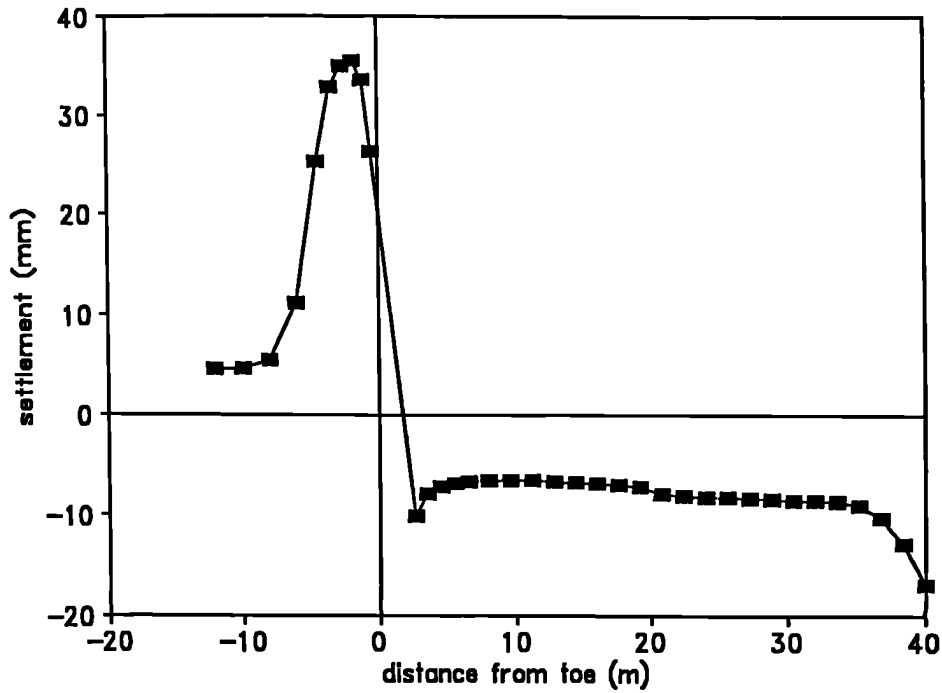


**Figure 4.12a - Surface settlement profile at failure for load controlled analysis of a rough footing on a subsoil with uniform strength/limited depth.**

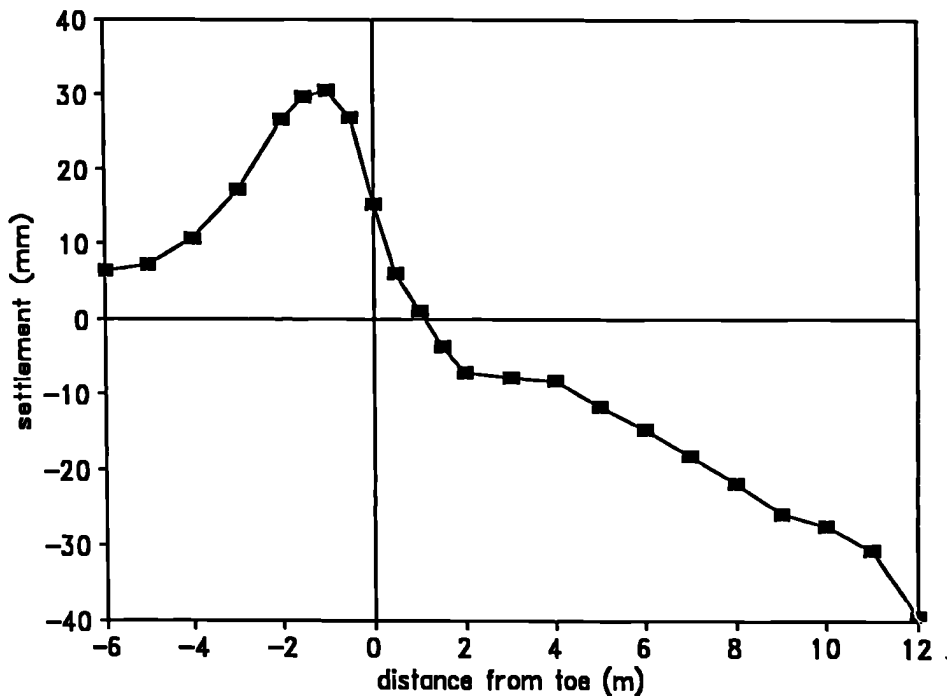


**Figure 4.12b - Surface settlement profile at failure for load controlled analysis of a rough footing on a subsoil with strength increasing linearly with depth.**

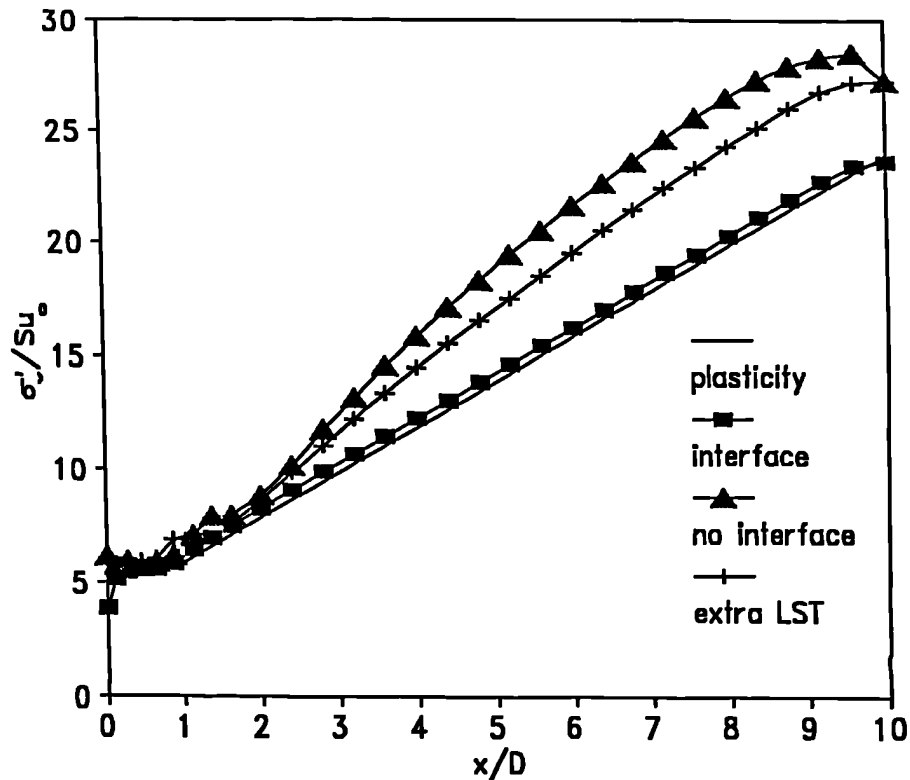


**Figure 4.13 - Vertical stress distributions at failure predicted using three different finite element meshes compared with plasticity theory.**

Two analyses, in addition to the analysis described previously, were performed. Firstly, an analysis using the mesh shown in Figure 4.5 but with no interface elements. Secondly, an analysis in which an extra row of triangular elements was introduced to the original mesh but, as for the first additional analysis, no interface elements were used. Each analysis was performed as described previously and the predicted vertical stress distributions at failure are presented along with the plasticity theory and the finite element analysis using interface elements (Figure 4.9) in Figure 4.13.

From Figure 4.13 it can be seen that the interface elements used to model the upper and lower rough boundaries produce a superior solution. The error in the predicted stress, at  $x/D=5$ , is 4% as compared to an error of 37% at the same point for the mesh without interface elements. Even when

the number of rows of linear strain triangles was increased, from three to four, the vertical stress distribution at failure still over-predicts the plasticity solution by a large amount, 24% at  $x/D=5$ , even though the number of degrees of freedom is similar to the original mesh including interface elements.

This result shows that the interface element can be used to analyse, accurately and economically, the behaviour at rough soil boundaries. The interface element also allows interface shear and normal stress information to be extracted easily from the analysis.

#### **4.2.5. Predicted Displacements for a Rough Footing on a Uniform Strength/Limited Depth Subsoil**

Using the method of characteristics it is possible to construct the slip line mesh for the rigid strip footing on soil of uniform strength and limited depth (Mandel and Salençon, 1973), Figure 4.14a, from which a hodograph can be established, Figure 4.14b. In the hodograph heave beyond the toe has not been shown. As noted earlier the hodograph provides information on the incremental relative displacement of blocks of soil for an increment of vertical displacement of the footing.

The incremental lateral displacements, predicted by both plasticity theory and the finite element analysis, at 2D, 4D, 6D and 8D from the footing toe are shown in Figure 4.15. The finite element lateral incremental displacements represent the lateral displacement from increment 90 to 100 predicted using the mesh shown in Figure 4.5 (with additional interface elements to model the upper rough boundary). At this stage of the analysis most of the soil beneath the footing is behaving plastically and should therefore provide an accurate comparison with the plasticity theory. The predicted incremental lateral displacements from the finite element analysis and plasticity theory are generally in good agreement.

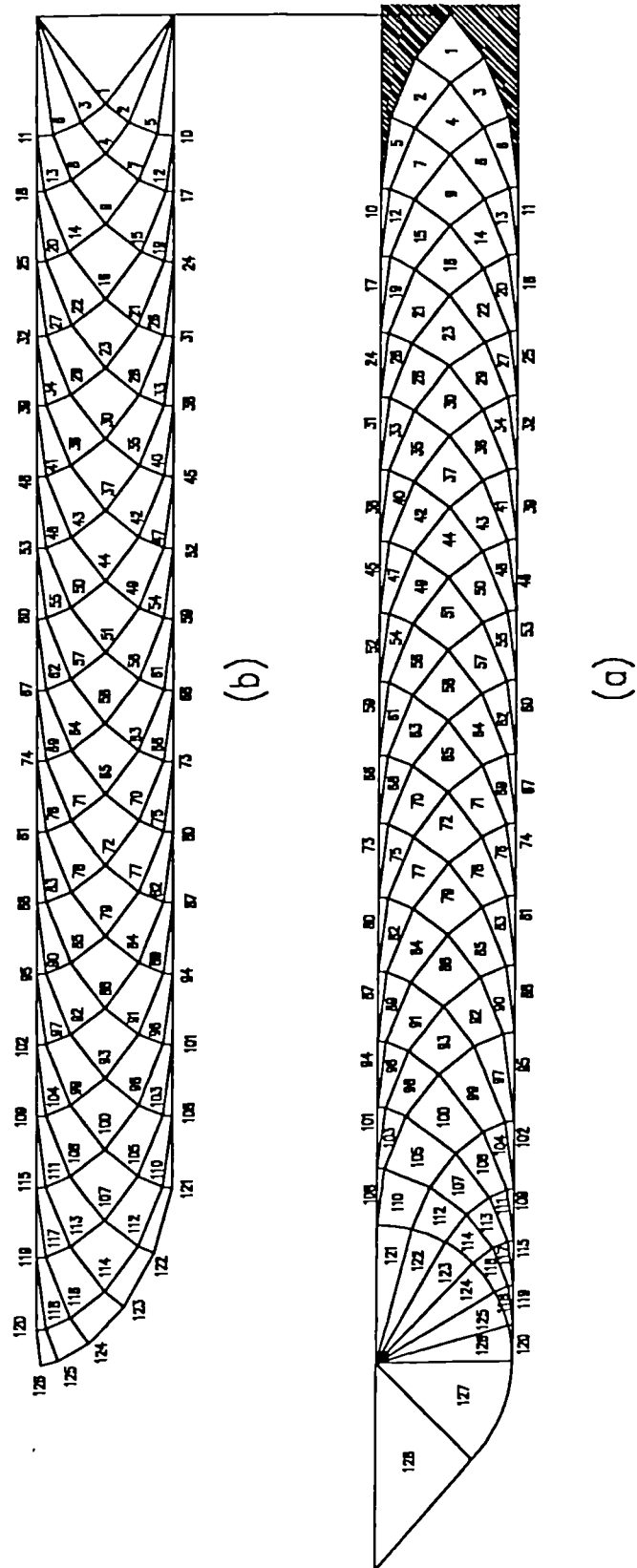


Figure 4.14 - Plasticity analysis of a rough rigid footing on a subsoil of uniform strength/limited depth: (a) slip line mesh; (b) hodograph.

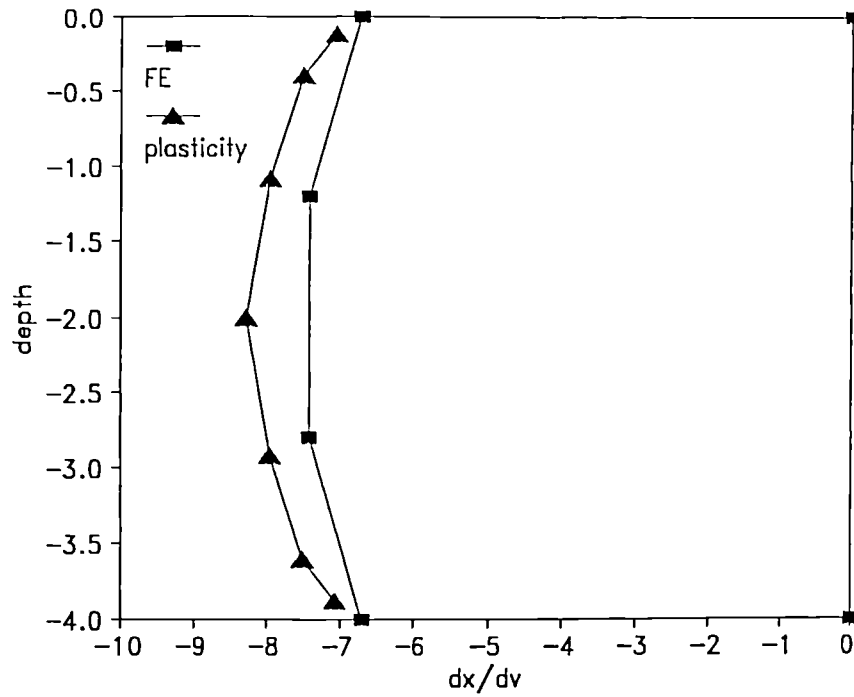


Figure 4.15a - Comparison of the lateral displacements predicted by finite element and plasticity analyses 2D from toe.

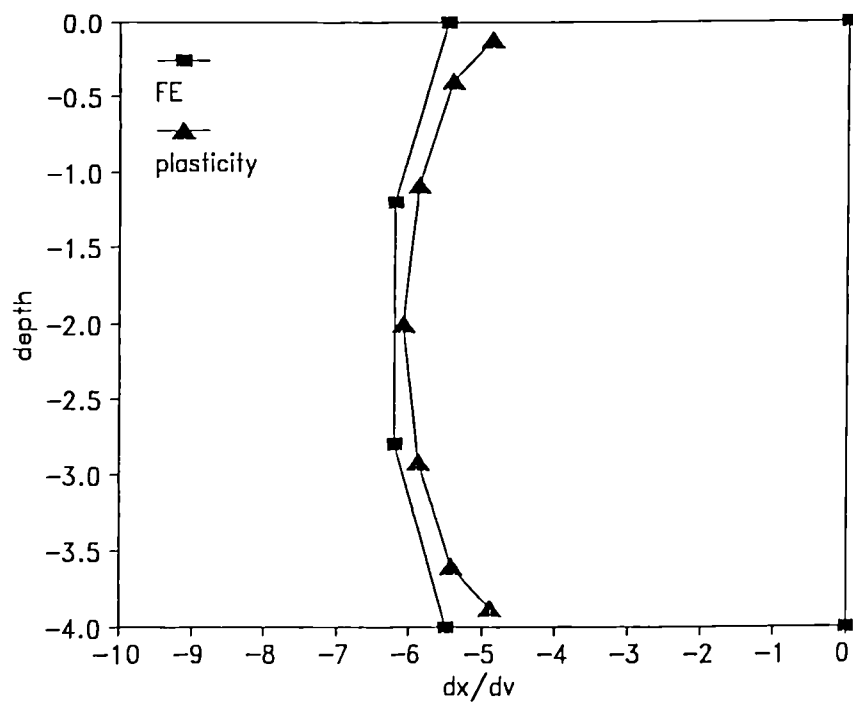


Figure 4.15b - Comparison of the lateral displacements predicted by finite element and plasticity analysis 4D from toe.

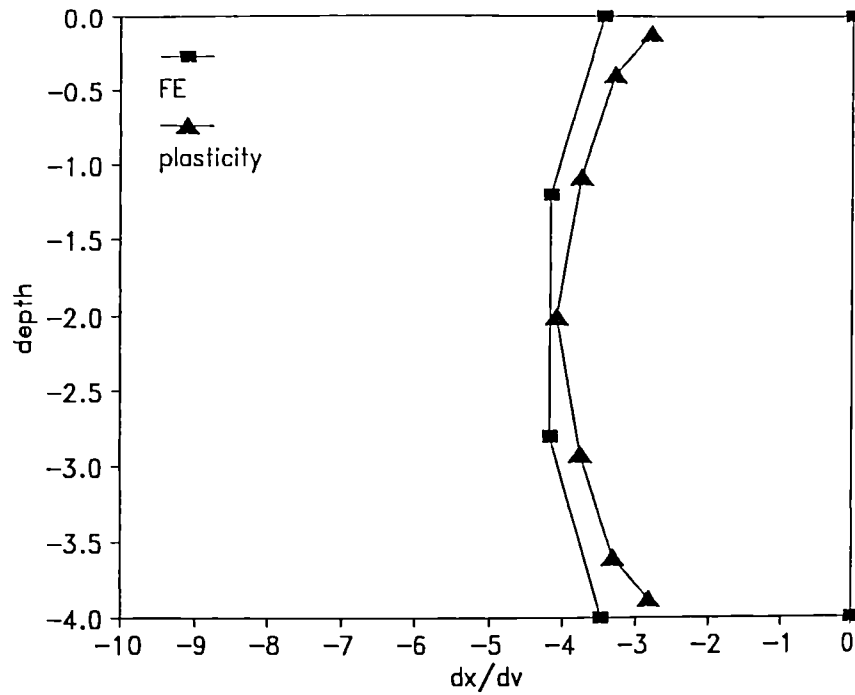


Figure 4.15c - Comparison of the lateral displacements predicted by finite element and plasticity analysis 6D from toe.

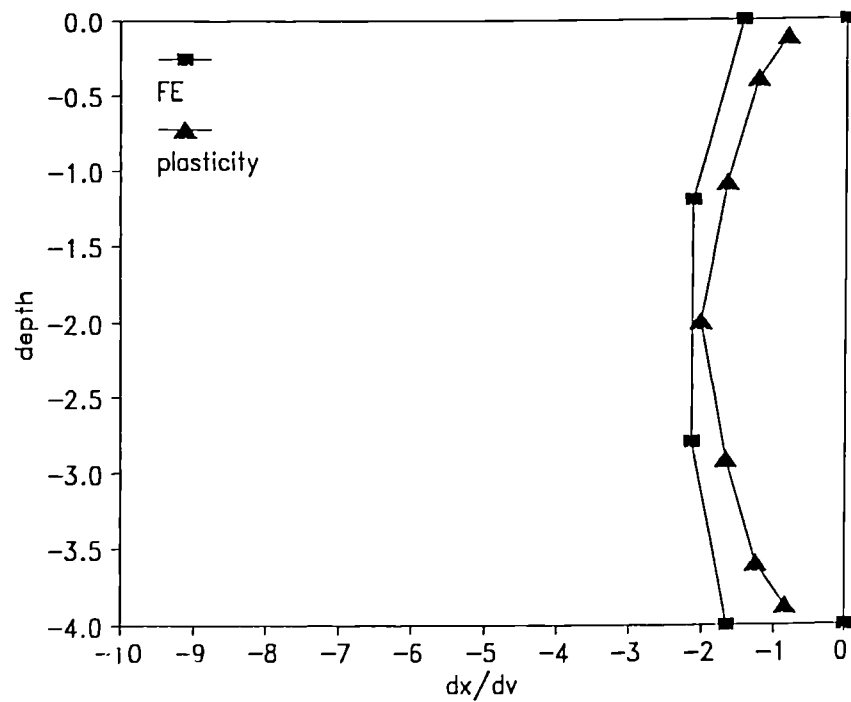


Figure 4.15d - Comparison of the lateral displacements predicted by finite element and plasticity analysis 8D from toe.

Towards the centreline the finite element displacements are larger than the plasticity displacements (Figures 4.15b, c and d). This may have been caused by the rigid area near the centreline in the hodograph, Figure 4.14b, being larger than that predicted by plasticity theory. This over-prediction of the extent of the rigid zone is a result of the relatively coarse slip line field which was used for the graphical solution, Figure 4.14a. If a finer slip field had been drawn, then the vertex of block 1, Figure 4.14a, would have coincided with the centreline of the footing, as predicted by plasticity theory. This would have reduced the extent of the rigid block and increased the lateral displacements predicted from Figure 4.14b.

At a distance  $2D$  from the toe, Figure 4.14a, the trend reverses and the plasticity displacements are larger than the finite element displacements. Two factors may have contributed to this. Firstly, the undrained behaviour is modelled by using a high value for the bulk modulus of water, but any non-infinite bulk modulus will result in some volumetric strain which will tend to produce smaller lateral displacements. This error is cumulative, becoming more significant with distance from the centreline. Secondly, if some of the soil was still elastic at increment 90 then a reduced lateral displacement would result.

#### **4.2.6. Further Analysis using Modified Cam-clay**

Finite element solutions using an elastic-perfectly plastic constitutive model for the soil can be compared directly with plasticity theory. However, this soil model may not necessarily be the best for representing soft clays and in the analyses in Chapters 6 and 7, modified Cam-clay (Roscoe and Burland, 1968) has been used to model the subsoil. For this reason a comparison was also made between the load distribution predicted by plasticity theory and from a finite element analysis using the modified Cam-clay model to represent the soil.

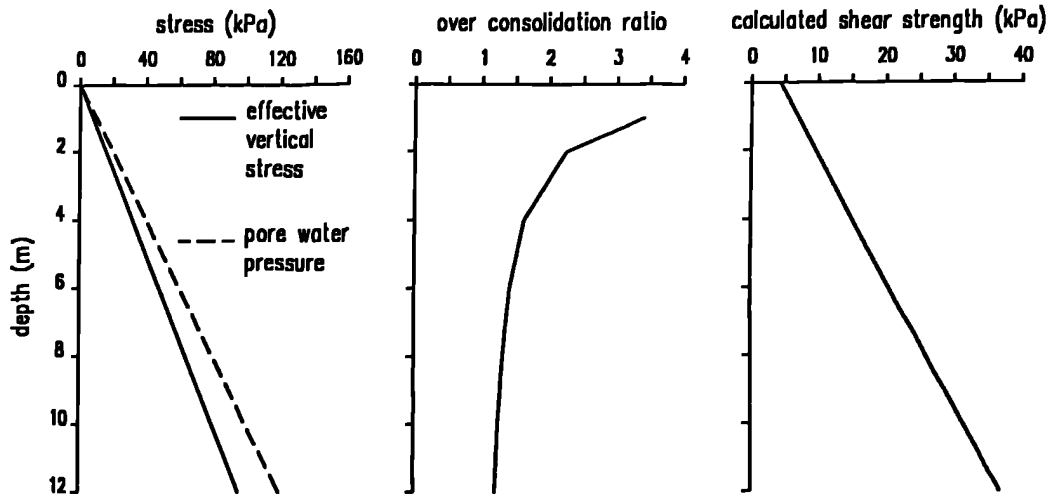


**Figure 4.16 - Stress and strength profiles used for the modified Cam-clay analysis.**

The analysis was conducted for a rough footing resting on a soil with strength increasing linearly with depth, the material parameters, using standard notation, were  $\lambda=0.25$ ,  $\kappa=0.07$ ,  $\Gamma=3.0$ ,  $M=1.0$  and  $\nu'=0.3$ . The predicted stress and strength profiles, Figure 4.16, were defined according to the equations developed in Appendix A. An error in the strength profile of Figure 4.16, pointed out by Potts and Ganendra (1991), is discussed below.

The analysis was performed using the mesh shown in Figure 4.6. Additional interface elements were included at the surface to model the rough boundary and the interface strength was  $s_{u0}=4.25\text{kPa}$ . The undrained shear strength was calculated to increase at a rate  $\rho=2.70\text{kPa/m}$ . The load settlement curves for three points at the subsoil surface are shown in Figure 4.17. Failure was defined to have occurred after 600 increments with a displacement of 0.06m.

At failure the vertical stress distribution beneath the footing can be compared with the plasticity solution, Figure 4.18. The prediction made using the modified Cam-clay model is in close agreement with the plasticity

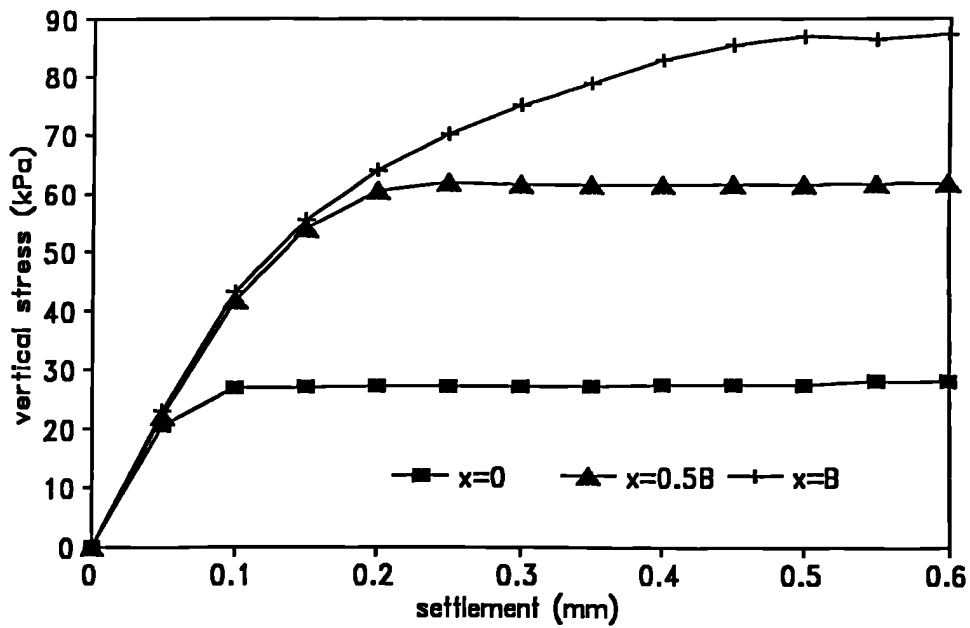


Figure 4.17 - Load settlement curves for a displacement controlled analysis using modified Cam-clay to model a subsoil with strength increasing linearly with depth.

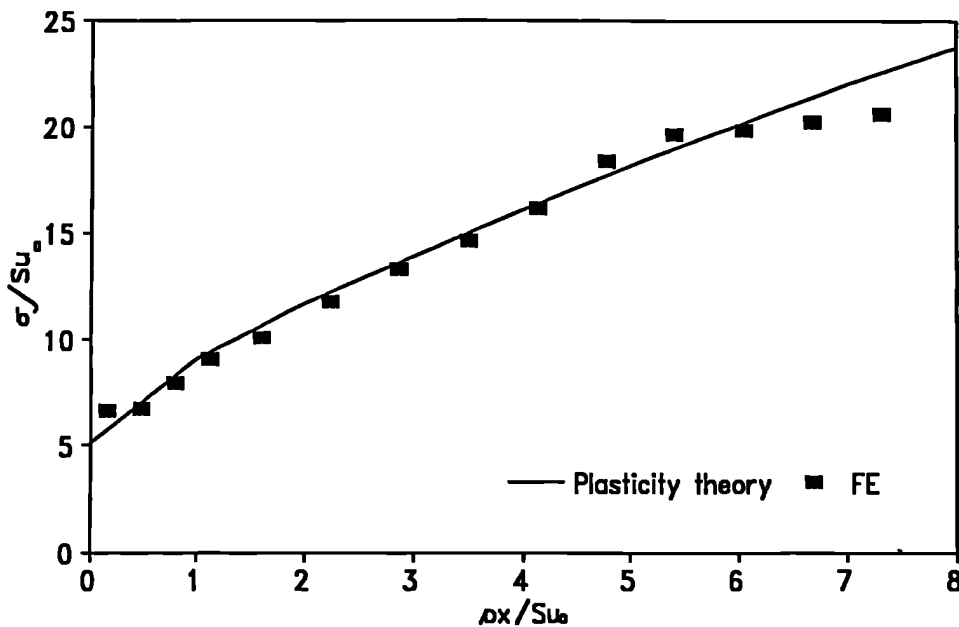


Figure 4.18 - Comparison of finite element and plasticity solutions for the stress distribution at failure beneath a rough footing on a subsoil with strength increasing linearly with depth (modified Cam-clay).

solution. Therefore, if modified Cam-clay constitutive model is selected in order to improve the modelling of the pre-failure behaviour, the prediction of collapse need not be adversely affected.

The number of increments used has increased by six times when compared with the equivalent elastic-perfectly plastic analysis, Section 4.2.2. Only a limited study was carried out to investigate the effect of the number of increments. However, the number of increments used is similar to that used to predict failure of a footing problem using the modified Cam-clay constitutive model with an incremental tangent stiffness solution (Potts et al, 1990).

### **Error in the Undrained Shear Strength Profile**

As pointed out by Potts and Ganendra (1991), in their discussion of Hird, et al (1990), the assumption of a linear undrained shear strength distribution, shown in Figure 4.16 is not strictly correct. The correct profile is defined by Equation 4.1 which is non-linear

$$s_u = (2.30z + 5.50) \left( \frac{4.29z + 1.37}{2.91z + 6.98} \right)^{0.28} \dots\dots\dots(4.1)$$

The two predictions of the undrained shear strength profile, Figure 4.16 and Equation 4.1, are shown in Figure 4.19. Also shown is the percentage error between the two predictions. The maximum error is 22% at the surface and rapidly decreases to less than 5% beyond 2m below ground level.

A best fit line through the profile predicted by Potts and Ganendra produces values of  $s_{u0}$ =4.13kPa and  $\rho$ =2.61kPa/m (compared with the values  $s_{u0}$ =4.25kPa and  $\rho$ =2.70kPa/m used in Figure 4.18). If these values are used to replot the data in Figure 4.18 a negligible difference occurs in the position of the data points.

The effect of the over-large interface strength (4.25kPa rather than 3.49kPa) appears to have had little effect on the final result. The analysis

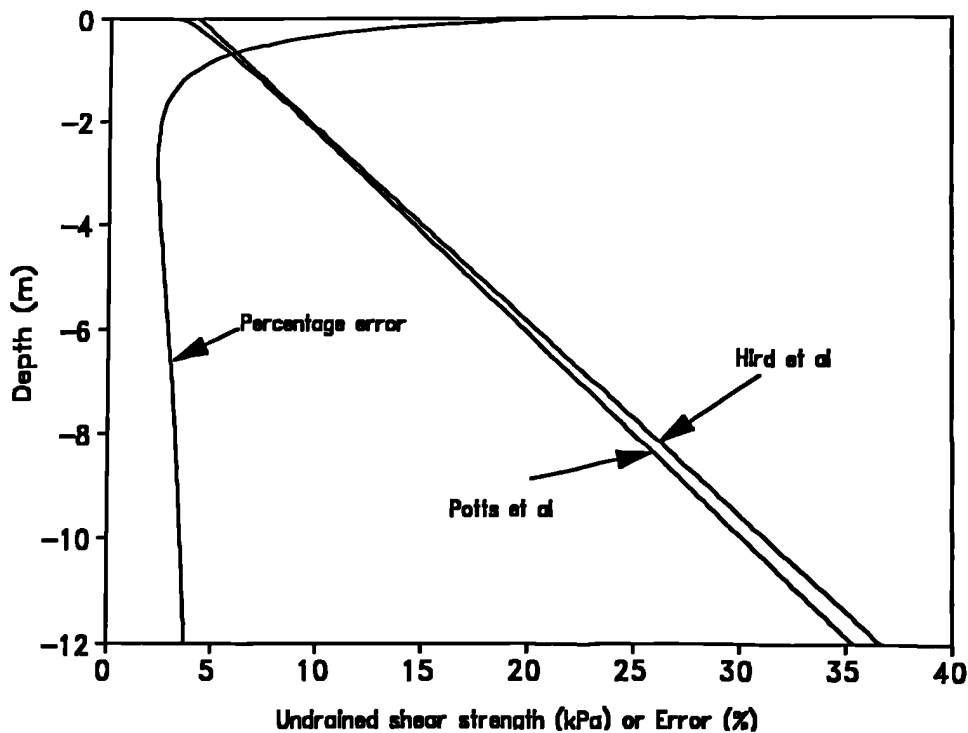
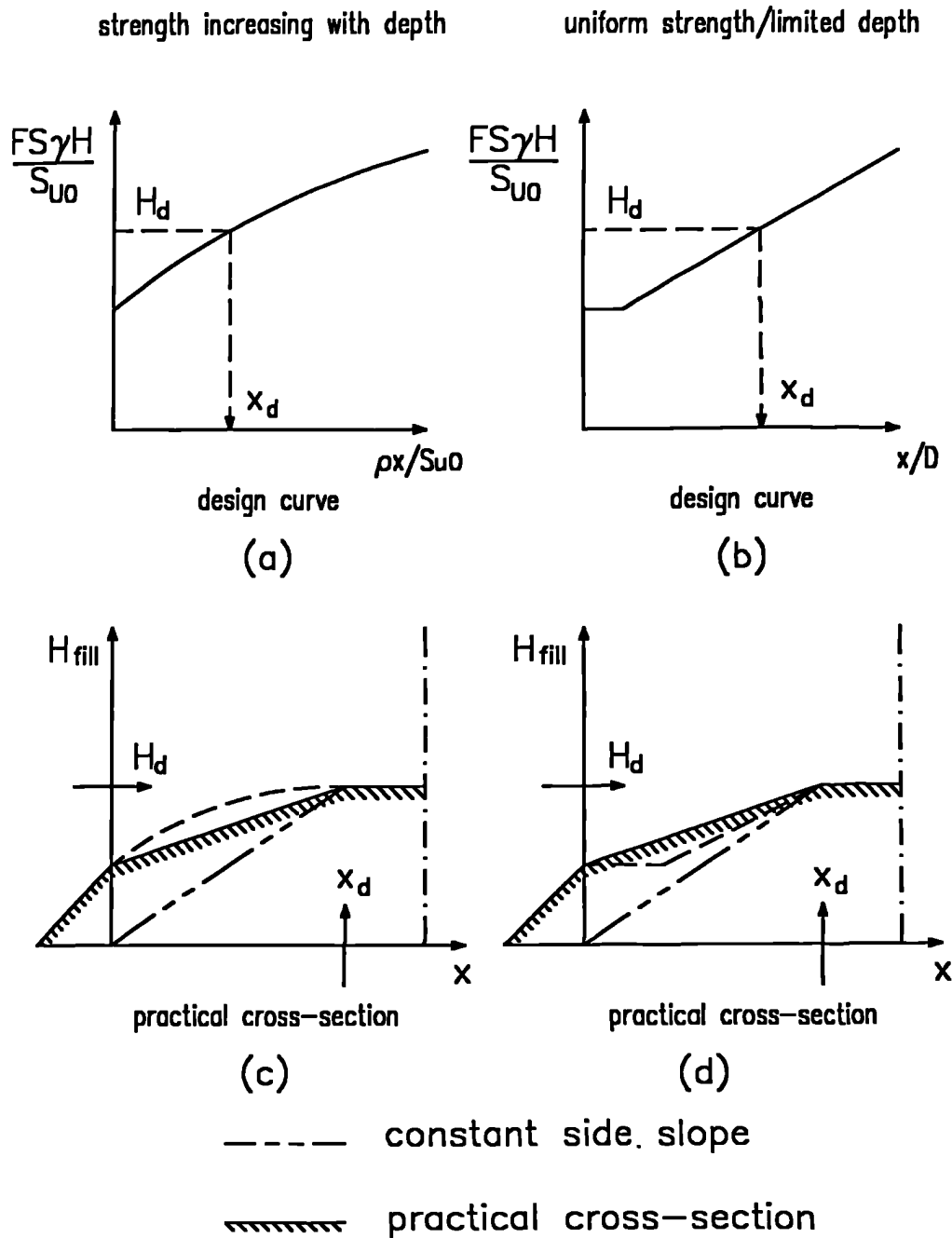


Figure 4.19 - Error in the undrained shear strength profile used for the modified Cam-clay analysis (after Potts and Ganendra, 1991).

showed that slip occurred on the interface beneath the loaded area even though the shear strength was lower at some integration points in neighbouring soil elements. This implies that yielding was constrained in those elements to some degree due to the discretization error at the surface.

### 4.3. Embankments with Constant Side Slope

Jewell (1988) has suggested that the design of an embankment built on either of the subsoils shown in Figure 4.3 can make use of the plasticity solutions to calculate the embankment profile for a single lift construction. Using the strength parameters defined in Figure 4.3, if an embankment is to be constructed to a design height  $H_d$  with a fill of unit weight  $\gamma$  and a factor of safety  $FS$ , then the vertical axis in Figure 4.4,  $\sigma_v/s_{u0}$ , becomes  $FS\gamma H/s_{u0}$ .



**Figure 4.20 - Proposed practical embankment shape to approximate ideal loading predicted by plasticity theory (after: Jewell, 1988) and a proposed simplified constant side slope design profile.**

Figure 4.20a and b. The plasticity curve can then be used to define the minimum safe single stage side slope length,  $x_d$ , Figures 4.20a and b, and cross section, Figures 4.20c and d.

The embankment shape which corresponds to plasticity theory involves a uniform slope within the plasticity region ( $x > 0$ ) and a stable, steeply sloping wedge beyond ( $x < 0$ ). Jewell (1988) compared limit equilibrium analyses of the plasticity cross sections (Figures 4.20c and d) with the plasticity solutions. Limit equilibrium analysis of subsoil with strength increasing linearly with depth were in good agreement with the plasticity curve but limit equilibrium analysis of the uniform strength and limited depth case exceeded the plasticity distribution by a large amount, this difference is discussed in Section 4.3.2. The embankment shape suggested by the plasticity cross section would be difficult to construct and would take additional land due to the triangle of soil required to avoid a vertical soil face at the toe.

Also shown on Figures 4.20c and d is a proposed embankment profile with a constant side slope which starts at the toe ( $x=0$ ) of the plasticity solution and at a distance  $x_d$  intersects the plasticity profile at the required design height,  $H_d$ . This profile would be easier to construct and would require less land than the plasticity cross section suggested by Jewell (1988). In order to investigate the proposed constant side slope profile a series of finite element analyses was carried out.

Finite element analyses were performed for fully reinforced embankments with constant side slopes on both types of idealized subsoil. The results of these analyses were compared with the plasticity solution to assess the validity of a design method using the plasticity distribution to predict the slope length of a constant side slope embankment.

### 4.3.1. Finite Element Analyses of Constant Side Slope

#### Loading

A series of load controlled analyses was carried out in order to investigate the possibility of using the plasticity solutions in the design of constant side slope embankments. The meshes shown in Figures 4.5 and 4.6, with additional interface elements at the surface, were used with the embankment fill represented by vertical loads. The subsoil was modelled as undrained using an elastic-perfectly plastic model with the same parameters as described in Section 4.2.2. The upper nodes of the surface interface elements were restrained in the horizontal direction thus modelling the fully reinforced case.

Analyses were carried out using five values of the design length of the side slope,  $x_d$ , for each of the two idealized subsoils. The procedure for calculating the applied loading was as follows. The side slope length,  $x_d$ , was chosen. The position on the abscissa of Figures 4.20a and b was therefore known. The embankment loading at  $x_d$  was found from the plasticity solutions, using a factor of safety of unity, as  $\sigma_v = \gamma H_d$ . The constant side slope loading was defined as increasing uniformly from the toe ( $\sigma_v = 0$  at  $x = 0$ ) to the crest ( $\sigma_v = \gamma H_d$  at  $x = x_d$ ) using vertical loads applied to the top of the interface elements.

The uniform strength/limited depth mesh, Figure 4.5, has a footing half width of  $10D$ . For the constant side slope analyses the ratios of  $x_d/D$  were 1, 3, 5, 7 and 9. The strength increasing linearly with depth mesh, Figure 4.6, has a footing half width of  $9.6\rho/s_{u0}$ . For the constant side slope analyses the ratios of  $x_d\rho/s_{u0}$  were 1.6, 3.2, 4.8, 6.4 and 8.0.

In each analysis the crest position remained constant and the vertical loads were increased proportionally across the loaded area.

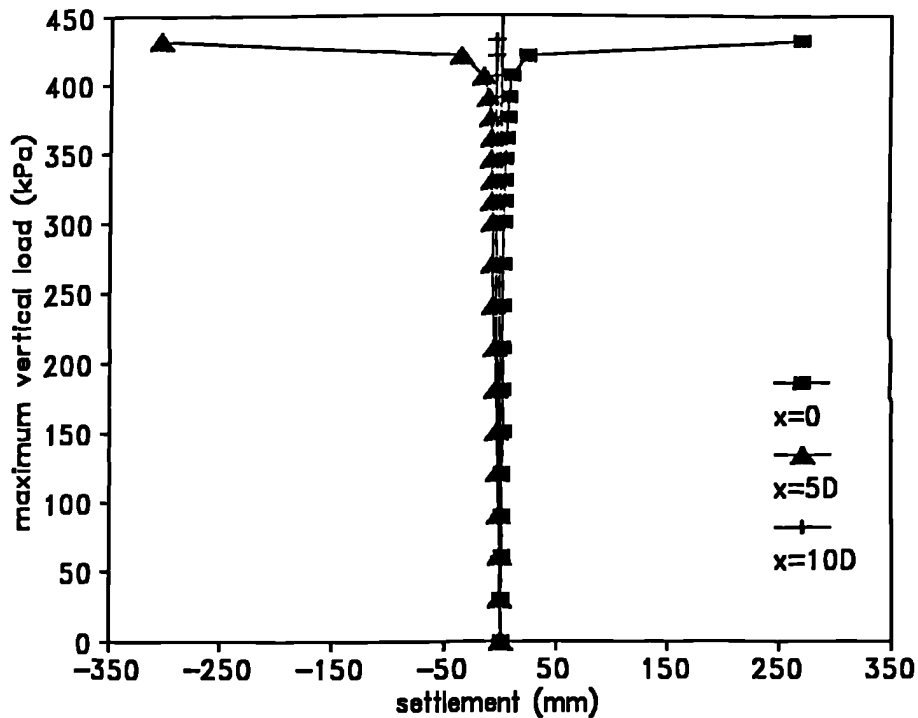
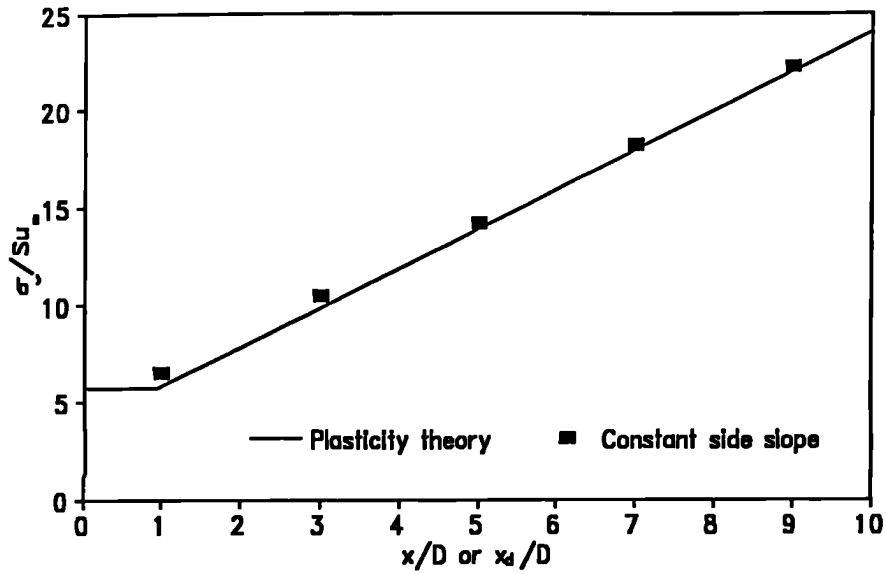


Figure 4.21 - Typical load displacement curve for a constant side slope analysis. Curve shown for a uniform strength limited depth subsoil analysis with  $x_v/D=5$ .

### 4.3.2. Results

The failure of the analysis was assessed from load-displacement curves for three points on the subsoil surface; these were located beneath the toe, the crest and the centreline. Typical curves are presented in Figure 4.21. Clearly defined failure loads could be assessed for all analyses as the load acting at the increment after which large displacements occurred at one or more of the observed points.

For each of these analyses the vertical stress applied beneath the crest was normalised with  $s_{u0}$  and plotted against the plasticity solution, Figure 4.22 and Figure 4.23 for the uniform strength and limited depth case and the strength increasing linearly with depth case respectively.



**Figure 4.22 - Comparison of the predicted collapse load of a constant side slope embankment with plasticity theory for a subsoil with uniform strength and limited depth.**

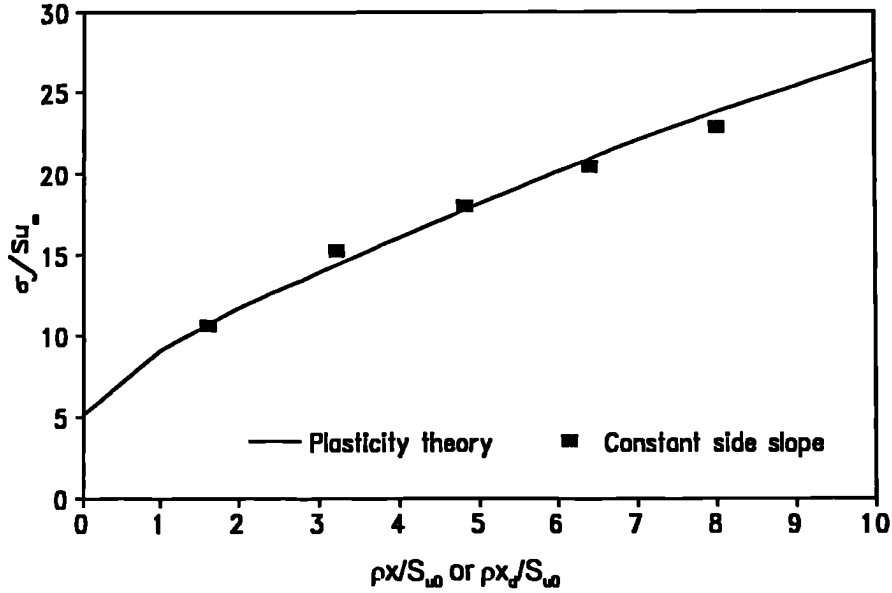


**Figure 4.23 - Comparison of the predicted collapse load of a constant side slope embankment with plasticity theory for a subsoil with strength increasing linearly with depth.**

The finite element predictions of the undrained failure of embankments with constant side slopes compare well with the profiles derived from plasticity theory. The vertical stress distribution from plasticity theory may be used to obtain a preliminary assessment of the length of slope required to build an embankment to the design height in a single lift.

#### **4.3.3. A Comparison of Limit Equilibrium and Finite Element Analysis for Embankments with Constant Side Slope**

Jewell (1988) compared limit equilibrium analyses with plasticity solutions for the two idealized subsoils. The slip circle analyses gave good agreement with the plasticity solution for the case of strength increasing linearly with depth, but the analyses of the uniform strength and limited depth subsoil over-predicted the stability by a large amount.

Using the finite element predicted displacements, the displacement vectors at failure can be produced, and an indication as to the mode of failure of the subsoil may be obtained. Displacement vectors at failure are plotted for three of the constant side slope analyses in Figures 4.24 and 4.25. The embankments shown indicate their relative size and position for each analysis.

The displacement vectors for the soil with strength increasing linearly with depth, Figure 4.25, show a rotational mechanism, thus confirming that a slip circle analysis is applicable in this case. The displacement vectors at failure for the uniform strength and limited depth case, Figure 4.24, show different mechanisms. When the side slope is very short, relative to the subsoil depth, a rotational mechanism can still develop, Figure 4.24a. However, as the side slope length becomes greater the subsoil is too shallow for a rotational mechanism to develop and the subsoil then fails with a translational mechanism with small rotational zones at either end, Figures 4.24b and c. For such a mechanism a slip circle analysis is no longer

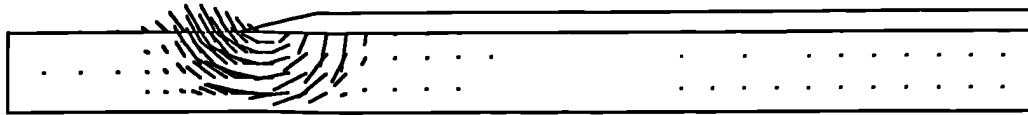


**Figure 4.24a - Displacement vectors at failure for a constant side slope embankment on a subsoil of uniform strength and limited depth;  
 $x_q/D=1$ .**



**Figure 4.24b - Displacement vectors at failure for a constant side slope embankment on a subsoil of uniform strength and limited depth;  
 $x_q/D=5$ .**



**Figure 4.24c - Displacement vectors at failure for a constant side slope embankment on a subsoil of uniform strength and limited depth;  
 $x_q/D=9$ .**

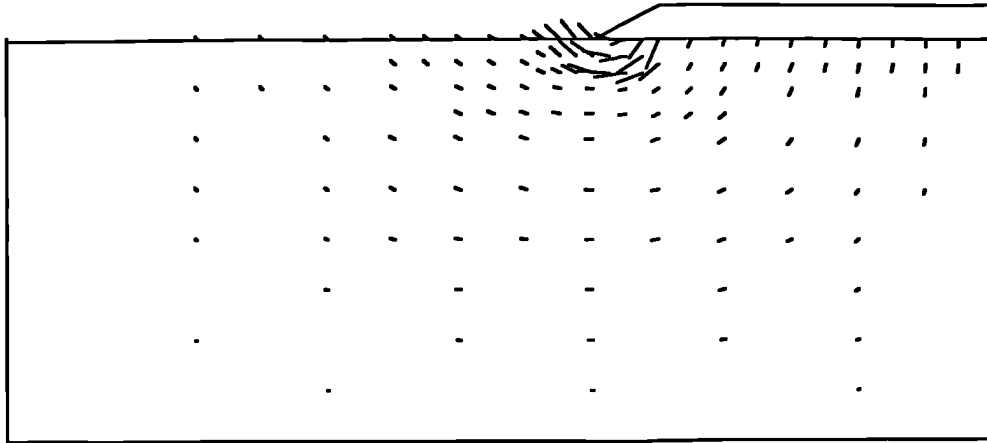


**Figure 4.25a - Displacement vectors at failure for a constant side slope embankment on a subsoil with strength increasing linearly with depth;  
 $\rho x_d/s_{u0}=1.6$ .**

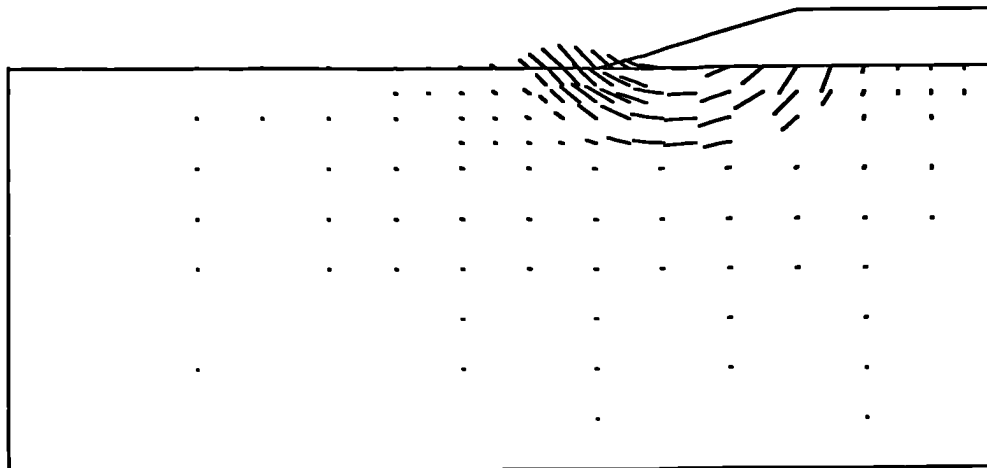


**Figure 4.25b - Displacement vectors at failure for a constant side slope embankment on a subsoil with strength increasing linearly with depth;  
 $\rho x_d/s_{u0}=4.8$ .**

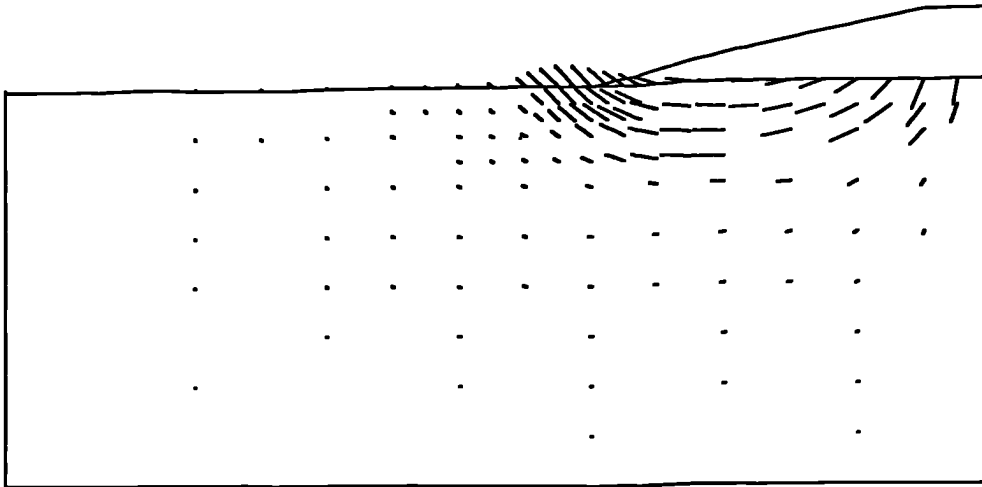


**Figure 4.25c - Displacement vectors at failure for a constant side slope embankment on a subsoil with strength increasing linearly with depth;  
 $\rho x_v/s_{u0}=8.0$**

appropriate, as observed by Jewell (1988).

In Figure 4.26 and Figure 4.27 the maximum shear strain contours at failure for two of the constant side slope analyses are shown. The regions of high shear strain indicate zones in which a slip surface is likely to develop. The intense shear gradients which are modelled accurately using the interface elements cannot be shown on the contour plot as the interface element has no thickness. These maximum shear strain contours further illustrate the failure mechanisms indicated in Figures 4.24 and 4.25.

## 4.4. Summary

A modified version of the finite element program CRISP has successfully predicted the undrained collapse of a strip footing on two idealized soil profiles using an elastic-perfectly plastic constitutive model. Both rough and

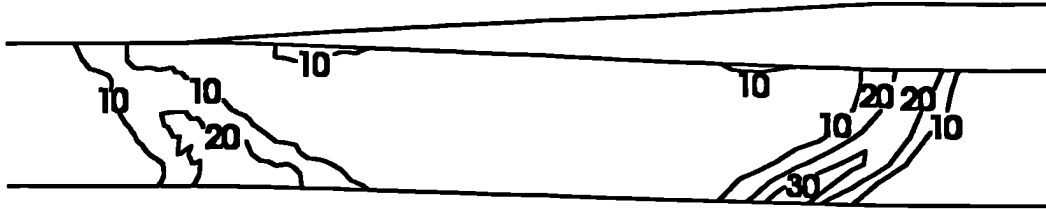


**Figure 4.26 - Maximum shear strain (%) contours at failure for an embankment with constant side slope on a subsoil of uniform strength and limited depth ( $x_v/D=5$ )**

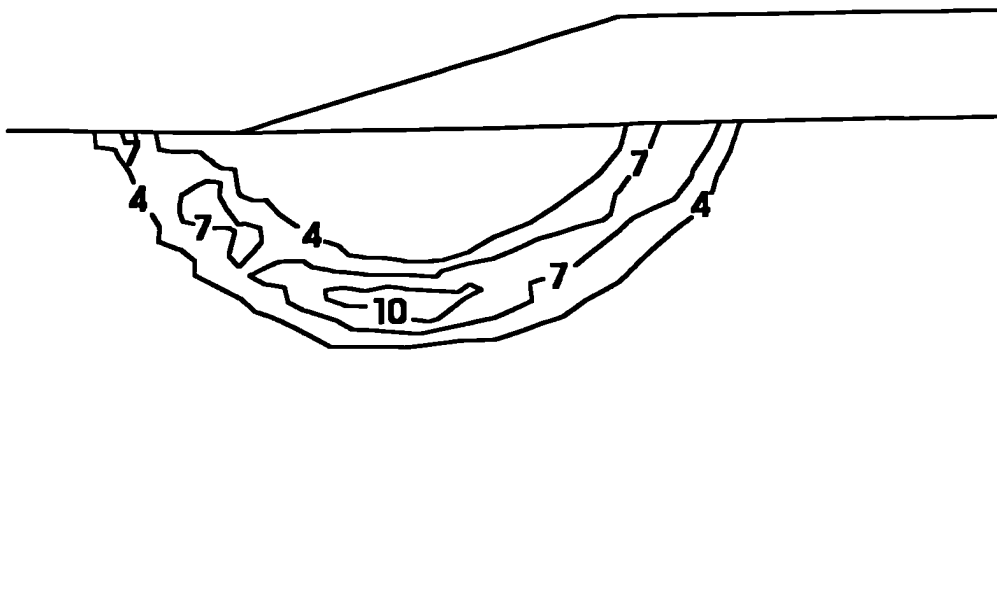


**Figure 4.27 - Maximum shear strain (%) contours at failure for an embankment with constant side slope on a subsoil with strength increasing linearly with depth ( $\rho x_v/s_{u0}=4.8$ )**

smooth footings were analysed representing different degrees of base restraint in a reinforced embankment. Predictions of failure loads agreed closely with plasticity theory for displacement controlled analyses, Figures 4.9 and 4.10.

Load controlled failures, which are more relevant to the construction of reinforced embankments, have been shown to be predictable using plasticity theory although the surface settlement profiles from finite element analyses and plasticity theory are different, Figure 4.12.

A displacement controlled analysis was performed modelling the subsoil using the modified Cam-clay constitutive model and having a profile of strength increasing, almost linearly, with depth. Comparison of finite element analysis and plasticity theory shows that, provided a sufficient number of increments are used, undrained failure, using the modified Cam-clay constitutive model, can be predicted accurately, Figure 4.18.

The lateral displacements predicted using finite element analysis for a subsoil of uniform strength and limited depth are in good agreement with the displacements predicted by plasticity theory, Figure 4.15. The comparisons were made for incremental lateral displacements, close to collapse, in a displacement controlled analysis.

A series of load controlled analyses of fully reinforced embankments with constant side slopes overlying the two idealized soil profiles was performed. From these analyses a simple design method, based on the plasticity solutions, which predicts the length of the embankment side slope for a required design height has been validated, Figures 4.22 and 4.23.

Both translational and rotational failure mechanisms have been observed in the finite element analyses, Figures 4.24 and 4.25. The type of mechanism which develops is dependent on the depth of the soft subsoil compared to the length of the embankment side slope. When performing a limit

equilibrium analysis it is essential that the correct type of mechanism is analysed. Failure to do so may lead to a serious over-estimate in the stability of the embankment (Jewell, 1988).

In all finite element analyses presented interface elements have been used to model the soil interface with rough boundaries. The interface was specified as having an undrained shear strength equal to that of the adjacent soil. The interface element has the capability of modelling accurately the discontinuity which develops at the rough boundary and produces superior predictions of failure loads compared to meshes in which interface elements are not used, Figure 4.13. The interface element also allows shear and normal stress information to be extracted easily from the finite element analysis.

# 5. Consolidation Around a Single Vertical Drain

## 5.1. Introduction

The installation of vertical drains in soft ground prior to embankment construction has become a well used construction technique since the invention of prefabricated band drains (Kjelleman, 1948) and their subsequent development. The drains increase stability by speeding up consolidation and therefore allow embankment construction to progress more quickly.

Vertical drains are most likely to be needed in clay soils with little or no fabric of the kind that facilitates natural drainage (Rowe, 1972), but they can also be effective in laminated or layered soils, where the permeability of the soil is markedly anisotropic (Horne, 1964). The quantification of mass permeability is widely recognised as one of the most difficult aspects of geotechnical design (Jamiolkowski et al, 1983). Perhaps because of the uncertainty associated with the permeability parameters, designers have apparently been content, until now, to rely on simplified analytical methods to quantify the effects of the drains. The most widely used methods (Barron, 1948; Hansbo, 1981) assume that consolidation takes place in a uniform soil column with linear compressibility characteristics in the absence of lateral movement. Such restrictive conditions are not likely to be realized in normally or lightly over-consolidated soils under embankment loading. The finite element method offers a less restrictive analysis which is also capable of incorporating the effects of reinforcement and stage construction. Furthermore, finite element analysis leads directly to the prediction of deformations and eliminates the need to extract information from a

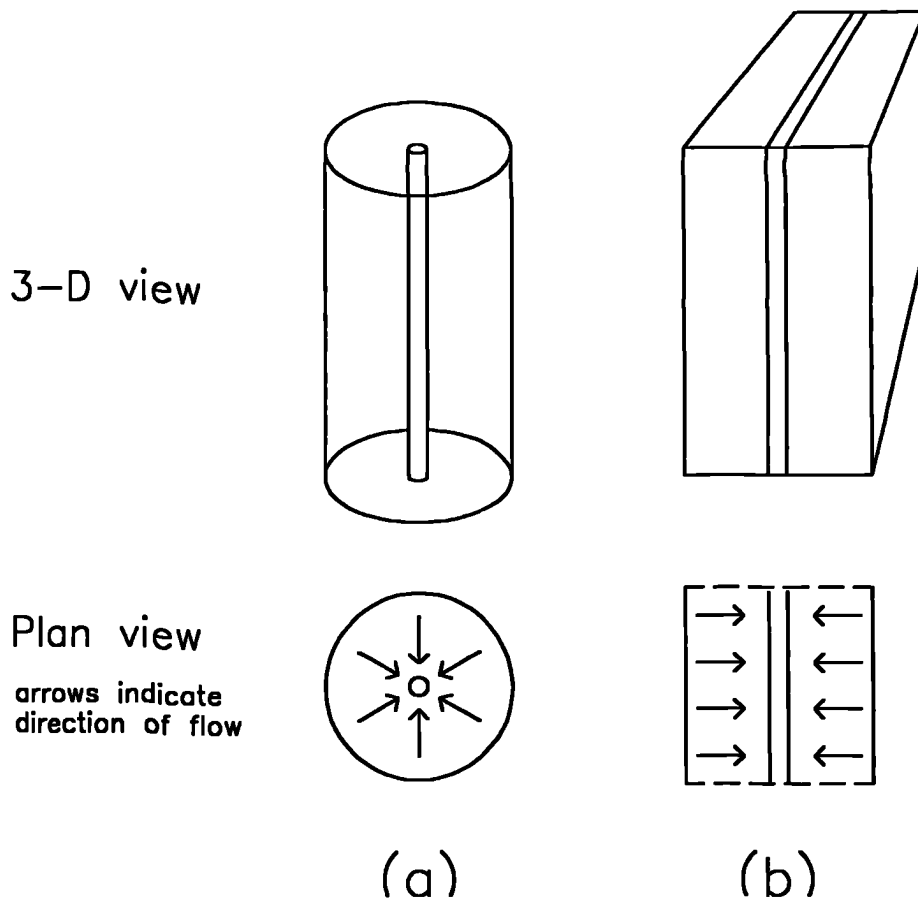


**Figure 5.1 - Unit cell and direction of flow: (a) axisymmetric conditions (b) plane strain conditions.**

consolidation analysis for subsequent use in a stability calculation. Despite its merits, however, the finite element analysis of vertical drains has only occasionally been reported (Zeng et al, 1987; Kumamoto et al, 1988; Sanchez and Sagaseta, 1990).

In this Chapter a methodology for the finite element analysis of ground incorporating vertical drains is developed. An obvious difficulty is that most numerical analyses of embankment problems are conducted for plane strain conditions, whereas the soil around an individual vertical drain is more appropriately modelled as axisymmetric, Figure 5.1. It is necessary,

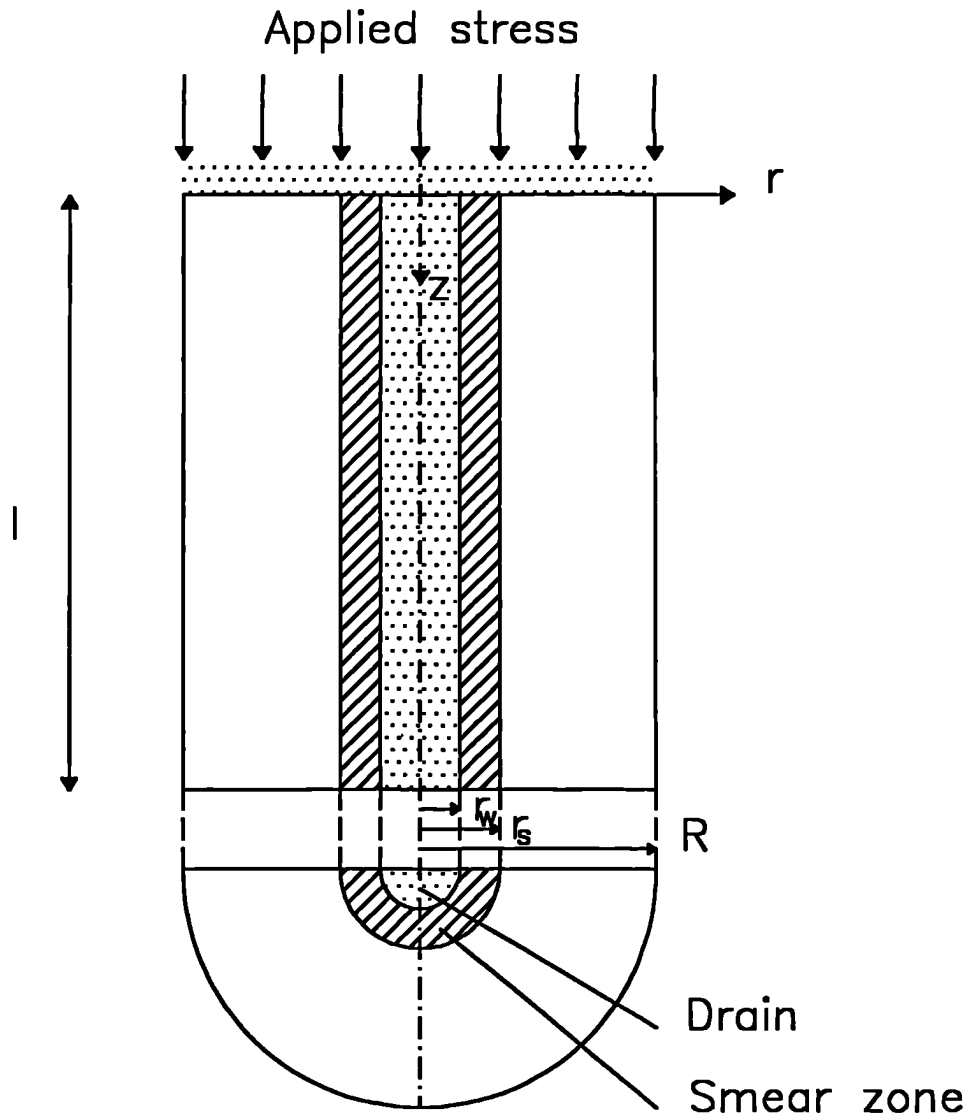


**Figure 5.2 - Unit cell adopted for analytical solution (After: Hansbo, 1981).**

therefore, to find a logical basis for the plane strain analysis. As previous approaches to this problem have left scope for improvement, Section 2.2.2, the equivalence of plane strain and axisymmetric consolidation has been re-examined and a new matching procedure developed.

The numerical analyses have been performed using the modified version of CRISP, Chapter 3, using the drainage element, Section 3.4, to model the vertical drains. Validation of the analysis was undertaken in two stages. Firstly, the results of axisymmetric analyses were compared with Hansbo's (1981) closed form solutions for consolidation around a single vertical drain. Secondly, comparative plane strain and axisymmetric analyses were conducted to test the matching procedure under the simplified conditions assumed in its derivation. In Chapter 6 the matching procedure is tested under more realistic ground conditions.

## 5.2. Comparison of Finite Element Analysis with a Closed Form Solution

Analytical solutions for the consolidation of soil by vertical drains have invariably involved the study of an axisymmetric unit cell, i.e. a cylinder of soil around a single vertical drain (Figure 5.1a), under simplified boundary conditions. Figure 5.2 shows a unit cell of fixed external radius  $R$  and initial length  $l$  containing a drain of radius  $r_w$ . The impervious bottom boundary is not free to move vertically, while the downward movement of the upper boundary may be permitted to develop freely under a constant applied stress (free strain) or may be constrained to be uniform (equal strain); the assumption of equal strain is usually adopted for mathematical convenience. As it is compressed, the soil exhibits uniform stress-strain behaviour. Drainage within the soil may take place both vertically and radially, although it is often reasonable to assume that radial flow dominates. The permeability of the soil,  $k$ , may reduce to a lower value,  $k_s$ , within a smeared zone of radius  $r_s$  caused by drain installation. Flow in the drain takes place vertically towards the top and is governed by the permeability,  $k_w$ , and radius of the drain.

The available theories vary in their degrees of rigour and complexity. The most rigorous, but mathematically most complex, solutions are based on Biot's (1941) consolidation theory and were derived for equal strain boundary conditions by Yoshikuni and Nakando (1974) and Onoue (1988). Both solutions allow for combined vertical and radial drainage in the soil and finite drain permeability (well resistance), but only Onoue's solution considers smear. Although the upper boundary is displaced uniformly, variation of vertical strain is permitted with both radius and depth. Less rigorous solutions, allowing for both well resistance and smear but neglecting vertical flow in the soil, have been obtained by Barron (1948), Hansbo (1981) and Zeng and Xie (1989). These are genuine equal strain analyses where the vertical strain is assumed to be uniform with radius and depth; the latter is clearly an approximation if well resistance is significant. The solutions of Hansbo and Zeng and Xie are relatively easy to compute compared with either Barron's solution or the more rigorous equal strain solution. Solutions for free strain boundary conditions have been obtained in the absence of well resistance (Barron, 1948) and even then tend to be complex.

It has been shown (Hansbo, 1981; Zeng and Xie, 1989; Onoue, 1988) that Hansbo's relatively simple theory compares well, not only with the philosophically similar solutions of Barron and Zeng and Xie, but also with more rigorous solutions. Being also simple to apply, the theory has gained wide acceptance and has been used in parametric studies (Jamiołkowski et al, 1983). It has therefore been used to validate the finite element analysis.

Under an instantaneous step loading the average degree of consolidation based on pore pressure,  $\bar{U}_h$ , on a horizontal plane at depth  $z$  and at time  $t$  is predicted by Hansbo to be

$$\bar{U}_h = 1 - e^{-8T_v/h^2} \dots\dots\dots(5.1)$$

where  $T_h$  is the time factor for horizontal drainage ( $c_h t/4R^2$ ) and

$$\mu = \ln(n/s) + (k/k_s) - 3/4 + z(2l-z)k/k_w r_w^2 \dots\dots\dots(5.2)$$

in which  $n=R/r_w$  and  $s=r_s/r_w$ .

Several groups of axisymmetric finite element analyses were carried out to obtain the results for comparison with Hansbo's theory. The mesh and boundary conditions for the first group of analyses, involving well resistance but no smear, are given in Figure 5.3. Loads were applied to the upper boundary of the mesh under a free strain rather than an equal strain condition, although, as will be shown later, the displacement of the upper boundary was practically uniform. Hansbo incorporated linear stress-strain behaviour of the soil by assuming a constant constrained modulus in the calculation of  $c_h$ ; in the finite element analyses linear elastic properties were specified,  $E'=10^4 \text{kN/m}^2$ , and  $\nu'=0$ . Hansbo's neglect of vertical flow in the soil was matched by setting its vertical permeability to zero. The horizontal permeability was taken to be  $10^{-8} \text{m/s}$ . The drain was assumed to possess negligible stiffness, but its finite permeability was varied to give different values of discharge capacity,  $q_w = k_w \pi r_w^2$ , and hence different values of the dimensionless parameter introduced by Yoshikuni and Nakando (1974),  $L=8kl^2/\pi q_w$ . At any particular stage in the analysis, the average degree of consolidation at the base of the drain could be evaluated by performing a simple numerical integration (trapezoidal rule) of the nodal pore pressures along the base of the mesh. The results are compared with those calculated by Hansbo for  $T_h < 2$  in Figure 5.4. It can be seen that the agreement is generally excellent. Also shown are almost identical results obtained by Yoshikuni and Nakando (1974).

Three more groups of analyses were conducted, with the aim of duplicating the parametric study reported by Jamiolkowski et al (1983). The effect of well resistance in the absence of smear was again investigated but a different mesh, Figure 5.5a, was used so that the geometry of the unit cell

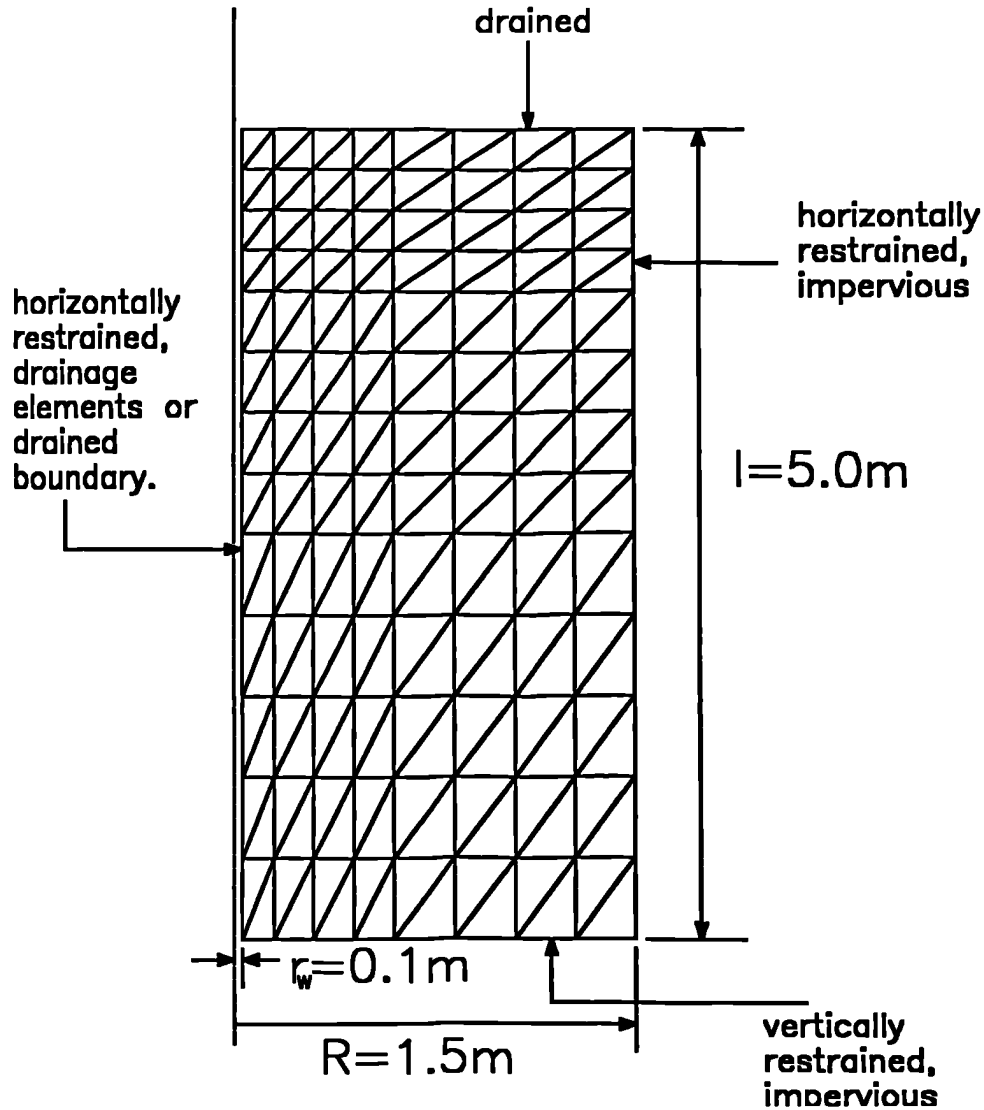


**Figure 5.3 - Finite element mesh used for unit cell analyses comparison with Hansbo (1981).**

would be consistent with that adopted in the other studies. Assumptions regarding the boundary conditions and material parameters remained unchanged. In the next group of analyses, the effect of the drain length was investigated for fixed values of the drain permeability. The variation of the drain length was achieved by shrinking or stretching the mesh in Figure 5.5a in the vertical direction so that  $R/l$  varied between 0.2 and 1.0. Finally, the effect of the smear zone was studied in the absence of well resistance

Consolidation Around a Single Vertical Drain

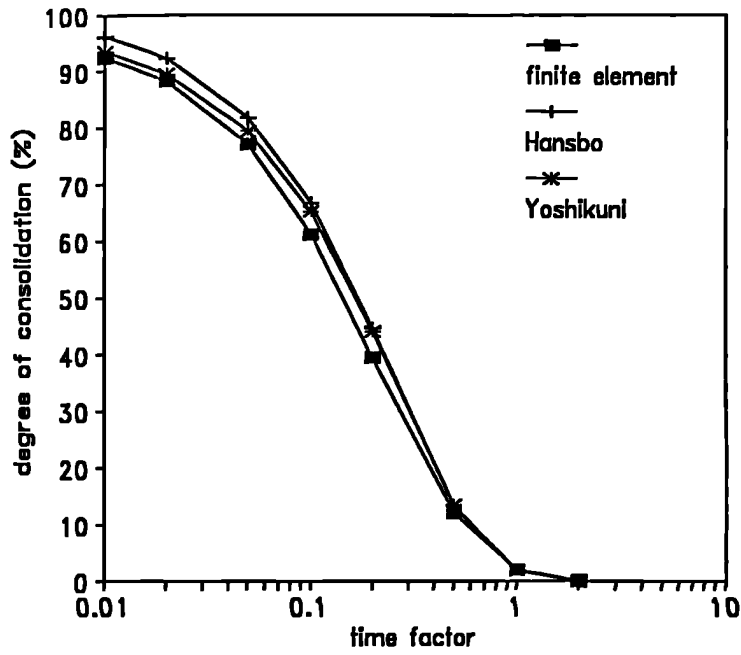


Figure 5.4a - Comparison of finite element and analytical results for consolidation of a unit cell :  $L=0.0$

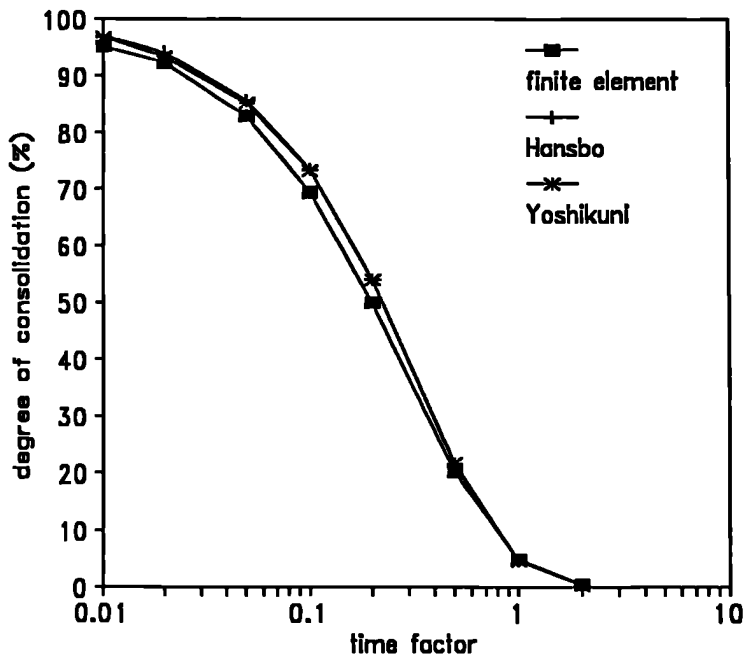


Figure 5.4b - Comparison of finite element and analytical results for consolidation of a unit cell :  $L=0.5$

### Consolidation Around a Single Vertical Drain

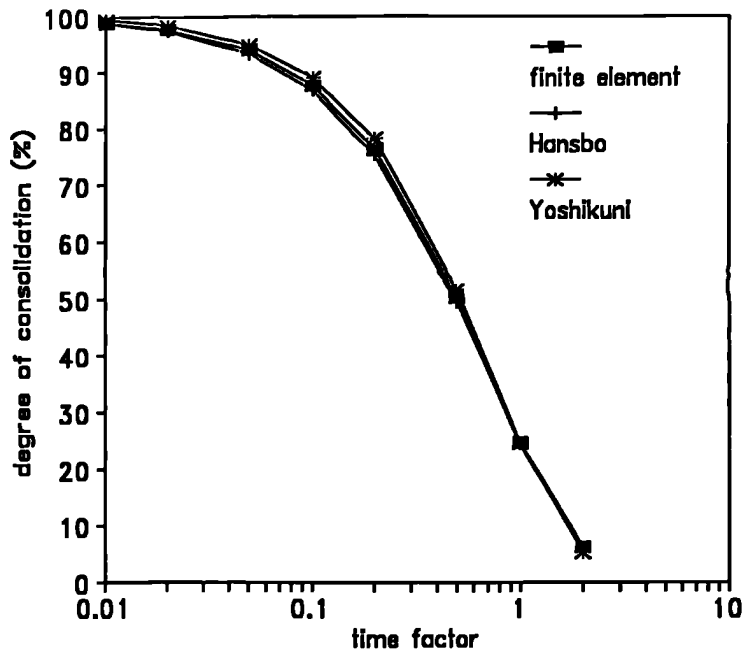


Figure 5.4c - Comparison of finite element and analytical results for consolidation of a unit cell : L=3.0

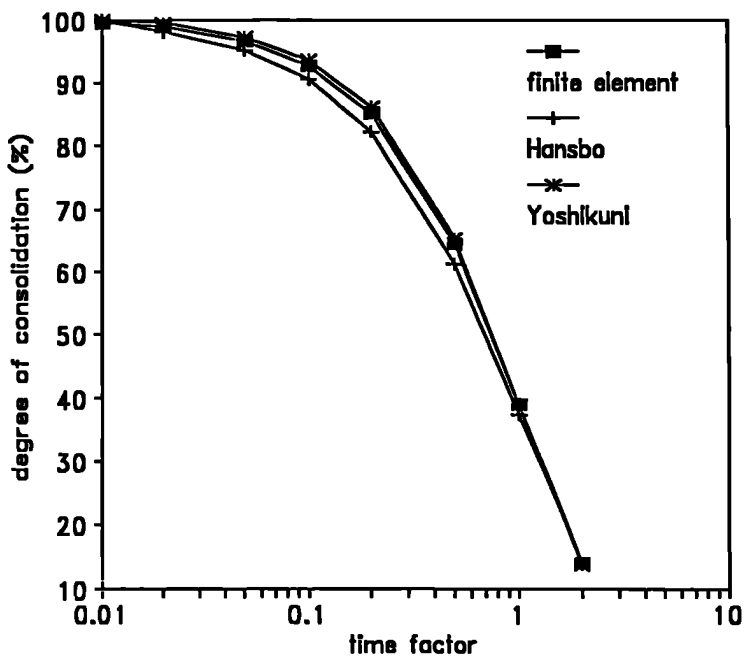


Figure 5.4d - Comparison of finite element and analytical results for consolidation of a unit cell : L=5.0

Consolidation Around a Single Vertical Drain

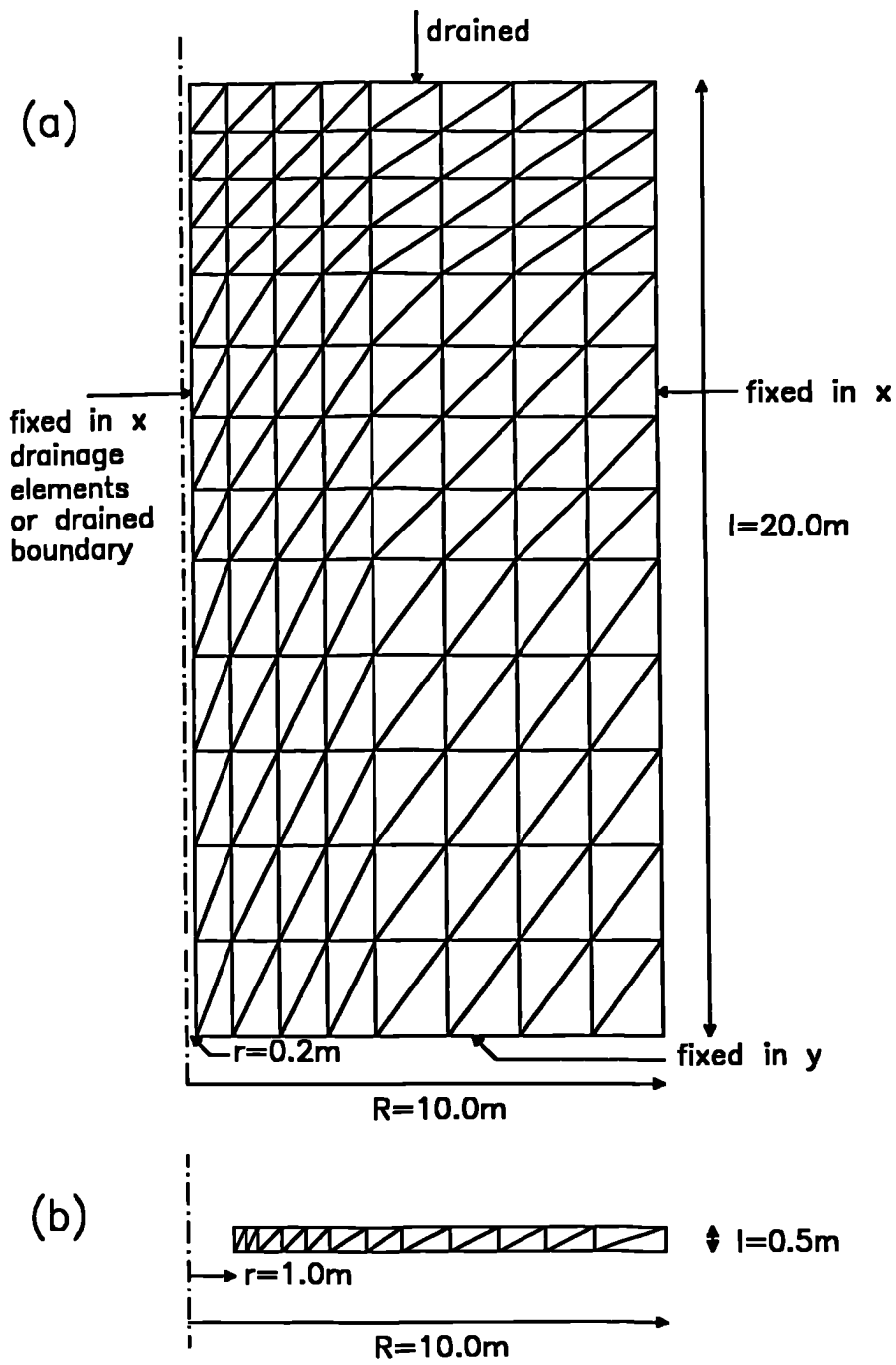


Figure 5.5 - Finite element meshes used for unit cell analyses : comparisons with Jamiolkowski et al (1983).

for a fixed drain spacing. In this case the analysis could be conducted more economically by using a single row of elements, Figure 5.5b, whose upper and lower boundaries were subject to the same conditions as those applied to the corresponding boundaries of the unit cell. To model the effect of smear, soil elements near the drain were reduced in size and given a permeability 10 times lower than the main body of soil (i.e.  $k/k_s=10$ ). An increase in the drain radius was also used to provide a value of  $s=r_s/r_w$  in the desired range.

Results for these three sets of predictions are presented alongside the theoretical predictions in Figures 5.6, 5.7 and 5.8. In each figure the time factor for 90% consolidation at mid-depth of the drain,  $T_{h90}$ , is expressed as a ratio of the corresponding theoretical factor for an ideal case in which there is no smear and no well resistance. Once again the agreement between the finite element analyses and the theoretical results is generally excellent. The trends shown in Figures 5.6, 5.7 and 5.8 are in close agreement with those shown by Jamiolkowski et al (1983). This is true despite a subtle difference of approach in the latter case, namely that in order to establish  $T_{h90}$  the average degree of consolidation was not just evaluated at the mid-depth but over its entire length.

As noted above, the finite element results were obtained under free strain conditions yet have been compared with an equal strain theory. It is of interest to plot the displacements of the upper boundary of the mesh to examine how far the boundary conditions for the finite element analyses deviate from the theoretical ones. The development of the surface displacement with time for three representative analyses is given in Figure 5.9; the settlements are expressed as proportions of the final settlement, which itself is uniform across the unit cell. The only significant non-uniformity occurs temporarily above the unusually thick smear zone in Figure 5.9c. The results explain why very similar solutions were obtained for free and equal strain conditions by Barron (1948).

Consolidation Around a Single Vertical Drain

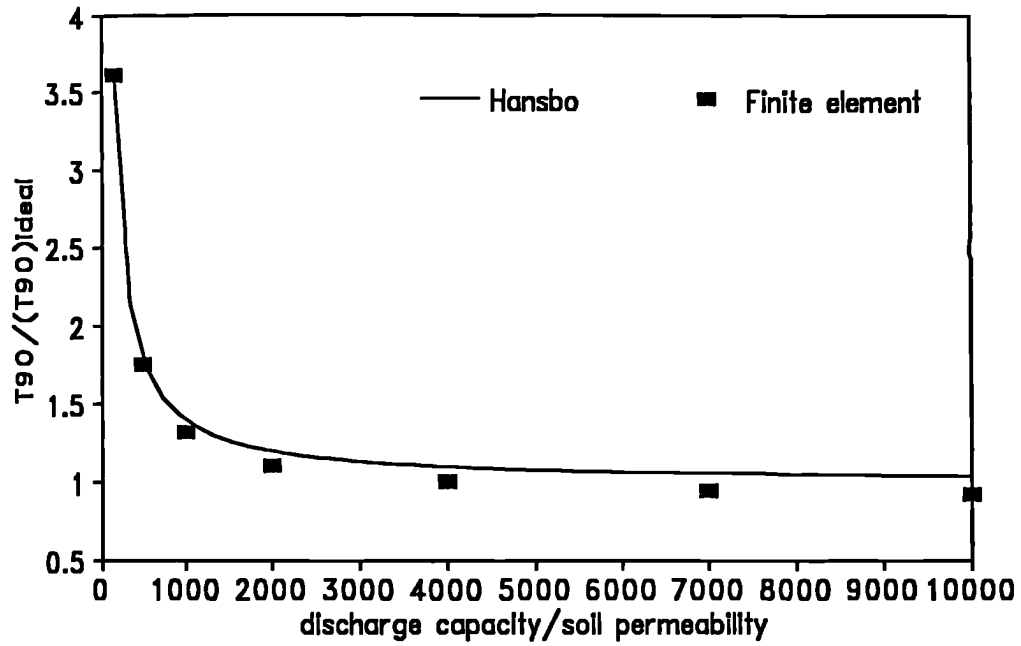


Figure 5.6 - Effect of well resistance on rate of consolidation.

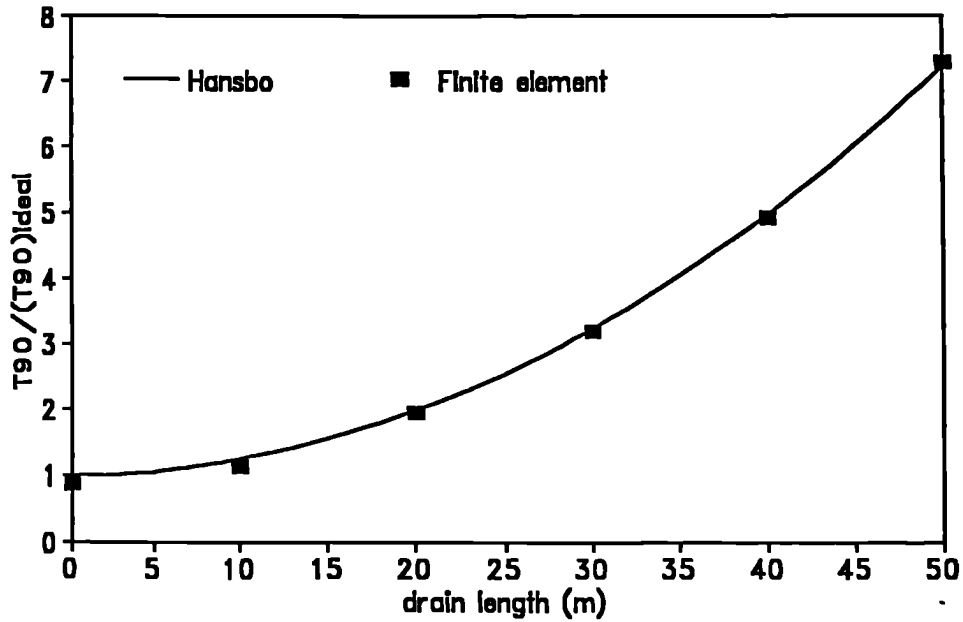
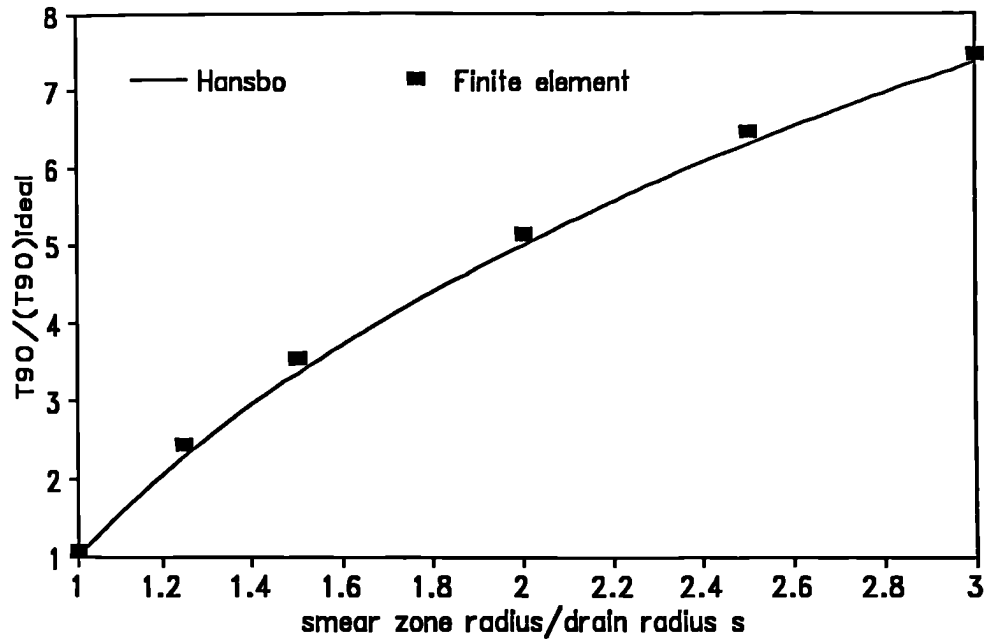


Figure 5.7 - Effect of drain length on rate of consolidation.



**Figure 5.8 - Effect of smear on rate of consolidation.**

The spatial variation of the vertical strain within the unit cell, neglected by Hansbo, is also readily obtainable from the finite element analyses. Figure 5.10 shows the variation obtained on the periphery of the unit cell at various stages of an analysis with high well resistance, when the largest variation of strain might be anticipated. The strain is expressed as a proportion of the final strain, which was uniform with depth. It is demonstrated that the variation of strain can be significant, although its effect on the overall rate of settlement, as given by Hansbo's solution, appears small.

**Consolidation Around a Single Vertical Drain**

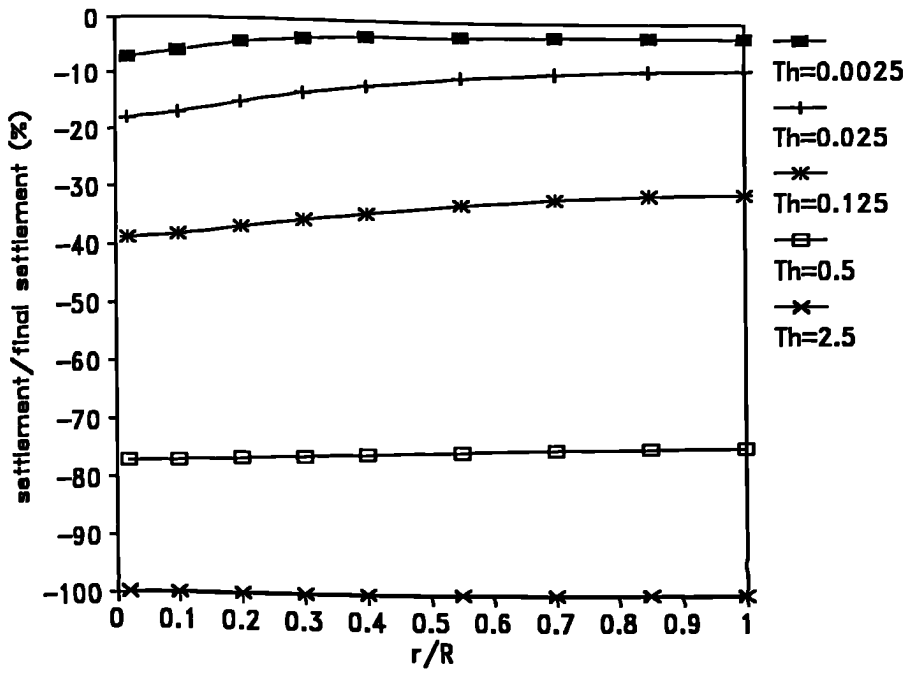


**Figure 5.9a - Development of surface settlement profile in finite element analyses without smear or well resistance.**

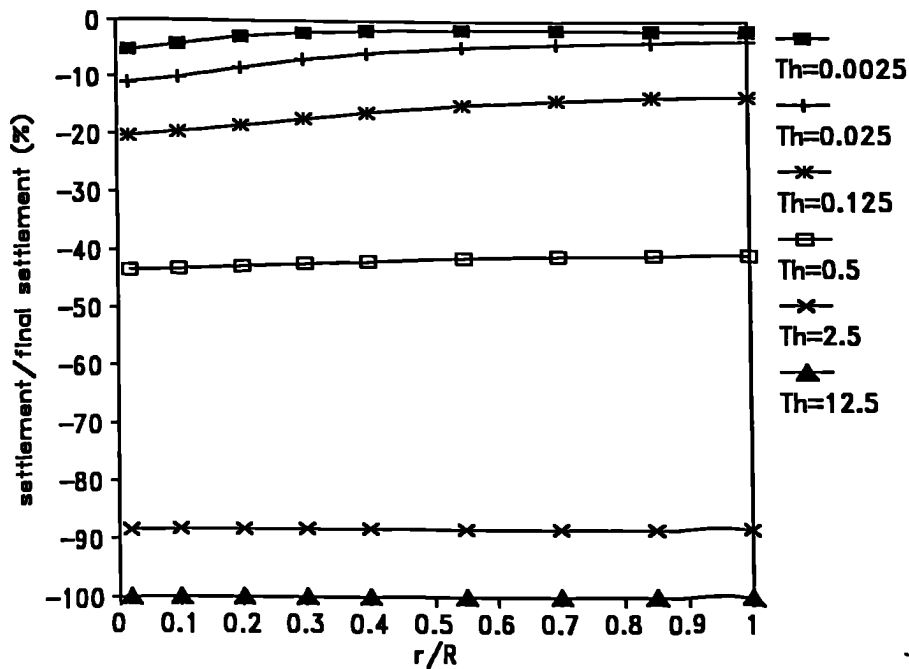


**Figure 5.9b - Development of surface settlement profile in finite element analyses without smear but with well resistance ( $q_w/k=150m^2$ ).**

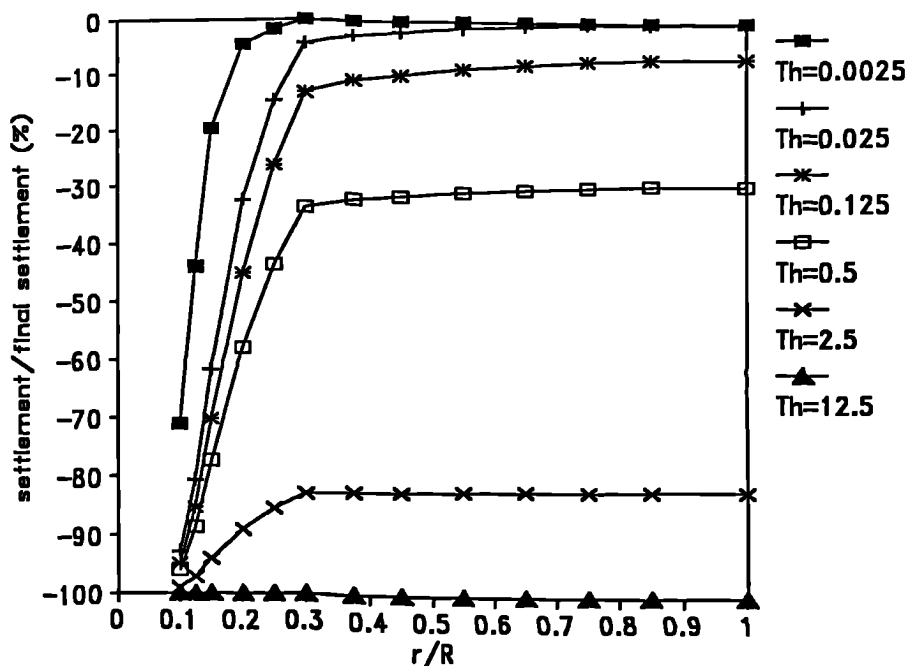


Figure 5.9c - Development of surface settlement profile in finite element analysis with smear (s=3.0) but without well resistance.

### 5.3. Matching Procedure for Plane Strain Analyses

Previous approaches for modelling the effect of vertical drains in plane strain analyses (Zeng et al, 1987; Sanchez and Sagaseta, 1990) have involved matching the time taken for a given degree of consolidation to be achieved by horizontal drainage under plane strain and axisymmetric conditions. Thus neglecting the effect of well resistance,

$$\frac{T_{hpl}B^2}{k_{pl}} = \frac{T_{hax}R^2}{k_{ax}} \dots\dots\dots(5.3)$$

where 2B is the drain spacing in plain strain and the subscripts (or subscript extensions) pl and ax identify the plane strain or axisymmetric conditions respectively. Either or both the drain spacing and the soil permeability may be manipulated to satisfy Equation 5.3. Unfortunately, the resulting values do not then apply for other than the chosen degree of consolidation, since

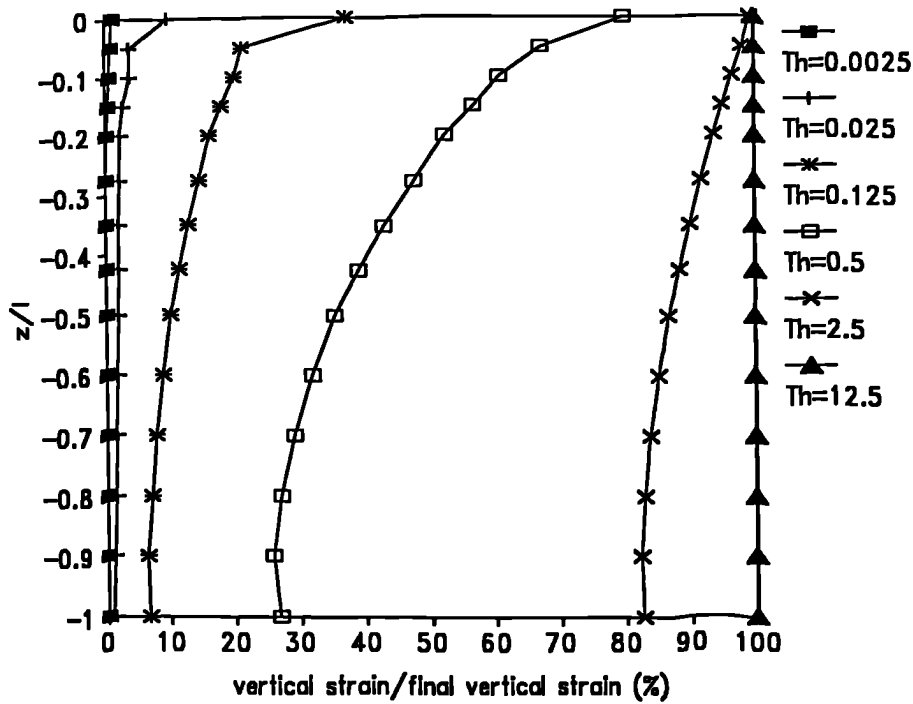


**Figure 5.10 - Variation of vertical strain with depth at unit cell periphery in finite element analysis with well resistance ( $q_w/k=150m^2$ ).**

the ratio of  $T_{hpr}/T_{hax}$  is not constant. Furthermore, in the presence of well resistance, the degree of consolidation varies with depth. In view of the generally good agreement between Hansbo's (1981) theory and finite element analyses seen in the previous section, a better basis for matching plane strain and axisymmetric unit cells was developed by adapting Hansbo's theory for plane strain.

Consider a plane strain unit cell of half width  $B$  containing a drain with discharge capacity  $Q_w$  per unit length. For matching purposes the drain is assumed to possess negligible thickness and no smear zone. As shown in Appendix B, it is possible to apply Equation 5.1 with  $T_h=c_h t/4B^2$  and  $\mu=(2/3)+2z(2l-z)(k/BQ_w)$ . For the rate of consolidation to be matched in the plane strain and axisymmetric unit cells, equality of the average degree of consolidation at every time and at every level in the cell is required. Hence

$$\bar{U}_{hpl} = \bar{U}_{hax} \dots\dots\dots(5.4)$$

from Equation 5.1

$$\frac{T_{hpl}}{\mu_{hpl}} = \frac{T_{hax}}{\mu_{ax}} \dots\dots\dots(5.5)$$

or

$$\frac{C_{hpl}t}{B^2\mu_{pl}} = \frac{C_{hax}t}{R^2\mu_{ax}} \dots\dots\dots(5.6)$$

Two types of matching are defined, firstly, geometry matching in which the permeability of the soil is the same in the plane strain and axisymmetric analyses and the width of the plane strain unit cell is adjusted. If the soil parameters are identical in the axisymmetric and plane strain unit cell, then Equation 5.6 becomes

$$B^2\mu_{pl} = R^2\mu_{ax} \dots\dots\dots(5.7)$$

The relevant expressions for  $\mu_{pl}$  and  $\mu_{ax}$  may be substituted into Equation 5.7 and the terms rearranged to give

$$\frac{2B^2}{3} - R^2 \left[ \ln\left(\frac{n}{s}\right) + \frac{k}{k_s} \ln(s) - \frac{3}{4} \right] = \left( \pi R^2 \frac{k}{q_w} - \frac{2Bk}{Q_w} \right) (2lz - z^2) \dots\dots(5.8)$$

The condition for geometric matching may be obtained by considering the case of negligible well resistance ( $q_w$  and  $Q_w \rightarrow \infty$ ). Therefore, geometric matching, including the effect of smear, is achieved if

$$\frac{2B^2}{3} - R^2 \left[ \ln\left(\frac{n}{s}\right) + \frac{k}{k_s} \ln(s) - \frac{3}{4} \right] = 0 \dots\dots\dots(5.9)$$

or

$$\frac{B}{R} = \sqrt{\frac{3}{2} \ln\left(\frac{n}{s}\right) + \frac{k}{k_s} \ln(s) - \frac{3}{4}} \dots\dots\dots(5.10)$$

The effect of well resistance is matched independently if

$$\pi \frac{R^2}{q_w} k - \frac{2B}{Q_w} k = 0 \dots\dots\dots(5.11)$$

or

$$Q_w = q_w \frac{2B}{\pi R^2} \dots\dots\dots(5.12)$$

A second procedure, referred to as permeability matching, is to maintain the same drain spacing in the plane strain and axisymmetric analyses and to adjust the plane strain horizontal soil permeability to achieve a matched analysis. From Equation 5.6 with B=R

$$\frac{k_{pl}}{\mu_{pl}} = \frac{k_{ax}}{\mu_{ax}} \dots\dots\dots(5.13)$$

substituting for the factors  $\mu_{pl}$  and  $\mu_{ax}$

$$k_{pl} = \frac{2k_{ax}}{3 \left[ \ln \left( \frac{n}{s} \right) + \frac{k_{ax}}{k_s} \ln(s) - \frac{3}{4} \right]} \dots\dots\dots(5.14)$$

and

$$Q_w = \frac{2q_w}{\pi R} \dots\dots\dots(5.15)$$

Although geometry and permeability matching procedures have been described separately, they can be used in combination by setting B to a desired value and re-deriving the requirements for  $k_{pl}$  and  $Q_w$ . This is useful in avoiding the necessity of modelling small equivalent drain spacings with excessively large numbers of finite elements in a full plane strain analysis.

### 5.3.1. Validation of the Matching Procedure

In order to validate the above theory, finite element analyses were undertaken for both an axisymmetric unit cell and the equivalent plane strain case, determined with the aid of Equations 5.10 and 5.12 or 5.14 and 5.15. The effects of both well resistance and smear were studied. As the matching theory considers only horizontal drainage in the soil, the vertical permeability of the soil was initially neglected. The mesh of Figure 5.5a was again used, stretched if necessary in the horizontal plane to achieve geometric matching. The stretching was done non-uniformly in such a way

that soil elements near the drain remained sufficiently small. The previously adopted values of the elastic parameters ( $E'$  and  $\nu'$ ) and horizontal permeability of the soil were retained, except when permeability was changed in accordance with the matching rules. As before the drain was assumed to possess no stiffness. In analyses with smear, the size of the smear zone and its permeability were fixed so that  $s=5$  and  $k/k_s=2$ . In the analyses with well resistance, the discharge capacity was chosen to give  $L=2$ .

The equivalence of these plane strain and axisymmetric analyses can be assessed on the basis of both settlement and pore pressure. Results for the overall average degree of consolidation,  $\bar{U}$ , calculated from the settlements of the surface nodes are given in Figure 5.11. The style of calculation was the same as that used to compute  $\bar{U}_h$  at a given depth from nodal pore pressures as described previously. The corresponding results for  $\bar{U}_h$  at the mid-depth of the drain are shown in Figure 5.12. For both  $\bar{U}$  and  $\bar{U}_h$  it can be seen that the geometry and permeability matching procedures produce almost identical results. However, in the absence of well resistance (Figures 5.11a, 5.11b, 5.12a and 5.12b) there are noticeable differences between the plane strain and axisymmetric results, especially at small time factors. When well resistance is significant (Figures 5.11c, 5.11b, 5.12c and 5.12d) better overall matching is achieved.

The matching errors displayed in Figures. 5.11 and 5.12 may be assessed, for geometric matching, by referring to Figures. 5.13a and 5.13b. The errors which are presented as differences in the degree of consolidation achieved at a given time factor, are probably attributable to the displacements at the upper boundary. For example, Figure 5.14a shows the displacement profiles at various stages of a matched analysis without smear or well resistance. In this plane strain analysis the settlement profile exhibits a much larger variation across the unit cell than in the corresponding

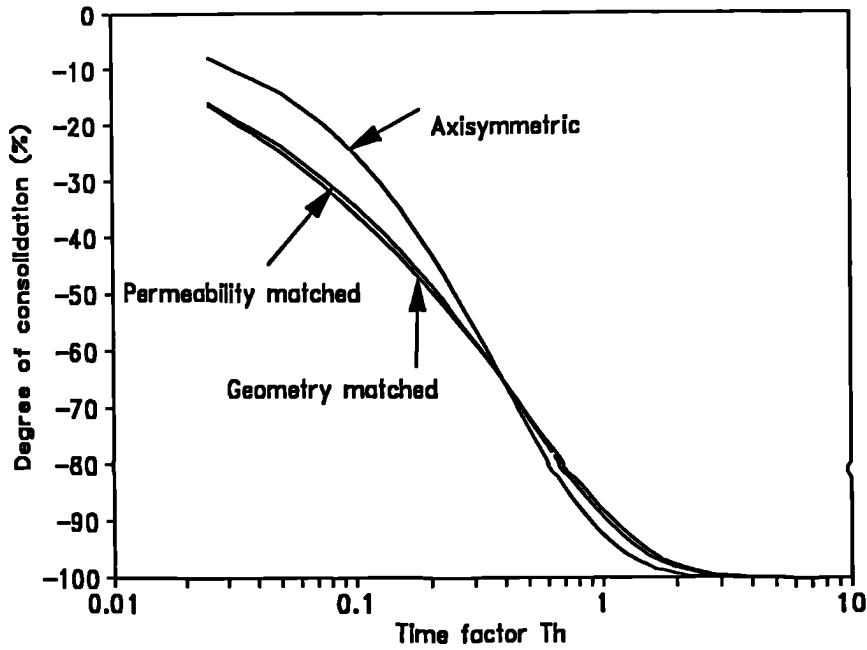


**Figure 5.11a - Comparison of the average surface settlement for axisymmetric and matched plane strain analyses : without smear or well resistance.**

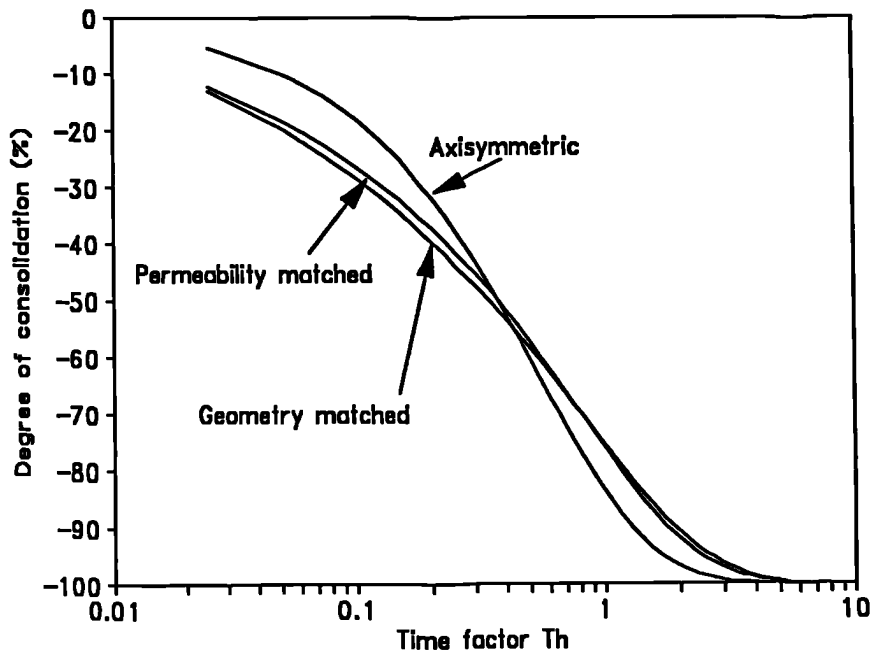


**Figure 5.11b - Comparison of the average surface settlement for axisymmetric and matched plane strain analyses : with smear but without well resistance.**

Consolidation Around a Single Vertical Drain

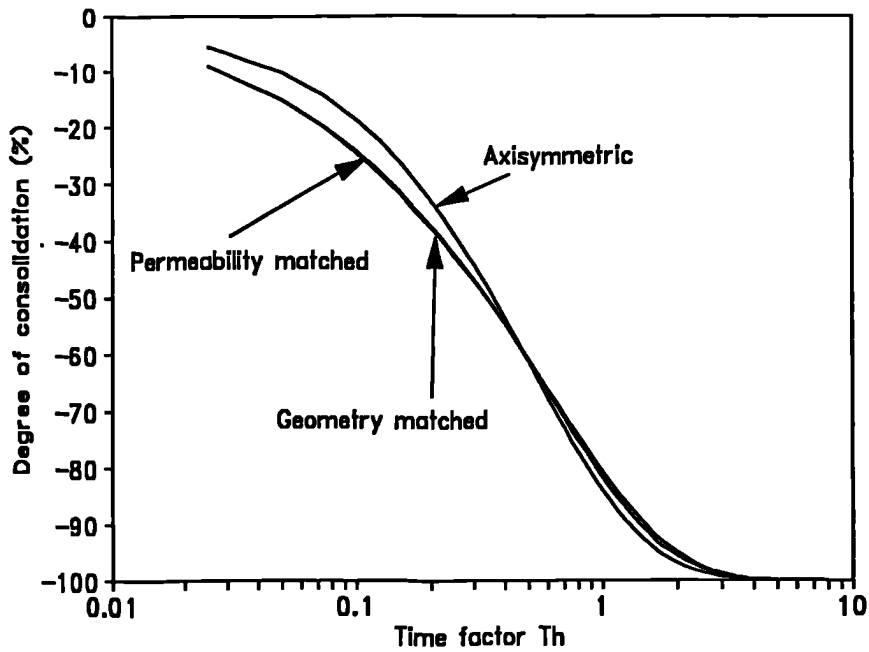


**Figure 5.11c - Comparison of the average surface settlement for axisymmetric and matched plane strain analyses : without smear but with well resistance.**

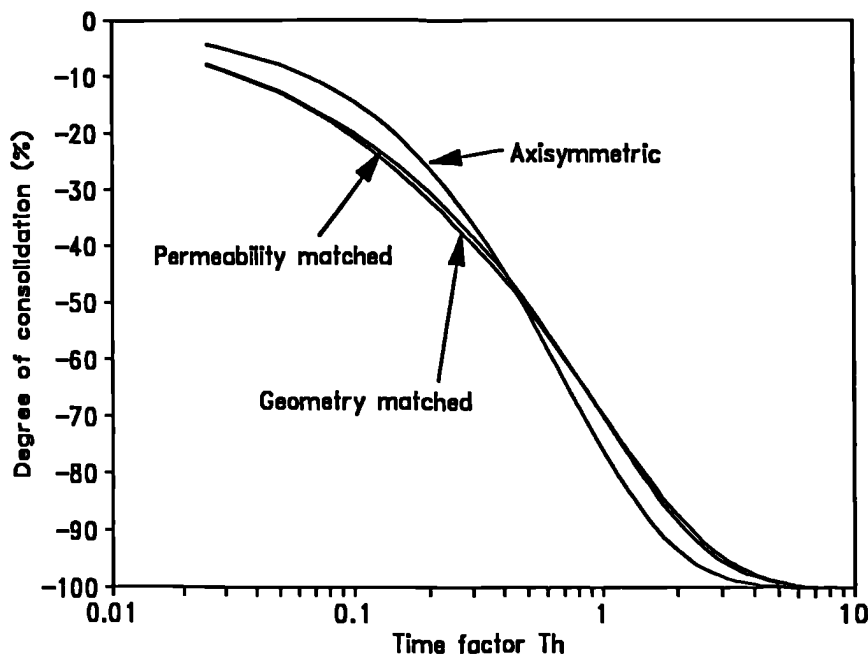


**Figure 5.11d - Comparison of the average surface settlement for axisymmetric and matched plane strain analyses : with smear and well resistance.**

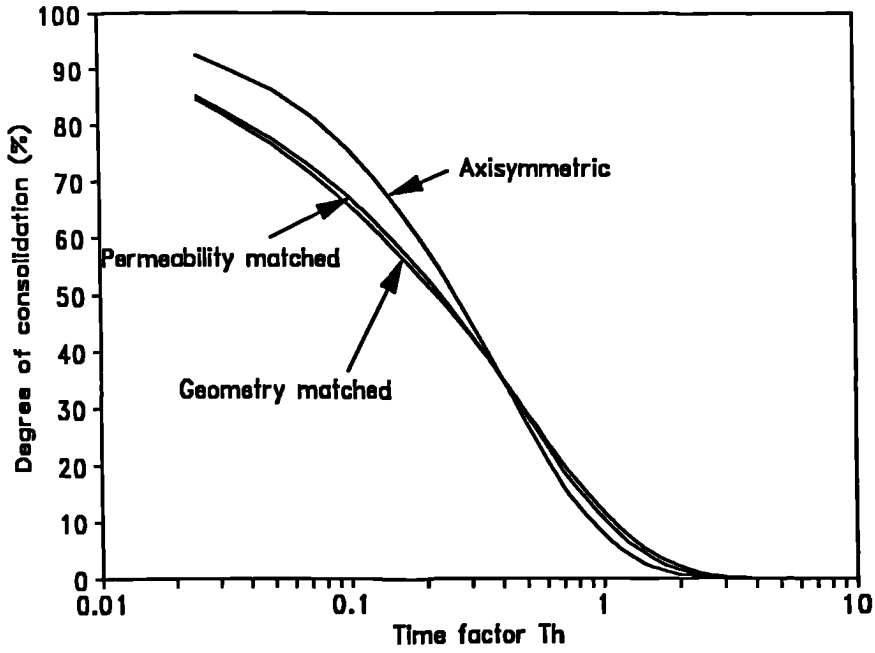


**Figure 5.12a - Comparison of the average excess pore pressure at mid-depth for axisymmetric and matched plane strain analyses : without smear or well resistance.**

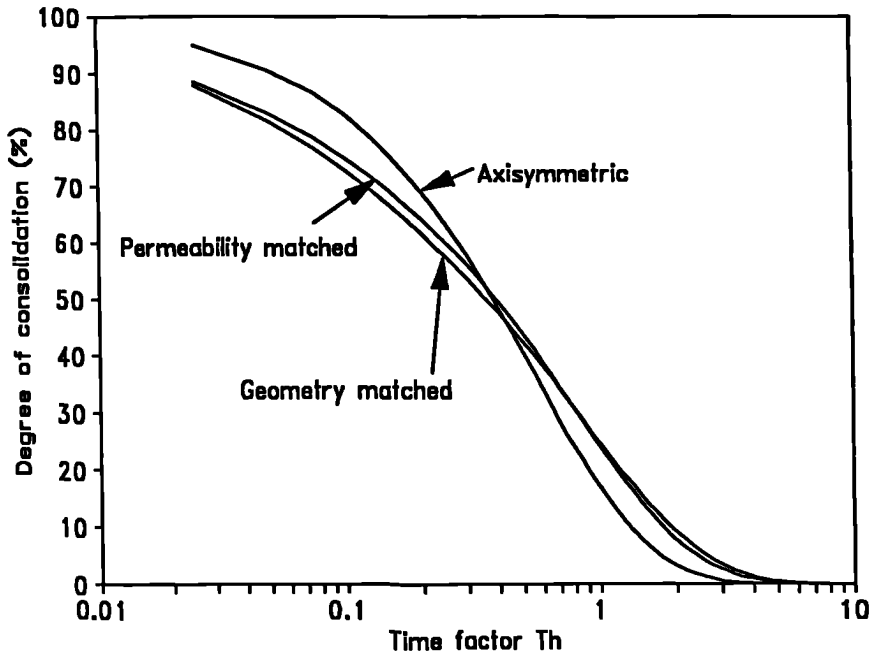


**Figure 5.12b - Comparison of the average excess pore pressure at mid-depth for axisymmetric and matched plane strain analyses : with smear but without well resistance.**

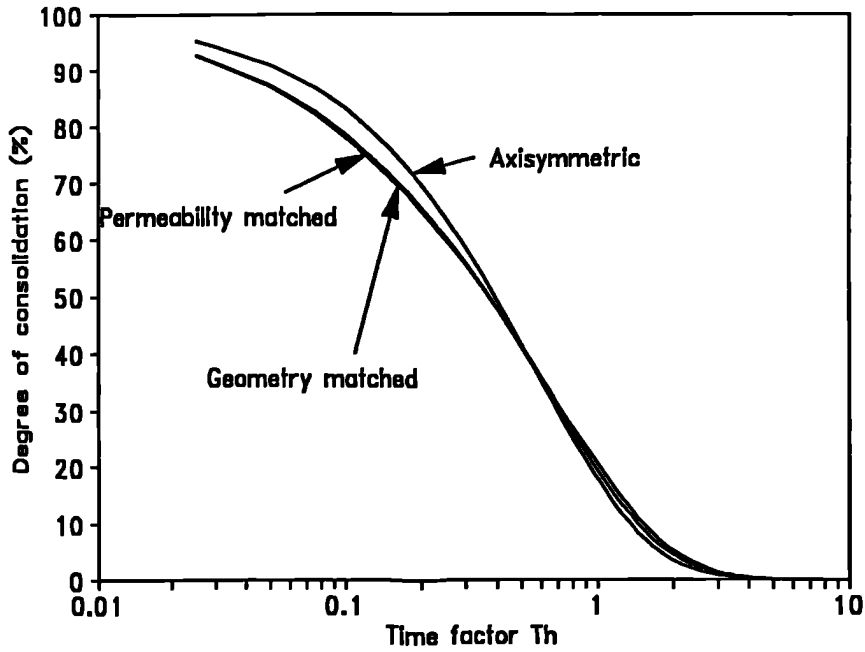


**Figure 5.12c - Comparison of the average excess pore pressure at mid-depth for axisymmetric and matched plane strain analyses : without smear but with well resistance.**

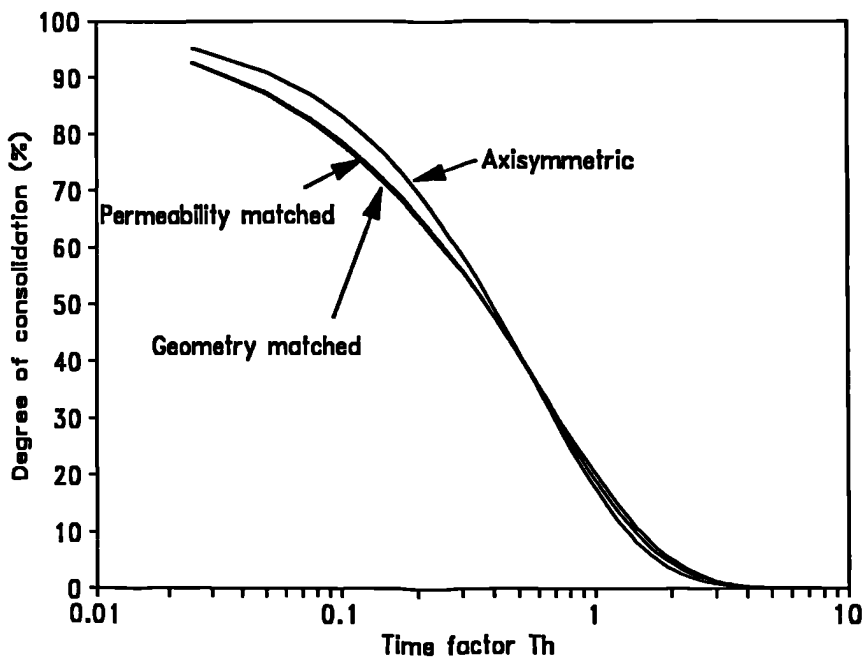


**Figure 5.12d - Comparison of the average excess pore pressure at mid-depth for axisymmetric and matched plane strain analyses : with smear and well resistance.**

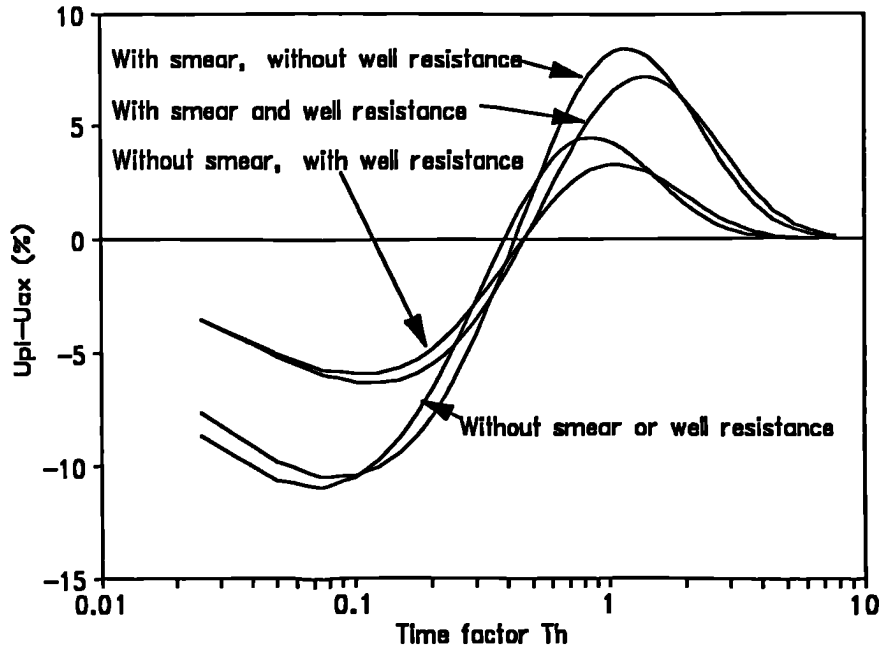


**Figure 5.13a - Errors in geometry matched plane strain analyses : based on settlements; results of Figure 5.11.**

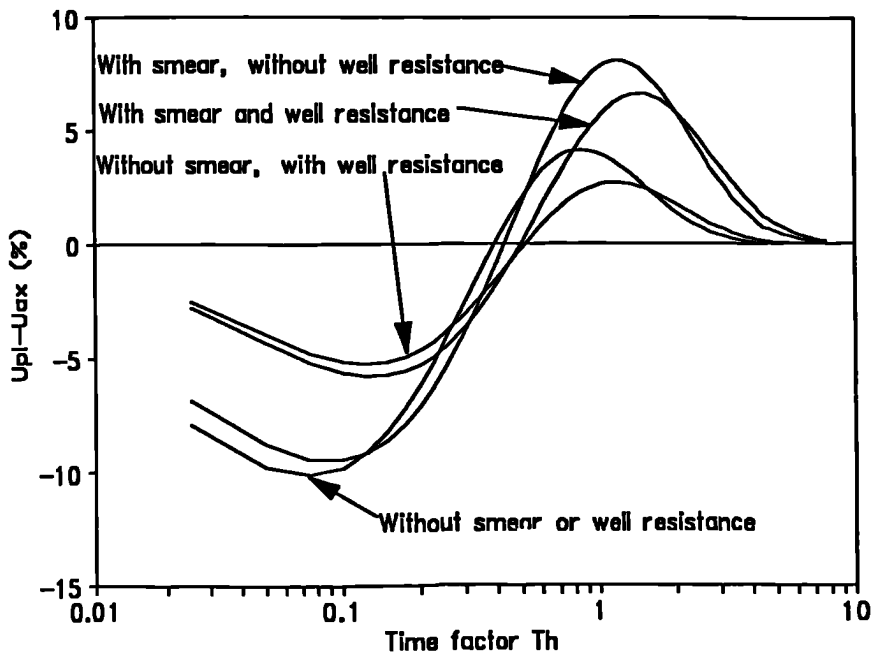


**Figure 5.13b - Errors in geometry matched plane strain analyses : based on pore pressure; results of Figure 5.12.**

axisymmetric analysis (Figure 5.9a) and clearly violates the equal strain assumption on which the matching theory is based. The improvement of the matching procedure obtained with well resistance, most marked at small time factors, corresponds to the attainment of slightly more uniform settlement profiles, Figure 5.14b. Fortunately the differential settlements seen in these unit cell analyses are less likely to occur in full embankment analyses, because of the stiffness contribution of the embankment elements, and superior matching can be anticipated.

### 5.3.2. Pore Pressure Variation Across Unit Cells

It is important to realize that, even if perfect matching is achieved, the excess pore pressures at corresponding points in the axisymmetric and plane strain unit cells will not be the same. This is illustrated in Figure 5.15 for a pair of analyses in which the difference in  $\bar{U}_h$  was negligible. In particular the maximum values of the excess pore pressures on the periphery of the unit cell (midway between drains) differ significantly.

The ratio of the pore pressures across the axisymmetric and matched unit cells ( $u_{ax}/u_{pl}$ ) has been derived in Appendix B, and at the periphery of the unit cells is

$$\frac{u_{ax}}{u_{pl}} = \frac{2 \ln(n) - 1}{3 \left( \ln(n) - \frac{3}{4} \right)} \dots\dots\dots(5.15)$$

From Equation 5.15 the ratio of the pore pressures at the periphery of the test unit cell, Figure 5.5, is 0.72. This compares well with the finite element predicted value of 0.68, from Figure 5.15. Equation 5.15 can therefore be used to predict the pore pressure which would develop in an axisymmetric unit cell from plane strain analysis results.

A notable difference in the theoretical solution (Barron, 1948; Hansbo, 1981) and the finite element solution to the consolidation of the unit cell is the excess pore pressure distribution at low time factors. As pointed out by

**Consolidation Around a Single Vertical Drain**

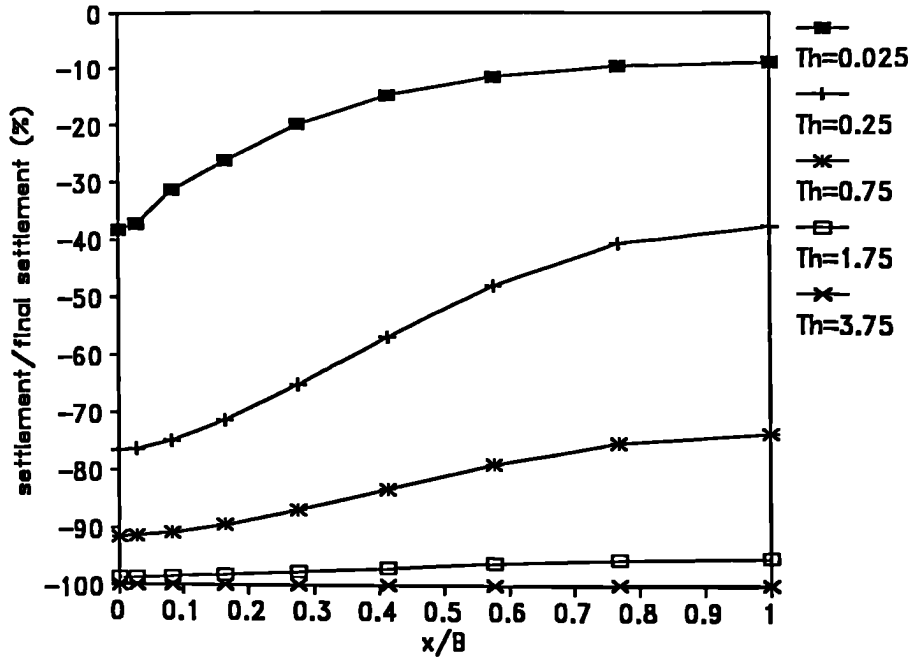


**Figure 5.14a - Development of surface settlement profile in geometry matched plane strain : without smear or well resistance.**

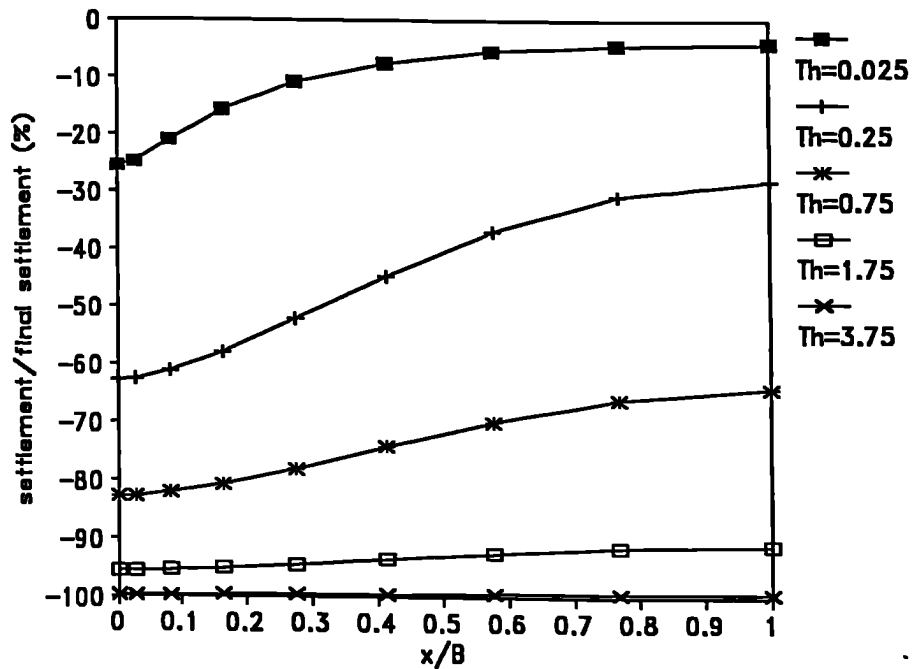


**Figure 5.14b - Development of surface settlement profile in geometry matched plane strain : without smear but with well resistance.**

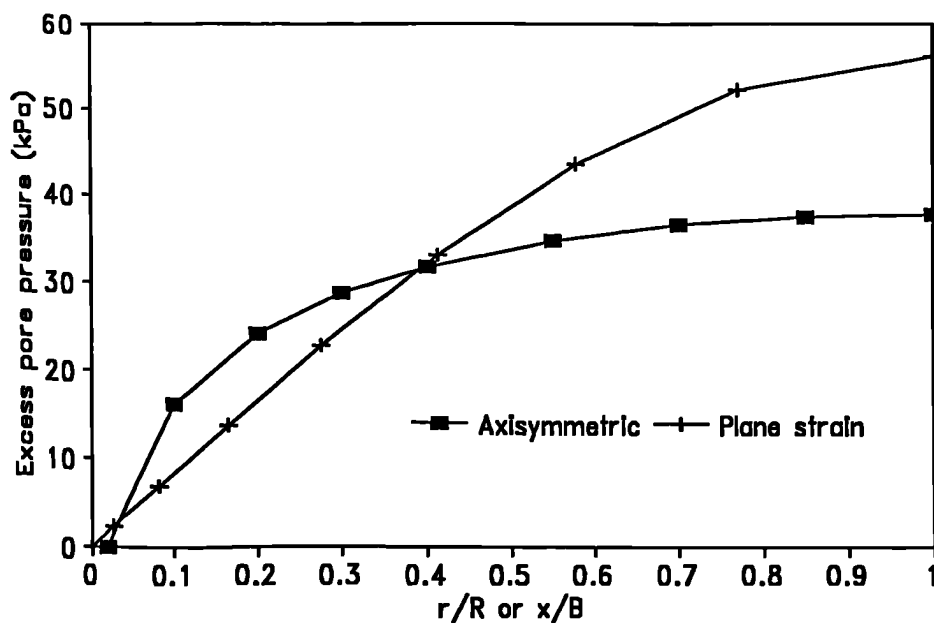


**Figure 5.15 - Comparison of pore pressure distributions from axisymmetric and geometry matched plane strain analyses without smear or well resistance (degree of consolidation = 65%).**

Barron, under equal strain conditions, the excess pore pressure distribution across an axisymmetric unit cell, at all times, must be parabolic. This results in an excess pore pressure greater than the applied load at early time factors near the periphery of the unit cell. In the finite element solution the initial excess pore pressure distribution is developed by applying the loading in an undrained increment; this results in the initial excess pore pressure being equal to the applied loading at every pore pressure node in the mesh. In order to limit the effect of pore pressure oscillations, the initial time step was chosen such that at no node was the excess pore pressure greater than the applied load after the first consolidation increment. The variation of pore pressure, at mid-depth, across the axisymmetric unit cells is shown in Figure 5.16 at the end of the first consolidation increment of an analysis with no smear zone and no well resistance. It is interesting to note that, even at this low time factor, a parabolic variation of excess pore pressure can be seen to have developed. However, the fact that the initial finite element

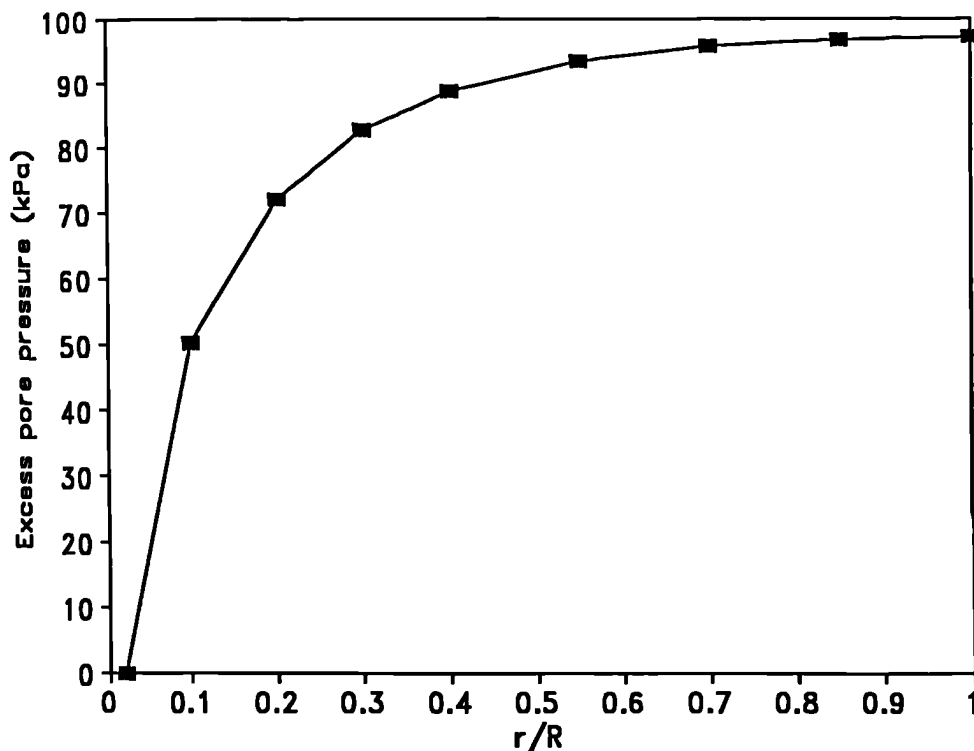


**Figure 5.16 - Excess pore pressure distribution after the first consolidation time increment from axisymmetric finite element analysis without smear or well resistance.**

excess pore pressure distribution cannot conform to the parabolic distribution discussed by Barron may contribute to the small differences between the theoretical and finite element results at low time factors, Figure 5.13.

### **5.3.3. Effect of Vertical Permeability on Matching Procedure**

So far the effect of vertical flow in the soil has not been considered. In order to check its influence on the matching procedure, two further pairs of analyses were conducted with equal horizontal and vertical permeabilities in the soil. Specimen results for  $\bar{U}_h$  at the mid-depth of the drain are shown in Figure 5.17 and indicate that the introduction of vertical flow does not invalidate the matching. In fact the matching errors in  $\bar{U}_h$  in Figure 5.18, are significantly reduced. This can be explained by the action of the vertical flow

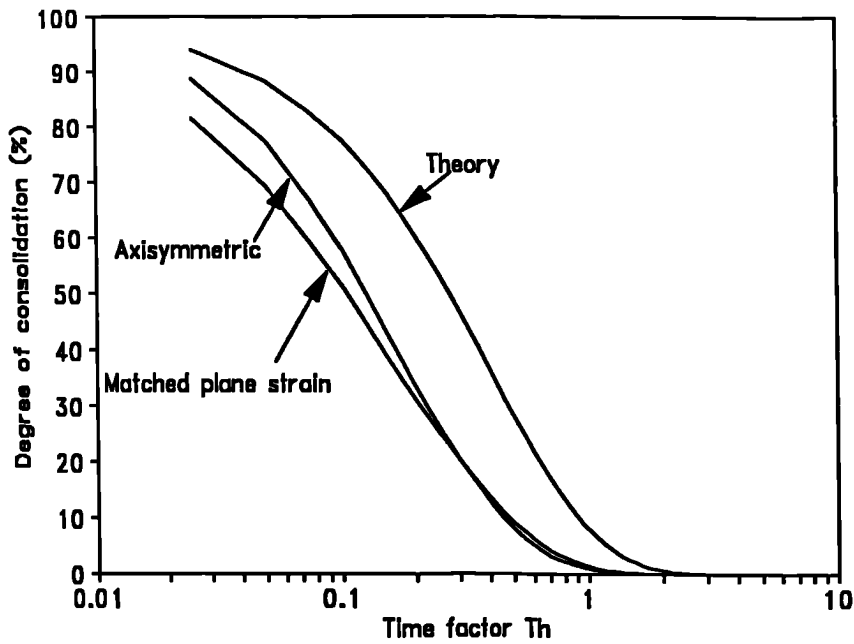


Figure 5.17a - Comparative results for axisymmetric and matched plane strain analyses with vertical flow ( $k_v=k_h$ ), degree of consolidation based on excess pore pressure without smear or well resistance.

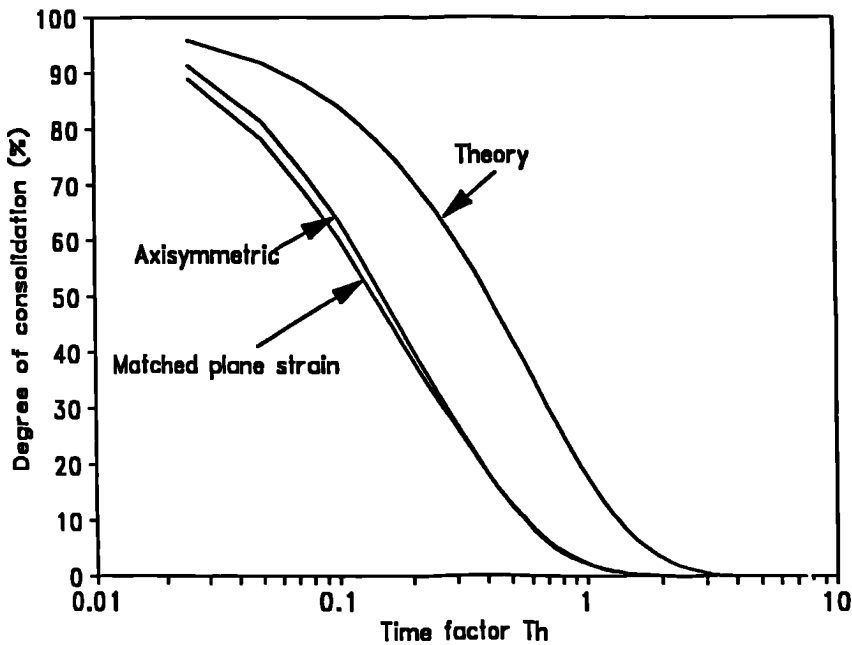
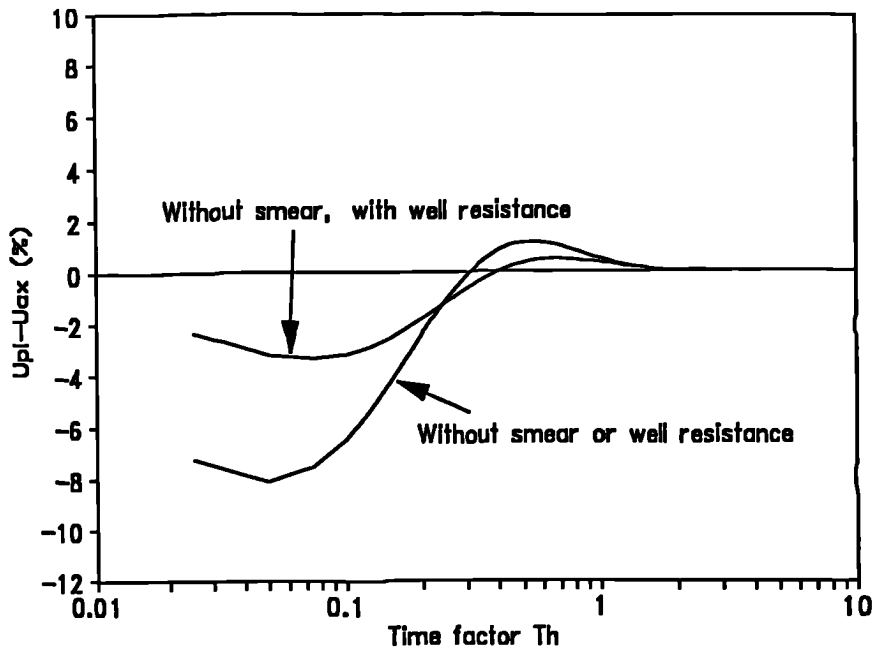


Figure 5.17b - Comparative results for axisymmetric and matched plane strain analyses with vertical flow ( $k_v=k_h$ ), degree of consolidation based on excess pore pressure without smear but with well resistance.



**Figure 5.18 - Errors in geometry matched plane strain analyses for unit cells with vertical permeability ( $k_v=k_h$ ) based on excess pore pressure.**

in promoting more uniform settlement profiles in the plain strain analysis. As in previous cases (Figure 5.13), the matching errors based on settlement were little different from those based on pore pressure and therefore they have not been presented. The influence of the vertical flow on the rate of consolidation is evident from the separation of the finite element and theoretical curves, Figure 5.17, but this is likely to be reduced in practical cases by two factors: firstly, the width of the unit cell (drain spacing) is likely to be less than that adopted for this study ( $R/l=B/l=0.5$ ) and, secondly, the vertical permeability is likely to be less than the horizontal permeability (Jamiolkowski et al, 1983).

## 5.4. Summary

A methodology has been developed for representing vertical drains in plane strain finite element analyses of embankments on soft ground, and has been validated by analysing the consolidation of soil around a single drain.

The methodology includes the use of a drainage element to represent the vertical drains, Section 3.4. The performance of CRISP has been checked under axisymmetric conditions against the theoretical solutions of Hansbo (1981) and found to be satisfactory. The trends obtained by Jamiolkowski et al (1983) in a parametric study of well resistance and smear have been reproduced successfully.

A procedure has been derived which permits equivalent plane strain and axisymmetric analyses to be conducted. Throughout the analysis, the average degrees of consolidation are matched at every level in the soil, although the pore pressures at corresponding points are not the same. The equivalent plane strain analysis can be achieved by manipulating the drain spacing and/or the horizontal permeability of the soil. The validity of the proposed matching procedure has been examined for drains with and without well resistance and smear, installed in a uniform soil with linear compressibility characteristics. The procedure is generally successful; at no time does the error in the average degree of consolidation, either at the mid-depth of the drain or over its whole length exceed 11%.

In practice the soil behaviour is likely to be non-linear and to vary with depth. Also in a full embankment analysis significant lateral strains may occur in the soil. Chapter 6 describes analyses of a case history in which a preloading embankment was constructed over a soil into which vertical drains had been installed. The matching procedure is used to model the vertical drains in these more realistic soil conditions and comparisons of observed and finite element predicted behaviour are made.

## **6. Case History: Porto Tolle**

### **6.1. Introduction**

A thermal power plant constructed on the Po river delta at Porto Tolle, Italy, required the construction of several large steel tanks. In order to limit settlement after the placement of these tanks pre-loading embankments were constructed and vertical drains installed in the subsoil. The amount of vertical drain used at the site (approximately 1,700,000m) justified a comprehensive site investigation followed by the construction of a trial embankment beneath which several types of vertical drain were installed. The trial was extensively monitored and used to assess each drain type.

The quality of the field and laboratory data (Hansbo et al, 1981) allowed the input parameters for a finite element analysis to be chosen with unusual confidence. Also, the large amount of instrumentation and sustained monitoring of the trial embankment enabled several comparisons between finite element analysis and observed behaviour to be made. The Porto Tolle case history therefore provides an excellent opportunity for comparing finite element analysis with reliable observed behaviour.

This Chapter is divided into three main Sections. Firstly, the Porto Tolle site and construction of the trial embankment are discussed. Secondly, analyses of axisymmetric and plane strain unit cells are presented; these analyses allow an assessment to be made of the matching procedure, developed in Chapter 5, for realistic soil conditions. Finally, a full plane strain analysis is presented and compared with the published observed behaviour.

## **6.2. Porto Tolle**

### **6.2.1. Subsurface Conditions**

The Porto Tolle site was subjected to intensive investigation (Croce et al, 1973; Garassino et al, 1979; Jamiolkowski et al, 1980; Hansbo et al, 1981; Jamiolkowski and Lancellotta, 1984). These investigations showed the subsoil, Figure 6.1, to consist of 6-9m of medium dense sand and silty sand, a 20-23m deep layer of silty-clay beneath which is a deep deposit of dense silty sand. The silty-clay deposit is normally consolidated, Figure 6.2, and contains very thin lenses and seams of silty sand from a few millimetres to a few centimetres thick. Jamiolkowski and Lancellotta (1984) observed that the permeable inclusions were discontinuous and that the clay layer behaved as a single consolidating stratum with drainage occurring towards the top and bottom. In the upper and lower part of the clay layer organic materials and gas pockets were observed. A summary of the published soft clay soil parameters is presented in Table 6.1. For the upper and lower silty sands only descriptive information was available.

Reclamation plants maintain the ground water level at 2-2.5m below mean sea level.

### **6.2.2. Construction of the Trial Embankment**

The original elevation of the site was between 1 and 2m below mean sea level; before construction of the embankment the ground level was raised, using a sand fill, to a level of 1-0.5m below mean sea level. All finite element analyses assume that the original ground level is at 0.5m below mean sea level and that pore pressures due to the sand layer completely dissipate before commencement of construction. This assumption was adopted as the vertical drains were installed in November 1976, over 4 months before construction started.

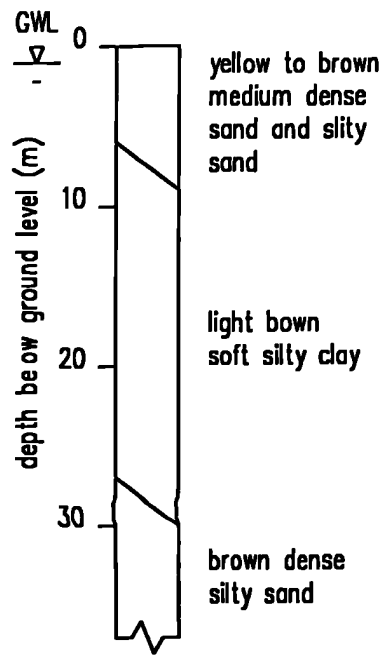


Figure 6.1 - Soil profile (after: Jamiolkowski and Lancellotta, 1984).

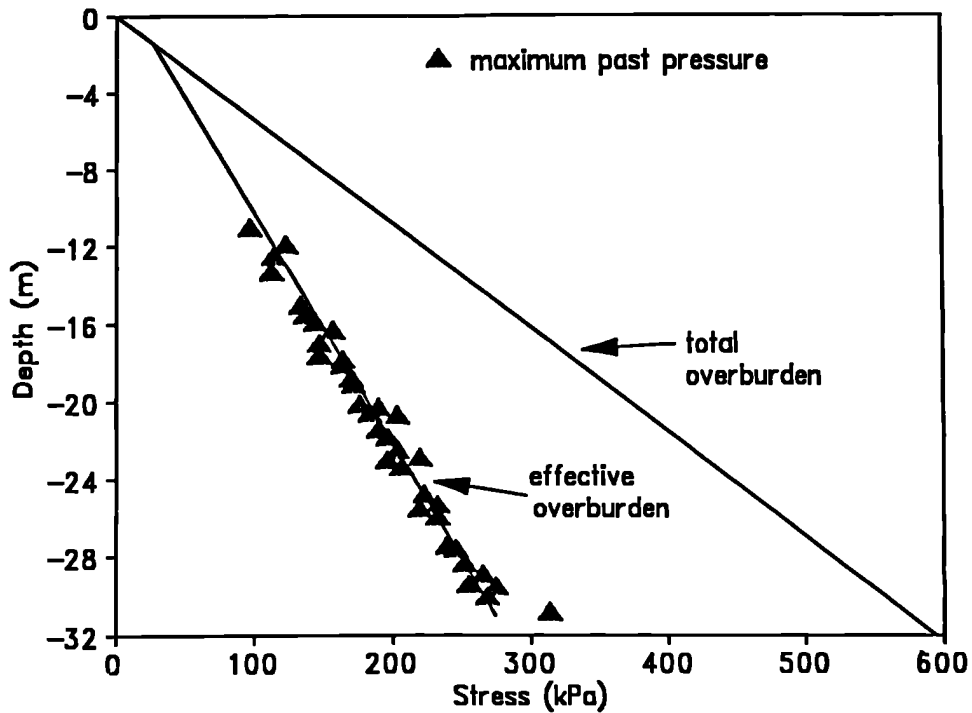


Figure 6.2 - Stress history and maximum overburden from one-dimensional consolidation tests according to Casagrande's procedure (after: Jamiolkowski and Lancellotta, 1984)

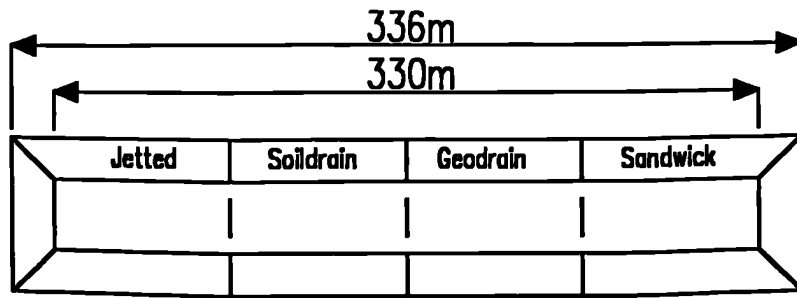
PARAMETER	VALUE
Compression Index	$C_c = 0.30 - 0.45$
$\phi'$ Triaxial compression	$\phi'_{ax} = 29^\circ$
$\phi'$ Plane strain compression	$\phi'_{pl} = 32^\circ$
Horizontal permeability	$k_h = 7.7 \times 10^{-9} - 9.6 \times 10^{-10} \text{ m/s}$
Vertical permeability	$k_v = 1.5 \times 10^{-10} - 5.5 \times 10^{-10} \text{ m/s}$
Total unit weight	$\gamma = 18.6 \text{ kN/m}^3$
Natural water content	$w_n = 35 - 40\%$
Liquid limit	LL=50 - 60%
Plasticity index	PI=25 - 40%

**Table 6.1 - Summary of Porto Tolle soft clay material properties.**

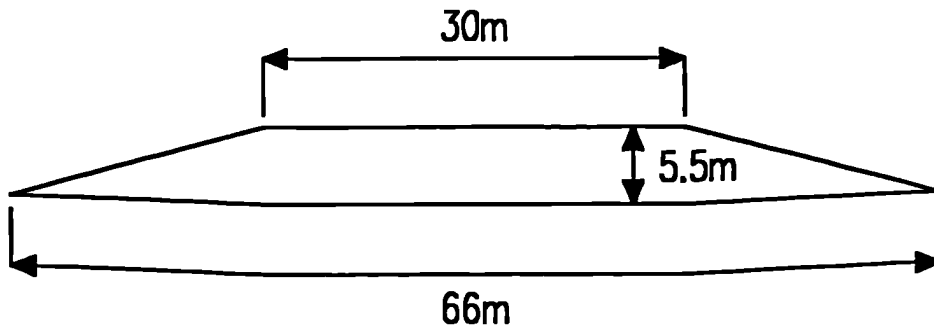
The cross section and plan view of the embankment are shown in Figure 6.3a and b and the rate of construction in Figure 6.3c. Four types of vertical drain were installed in the clay stratum, Figure 6.3b. The finite element analyses concentrate on the Geodrain area, although little variation in performance of the four zones was observed (Hansbo et al, 1981). The embankment was constructed at a constant rate to a height of 5.5m in a period of 3.5 months; this implies a load due to the fill of  $99 \text{ kN/m}^2$  beneath the crest (unit weight of fill  $18 \text{ kN/m}^3$ , Jamiolkowski and Lancellotta, 1984). A consolidation period of 10 months was then allowed before removal of the embankment.

### 6.2.3. Vertical Drains

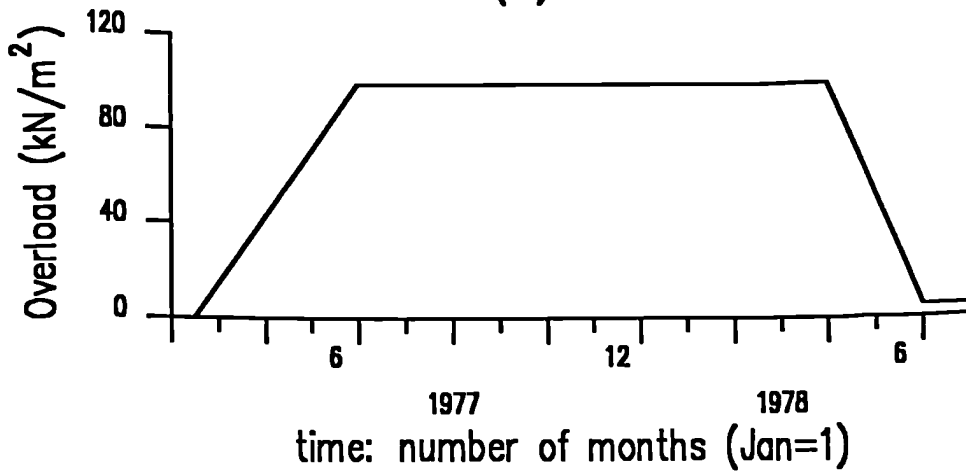
The vertical drains were installed in a triangular grid as reported by Mogilarardi and Torstensson (1977). The Geodrain spacing was 3.80m and the equivalent diameter of the drain was 62mm (Jamiolkowski et al, 1983). This drain spacing results in an area of influence of each drain of 3.99m and



(a)



(b)



(c)

Figure 6.3 - Porto Tolle trial embankment: (a) Plan view; (b) Cross-section; (c) Construction schedule.

therefore the unit cell radius is 1.995m.

No information regarding the discharge capacity of the drains was available and for the initial finite element analyses conservative values were assumed.

#### **6.2.4. Instrumentation**

The trial embankment was heavily instrumented with settlement plates, several types of piezometer and vertical and horizontal inclinometers (Garassino et al, 1979). Field measurements were taken during the construction and consolidation stages.

### **6.3. Unit Cell Analyses**

A series of fully coupled consolidation analyses has been performed. The aims of these analyses were, firstly, to assess the likely affect of the well resistance of the vertical drain and, secondly, to assess the quality of the matching procedure developed in Chapter 5 under more realistic soil conditions. In all of these analyses only the clay layer, Figure 6.1, has been modelled.

#### **6.3.1. Finite Element Mesh and Material Parameters**

The finite element mesh and boundary conditions used for the axisymmetric unit cell analyses are shown in Figure 6.4.

The clay layer was modelled using modified Cam-clay (Roscoe and Burland, 1968). The material parameters were obtained from the published data, summarized in Table 6.1, as follows. The compression index varies between 0.30 and 0.45, corresponding to a  $\lambda$  of 0.13-0.195. A single value,  $\lambda=0.16$ , was used in all analyses; this approximates to the mean of the range and also agrees well with an empirical relationship between  $\lambda$  and plasticity index proposed by Yudhbir and Wood (1989). For many clays  $\kappa$  is

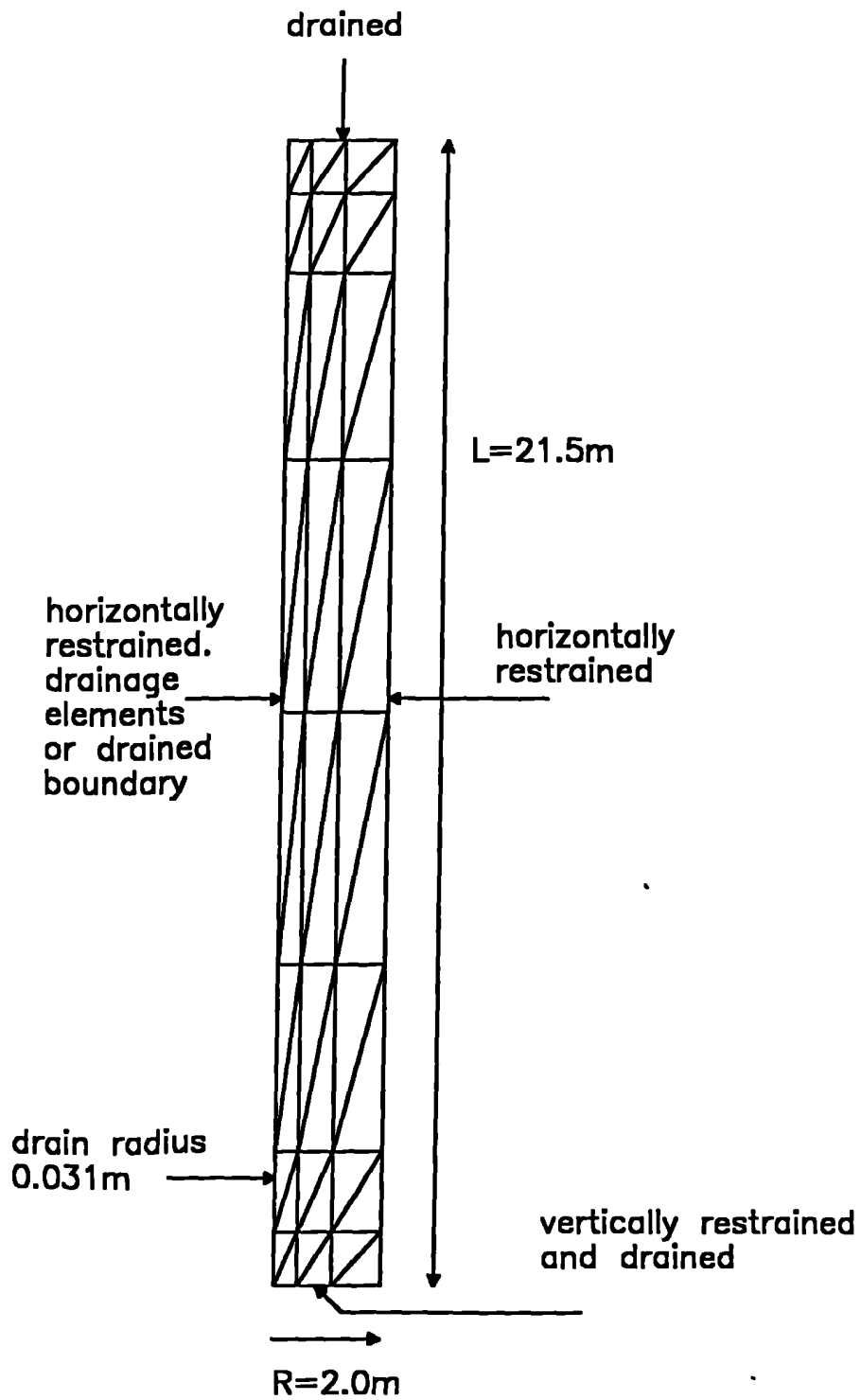


Figure 6.4 - Mesh used for axisymmetric finite element analyses.

approximately 20% of  $\lambda$  (Wroth, 1984), therefore,  $\kappa$  was estimated as 0.032. To ensure that the initial finite element voids ratio was approximately correct a value for  $\Gamma$  of 2.58 was used. To ensure that the predicted undrained shear strengths in plane strain and axisymmetry were correct, Section 6.3.3, different values of  $M$  were used (see Appendix A). The values were derived from the angle of shearing resistance,  $\phi'$ , in triaxial and plane strain compression tests as  $M_{ax}=1.16$  and  $M_{pl}=0.92$ , which correspond to  $\phi'_{ax}=29^\circ$  and  $\phi'_{pl}=32^\circ$  (where the subscripts ax and pl refer to axisymmetry and plane strain respectively). A typical value for the Poissons ratio,  $\nu'=0.3$ , was used (Tomlinson, 1986). The horizontal and vertical permeability parameters,  $k_h=4.1 \times 10^{-9} \text{m/s}$  and  $k_v=3.5 \times 10^{-10} \text{m/s}$ , were the averages of the respective ranges which were based on a combination of field and laboratory tests.

The above parameters are summarised in Table 6.2.

Parameter	Value
$\lambda$	0.16
$\kappa$	0.032
$\Gamma$	2.58
$M_{ax}$	1.16
$M_{pl}$	0.92
$\nu'$	0.3
$k_h$	$4.1 \times 10^{-9} \text{m/s}$
$k_v$	$3.5 \times 10^{-10} \text{m/s}$

**Table 6.2 - Summary of parameters used to model Porto Tolle clay.**

### **6.3.2. In Situ Stresses**

The vertical effective and total stresses were derived using a unit weight for the soil of  $18.6\text{kN/m}^3$ , both above and below the water table which was assumed to be 1.4m below ground level. The coefficient of earth pressure at rest was calculated according to modified Cam-clay theory, Appendix A, as  $(K_0)_{ax}=0.64$  and  $(K_0)_{pl}=0.74$ . These values are considerably higher than published,  $K_0=0.48-0.54$  (Garassino et al, 1979), but must be used if the correct response to one-dimensional loading is to be obtained. To calculate the size of the initial yield locus the layer was modelled as be normally consolidated, Figure 6.2.

### **6.3.3. Undrained Analyses to Assess Shear Strength**

Two analyses were carried out to check that the undrained shear strength of the soil was modelled correctly in both plane strain and axisymmetry. The mesh shown in Figure 6.4 was used with all boundaries undrained, the right hand boundary was incrementally displaced and the deviator and shear stress of the elements monitored. When no increase of stress occurred for an increment of displacement the unit cell was said to have failed. The finite element predicted undrained shear strength profiles are plotted against the theoretical values (using equations from Appendix A) in Figure 6.5.

The results presented were obtained using 50 increments with total displacements of 0.08 and 0.25m for the axisymmetric and plane strain analyses respectively. Additional analyses with 200 increments and double the number of elements in both the vertical and horizontal direction produced negligible differences in the predicted undrained shear strengths

### **6.3.4. Axisymmetric Unit Cell Consolidation Analyses**

Two axisymmetric analyses were conducted using the mesh shown in Figure 6.4. The embankment loading was represented by a uniform stress of  $99\text{ kN/m}^2$  applied to the top boundary of the mesh. The load was applied

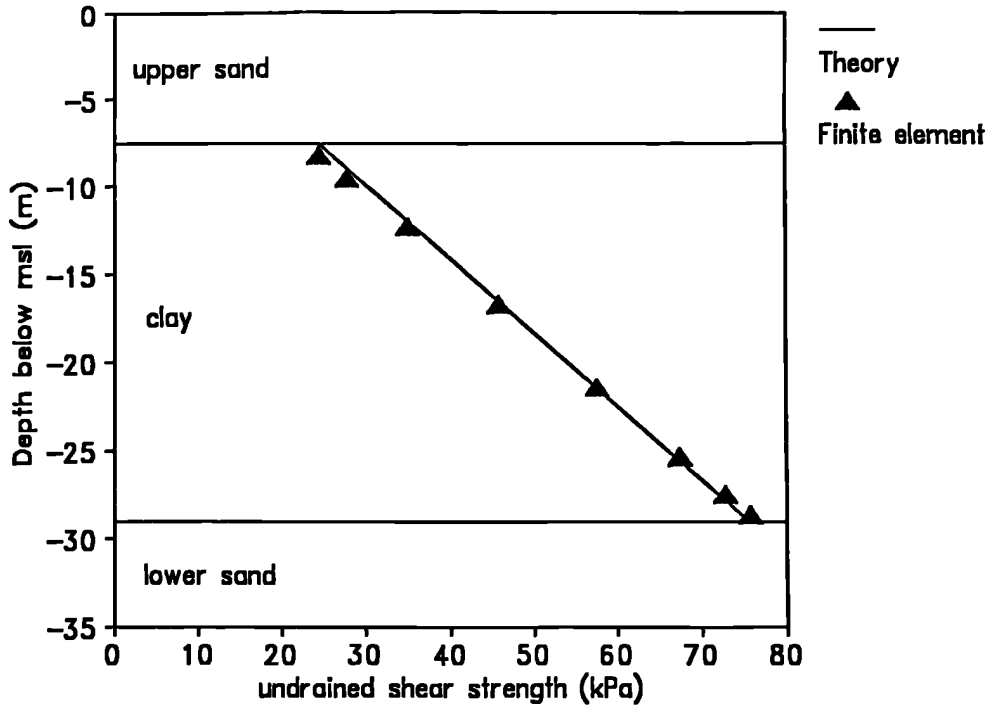


Figure 6.5a - Undrained shear strength in plane strain.

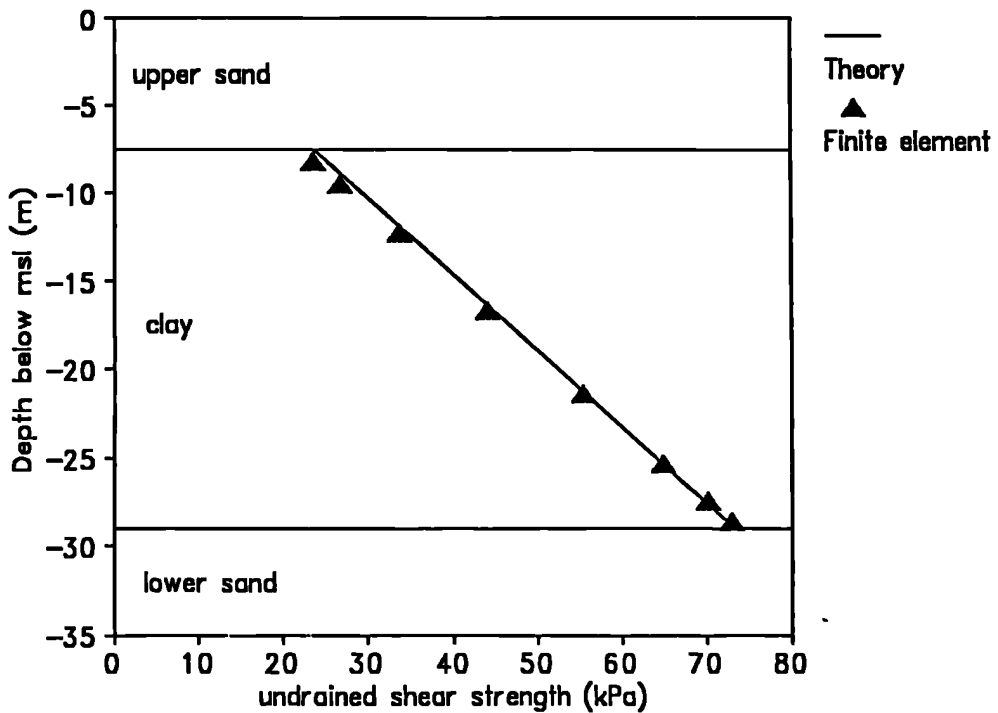


Figure 6.5b - Undrained shear strength in axisymmetry.

at a constant rate over 50 equal time increments totalling 3.5 months. The consolidation was modelled using 50 equal time increments totalling 10 months.

The first analysis used drainage elements, Section 3.4, to model the vertical drain, with a discharge capacity of  $140\text{m}^3/\text{year}$  corresponding to the minimum likely value (Holtz et al, 1991). The second modelled the drain as infinitely permeable by setting the excess pore pressure to zero at the left hand mesh boundary, Figure 6.4. The average surface settlement for each analysis is plotted against time in Figure 6.6; as can be seen even the lowest likely discharge capacity has a negligible effect on the rate of consolidation. The maximum hydraulic gradient in the drain, used for the first analysis, occurred transiently near the surface and was equal to 0.11. As the actual discharge capacity is likely to be significantly higher than that assumed, the effect of well resistance can be ignored and the vertical drain modelled as a boundary with zero excess pore pressure.

In the remainder of this Chapter the analysis without vertical drainage elements will be referred to as the axisymmetric analysis.

### **6.3.5. Comparison of Finite Element and Observed Behaviour**

The rate of consolidation of the axisymmetric unit cell can be compared with the observed pore pressure dissipation and rate of surface settlement during the trial. The unit cell analyses neglect the sand layers and the lateral deformation of the soil; however, as the sand is relatively incompressible and the relevant observations were made beneath the embankment centreline these effects were considered negligible.

The excess pore pressure at the periphery of the unit cell is compared with observed values in Figures 6.7a and b for depths of 19.7 and 12.6m below ground level respectively; the peripheral value was used for comparison as the piezometers were placed at the centre of the triangularly spaced drains.

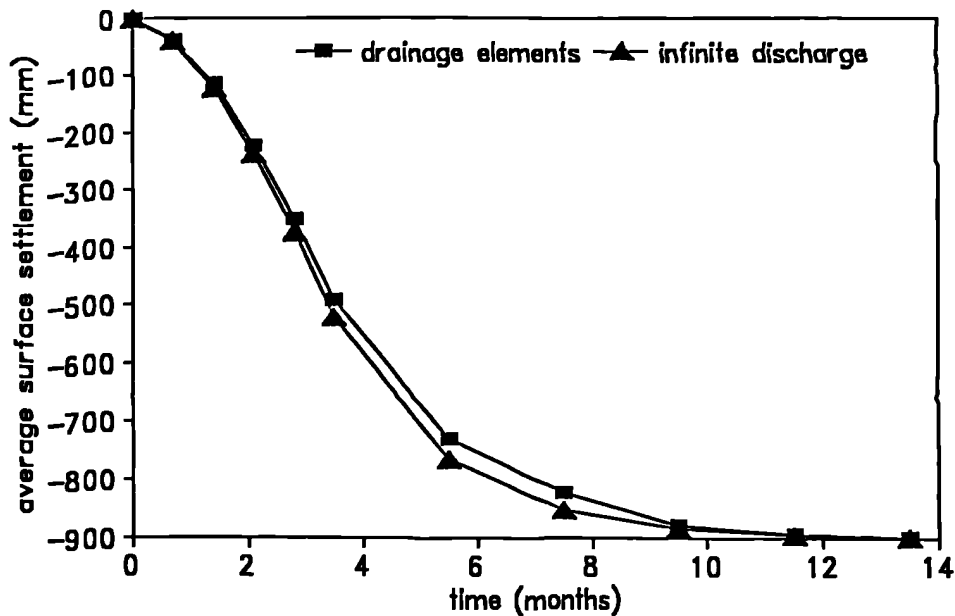


**Figure 6.6 - Axisymmetric unit cell consolidation based on average surface settlement.**

The settlement of the top right hand corner of the unit cell is compared with observed values in Figure 6.8.

During construction the agreement between predicted and observed pore pressures and settlements is very good, therefore validating the choice of material parameters. However, during the ten month consolidation period, although the predicted settlement is still very close to that observed Figure 6.8, the predicted pore pressures show a marked deviation from the monitored values, Figure 6.7. The finite element predictions of both pore pressures and settlements are consistent, with the settlement reaching a final constant value as the excess pore pressures approach zero. This trend is not seen in the observed values. Although the observed settlement appears to be levelling off, implying the end of primary compression, there is little dissipation of the excess pore pressure after the end of construction. Jamiolkowski and Lancellotta (1984) suggested that the observed pore

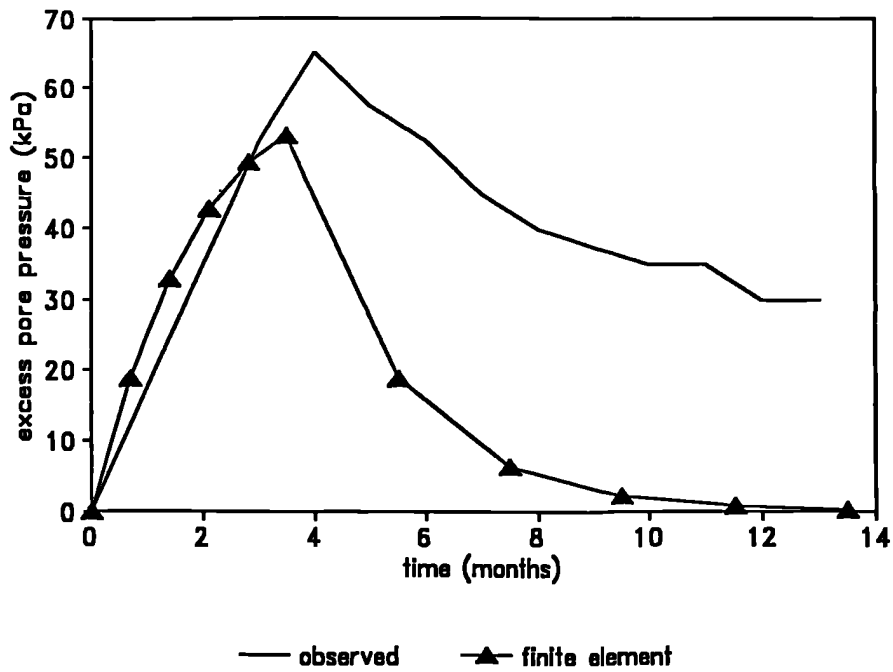


Figure 6.7a - Excess pore pressure 19.7m below ground level on the centreline of the embankment.

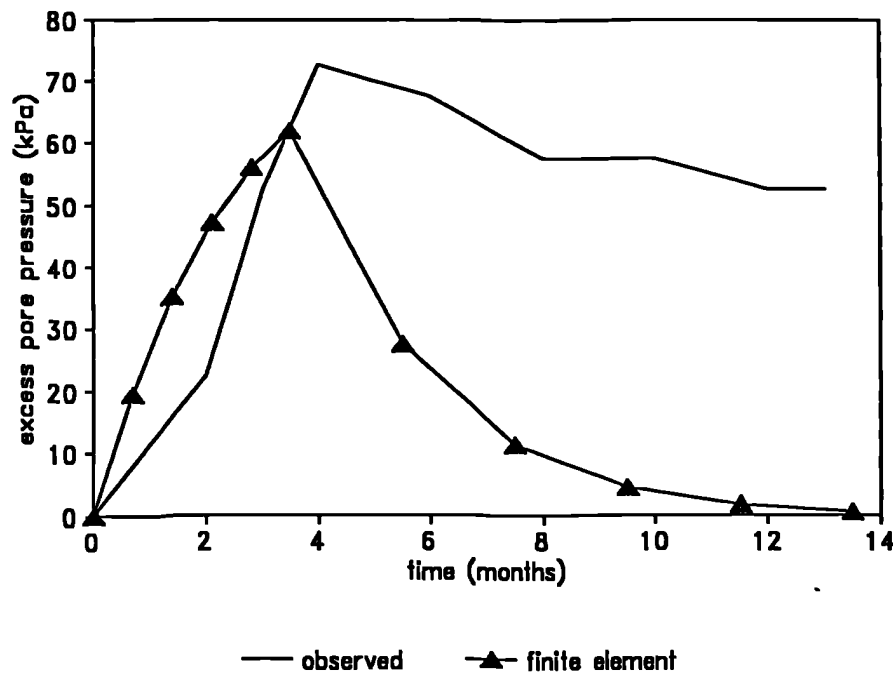


Figure 6.7b - Excess pore pressure 12.6m below ground level on the centreline of the embankment.

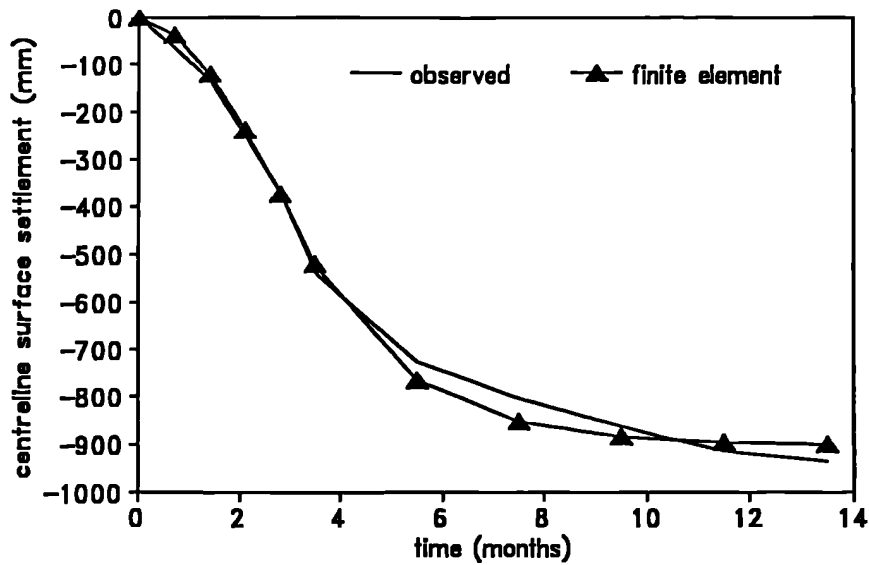


Figure 6.8 - Rate of surface settlement at centreline of the embankment.

pressures during the consolidation stage may have been unreliable, and stated that the unsatisfactory long term performance of the piezometers may have been due to the presence of organic gas. However, the malfunction of the piezometers may have masked the effect of phenomena, such as destructuring of the soil (Burland, 1990), which would also have resulted in higher observed excess pore pressures than predicted by the finite element analysis. As the monitored excess pore pressures during the consolidation stage may be in error, the material parameters used for the axisymmetric analysis were retained in further analyses.

From Figure 6.7 it is interesting to note that the pore pressure at 19.7m below ground level is lower than at 12.6m below ground level. This behaviour appears incorrect as with an infinitely permeable drain the rate of consolidation of an isotropic material should be the same at every depth, and the effect of the small vertical permeability would imply lower pore

pressures closer to the top or bottom boundaries. The cause of this apparent anomaly is the way in which the modified Cam-clay model has been implemented in CRISP. The coefficient of consolidation depends on both the permeability and the compressibility of the material; in CRISP the permeability is constant for a given material but the compressibility, which is dependent on both stress level and voids ratio, varies with depth. This results in the coefficient of consolidation reducing with depth in a modified Cam-clay analysis and is the cause of the above variation in the dissipation of excess pore pressure with depth. At Porto Tolle this variation was not large but as will be seen in Chapter 7 this effect may cause a much larger variation in other circumstances.

### **6.3.6. Plane Strain Unit Cell Consolidation Analyses**

Two plane strain analyses have been carried out to assess the quality of the matching procedure developed in Chapter 5. In the first analysis the width of the unit cell has been changed and the soil permeability left the same as for the axisymmetric analysis; this is referred to as geometry matching. In the second analysis the horizontal permeability has been changed whilst maintaining the same unit cell dimensions; this is referred to as permeability matching.

Details of the procedure are given in Chapter 5. Applying Equations 5.10 and 5.14, in which the effect of smear and well resistance has been ignored, the plane strain unit cell width for the geometry matched case is  $B=4.5\text{m}$  and the horizontal permeability for the permeability matched analysis is  $k_h=8.0 \times 10^{-10}\text{m/s}$ .

The two analyses in plane strain were conducted in the same way as those in axisymmetry. The vertical drain was again modelled as infinitely permeable. Comparisons of the average surface settlement and average excess pore pressure at mid depth are shown in Figures 6.9 and 6.10. The average values were calculated using the trapezium rule. Only the geometry

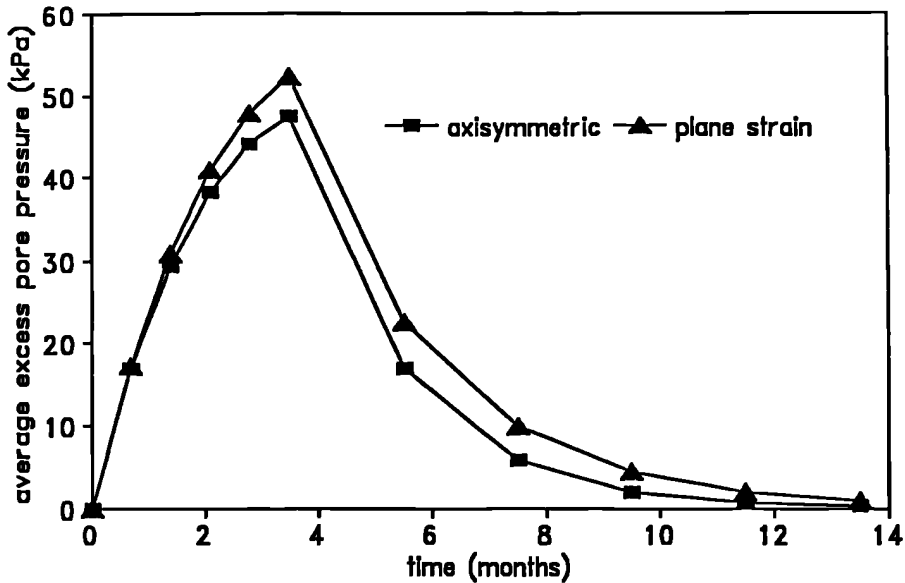


Figure 6.9 - Unit cell rate of consolidation based on the average excess pore pressure at mid-depth.

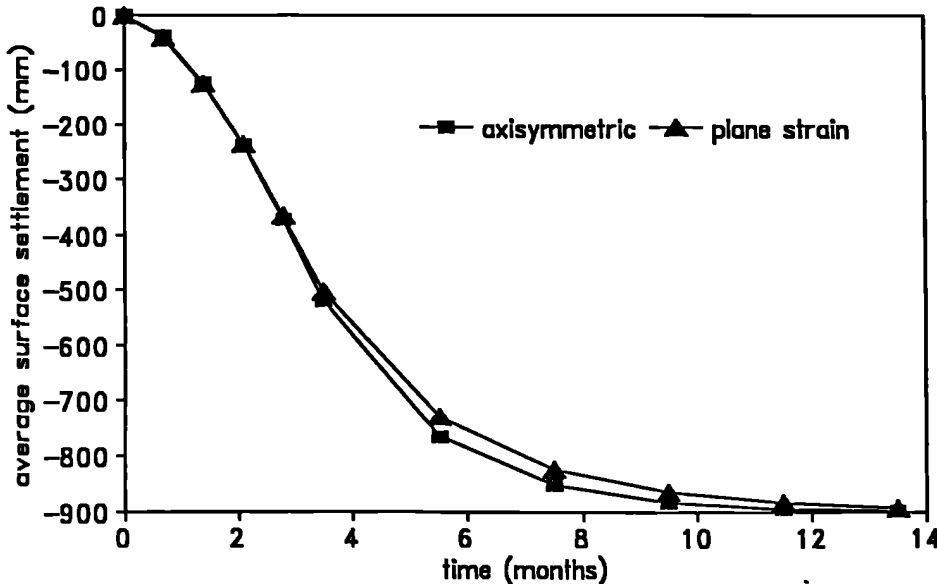


Figure 6.10 - Unit cell rate of consolidation based on the average surface settlement.

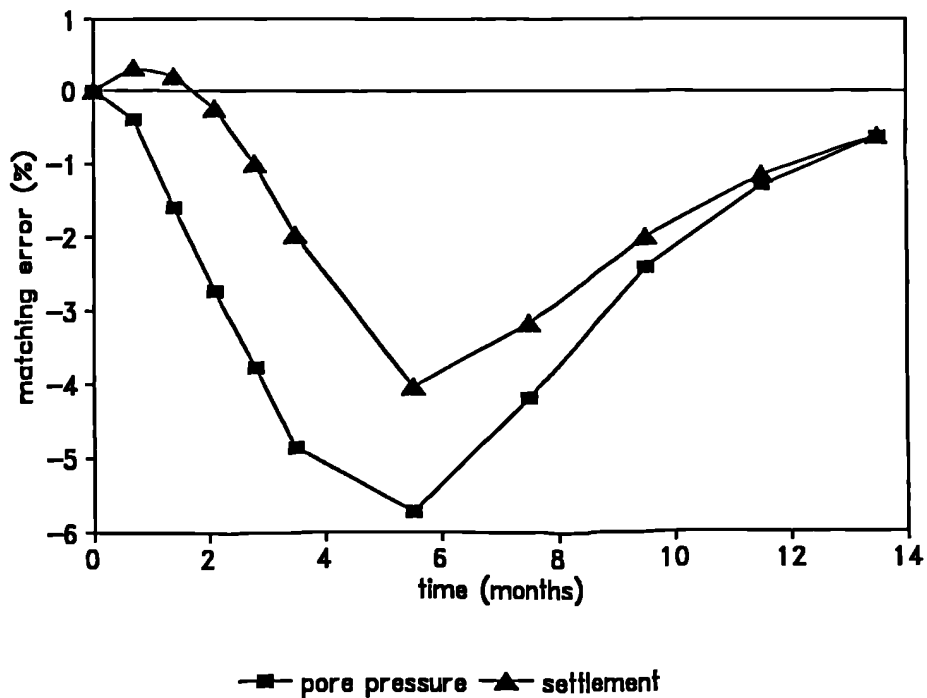


Figure 6.11 - Unit cell rate of consolidation matching errors.

matched analysis has been plotted as the difference between the two plane strain analyses was too small to be noticeable.

For both settlement and pore pressure the agreement between axisymmetric and plane strain analyses is very good. It is possible to define matching errors as

$$(\text{ERROR})_{PWP} = \frac{\text{DIFFERENCE IN PREDICTED AVERAGE EXCESS PORE PRESSURE}}{\text{APPLIED LOAD}} \times 100 \quad \dots\dots(6.1)$$

$$(\text{ERROR})_{SET} = \frac{\text{DIFFERENCE IN PREDICTED AVERAGE SETTLEMENT}}{\text{FINAL SETTLEMENT}} \times 100 \quad \dots\dots\dots(6.2)$$

These errors are plotted against time in Figure 6.11 from which it can be seen that the matching error is never greater than 6%.

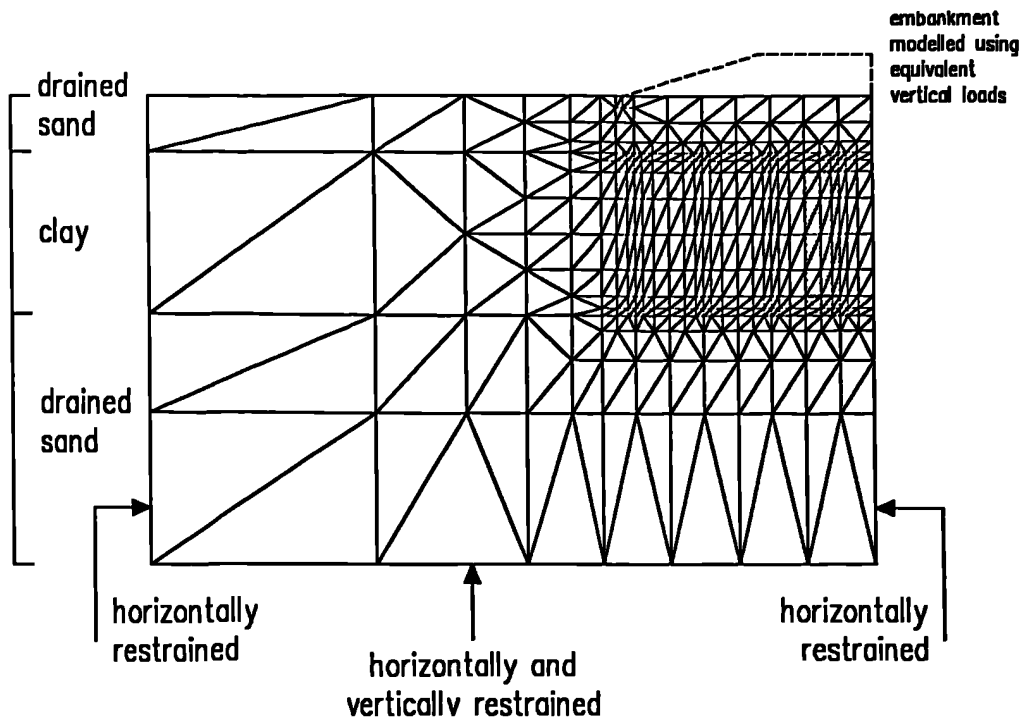


Figure 6.12 - Mesh used for full plane strain analysis.

## 6.4. Full Plane Strain Analysis

Having established that well resistance was not a significant factor and that the proposed matching procedure was reliable a full plane strain analysis was carried out.

### 6.4.1. Finite Element Mesh and Boundary Conditions

The finite element mesh used for the full plane strain analysis is shown in Figure 6.12. Both the upper and lower sands have been modelled as drained layers. The unit cell mesh, Figure 6.4, has been stretched to a width of 4.5m, as used in the geometry matched unit cell analysis, and repeated to model the area of soil improved with vertical drains. The boundary conditions used in the analysis are also shown. The embankment was

modelled using vertical loads applied in the same number of increments and time as for the unit cell analyses.

## 6.4.2. Material Parameters

### Clay Layer and Drains

The material parameters for the clay layer were as defined in Table 6.2. The drains were modelled as lines of nodes at which no excess pore pressure could develop, thus representing an infinitely permeable drain (Section 6.3.4).

### Sand Layers

Only descriptive information was available for the upper and lower sand layers and it was therefore necessary to adopt typical parameter values to model these materials. The layers were modelled as drained elastic-perfectly plastic materials for which five parameters are required: the cohesion ( $c'$ ), the angle of shearing resistance ( $\phi'$ ), the Young's modulus ( $E$ ), the Poissons ratio ( $\nu'$ ) and the unit weight ( $\gamma$ ). The cohesion was taken to be zero,  $c'=0$ . The angle of shearing resistance was defined as  $\phi'=44.4^\circ$  following Jewell (1990). A typical value for the Poissons ratio under drained conditions was used,  $\nu'=0.2$ , (Lade, 1977). The unit weight of the sand was assumed to be the same as for the clay, i.e.  $\gamma=18.6\text{kN/m}^3$ . Again following Jewell (1990), the Youngs modulus for the soil was derived from an empirical relationship proposed by Hardin and Black (1966) for the initial elastic shear modulus of soil,  $G_i$ ,

$$G_i = 700 \frac{(2.17-e)^2}{(1+e)} \left( \frac{s'_v}{s'_r} \right)^{0.5} \dots\dots\dots(6.3)$$

where  $s'_r=100\text{kN/m}^2$  is included for dimensional consistency,  $s'_v$  is assumed to be equivalent to the mean effective stress ( $p'$ ) for plane strain conditions and  $e$  is the voids ratio, assumed equal to 0.5. Equation 6.3 was used to evaluate an initial shear modulus,  $G_i$ . In order to use a shear modulus more

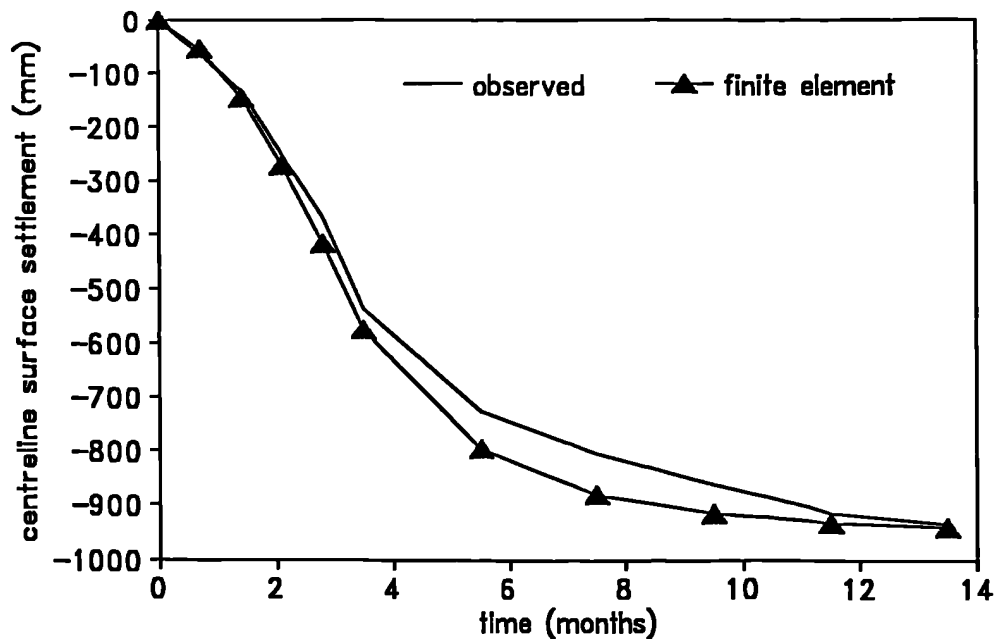


Figure 6.13 - Surface settlement at centreline.

appropriate to the strain levels that may develop in the embankment before yielding, a value for the shear modulus of  $G=0.5G_c$  was used. The Young's modulus was then related to the shear modulus as  $E=2(1+\nu')G$ .

Three sand layers were defined, namely:  $z=0-7.5\text{m}$ ,  $29-42\text{m}$  and  $42-62\text{m}$  below ground level and the Young's modulus values in these layers were  $5.9 \times 10^4$ ,  $14.5 \times 10^4$  and  $17.4 \times 10^4 \text{ kN/m}^2$  respectively.

### 6.4.3. Comparison of Observed and Predicted Behaviour

#### Settlement

The surface settlements on the embankment centreline are plotted in Figure 6.13. The observed and predicted values are in good agreement. However, while the predicted settlement has reached a steady value at the end of the analysis, indicating complete consolidation, the observed settlement is

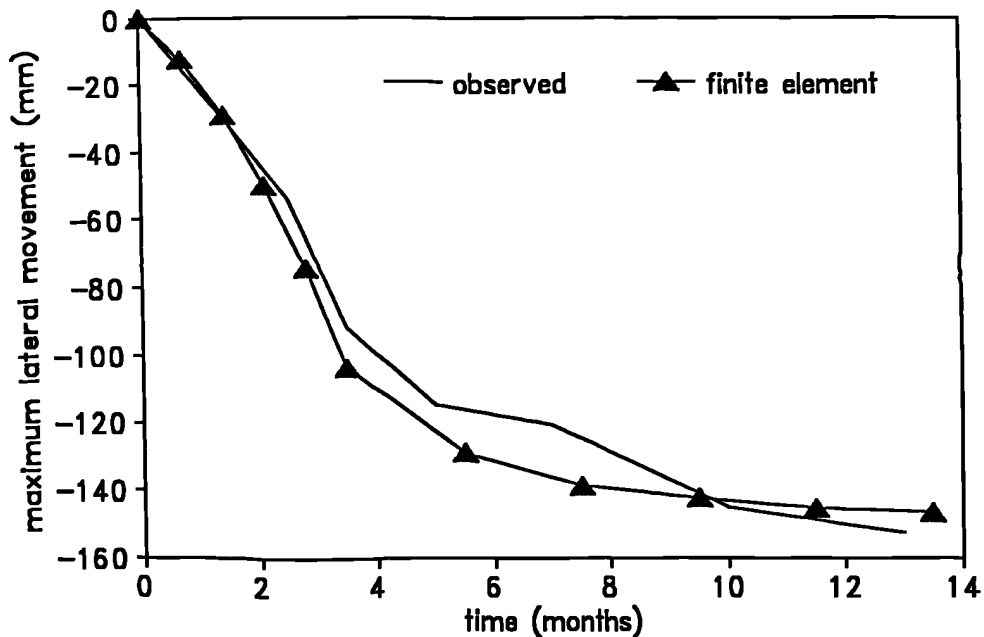


Figure 6.14 - Maximum horizontal displacement.

continuing at a reduced rate. This may be due to secondary compression. Garassino et al (1979) quoted a value for the coefficient of secondary compression of  $c_{\alpha}=0.46\pm 0.22\%$  measured in oedometer tests. If it is assumed that 90% consolidation occurs in 6 months and that secondary compression then starts, the estimated settlement over the remaining 7.5 months is approximately 15mm. This suggests that the inability of CRISP to model secondary compression is not a significant limitation in this case.

### Lateral Movement

An inclinometer was installed beneath the embankment approximately 9m from the toe. The development of the maximum lateral movement, which was predicted by the finite element analysis to occur at around 10m below ground level, is plotted in Figure 6.14. Again the agreement between analysis and observation is encouraging. The observed lateral displacement

has not reached a constant value at the end of the period considered; this may again be explained by the continued creep of the soil which is not modelled in the finite element analysis.

The lateral movement profiles at the end of construction and at the end of consolidation are plotted in Figure 6.15. The maximum values of lateral movement are in good agreement, although the observed small inward movement of the surface has been exaggerated in the finite element analysis. This may be a result of modelling the embankment simply using vertical loads which does not allow the development of outward shear stresses at the ground surface, as may occur in practice.

The inward movement cannot be explained as being caused simply by settlement of the embankment. If the embankment was assumed to remain the same length (33m) and the settlement increased linearly from the toe to the centreline value of 900mm, then the toe would move inwards by only 2mm. Most of the predicted inward movement must be caused by the initial elastic behaviour of the sand. It may be noted that for a footing moving rigidly into an elastic layer an inward movement at either end of the footing is predicted (Poulos and Davis, 1974).

### **Pore Pressure**

Piezometers were placed on the centreline of the embankment at depths of 19.7 and 12.6m below the surface. The piezometers were positioned at the centre of a triangle of drains so as to record the highest pore pressures. In Figure 6.16 comparisons of the observed and finite element predicted pore pressures are shown.

The excess pore pressure calculated from the finite element program is for a plane strain analysis and as discussed in Chapter 5 the matching procedure ensures that the average pore pressure across the axisymmetric and plane strain unit cell are equal at every depth and at every time. However, the distribution of pore pressure across each unit cell is not the

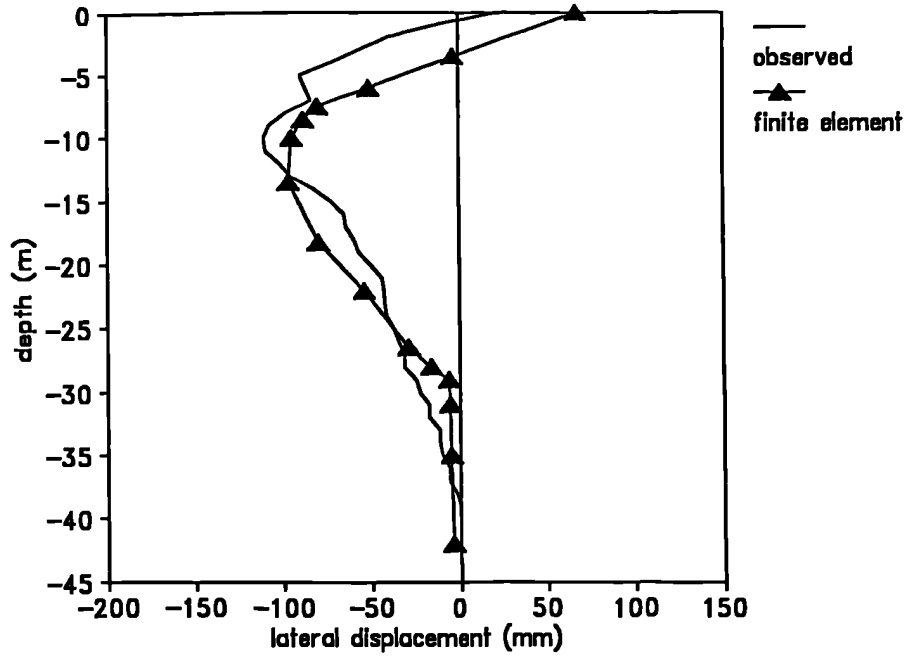


Figure 6.15a - Lateral movement profile at the inclinometer position at the end of the construction stage.

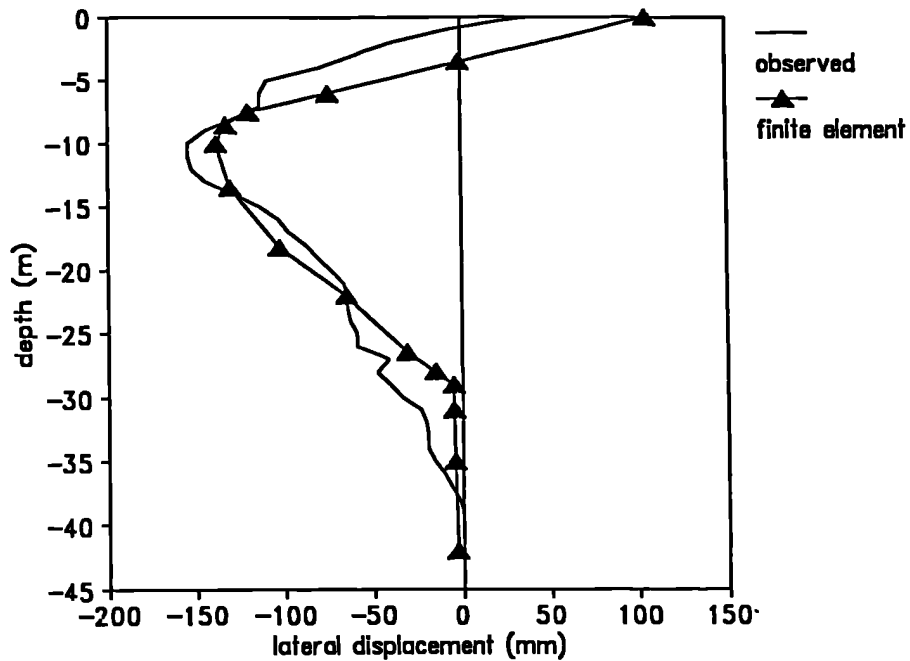


Figure 6.15b - Lateral movement profile at the inclinometer position at the end of the consolidation stage.

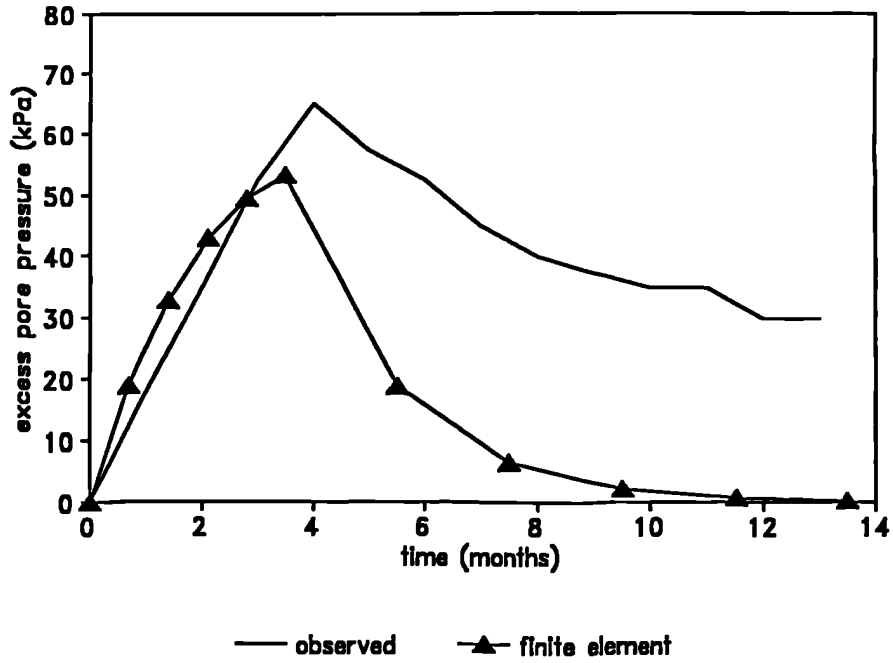


Figure 6.16a - Excess pore pressure 19.7m below ground surface on centreline.

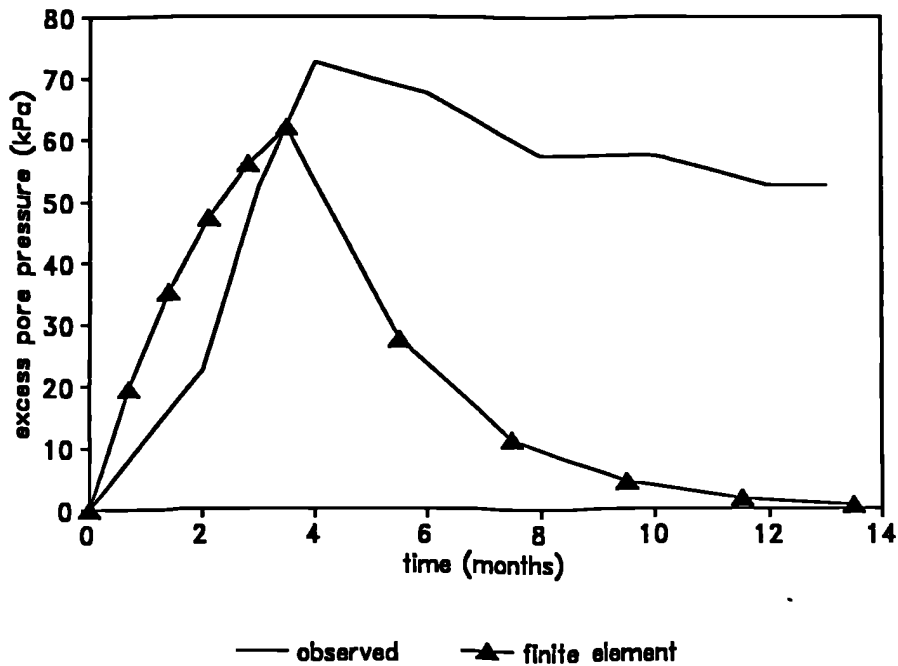


Figure 6.16b - Excess pore pressure 12.6m below ground surface on centreline.

same and in the present case, at the periphery of the unit cell, the axisymmetric pore pressure is only 72% of that predicted in plane strain, as predicted using Equation B33, Appendix B. It is therefore necessary to correct the plane strain pore pressure at the periphery of the unit cell by multiplying by a factor of 0.72 before comparison with the observed data can be made.

From Figure 6.16 it can be seen that the predicted excess pore pressures during construction are in good agreement with those observed. However, as seen in the axisymmetric unit cell analyses, Section 6.3.5, the agreement after the end of construction is not good. As previously discussed the likely cause of this discrepancy is the unsatisfactory long term performance of the piezometers due to the presence of organic gas, resulting in incorrect recorded values. However, other factors may result in an increased observed excess pore pressure (Eg. destructuring of the subsoil) and should ideally be considered in future analyses.

## **6.5. Summary**

The matching procedure developed in Chapter 5 has been applied to a normally consolidated clay deposit modelled using modified Cam-clay. The comparisons of the rate of consolidation based on both average surface settlement and average pore pressure at the mid depth of axisymmetric and plane strain unit cells are good. The matching procedure has therefore been shown to be capable of providing an accurate representation of soil improved using vertical drains analysed in plane strain.

A full plane strain analysis of the Porto Tolle trial embankment has been carried out in which the matching procedure was used to calculate the spacing of the vertical drains in plane strain. The finite element predicted vertical and lateral displacements and pore pressure on the centreline are, with the exception of excess pore pressures after construction, in good agreement with the observed values. The study shows that with accurate

soil parameters obtained from high quality field and laboratory tests and with careful finite element modelling accurate predictions of the behaviour of soils improved with vertical drains can be made.

# 7. Multi-Stage Embankment Construction

## 7.1. Introduction

The maximum single stage height of an embankment, with a given side slope length, built on soft clay can be estimated using plasticity theory (as described in Chapter 4). If the required embankment height is greater than this then a multi-stage construction approach could be used in which the subsoil is allowed to consolidate and gain strength between each, of several, loading stages. Vertical drains are often installed in the subsoil to increase the rate of consolidation and therefore shorten the required consolidation stages.

The design of a multi-stage embankment requires the accurate prediction of the strength increase of the subsoil and the application of the correct analysis method to each loading stage. Three approaches have been summarized by Ladd (1991).

- 1 Total stress analysis - Construction and failure are assumed to occur in a sufficiently short time so that the strength increase of the subsoil is negligible. The shear strength of the subsoil is based on unconsolidated undrained laboratory tests or field vane shear tests. This method cannot take account of the increase of shear strength due to consolidation and is only applicable to a single lift embankment analysis.
- 2 Effective stress analysis - Effective strength parameters are measured in consolidated drained laboratory tests and insitu measured pore pressures are used to calculate the available shear strength along a potential slip surface. The implicit assumption is

that no excess pore pressures are generated during failure. However, observations indicate that embankment failures generally occur in a matter of minutes. This would imply the generation of significant pore water pressure during failure, thus reducing the effective stress and therefore the factor of safety from that which would be predicted from an effective stress analysis.

- 3 Undrained strength analysis - The effective stresses are used to predict the undrained shear strength of the subsoil. These strengths are then used in a total stress analysis. This procedure, proposed by Ladd (1991), Jardine and Hight (1987) and Leroueil et al (1990), allows for increases of strength in the subsoil and appreciates that failure is likely to occur sufficiently quickly so as to be undrained in nature.

The undrained strength analysis provides a logical method for the analysis of stage constructed embankments. However, the designer still has to decide how to estimate the effective stresses in the subsoil at any time and how to use these stresses to predict accurately the undrained shear strength before analysis of a loading stage. In this Chapter a finite element analysis of an idealized two stage construction is performed and the undrained shear strength increases of the subsoil are calculated. Simple methods of estimating the subsoil undrained shear strength increase are then proposed and compared with the finite element predictions. These simple methods are also used to predict undrained shear strength increases for the Porto Tolle case history presented in Chapter 6 and compared with the finite element results.

## **7.2. Idealized Two-Stage Construction**

An idealized reinforced embankment constructed in two lifts on a soft clay subsoil containing vertical drains has been modelled using CRISP. The finite element analysis has been used to predict the strength increase of the

subsoil after a period of consolidation. The finite element analyses were carried out in conjunction with limit equilibrium analyses, of the same idealized embankment, performed by Jewell (1991)<sup>1</sup>.

### **7.2.1. Finite Element Analysis of Idealized Two-Stage Construction**

The material parameters and embankment geometry were chosen to be typical of embankments built over soft clay subsoils. Reinforcement at the base of the embankment and vertical drains in the subsoil were modelled. Fully coupled consolidation analyses have been performed in which the subsoil was allowed to consolidate with the embankment modelled as fully drained. The embankment was constructed in two lifts applied relatively quickly with a period in between in which significant consolidation occurred.

#### **Geometry**

The embankment and subsoil geometry are defined in Figure 7.1. The soft clay was assumed to overly a rough rigid layer. The heights of the first and second lift were calculated by Jewell (1990), using a limit equilibrium method, to provide a factor of safety of 1.1 at the end of each lift.

#### **Soft Clay Subsoil**

The soft clay was modelled using modified Cam-clay, with parameters:  $M_{PL}=0.7$ ,  $\lambda=0.25$ ,  $\kappa=0.05$ ,  $\Gamma=3.0$ ,  $\nu'=0.3$  and  $\gamma_{bulk}=18\text{kN/m}^3$ . Following Appendix A these parameters imply  $\phi'_{PL}=24^\circ$ ,  $K_{ONC}=0.83$  and  $(s_v/\sigma'_v)_{NC}=0.218$ .

An over-consolidated profile was modelled by assuming that the present water table at 1m below ground level had at some time previously been lowered to 2m below ground level. The above material parameters and stress history defines the subsoil strength and initial stress conditions shown in Figure 7.2.

---

<sup>1</sup> Private communication.

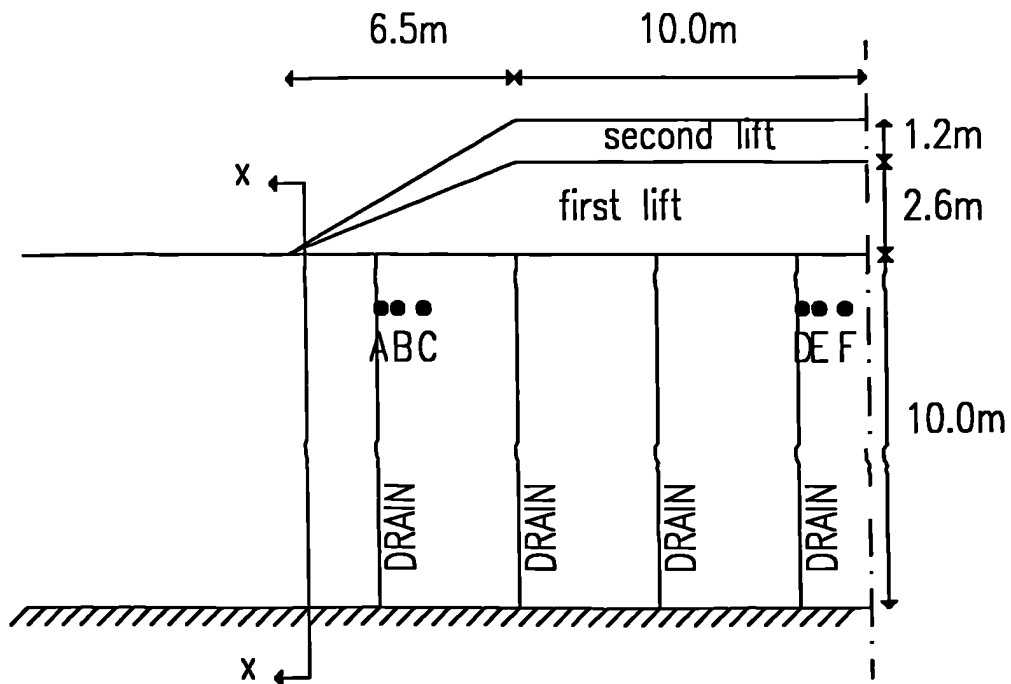
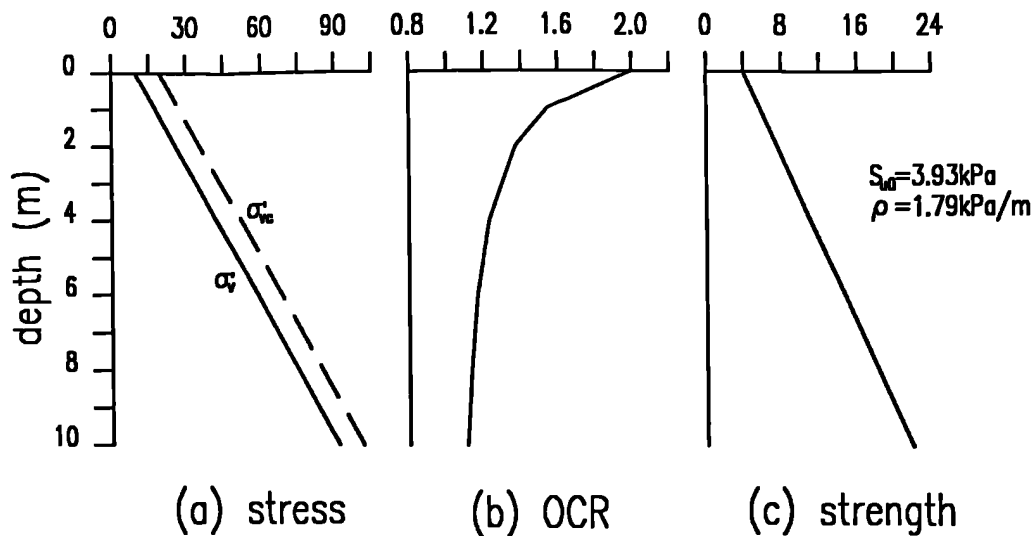


Figure 7.1 - Idealized two-stage embankment geometry.

The horizontal permeability was  $k_h=3 \times 10^{-9} \text{m/s}$  with a negligible vertical permeability so that flow was predominantly towards the vertical drains, which were the only draining boundaries. Vertical flow was minimised so that the subsoil surface did not consolidate and gain strength quicker than the soil mass. Hansbo's (1981) equation for consolidation around a vertical drain could therefore be used to generate comparisons between simpler design methods and the finite element analyses.

#### Embankment Fill

The fill was modelled as a fully drained elastic-perfectly plastic material with a Mohr-Coulomb yield criterion representing a granular fill. The fill was defined as having a bulk density of  $\gamma_{\text{bulk}}=20 \text{kN/m}^3$  and elastic parameters:  $E=10^5 \text{kN/m}^2$  and  $\nu=0.2$ . The strength parameters were  $\phi'=30^\circ$  and  $c'=5 \text{kN/m}^2$ .



**Figure 7.2 - Idealized soil (a) stress (b) Over-consolidation ratio (c) Initial undrained shear strength.**

The small cohesion was necessary in order to avoid numerical problems in the finite element solution and is justifiable as some suction would be present in the fill material. This embankment model may allow tensile stresses to develop, so the analysis was monitored to ensure that any tensile stresses that developed did not become unrealistically large.

### Reinforcement

The reinforcement was modelled as a linear elastic material with a stiffness  $J=2000\text{kN/m}$  placed at the base of the embankment.

### Vertical Drains

A design consolidation period of 6 months was allowed in which a system of vertical drains would produce 60-70% consolidation. Using Hansbo's (1981) equation for the consolidation of soil around a vertical drain and using a typical effective drain diameter of 65mm (Jamiolkowski et al, 1983) a drain spacing of 2.5m was estimated to cause approximately 62% dissipation of

excess pore water pressure beneath the centre of the embankment. This calculation assumes that the drains have no well resistance and cause no smearing of the soil during installation and that the subsoil undergoes one-dimensional loading.

In the finite element analysis the drains were modelled as infinitely permeable by defining boundaries at which the excess pore pressures were set to zero. The matching procedure, Chapter 5, was used to provide a finite element drain spacing of 4m by modifying the horizontal subsoil permeability to  $k_h=1.77 \times 10^{-9} \text{m/s}$ . The positions of the drains in the finite element analysis are shown in Figure 7.1.

### **Soil/Reinforcement Interfaces**

In order to represent accurately the behaviour of the reinforcement it was necessary to model the (lower) subsoil/reinforcement and (upper) reinforcement/fill interfaces. The stiffness parameters of both interfaces were: normal stiffness,  $k_n=10^4 \text{kN/m}^2$  and, shear stiffness,  $k_s=10^6 \text{kN/m}^2$ . Stiffness values in this range have been shown by Kwok (1987) to produce satisfactory results.

The upper interface yield criterion was modelled with  $\phi=30^\circ$  and  $\delta=5 \text{kN/m}^2$  so that the full shear strength of the fill material was assumed to be mobilised along the upper interface at failure.

The lower interface yield criterion was modelled as purely cohesive with a value of  $\delta=3.93 \text{kN/m}^2$ , equal to the initial undrained shear strength of the subsoil surface, during the first lift and the consolidation stage. The interface strength was increased for the final lift to represent the enhanced subsoil surface strength. The increased interface shear strength was the average of the undrained shear strengths in the surface elements, of each unit cell, as shown in Figure 7.3.

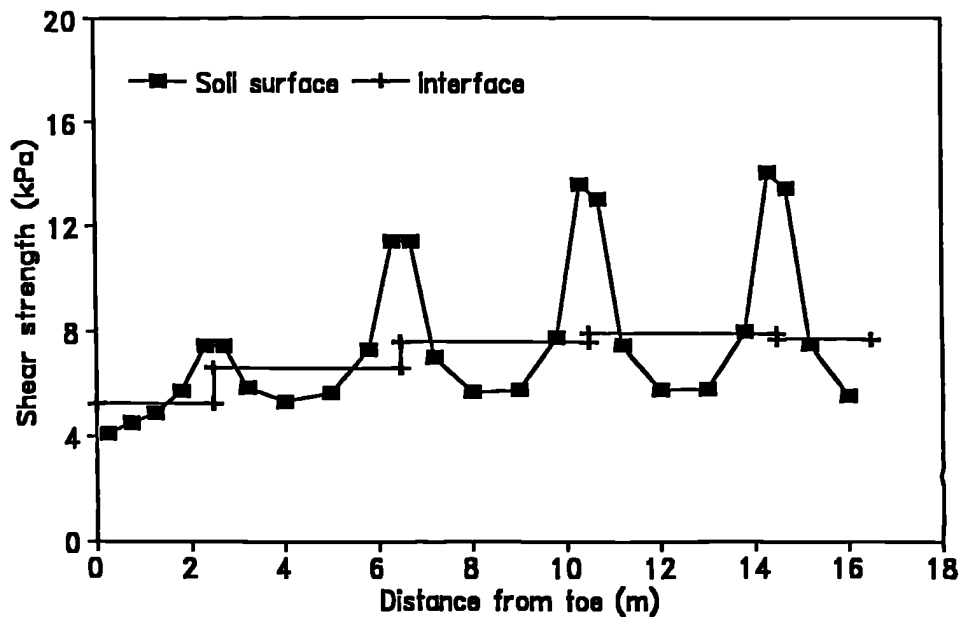


**Figure 7.3 - Lower interface shear strength after the consolidation stage.**

### Construction Sequence

The first lift of 2.6m was applied in 20 days, during which some consolidation of the elements adjacent to the drains occurred. A further 180 days was allowed in which the subsoil consolidated and gained strength. The embankment was then constructed at a steeper side slope, so that the crest position remained constant, to a height of 3.8m in 20 days, Figure 7.1.

Each of the loading stages was modelled using 200 increments and the consolidation period occurred over 50 time increments of increasing size.

### Undrained Loading to Failure

At the end of both the first and second lifts an undrained analysis was carried out in order to assess the factor of safety. A uniform surcharge load was applied to the crest of the embankment, and increased until failure of

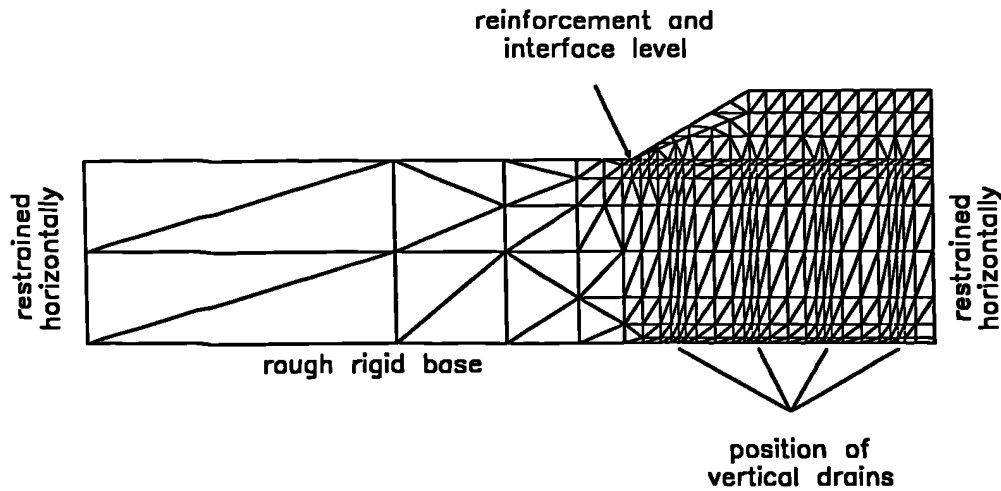


**Figure 7.4 - Finite element mesh and boundary conditions.**

the subsoil occurred. Failure was defined as the increment during which the increase in settlement was greater than the increase in the height of fill, represented by the surcharge loading. This definition of failure has been previously used by Rowe and Soderman (1987) and is discussed further in Section 7.2.2.

### **Finite Element Mesh and Boundary Conditions**

The mesh and boundary conditions used for the finite element analysis are shown in Figure 7.4. Four vertical drains have been modelled at the positions shown.

## **7.2.2. Finite Element Results**

### **Displacements**

The vertical displacements of points directly below the toe, the crest and the centreline on the surface of the subsoil are plotted against embankment

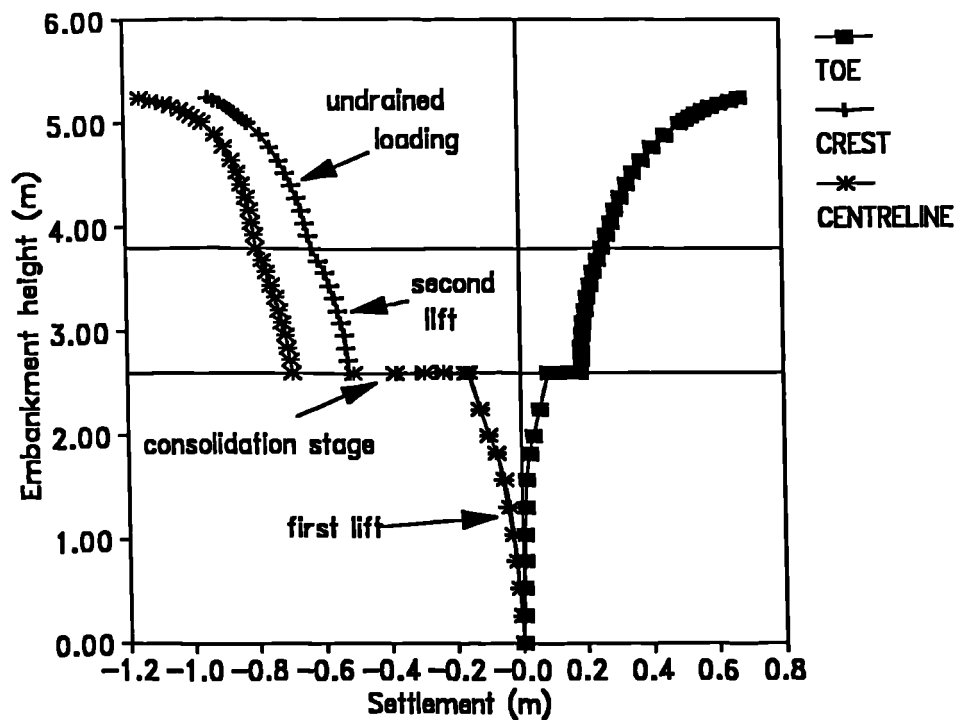


Figure 7.5 - Settlement of points at the subsoil surface against embankment height.

height in Figure 7.5. At the end of the first lift the settlement response is non-linear indicating significant yielding of the subsoil. During the consolidation stage significant settlement occurs with no increase of embankment height as the subsoil consolidates and gains strength. The final lift, to 3.8m, again shows a non-linear response. Beyond a height of 3.8m the undrained surcharge loading causes large displacements, with the curves for the three positions flattening out and indicating the approach of failure.

A change of gradient of the crest and centreline settlement results can be seen when the analysis changes from consolidated to undrained, i.e. at the end of the second lift and the start of surcharging. A steeper settlement load curve would be expected in an undrained analysis as the large bulk modulus of water,  $K_w = 5 \times 10^5 \text{ kN/m}^2$ , allows negligible volumetric strain and

the settlement due to the loss of water from the system can no longer occur. Further research into the change from consolidated to undrained analyses may be required to ensure that the undrained failure predicted is accurate.

The maximum centreline surface settlement at the end of the consolidation was 691mm, this value is comparable to an estimate of the one dimensional consolidation settlement beneath the embankment crest, performed before the finite element analysis, of 0.71m. This calculation was based on an average coefficient of volume change,  $m_v=2.2 \times 10^{-3} \text{m}^2/\text{kN}$ , and assuming that 62% of the excess pore pressures dissipated during the consolidation stage, Section 7.2.1.

The centreline settlement increased to 799mm by the end of the second lift as a result of mainly distortional deformations, although some small volume change did occur. At failure the final centreline settlement was 1147mm, indicating large distortional deformations with the development of a rotational mechanism, Figure 7.10.

The surface settlement profiles at the end of each of the three stages and at failure are shown in Figure 7.6. Heave occurred near the toe and the greatest settlement occurred beneath the crest. The ratio of the maximum heave to the maximum settlement increased with the application of load. The ratio was 0.48 after the first lift, 0.31 after consolidation, 0.38 after the second lift and 0.68 at failure.

The lateral displacements of a section through the toe are shown in Figure 7.7. The maximum lateral movement occurs at a depth of 1-2.5m below ground level. The lateral movement profile is typical of that observed in finite element analyses but differs from those often observed which are significantly more concave below the peak movement.

The maximum surface displacement is plotted against the maximum lateral movement in Figure 7.8. The form of this curve is similar to those produced by Jardine and Hight (1987) and Leroueil et al (1991) with the ratio of lateral

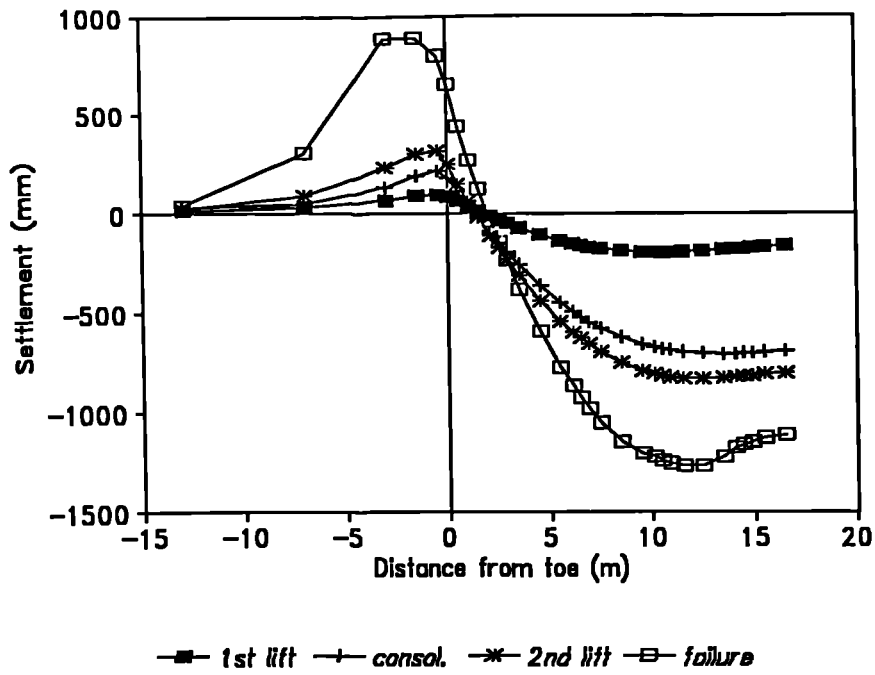


**Figure 7.6 - Surface settlement profiles.**

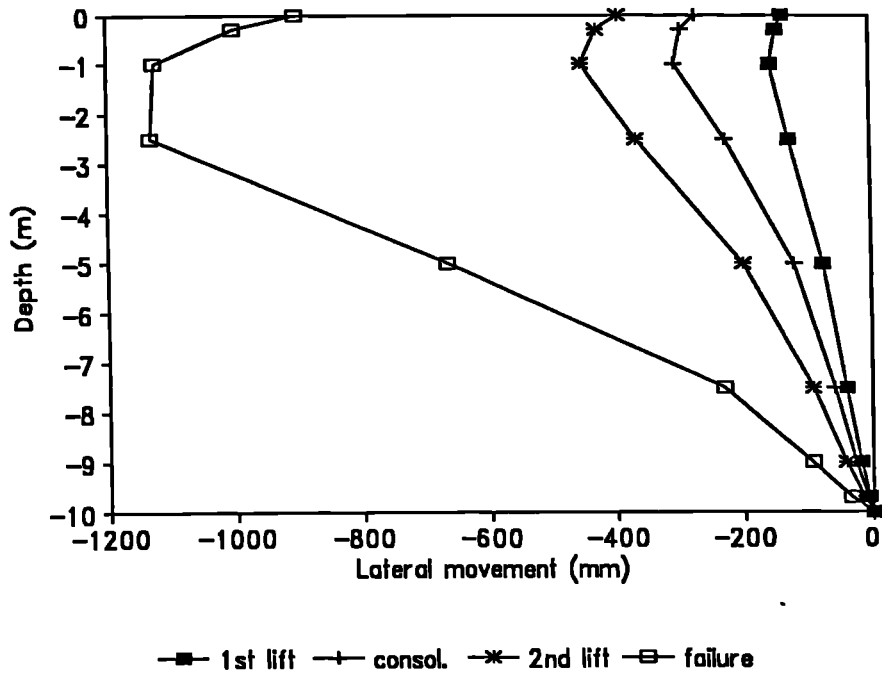


**Figure 7.7 - Lateral movement of a section through the toe.**

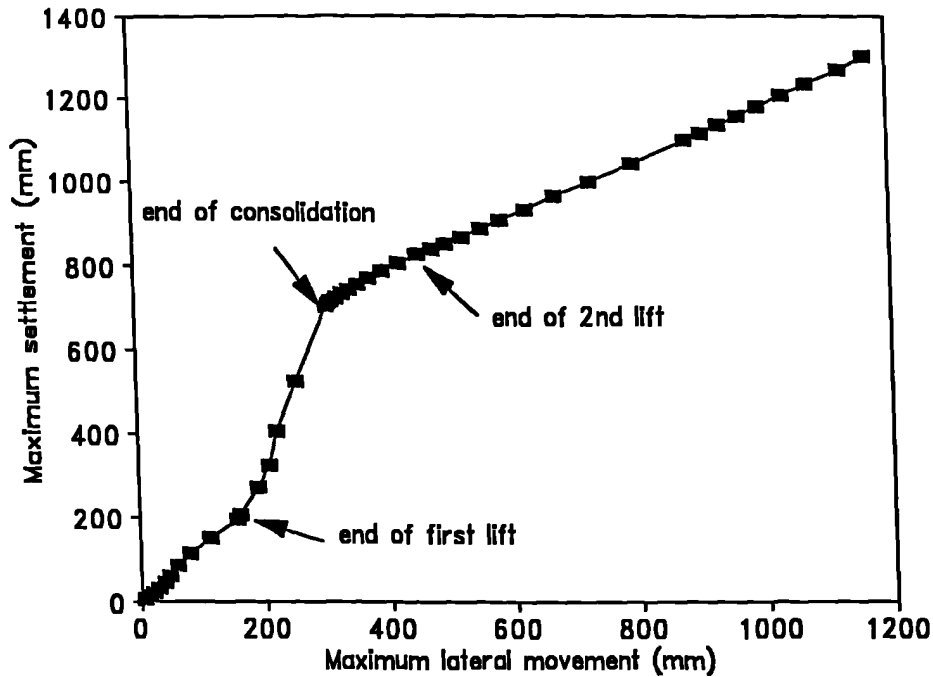


**Figure 7.8 - Maximum surface settlement against maximum lateral movement beneath the toe.**

deformation to settlement being greater during loading than during consolidation. It is interesting to note that at failure the ratio is approaching unity, similar behaviour being observed physically for the Queensborough bypass and a centrifuge model test (see Jardine and Hight, 1987).

### **Factor of Safety**

In order to define the failure height of the embankment the ratio of the change in the maximum surface settlement, over ten increments, to the depth of fill placed has been plotted in Figure 7.9. When the ratio is equal to unity the settlement of the subsoil is greater than the depth of fill placed and there is no net gain in height, therefore failure is deemed to have occurred. From this graph the failure of both undrained loading stages can be defined to give an indication of the factors of safety of the first and second lifts. The first lift fails with an additional surcharge equivalent to 1.33m of fill and the

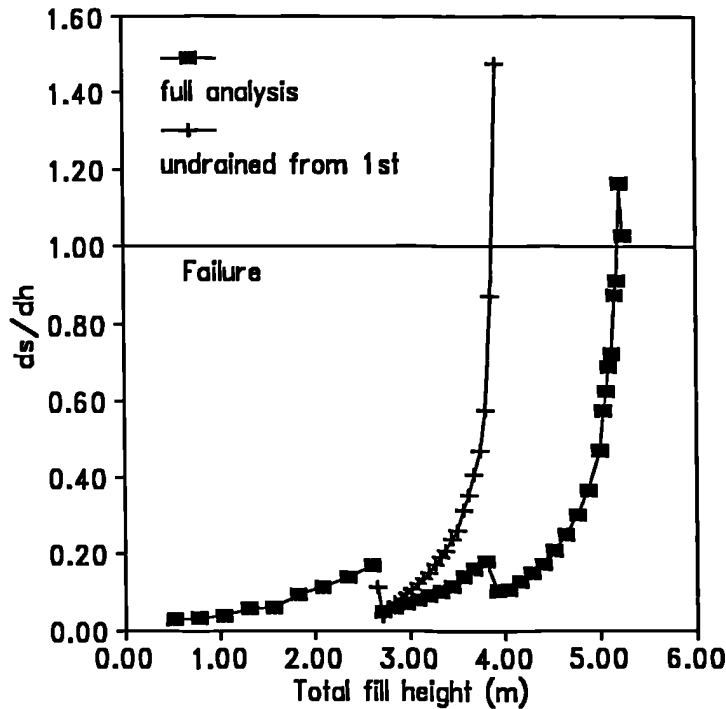


**Figure 7.9 - Ratio of maximum settlement to maximum lateral movement against embankment height (ds=change in maximum settlement, dh=height of fill added).**

second lift with 1.40m. This additional loading can be used to define a factor of safety as

$$FS = \frac{(H + \Delta H)}{H} \dots\dots\dots(7.1)$$

where H is the height before surchargeing and ΔH is the height of surcharge required to cause failure.

From this definition the factor of safety of the first lift is 1.5 and the second lift is 1.4. The corresponding factors of safety calculated by Jewell (1991) using a limit equilibrium approach was 1.1 for both lifts. However, it is difficult to directly compare the finite element and limit equilibrium factors of safety for several reasons

- 1 The finite element analysis allowed 20 days for the placing of the first and second lifts in which time the soil adjacent to the drains would have partially consolidated and gained strength. This would result in a higher factor of safety as the limit equilibrium assumed undrained loading.**
- 2 The strength increases during the consolidation stage adopted in the limit equilibrium calculations were significantly different to those observed in the finite element analysis. This aspect is discussed further in Section 7.3.**
- 3 The limit equilibrium calculation used a factor of safety based on the available shear strength and the applied loading. The calculated factor of safety of 1.1, therefore, implied that the embankment height could be increased by a factor of 1.1 across the whole section. The finite element calculation applied a surcharge loading along the crest and not on the side slope. The mechanism which develops in the finite element analysis would have been different to that produced if the embankment loading was proportionally increased at all points.**
- 4 When predicting undrained collapse using modified Cam-clay a large number of increments need to be used to ensure that the collapse load is not over-predicted. The only certain method of prediction is to perform a sensitivity study with increasing numbers of increments until the collapse is unaffected by an increase in the number of increments. Such a sensitivity study was not carried out for in this case but a large number of increments were used. The first lift failed in the 660<sup>th</sup> increment the first 200 increments were consolidated, the second lift failed in the 690<sup>th</sup> increment with the first 450 increments consolidated.**

**To compare the limit equilibrium and finite element predicted failure directly it would be necessary to carry out a limit equilibrium analysis using the finite**

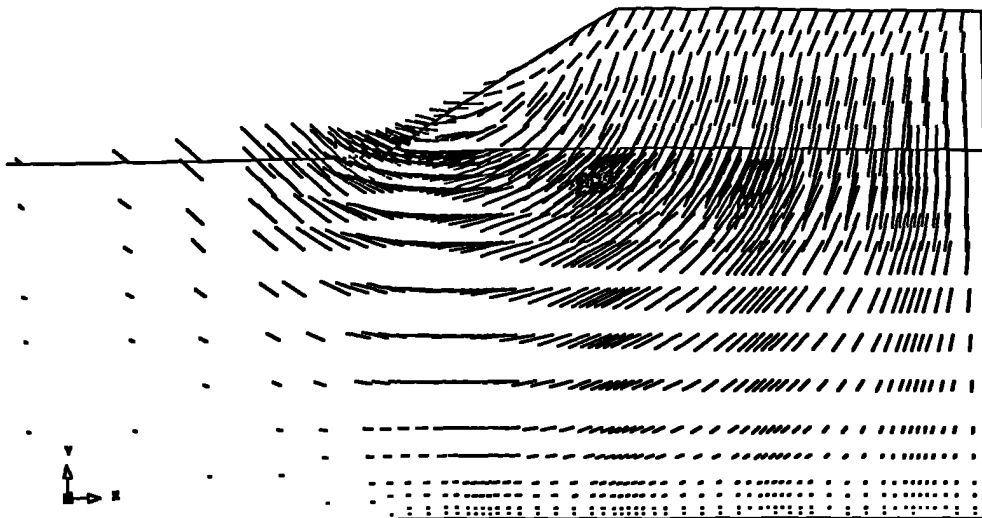


**Figure 7.10 - Displacement vectors at failure.**

element predicted strength at the end of the consolidation stage and to perform a finite element analysis in which the second lift loading is undrained and the additional surcharge loading is applied proportionally across the whole embankment.

The displacement vectors at failure are shown in Figure 7.10. For a subsoil of this type and geometry a rotational failure mechanism would be expected to develop, Chapter 4. Such a mechanism can be seen to have developed at failure.

### **Subsoil Stresses**

The finite element analysis can be used to investigate the subsoil stresses at key positions. Investigations beneath the slope and the beneath the crest have been carried out, considering elements at increasing distances from vertical drains. The positions of the elements (A, B, C, D, E and F) are shown in Figure 7.1.

In Figure 7.11 the stress paths for the six positions in the subsoil are plotted. Figure 7.11a shows the stress paths for points beneath the slope.

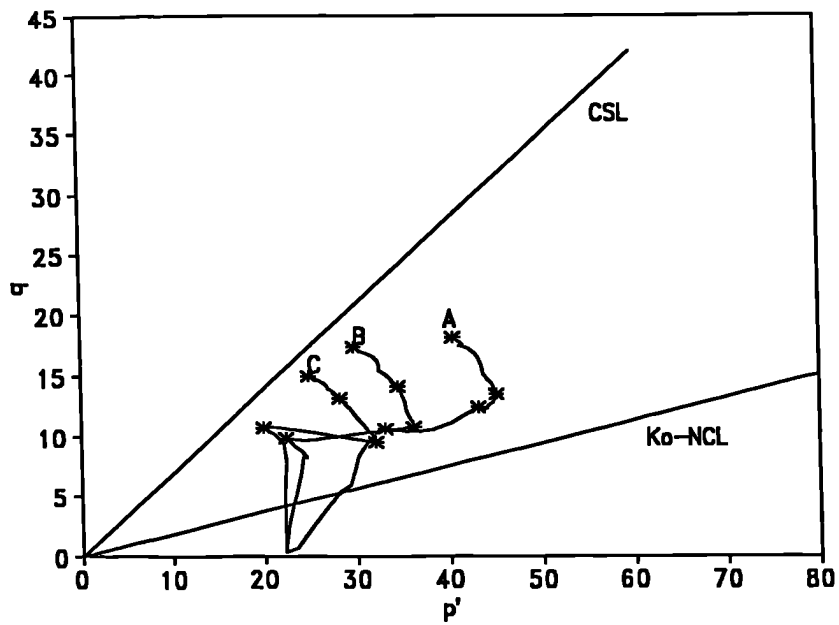


**Figure 7.11a - Stress paths of the subsoil beneath slope (\* indicate change of loading).**

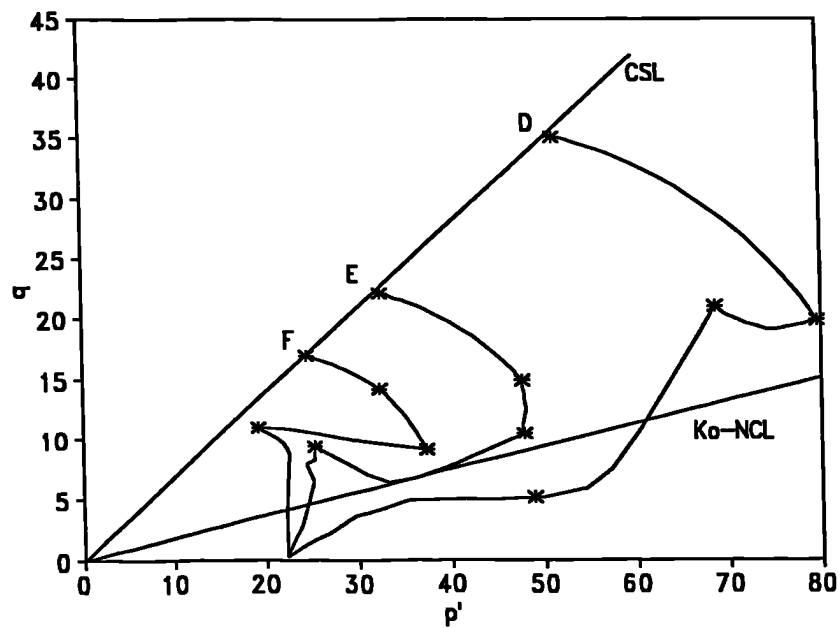


**Figure 7.11b - Stress paths of the subsoil beneath crest (\* indicate change of loading).**

None of these elements reach the critical state but it can be seen that the response during loading is increasingly undrained as the distance from the drain increases. Position C, furthest from the drain, shows an almost undrained response whilst position A, closest to the drain, shows a virtually drained response, and is almost parallel to the  $K_0$  line during the consolidation stage, until the undrained loading is applied. Figure 7.11b shows the stress paths for positions close to the centreline and the general trend of behaviour is the same as beneath the slope. Some of the soil is approaching the critical state at failure of the embankment. These stress paths follow a similar pattern to those observed by Almeida et al (1985, 1986) and Smith(1984).

The rotation of the principal stress direction within the subsoil is of significance as the subsoil undrained shear strength is known to be dependent on the orientation of principal stresses (Eg: Ladd, 1991; Hight et al, 1987), this aspect will be discussed in more detail in Section 7.3. The rotations beneath the crest are shown in Figure 7.12b. At position D principal stress directions are exchanged during the first increment with the horizontal stress becoming the maximum principal stress. However, apart from this, the principal stress rotations are less than  $10^\circ$  and conditions beneath the crest approximate to those in a one dimensional compression test. The rotations beneath the slope, Figure 7.12a, are much larger throughout the analysis although the rotations reduce sharply as failure is approached. This variation of rotation across the subsoil is complicated by the inclusion of the vertical drains but compares well with that observed by Smith (1984).

The parameter introduced by Bishop (1966)

$$b = \frac{\sigma_2' - \sigma_3'}{\sigma_1' - \sigma_3'} \dots\dots\dots(7.2)$$

can be modified so that  $\sigma_1'$  and  $\sigma_3'$  are the in plane maximum and minimum principal stresses and  $\sigma_2'$  is the out of plane stress,  $\sigma_z'$ . Now b is redefined

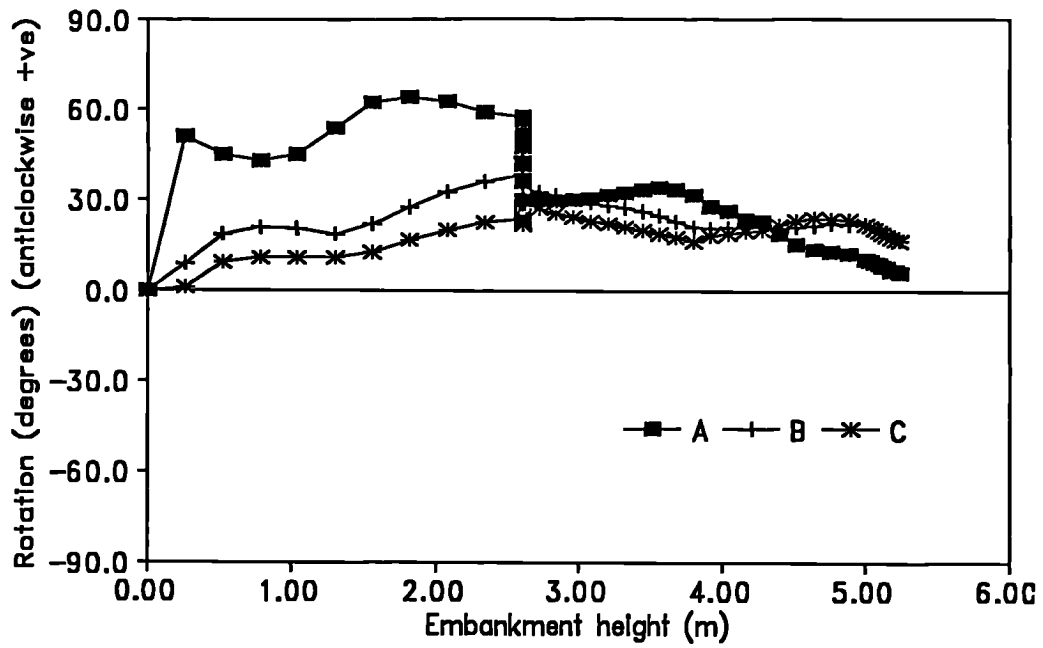


Figure 7.12a - Principal stress rotations beneath the slope.

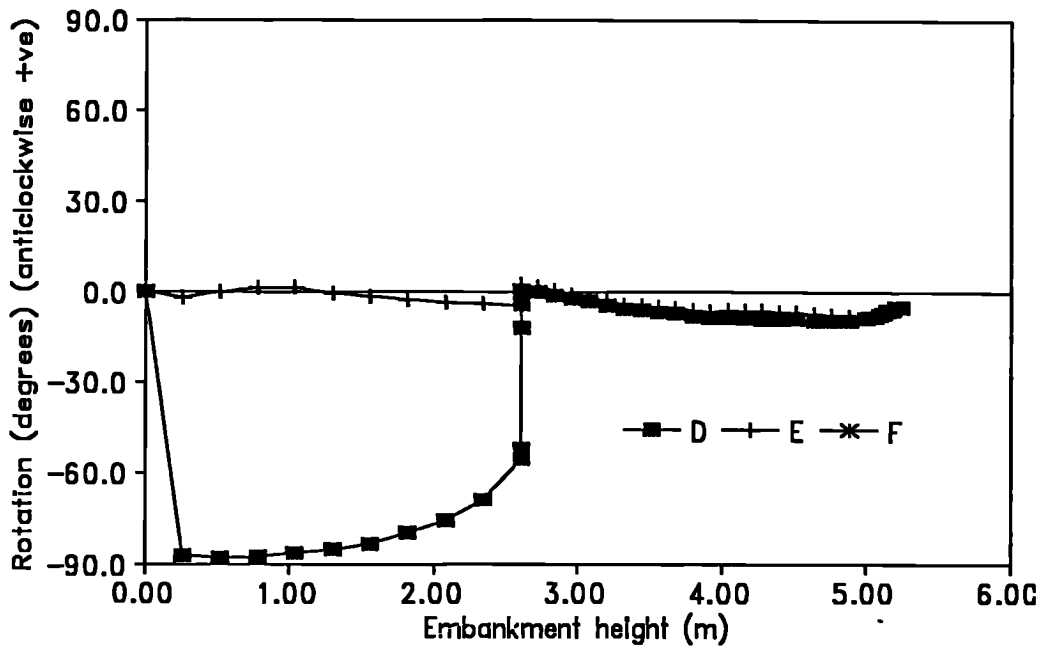


Figure 7.12b- Principal stress rotations beneath the crest.

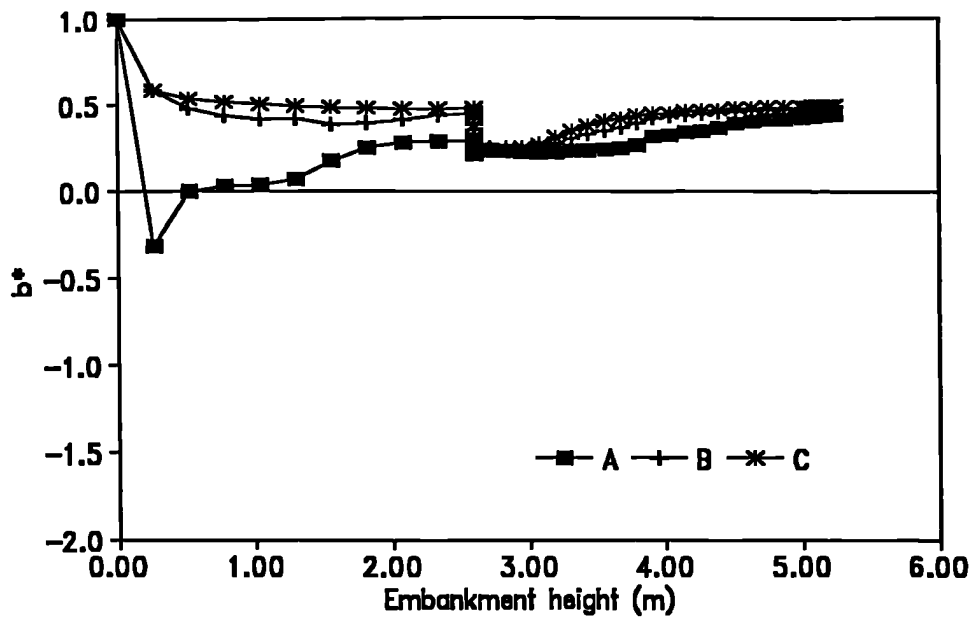


Figure 7.13a - Modified Bishop stress ratio beneath the slope.

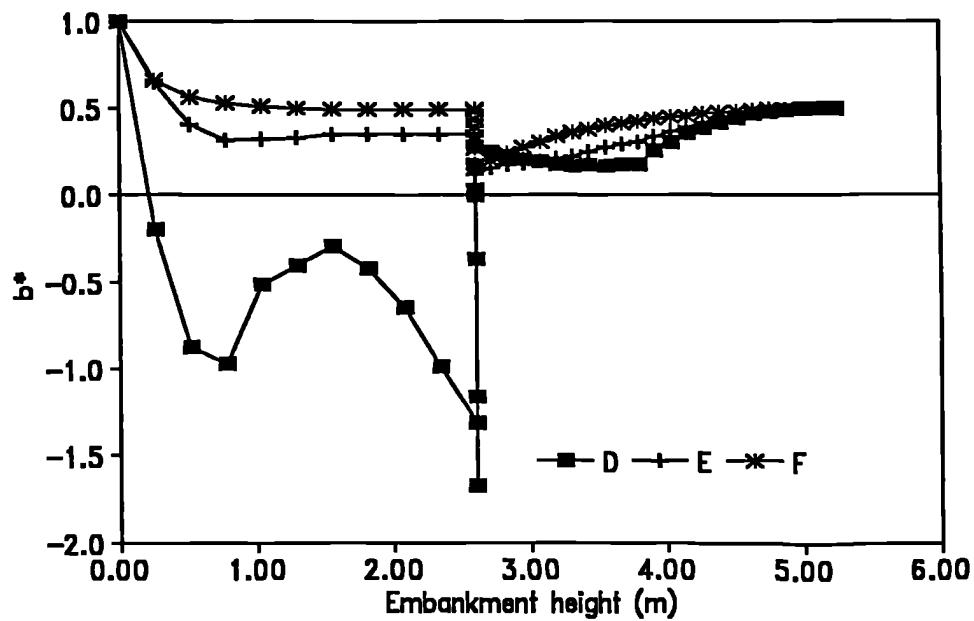


Figure 7.13b - Modified Bishop stress ratio beneath the crest.

as

$$b^* = \frac{\sigma'_2 - \sigma'_3}{\sigma'_1 - \sigma'_3} \dots\dots\dots(7.3)$$

This implies that, if  $\sigma'_2 > \sigma'_1$  then  $b^* > 1$  if  $\sigma'_2 < \sigma'_3$  then  $b^* < 0$  and if  $\sigma'_3 > \sigma'_2 > \sigma'_1$  then  $b^* = b$ .

The variation of  $b^*$  with embankment height has been plotted in Figure 7.13. Beneath both the slope and crest during the first lift the element nearest the drain has an out of plane principal stress that is less than the minimum in plane principal stress. This is consistent with the soil nearest the drain consolidating quickly, causing little out of plane stress, and the soil further from the drain becoming increasingly undrained and undergoing stress increases in all directions due to the increased vertical stress. During the consolidation stage for all positions  $b^*$  reaches a value between 0.0 and 0.5. In the second lift the elements away from the drain are approaching the failure value of  $b^* = 0.5$  with the soil adjacent to the drain having a relatively constant value. Finally the undrained loading causes all points to approach a value of  $b^* = 0.5$ . This is consistent with Figure 7.11 in which the stress paths are approaching the critical state.

The strength at the end of each increment can be calculated from the void ratio, Appendix A, Equation A30. The ratio of the strength to the effective vertical stress ( $s_v/\sigma'_v$ ) is plotted in Figure 7.14 and the ratio of the strength to the maximum in plane principal effective stress ( $s_v/\sigma'_1$ ) is plotted in Figure 7.15. Two points are noted from these graphs; firstly, at no stage of the analysis does either ratio fall below the normally consolidated ratio  $s_v/\sigma'_1 = 0.218$  and, secondly, the ratio  $s_v/\sigma'_v$  is always equal to or greater than the ratio  $s_v/\sigma'_1$  as the effective vertical stress can never be greater than the maximum in plane principal stress. These points are significant when developing strategies for calculating strength increases.

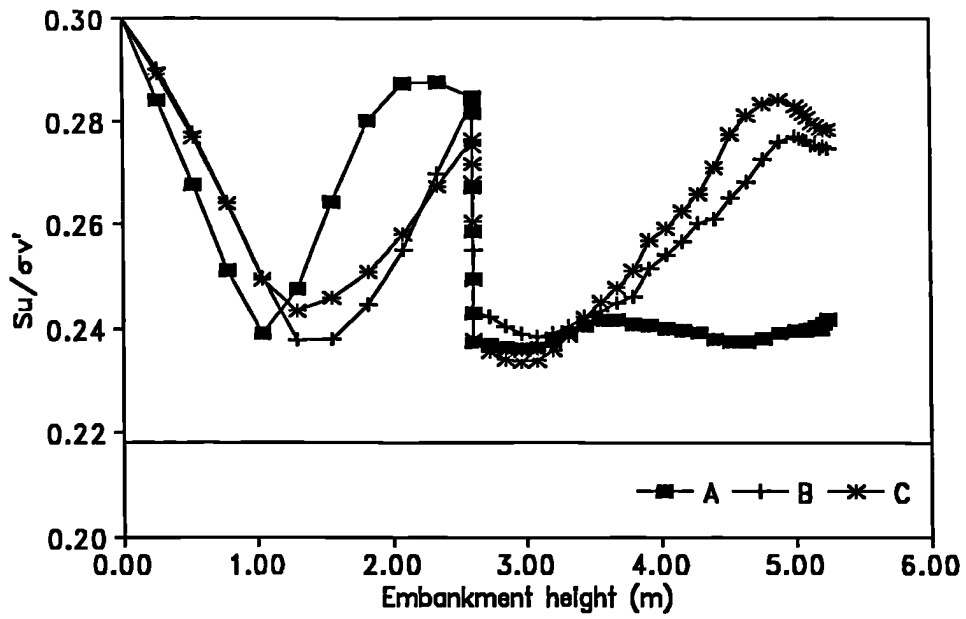


Figure 7.14a - Variation of  $s_u/\sigma'_v$  beneath slope.

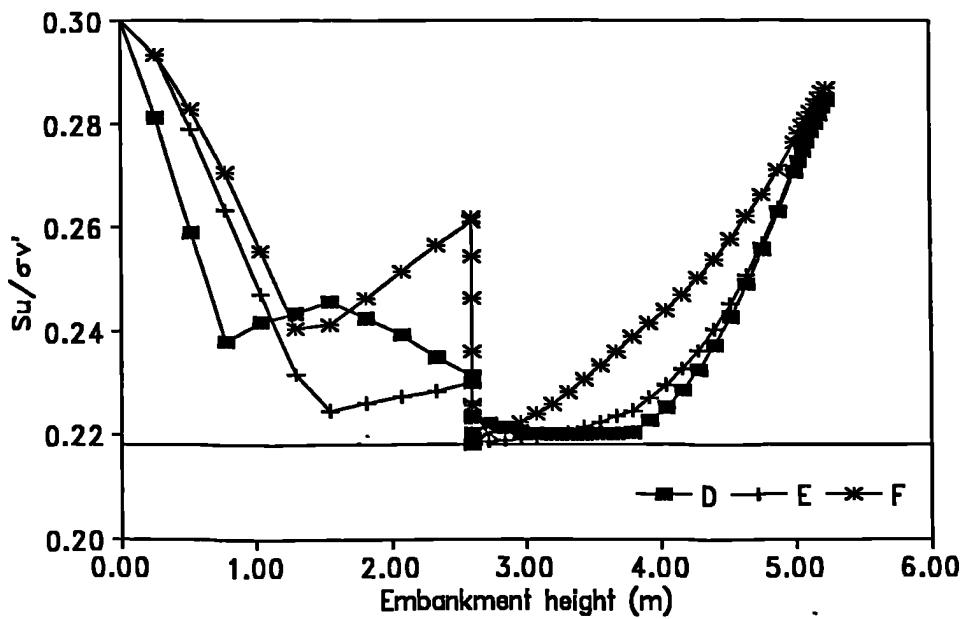


Figure 7.14b - Variation of  $s_u/\sigma'_v$  beneath the crest.

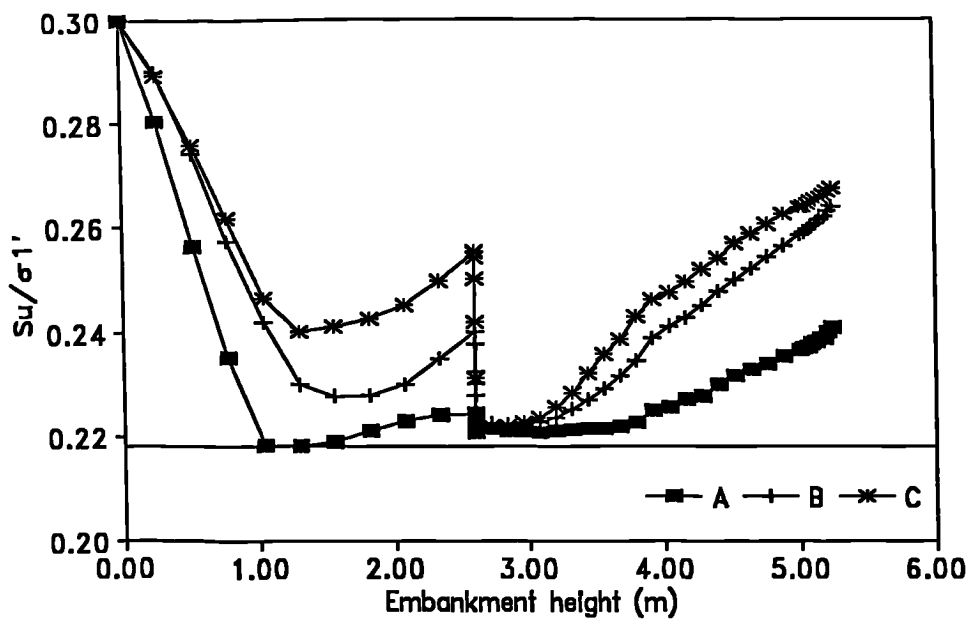


Figure 7.15a - Variation of  $s_u/\sigma'1'$  beneath the slope.

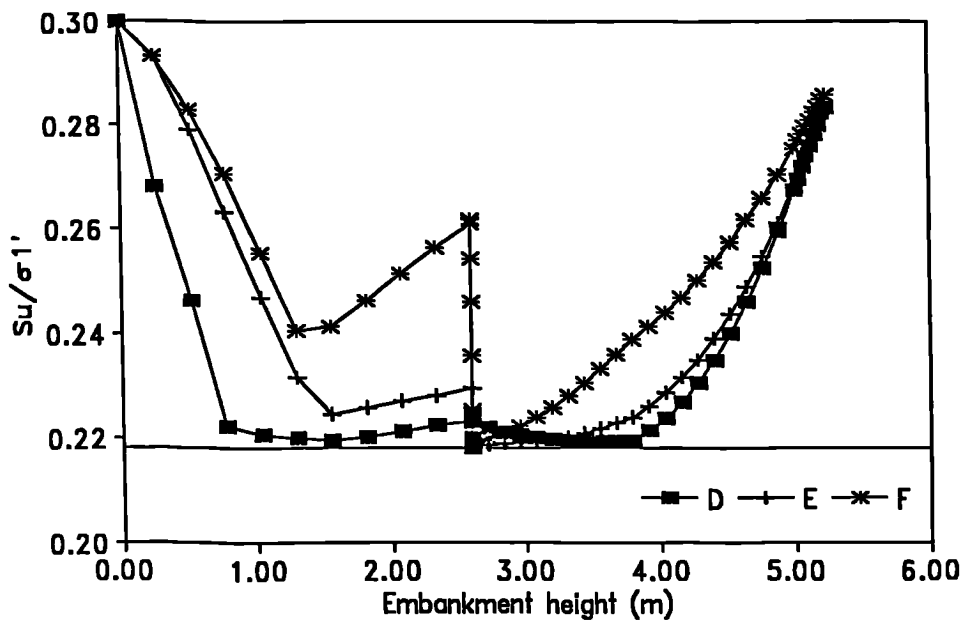


Figure 7.15b - Variation of  $s_u/\sigma'1'$  beneath the crest.

During the first lift the strength ratios for all points reduce until yielding occurs. Once the soil has yielded the value of  $s_v/\sigma_1'$  is dependent on the ratio  $q/p'$ . By comparing Figure 7.11 with 7.15 it can be seen that an increasing  $q/p'$  ratio causes an increase in  $s_v/\sigma_1'$  and vice versa. Points D, E and F are at the critical state, Figure 7.11, with a constant  $s_v/\sigma_1'$  of approximately 0.28. During the loading stages the undrained shear strength remains virtually constant. The increase in the ratio is, therefore, a result of a reduction in the effective stress due to increasing pore pressures.

### **Reinforcement and Interface Behaviour**

The reinforcement strain is plotted at the end of each of the four stages in Figure 7.16. From the profiles it can be seen that the reinforcement strain is slightly reduced near vertical drains (at 2, 6, 10, and 14m from toe). This is due to the soil adjacent to the drains consolidating and gaining strength more quickly. The reinforcement strain increases during the consolidation stage. This increase is not caused purely by the differential settlement of the embankment but also by to an increasing lateral movement, Figure 7.7. The reinforcement strain profile at failure shows a final reinforcement strain of over 8%.

The interface elements can be used to plot the shear stress distributions at the interfaces above and below the reinforcement, Figure 7.17. The sign convention used to define the direction of the interface shear stresses is shown in Figure 3.4.

The (upper) reinforcement/fill shear stress profile, Figure 7.17a, shows significant oscillation of stress, particularly at failure. However, trends can be discerned from the profiles and in all cases the shear stress on the reinforcement is outwards for the first 8-10m beyond the toe, indicating that the embankment is spreading laterally and inducing a tensile strain in the reinforcement. Beyond this (nearer the centreline) the embankment

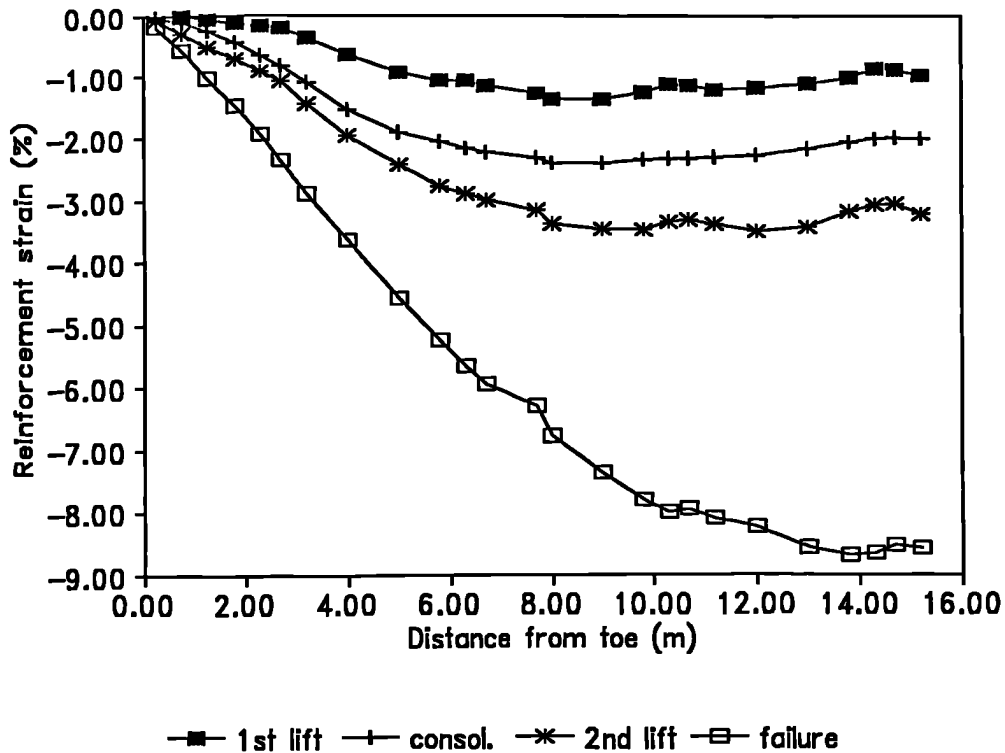


Figure 7.16 - Reinforcement strain.

provides an inward shear stress indicating that the embankment is providing some restraint to the subsoil which is spreading outwards.

The (lower) reinforcement/subsoil interface shear stress profile is shown in Figure 7.17b. For the majority of the profile the shear stress on the reinforcement is in an outward direction, indicating that the soil is moving outwards relative to the reinforcement. At the end of the first lift some of the interface has reached failure at 3.93kPa. Again variation of the shear stress across a unit cell can be observed as the shear stress tends to be reduced near a drain and increased away from it (drains are positioned at 2, 6, 10 and 14m from the toe). After the consolidation stage the interface shear stress, generally, reduces with none of the soil at failure. For the second lift and the undrained loading to failure the interface shear strength was

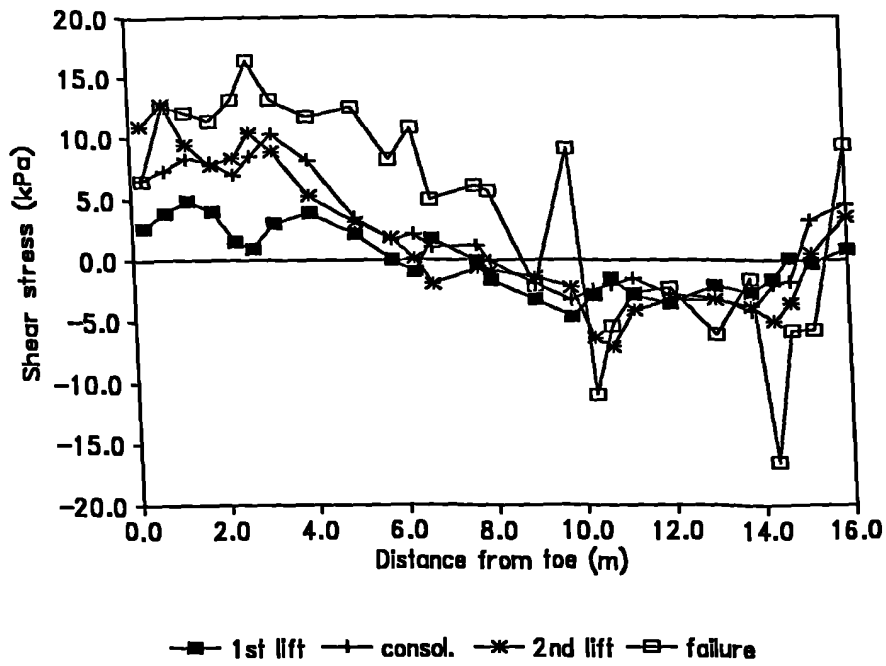


Figure 7.17a - Shear stress on the reinforcement/fill interface.

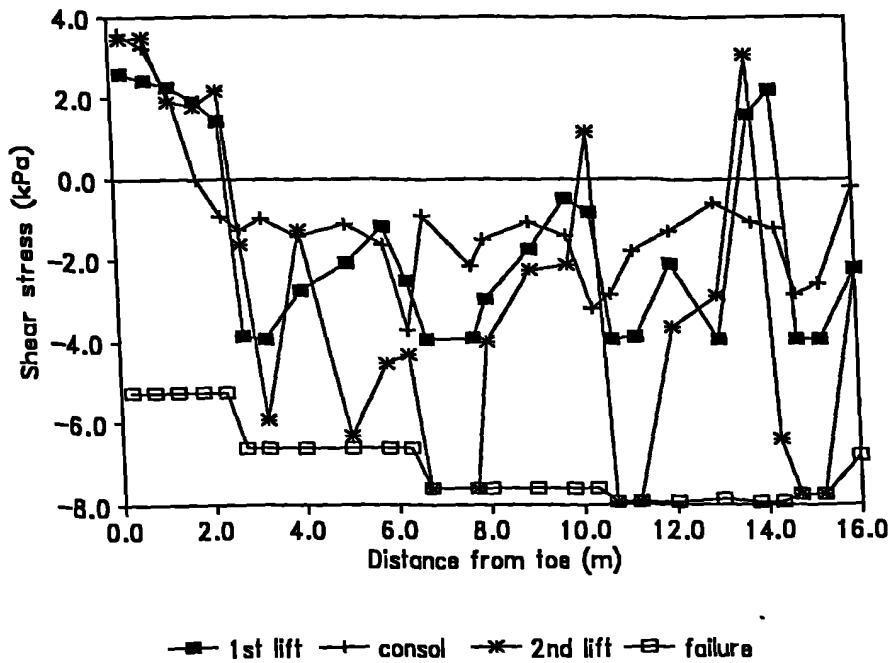


Figure 7.17b - Shear stress on the reinforcement/clay interface.

increased, according to Figure 7.3, to take account of the increase in the surface strength of the subsoil. After the second lift the shear stress has, in general, increased with some of the elements reaching their limiting strength. The profile plotted at failure was taken from a slightly earlier increment to avoid the oscillations which occurred during the failure increment. The shear strength has been reached over almost all of the interface indicating slip between the reinforcement and the soil. At failure the shear stress is in an outward direction along the whole of the interface.

## **7.3. Subsoil Strength Increase**

In order to carry out an accurate stability analysis of a multi-stage embankment it is necessary to make a safe assessment of the increase in undrained shear strength during the consolidation stage of construction and then to use these in a total stress limit equilibrium analysis. In this Section methods for estimating the increase in undrained shear strength and the assumptions which account for the observed behaviour of soft clay are discussed. The strength increases predicted by several simple methods are compared with the increases observed from the idealised two stage construction finite element analysis. The simple methods which best fit with the finite element results have then been used to predict strength increases for the Porto Tolle case history (Chapter 6) and these are also compared with finite element results.

### **7.3.1. Simple Calculation Methods**

#### **Calculation of Undrained Strength from Vertical Effective Stress**

Before construction of an embankment the subsoil will almost always be in a  $K_0$  condition with the principal stresses vertical and horizontal. As construction proceeds the stress conditions become more complex with rotation of the principal stress directions at all positions in the subsoil except directly beneath the embankment centreline. Figure 7.18 shows a subsoil

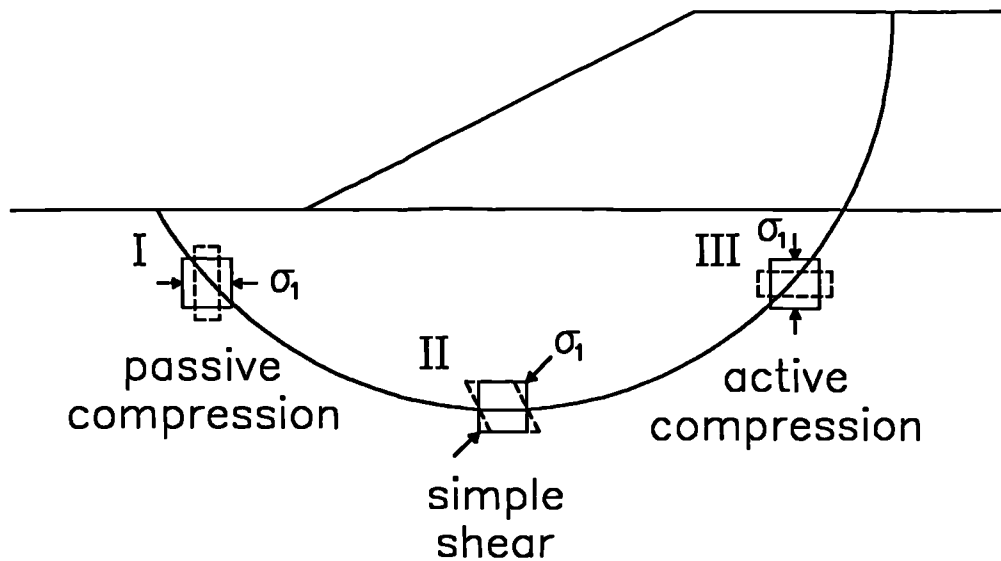


**Figure 7.18 - Stress state on a potential failure surface in a soil near failure subject to embankment loading.**

near failure. A potential rotational failure surface is shown, but depending on the subsoil conditions, the mechanism could equally well be translational (see Section 4.3.3). From the orientation of the slip surface the principal stress directions at I, II and III can be inferred, with I undergoing active compression, II simple shear and III passive extension. This complex stress distribution is further complicated by the inclusion of vertical drains. From Figure 7.12 it can be seen that for positions beneath the mid-slope and the centreline there is a variation of the principle stress rotation as the distance from a vertical drain increases.

In the laboratory it is possible to perform a number of tests with the principal stress directions in fixed positions. Figure 7.19 shows results of a series of such tests on normally consolidated clays and silts (as summarized by Ladd, 1991), with each line representing the best fit to a number of tests results. It can be argued that an undrained triaxial compression test

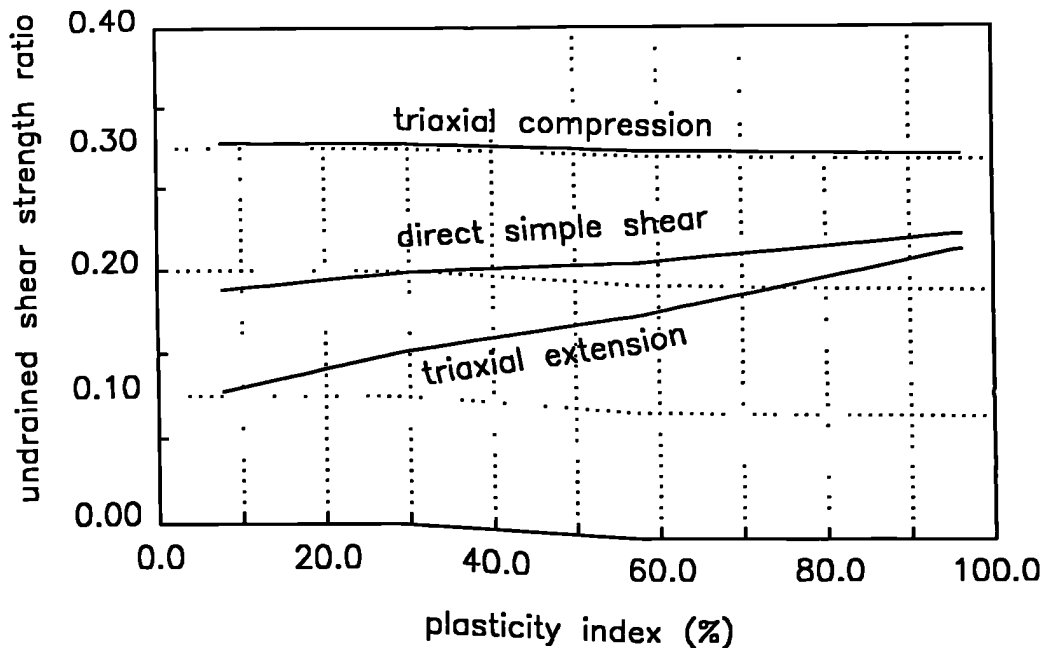


Figure 7.19 - Undrained strength anisotropy of normally consolidated clays.

represents the stress state at I, and correspondingly a direct simple shear test at II and a triaxial extension test at III. To obtain a simple analysis method an average of these three results would give a measure of the average strength along the failure surface shown in Figure 7.18. The average value from the three tests corresponds approximately with the direct simple shear test result, although this is not the case with varved deposits which often produce low undrained strengths in simple shear. The Cam-clay constitutive model implemented in CRISP does not reproduce the observed strength anisotropy but calculates a constant undrained shear strength independent of the direction of the principal stresses.

The strength ratio  $(s_u/\sigma_1')_{NC}$  can be used to provide a safe estimate of the undrained shear strength of the subsoil at any time providing the value of  $\sigma_1'$  is known. The variation of the strength ratio with embankment height has

been plotted for the idealised study in Figures 7.14 and 7.15. From these plots it can be seen that the initial strength ratio provides a lower bound to the strength ratio during construction. However, It is difficult to simply yet accurately estimate the value of  $\sigma_1'$  and an easier quantity to evaluate is the effective vertical stress  $\sigma_v'$ . Using this value with the initial strength ratio must provide a conservative strength as  $\sigma_v' < \sigma_1'$ . The strength at any time can therefore be calculated from

$$s_u = \left( \frac{s_u}{\sigma_1'} \right)_{NC} \sigma_v' \dots\dots\dots(7.4)$$

**Vertical Stress Increase due to Embankment Loading**

In order to apply Equation 7.4 it is necessary to calculate the increase in the effective vertical stress ( $\Delta\sigma_v'$ ) due to the embankment loading. This involves firstly, the calculation of the total vertical stress increase ( $\Delta\sigma_v$ ) and secondly, the excess pore water pressure ( $u$ ) due to incomplete consolidation. In this Section two methods for the estimation of the total vertical stress increase are proposed.

Method 1 (Figure 7.20a) - In this method the load is assumed to act one-dimensionally, i.e. the loading of the subsoil is due only to the weight of fill material above. This results in no stress increase, and therefore no strength increase, beyond the toe.

Method 2 (Figure 7.20b) - This method relies on the use of an elastic solution to the embankment loading problem (Gray, 1936). The application of the solution is only strictly valid for elastic conditions. However, the solution does provide a convenient method of calculation of the vertical stress increase and has been shown to provide realistic values (Watson et al, 1984).

These methods provide an upper and lower bound on the sophistication which is appropriate in this type of calculation. An intermediate calculation method assumes that a constant load spreading angle can be applied at the

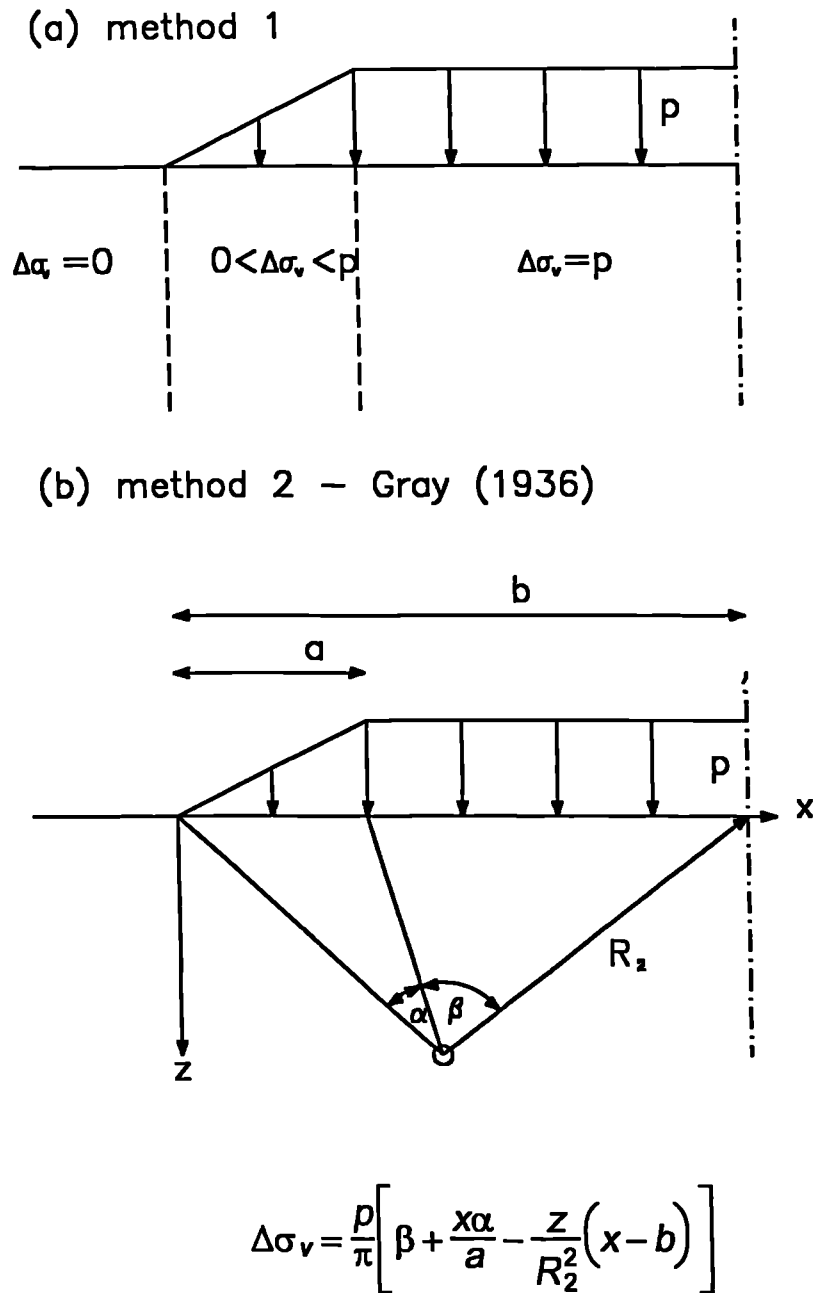


**Figure 7.20 - Estimation of vertical stress increase in a soil due to embankment loading: a) one-dimensional; b) according to Gray (1936).**

toe and that this angle reduces linearly towards the centreline. If the load spreading angle was zero, this method would be equivalent to method 1 (above).

**Generation of Excess Pore Water Pressure due to Embankment Loading**

At the end of a loading stage excess pore pressures will have been generated in the subsoil. For the purpose of this investigation the simplest possible estimation of the value of these excess pore pressure increase ( $\Delta u$ ) has been made, i.e. that the excess pore pressure increase is equal to the increase in total vertical stress calculated using Grays (1936) elastic theory

$$\Delta u = \Delta \sigma_v \dots\dots\dots(7.5)$$

This approach is only correct beneath the centreline of the embankment as no account has been taken of the generation of pore pressures due to shear stress increase. Other simple approaches to the calculation of excess pore pressure generation have been used. Murray and Symons (1974) used Skempton's (1954) equation for the pore pressure developed in a saturated soil under undrained conditions

$$\Delta u = \Delta \sigma_3 + A(\Delta \sigma_1 - \Delta \sigma_3) \dots\dots\dots(7.6)$$

and assumed that Skempton's pore pressure parameter  $A=1$  at failure for a normally consolidated soil, so that

$$\Delta u = \Delta \sigma_1 \dots\dots\dots(7.7)$$

with  $\Delta \sigma_1$  calculated using an elastic solution.

Parry (1972) used a similar approach for the comparison of predicted and observed pore pressures for an embankment constructed over a soft clay soil. The excess pore pressure was linked to the stress increment by

$$\Delta u = \alpha A \Delta \sigma_1 \dots\dots\dots(7.8)$$

where  $A$  is the pore pressure parameter measured at failure for undisturbed samples in an undrained triaxial compression test,  $\Delta\sigma_1$  is the increment in the maximum principal total stress calculated using elastic theory and  $\alpha$  was a constant value equal to 1.25 for the embankment studied.

Burland (1972) proposed a method for the prediction of the generation of excess pore pressures which allowed for local failure of the subsoil. The method still relied on elastic solutions for the calculation of stresses but showed encouraging results when predictions were compared with observations for three embankments constructed over soft clays.

The method used for the calculation of excess pore pressures in this Thesis is likely to underestimate the actual pore pressures generated under undrained conditions. Whilst the present method has the merit of simplicity, further calculations should be carried out to assess the applicability of other relationships.

### **Estimation of Dissipation of Excess Pore Water Pressure**

The excess pore water pressure generated during loading will reduce during the consolidation stages. In order to calculate the effective stress conditions, and thus the undrained shear strength, it is necessary to estimate the amount of dissipation which occurs. When analysing a subsoil containing vertical drains it is likely that the flow will be predominantly horizontal and it may be appropriate to use one of the solutions for a unit cell reviewed in Chapter 5. For this study Hansbo's (1981) solution has been used. For the idealised two-stage analysis the vertical permeability was negligible so that it was possible to apply Hansbo's equation without consideration of vertical flow. In general the vertical permeability will not be negligible and soil close to horizontal drained boundaries will consolidate more quickly than would be predicted using purely radial flow in a unit cell calculation. The increased rate of consolidation would lead to surface strengthening which is important, particularly for reinforced embankments,

where the soil strength at the soil/reinforcement interface significantly affects the failure load of the subsoil. Using Hansbo's equation should therefore give a conservative estimate of the dissipation of pore water pressure in this critical region provided the material parameters used, and assumptions regarding well resistance and smear, are realistic.

Hansbo's equation can be used to calculate the average degree of consolidation as

$$\bar{U}_h = 1 - e^{-8T_h/\mu} \dots\dots\dots(7.9)$$

where  $T_h$  is the time factor and  $\mu$  is a factor dependent on geometry, smear and well resistance; these factors are discussed in detail in Chapter 5.

Equation 7.9 can be used to estimate the dissipation of excess pore water pressure during a consolidation stage. If the time taken to place the fill is sufficiently short, the consolidation which occurs during construction, is negligible. However, if the rate of loading is relatively slow a calculation of the pore pressure dissipation can be made using the equations developed in Appendix C, which modify Hansbo's equation to allow for ramp loading

$$\bar{U}_h = 1 - \frac{\alpha\mu(1 - e^{-8T_h/\mu})}{T_h} \dots\dots\dots(7.10)$$

where  $\alpha$  is the rate of loading.

### **7.3.2. Factors Influencing the Strength Increase of Soft Clays**

In the previous Sections a method for calculating the strength increase of a clay soil has been proposed and the method can be summarized as

- 1 Calculate the increment of total vertical stress in the subsoil using either a one-dimensional approach or an elastic solution, Figure 7.20.
- 2 Assume that the increase in vertical stress causes an equal increment of excess pore pressure at the end of the loading stage.

- 3 Calculate the dissipation of the excess pore water pressure, before the start of the next loading stage, using Equation 7.9 and/or Equation 7.10 and combine with the increment of total vertical stress to calculate the increment of effective vertical stress.
- 4 Calculate the new undrained shear strength using the increment of effective vertical stress with Equation 7.4.

This procedure could be used to calculate the strength increase in any clay subsoil. However, some other aspects of the behaviour of soft clays need be taken into account to achieve an accurate estimation of the subsoil strength increase.

### Lightly Over-Consolidated Clays

It is unlikely that a soft clay subsoil will be normally consolidated; over-consolidation could occur for one of several reasons, such as the removal of overburden, fluctuations in ground water level, dessication of the clay surface or ageing. The over-consolidation has several important consequences in relation to the strength increase due to loading of the soil. In order to evaluate these effects the soil behaviour will be discussed within a critical state frame work.

The plane strain undrained strength ratio of an over-consolidated (OC) clay is shown in Appendix A to be

$$\left(\frac{s_{LD}}{\sigma_v'}\right)_{OC} = \left(\frac{s_{LD}}{\sigma_v'}\right)_{NC} \frac{(1+2K_0)}{(1+2K_{0NC})} \left[ \frac{OCR(1+2K_{0NC})}{(1+2K_0)} \right]^{\lambda} \dots\dots\dots(7.10)$$

As the over-consolidation ratio (OCR) is, by definition, greater than 1 and, from Appendix A,  $K_0 > K_{0NC}$ , the over-consolidated strength ratio must be greater than the normally consolidated ratio, which is often observed to be  $0.22 \pm 0.02$  (Hight et al, 1987; Ladd, 1991).

When embankment construction commences the soil is reloaded from its over-consolidated state and modest strength increases will be expected

until the preconsolidation pressure is reached. For a typical ratio of  $\kappa/\lambda=0.2$  the strength increase in the over-consolidated range is only 20% of that in the normally consolidated range for the same change in vertical stress. It is therefore a realistically conservative assumption to ignore any strength increase due to effective stress increases whilst the soil is over-consolidated. Any soil which remains in the over-consolidated range is assumed to fail at its insitu undrained shear strength.

A second effect is the increased rate of pore water pressure dissipation in the over-consolidated range (Tavenas and Leroueil, 1980; Hight et al, 1987; Leroueil et al, 1991). The change in volume of an over-consolidated clay compared with that of a normally consolidated clay for the same variation in vertical effective stress is small. Therefore, for soil loaded in the over-consolidated range the excess pore pressures generated may be small.

### **Variation of the Coefficient of Consolidation**

When using Hansbo's (1981) equation to assess the rate of consolidation of a soil it is implicitly assumed that the coefficient of consolidation is constant. In reality the coefficient initially varies with depth and also varies with time as the loading is applied and consolidation occurs. The coefficient of consolidation is defined as

$$c_h = \frac{k}{m_v \gamma_w} \dots\dots\dots(7.11)$$

where the coefficient of volume change for the initial one-dimensional conditions can be defined as  $m_v = \lambda/\sigma'_v(1+e)$ ,  $k$  is the permeability and  $\gamma_w$  is the unit weight of water.

The coefficient of volume change is dependent on both the void ratio and the vertical effective stress and will therefore vary with depth. For the idealized case described in Section 7.2, the values of  $m_v$  at the top and bottom of the soft clay were  $9.4 \times 10^{-3}$  and  $1.4 \times 10^{-3} \text{m}^2/\text{kN}$  respectively. This

implies an initial coefficient of consolidation almost seven times larger at the bottom than the top. This effect is offset, to some extent, by the observed decrease of permeability with decreasing void ratio, Tavenas et al (1983), proposed the following relationship

$$\log k = \log k_0 - \left( \frac{e_0 - e}{0.5e_0} \right) \dots\dots\dots(7.12)$$

where  $e_0$  and  $k_0$  are the initial void ratio and permeability respectively.

Applying Equation 7.12, to the idealized case, results in a permeability which is five times greater at the surface than at the base. Combining the effects of the variation of the coefficient of volume change and permeability gives a slightly larger coefficient of consolidation at the surface than at the base.

In the finite element analysis of the idealized case the variation of the coefficient of volume change was automatically accounted for when using the modified Cam-clay constitutive model. However, the permeability was constant throughout the depth. Therefore, the upper layers of the finite element mesh consolidated more quickly than those lower down.

In general, when performing a finite element analysis of an embankment constructed on a soft soil it is necessary to model accurately the coefficient of consolidation throughout the depth of the deposit. To achieve this, using the modified Cam-clay model implemented in CRISP, it would be necessary to define several horizontal layers of elements and define a different value for the permeability in each.

As well as its initial variation with depth, the permeability will also display further changes with loading. This can be considered using Equation 7.12. The variation of permeability with stress level has been implemented in CRISP, Section 3.4, but has not been used in the idealized analysis.

### 7.3.3. Comparison of the Strength Increases Predicted by Finite Element and Simple Methods

In this Section the simple analysis methods outlined above are applied to the idealized embankment and compared with the strength increases derived from the finite element analysis at the end of the consolidation stage.

#### Strength Increases Computed from Finite Element Results

The void ratio,  $e$ , for the centroid of each element is included in the output from the finite element analysis and can be used to calculate the undrained shear strength in plane strain (Appendix A, Equation A34) as

$$S_{u0} = \frac{M}{\sqrt{3}} \exp\left[\frac{e_0 - e}{\lambda}\right] \dots\dots\dots(7.13)$$

where  $e_0 = \Gamma - 1$ .

The undrained shear strength increases for each row of elements in each unit cell are then averaged to give eight values of strength with depth (per unit cell).

The matching technique (developed in Chapter 5) only ensures that the average value of the excess pore pressure in the plane strain unit cell is equivalent to that which would occur in an axisymmetric unit cell. The variation of the excess pore pressure across the unit cells will be different (Section 5.3.2) and therefore the undrained shear strength variation across the unit cell will be different. In order to use the results from a plane strain finite element analysis to predict undrained shear strengths which are likely to occur in the subsoil, it is necessary to average the void ratio at various levels in each of the unit cells and to calculate the undrained shear strength from these average values.

### **7.3.4. Strength Increases Calculated from Simple Methods**

A total of eight combinations of the assumptions outlined in Sections 7.3.1 and 7.3.2 were used to compare simple design methods with the finite element results. These combinations are summarized in Table 7.1 and the main assumptions are outlined below

- 1 Calculation of loading - the stress increase in the subsoil was calculated either using a one-dimensional approach or Gray's (1936) elastic solution, Figure 7.20.
- 2 Variation of the coefficient of volume change,  $m_v$  - the value of  $m_v$  varies significantly with depth in the finite element analysis. Simple calculations have been carried out with either a constant  $m_v$  or with the value  $m_v$  varying with depth as in the finite element analysis.
- 3 Pore pressure dissipation in the over-consolidated range - increased rates of the dissipation of the excess pore pressure occur in the over-consolidated range. This observation has been accounted for in the simple analyses by considering the two extremes of behaviour. At one extreme, the rate of consolidation is assumed equal in both the over-consolidated and normally consolidated soil. At the other extreme, immediate dissipation is assumed in the over-consolidated range. The remaining excess pore water pressure dissipates during the consolidation period according to Equation 7.5.

In all cases only the vertical effective stress increase above the preconsolidation pressure has been used to compute the increase in strength. Positions at which the soil has not reached the preconsolidation pressure are assumed to have no change in strength.

Method	Loading	$m_v$ varies with depth	Immediate pore pressure dissipation in OC range
A	one-dimensional	no	no
B	Gray	no	no
C	one-dimensional	yes	no
D	Gray	yes	no
E	one-dimensional	no	yes
F	Gray	no	yes
G	one-dimensional	yes	yes
H	Gray	yes	yes

**Table 7.1 - Summary of the assumptions used in the simple methods used to predict strength increases.**

**Comparison of Simple Methods and Finite Element Results for Strength Increase**

All eight simple methods were used to compute the strength increase in the unit cell closest to the centreline. At this point the conditions are almost one-dimensional and comparisons between the simple methods and the finite element analysis should be most favourable. The calculated undrained shear strength increases at the end of the consolidation stage are plotted in Figure 7.21 and the absolute value of strength in Figure 7.22.

From Figure 7.21 it can be seen that the methods which assume a constant coefficient of volume change with depth (A, B, E and F) do not predict accurately the trend of strength increase observed in the finite element results. As discussed above this result is somewhat artificial, arising from the variation of coefficient of volume change in the finite element analysis without the compensating variation of permeability. However, when the variation of the coefficient of volume change is used in the simple

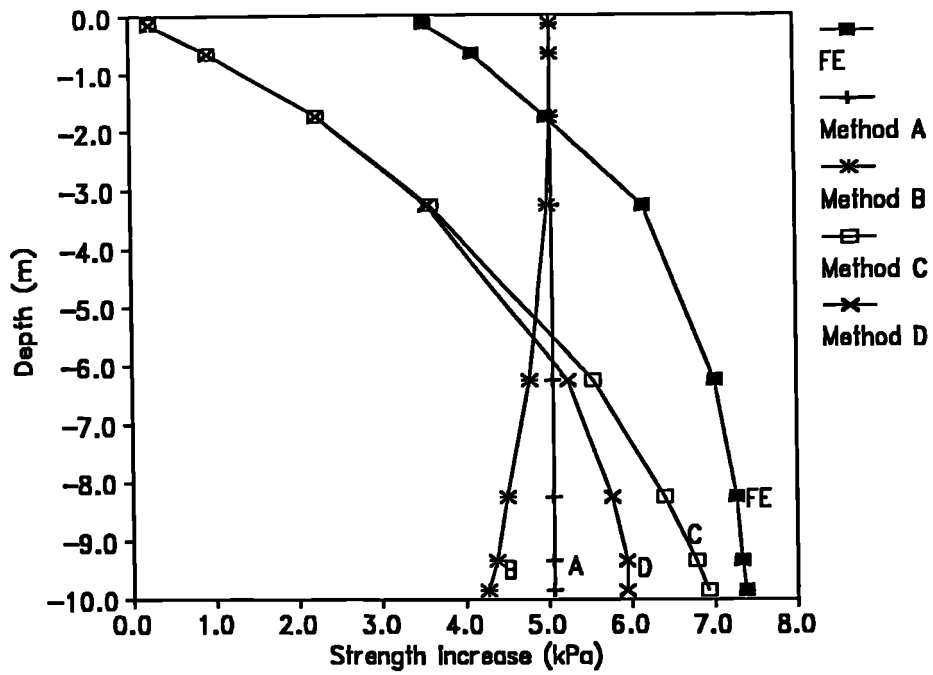


Figure 7.21a - Predicted strength increase near centreline; Methods A-D.

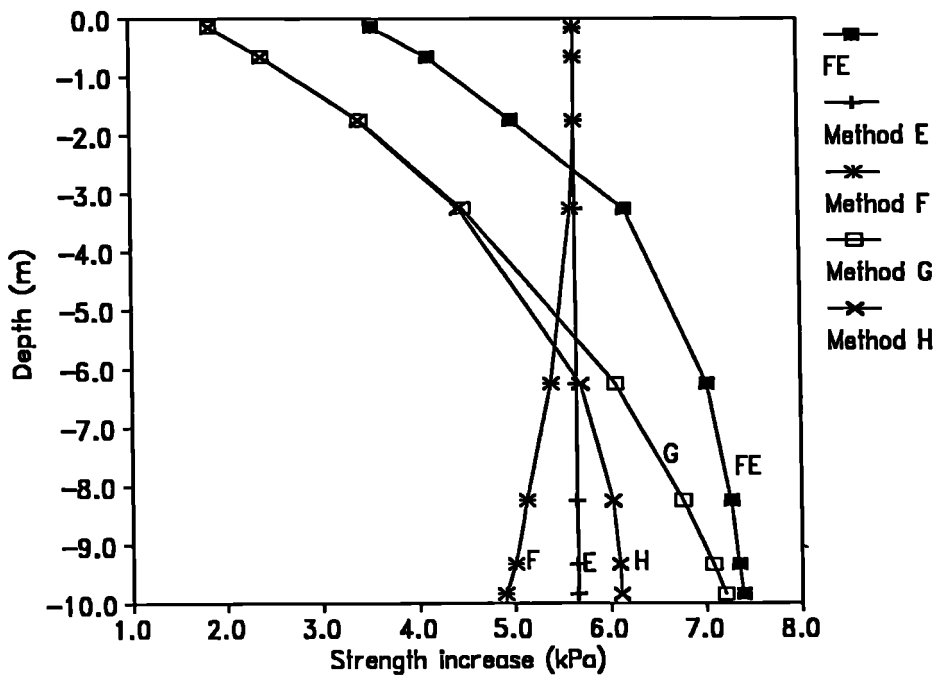


Figure 7.21b - Predicted strength increase near centreline; Methods E-F.

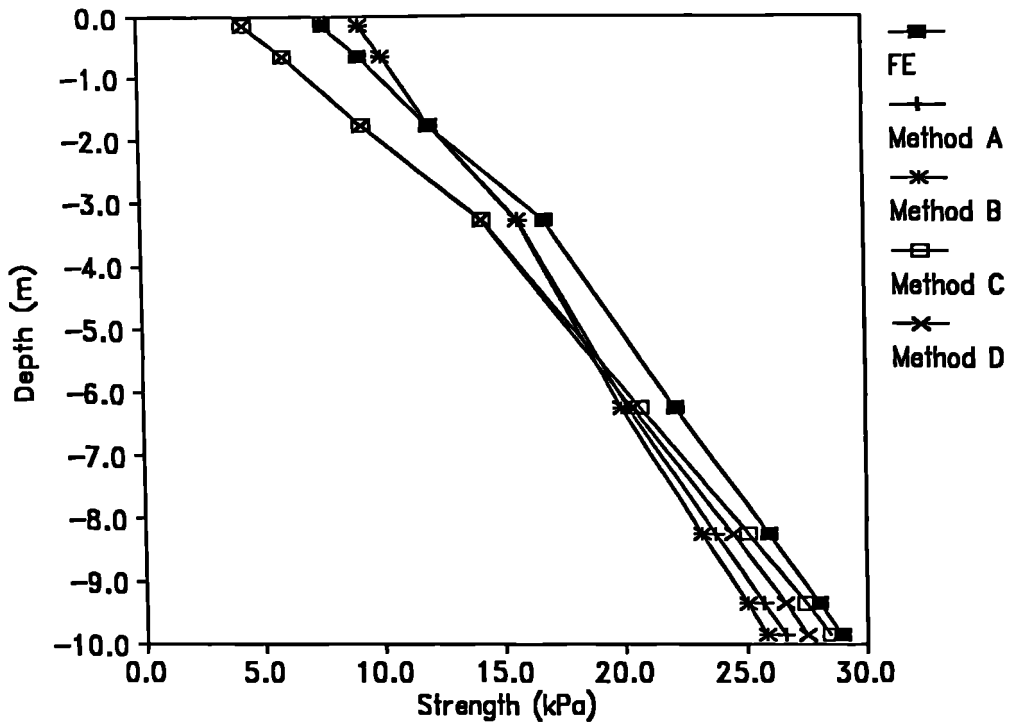


Figure 7.22a - Predicted strength near centreline; Methods A-D.

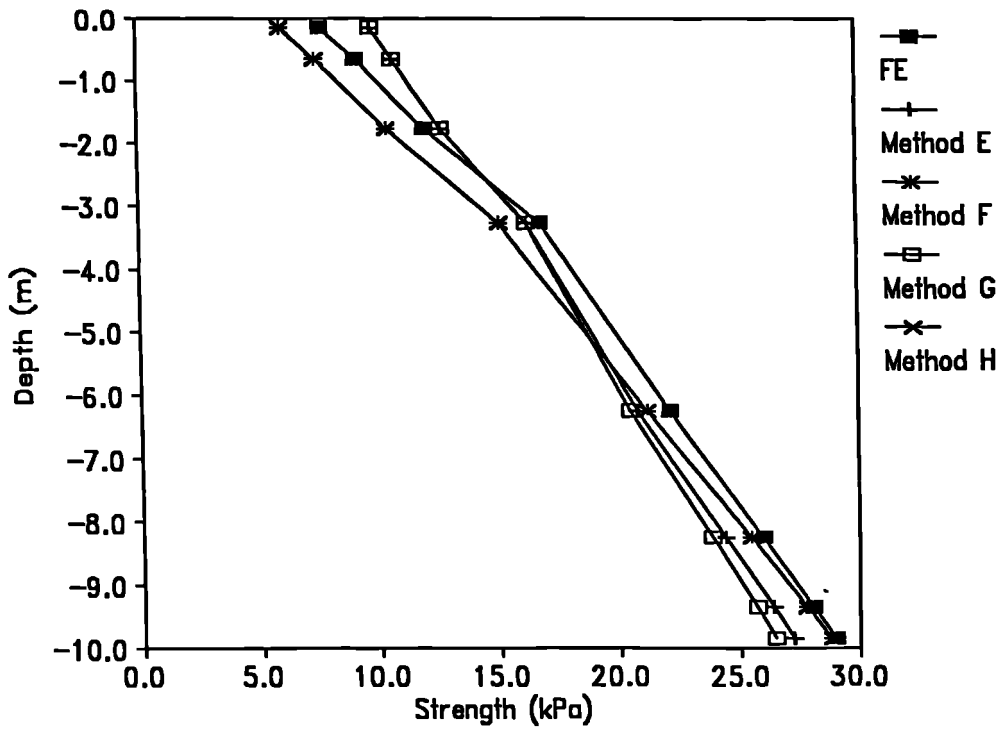


Figure 7.22b - Predicted strength near centreline; Methods E-F.

calculations, (C, D, G and H) it is reassuring that the finite element predicted variation of strength increase with depth at the centreline can be qualitatively reproduced. For comparisons of the undrained shear strength increases over the whole cross section, to be made below, only methods which allow for the variation of coefficient of volume change with depth will be considered.

The effect of the method of calculation of the vertical stress due to embankment loading can be observed by comparing method C with D and method G with H. Near the surface the predicted strength increases are identical, but lower down Gray's elastic solution predicts a smaller vertical stress (and hence strength) increase. Gray's elastic solution was developed for a semi-infinite half space whereas the finite element analysis considers a 10m depth of clay overlying a rough rigid layer. A comparison of Gray's solution with an elastic finite element analysis showed only minor differences in the predicted vertical stresses, with the maximum difference occurring at the surface, but in an elasto-plastic analysis of the subsoil the rigid bottom boundary effect on the vertical stress distribution may be more significant. In order to provide more general comparisons, the simple methods were used to calculate strength increases over the whole cross section employing both the one-dimensional and Gray vertical stress distributions.

The effect of immediate dissipation of pore water pressure in the over-consolidated range can be observed by comparing Figures 7.21a and b. In all cases the analyses assuming immediate dissipation (E, F, G and H) predicted a larger increase in strength and produced a strength increase profile which was closer to that predicted by the finite element analysis. Therefore, only methods which assume immediate dissipation of excess pore water pressure in the over-consolidated range will be considered further (i.e. Methods G and H).

Following the study of strength increases at the centreline methods G and H have been used to predict strength increases throughout the subsoil. Contours of the finite element predicted strength increase and absolute strength after the consolidation stage are shown in Figure 7.23.

The corresponding strength increase contours for methods G and H are plotted in Figure 7.24 with the absolute strength in Figure 7.25. In all of the contour plots it can be seen that the simple methods predict accurately the trend for the strength increase and absolute strength as defined from the finite element results. The differences between the finite element and simple methods for the undrained shear strength are plotted in contour form in Figure 7.26 (a positive value indicates a lower predicted strength increase from the simple method than from the finite element analysis).

## **7.4. Porto Tolle**

An analysis of the strength increase predicted for the Porto Tolle case history, reported in Chapter 6, can be carried out in the same manner as that described for the idealized case. For the idealized case the simplified methods which best reproduced the finite element analysis strength increases were methods G and H, see Table 7.2. These same assumptions were used to calculate the strength increase at Porto Tolle.

No consideration of the behaviour of the soil in the over-consolidated range was required as the soil was modelled as normally consolidated.

Comparison of the predicted degree of dissipation of excess pore pressures using the simplified procedure with those predicted from the finite element analysis are shown in Figure 7.27a for the end of the consolidation period. The degree of consolidation near the top of the clay layer is greater in the finite element analysis. This is due to the vertical flow of pore water which is not accounted for in the simplified (Hansbo) analysis. At greater depths the predicted dissipation agrees well, indicating that the variation of the

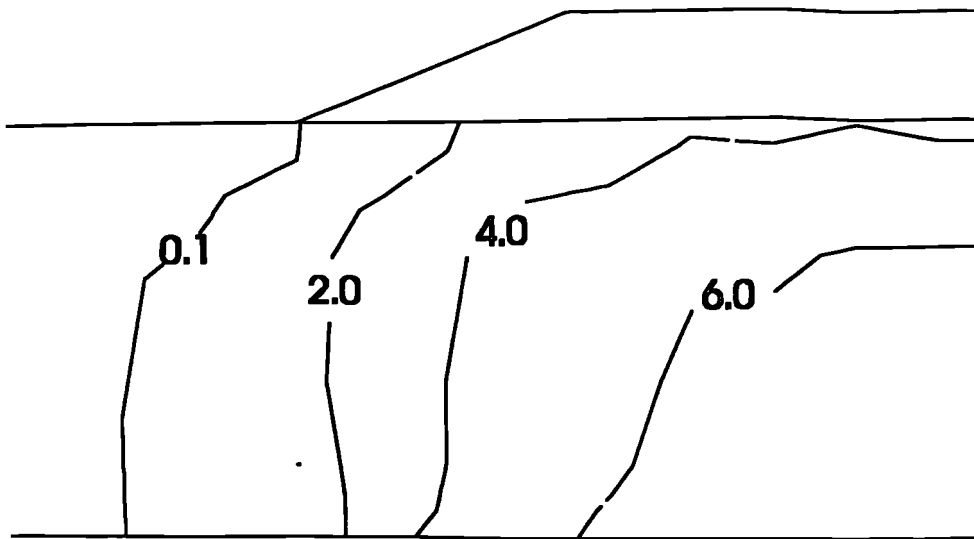


**Figure 7.23a - Contours of the strength increase at the end of the consolidation stage predicted by the finite element analysis.**

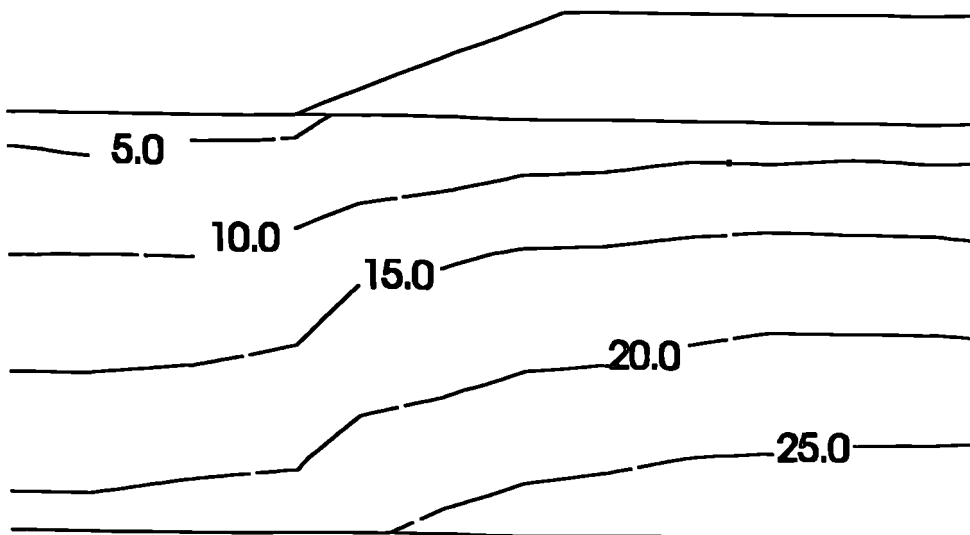


**Figure 7.23b - Contours of the absolute strength at the end of the consolidation stage predicted by the finite element analysis.**

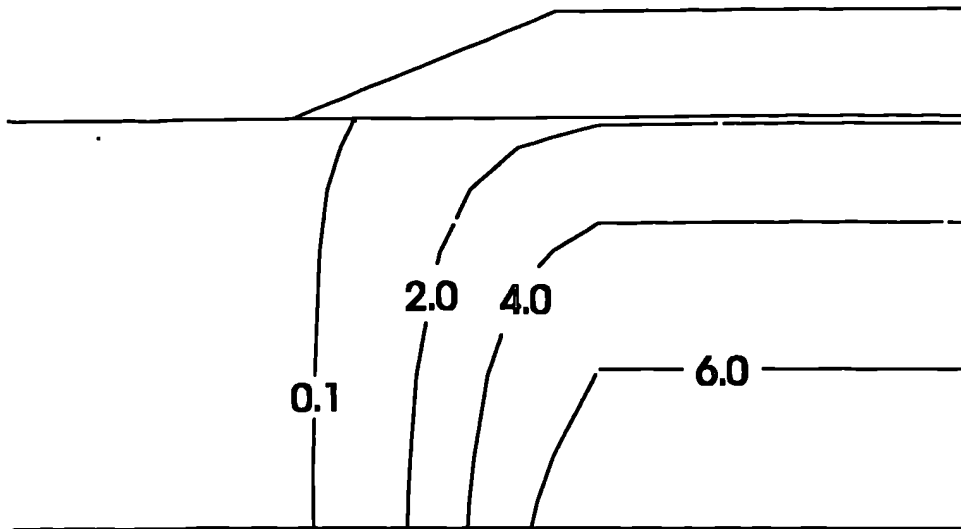


**Figure 7.24a - Contours of the strength increase at the end of the consolidation stage predicted using Method G (see Table 7.2).**

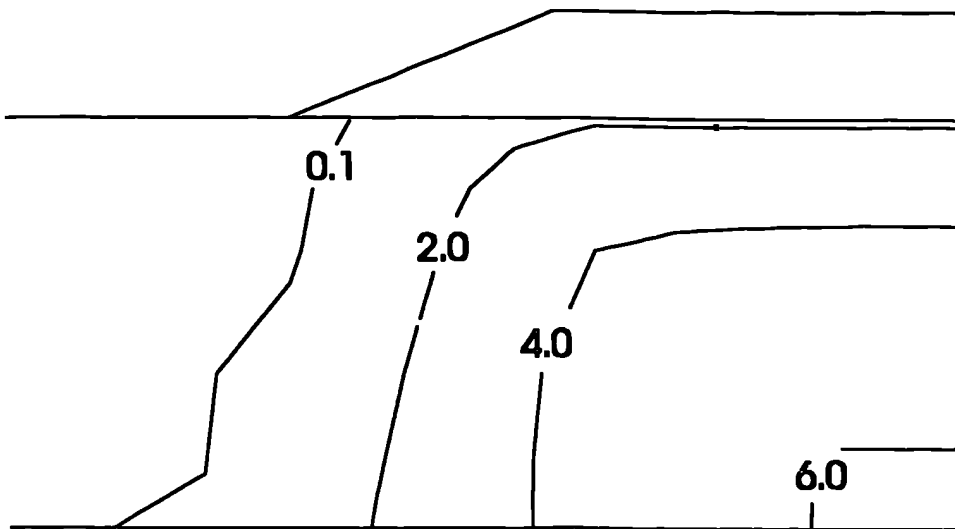


**Figure 7.24b - Contours of the strength increase at the end of the consolidation stage predicted using Method H (see Table 7.2).**

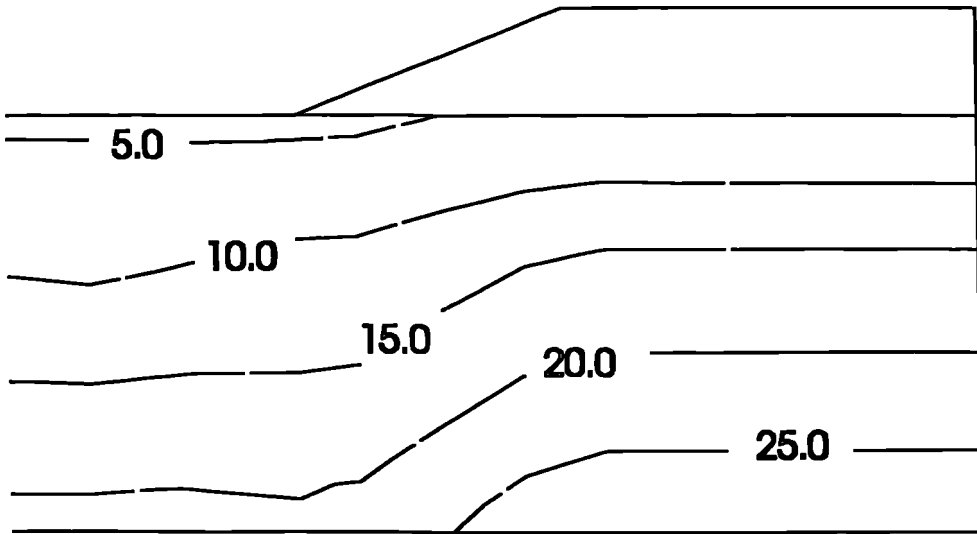


**Figure 7.25a - Contours of the absolute strength at the end of the consolidation stage predicted using Method G (see Table 7.2).**

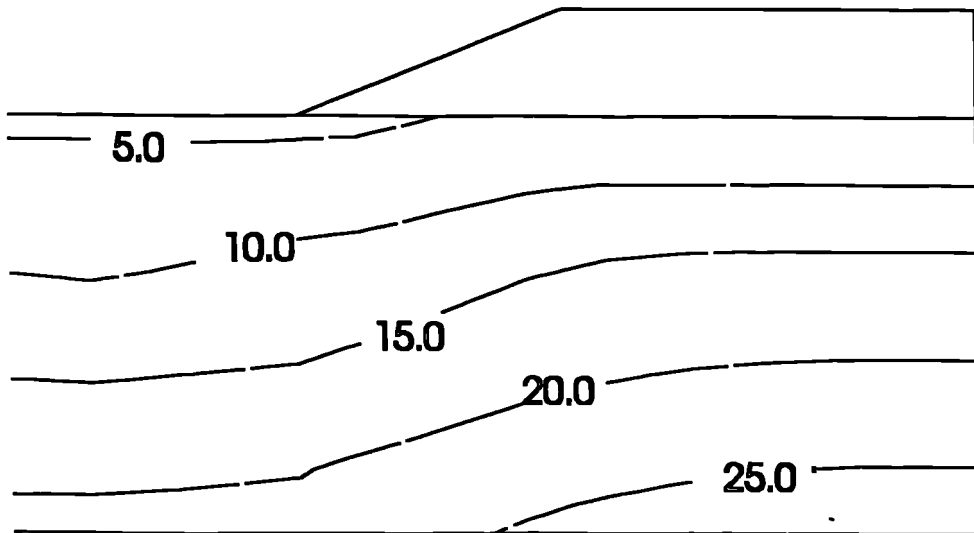


**Figure 7.25b - Contours of the absolute strength at the end of the consolidation stage predicted using Method H (see Table 7.2).**

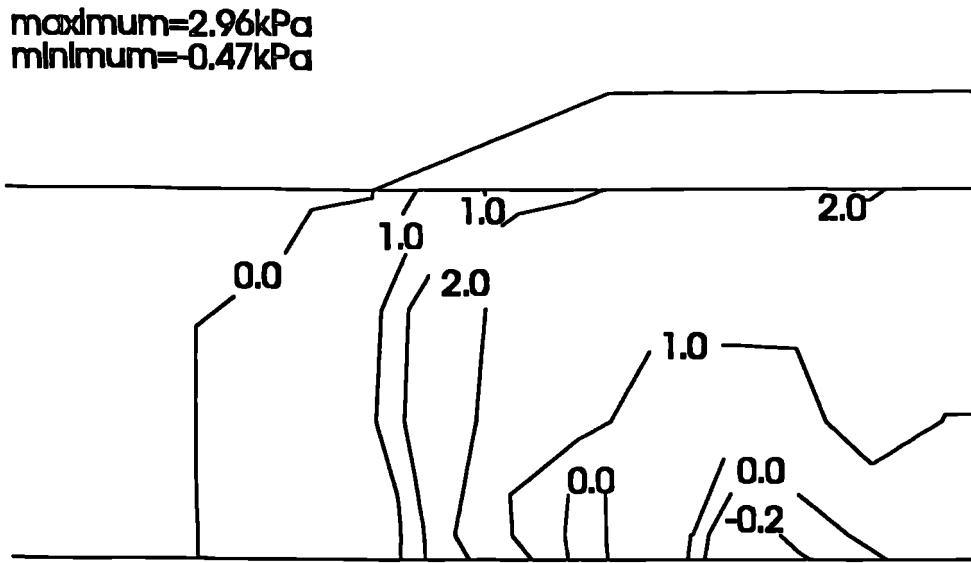


Figure 7.26a - Contours of the strength difference between Method G and finite element at the end of the consolidation stage.

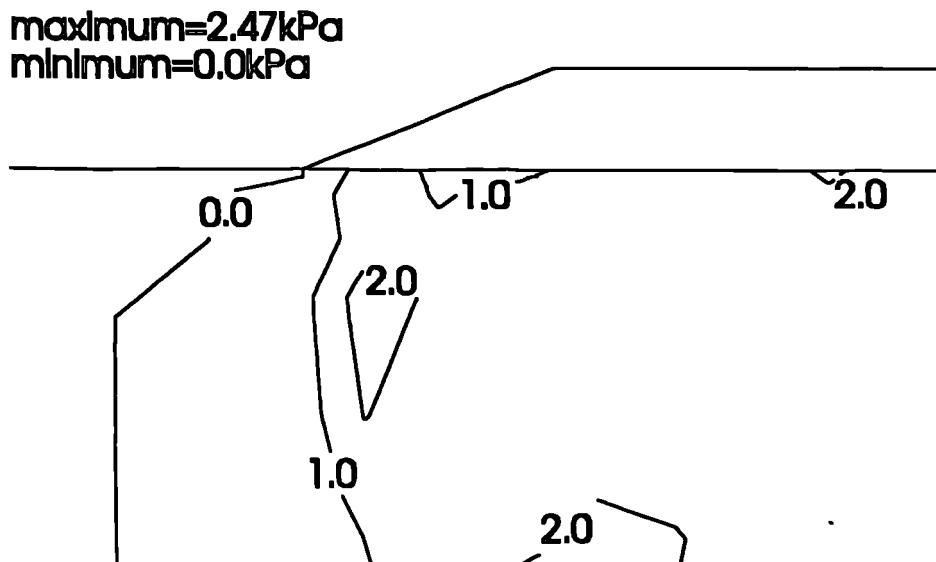


Figure 7.26b - Contours of the strength difference between Method H and finite element at the end of the consolidation stage.

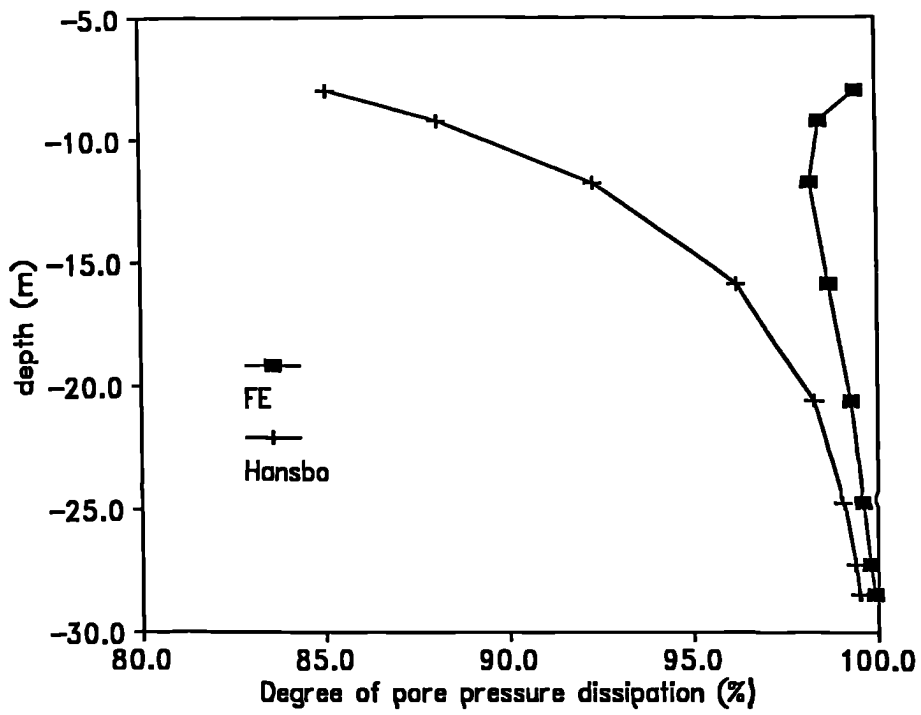


Figure 7.27a - Predicted degree of consolidation.

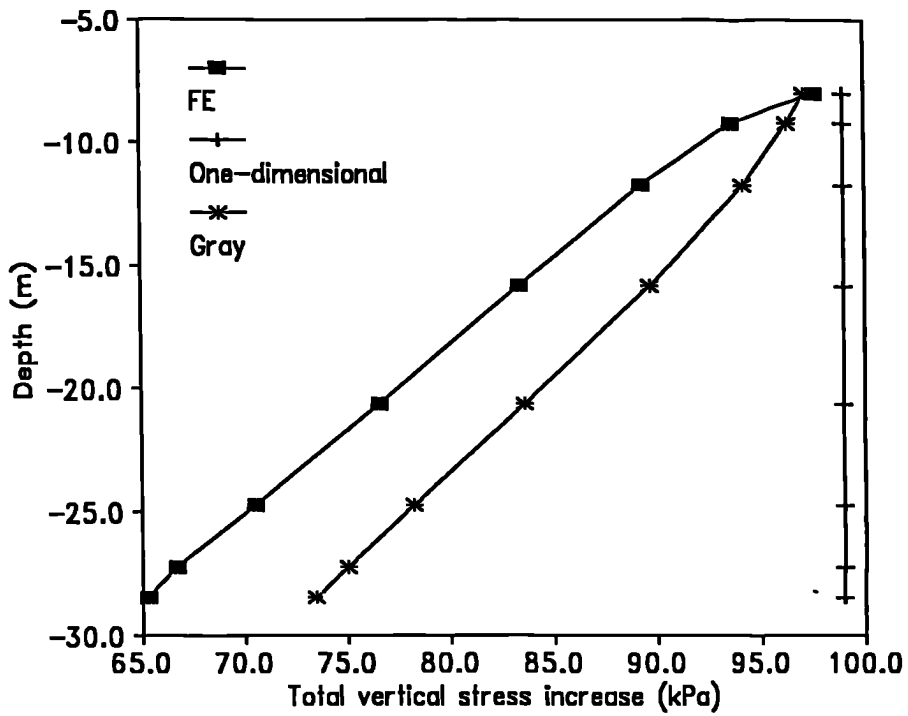


Figure 7.27b - Predicted increase in total vertical stress.

coefficient of volume change with depth, which would have occurred in the finite element analysis, was correctly reproduced by the simple method.

Figure 7.27b shows a comparison of the total stress increase near the centreline, calculated using both a one-dimensional approach and using the Gray (1936) elastic solution with the average finite element prediction in the unit cell closest to the centreline. The one-dimensional approach predicts a uniform stress increase equal to the applied load, and is increasingly in error with depth. The elastic solution represents more accurately the profile of total stress increase with depth, but still exceeds the finite element prediction.

After combining the predicted degree of consolidation (Figure 7.27a) and the increase in total vertical stress (Figure 7.21b) to predict the increase in effective vertical stress, the undrained strength ratio,  $(s_u/\sigma_v')_{NC}=0.272$ , can be used to predict the strength increase. These predictions are compared with the undrained shear strengths calculated from the finite element analysis near the centreline in Figure 7.28a. The underestimation of the degree of consolidation causes the simplified method to underestimate the strength at the surface. The one-dimensional calculation of total stress increase (Method G) results in a large error in the predicted strength. However, the superior total stress predictions using the elastic solution (Method H) result in a better prediction of the strength increase and produce the observed trend at the centreline.

The Gray solution has been used to calculate the stresses throughout the soft clay layer and predictions of strength increase from both the finite element analysis and the simplified method are presented in Figure 7.29. A comparison of the two predictions is made in Figure 7.30 where the strength calculated using the simplified method has been subtracted from those predicted in the finite element analysis. The maximum error on the safe side is 14.10kPa and this is due to the simplified method neglecting the effect of vertical permeability. The maximum unsafe error is -3.37kPa and is caused

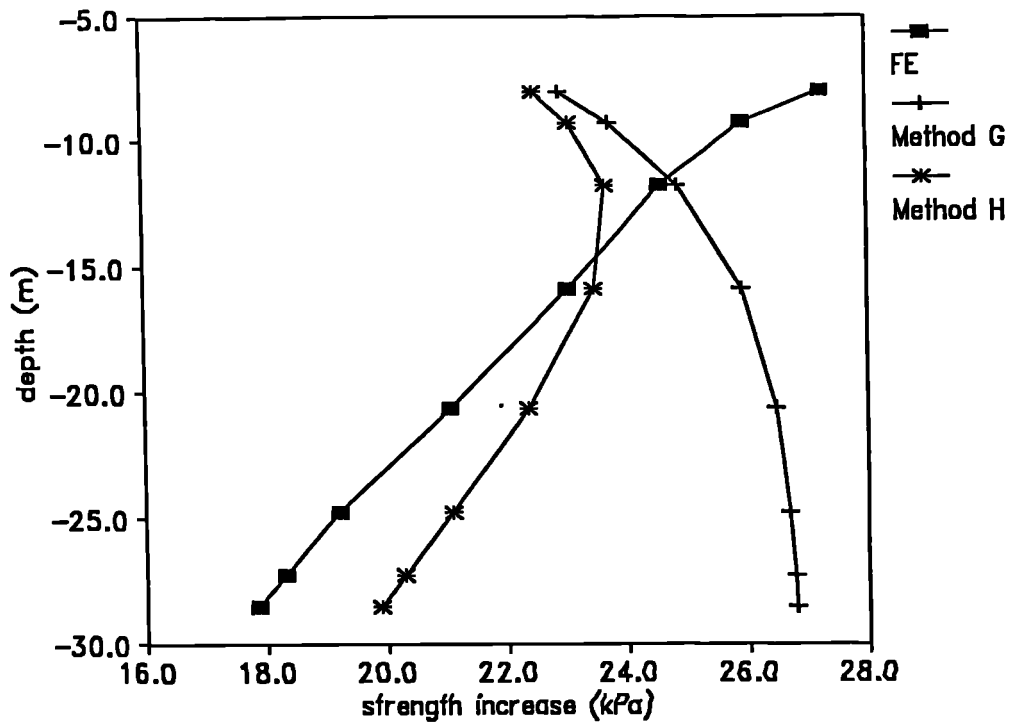


Figure 7.28a - Predicted undrained shear strength increase

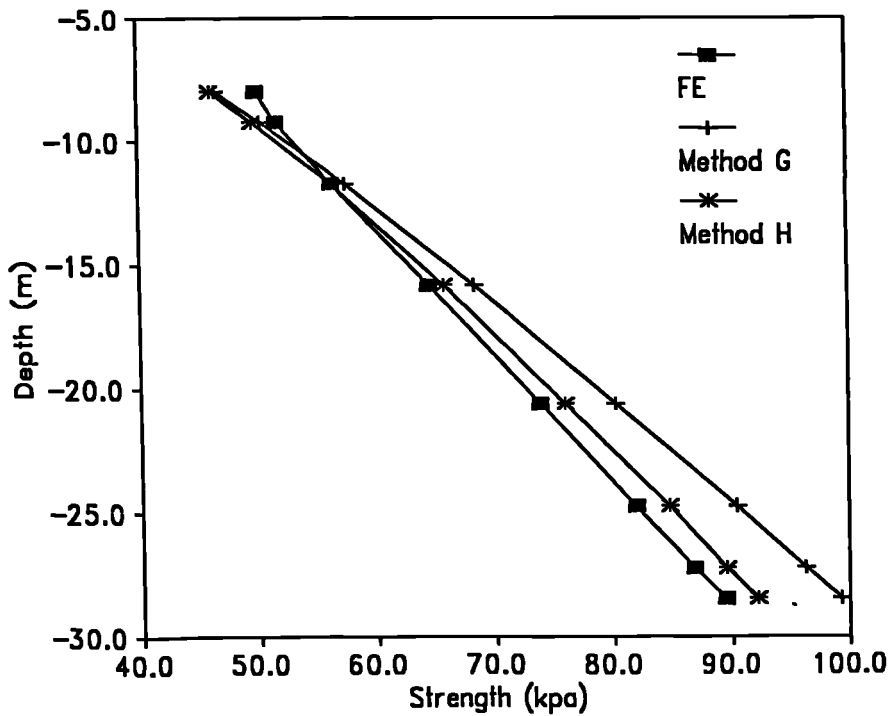
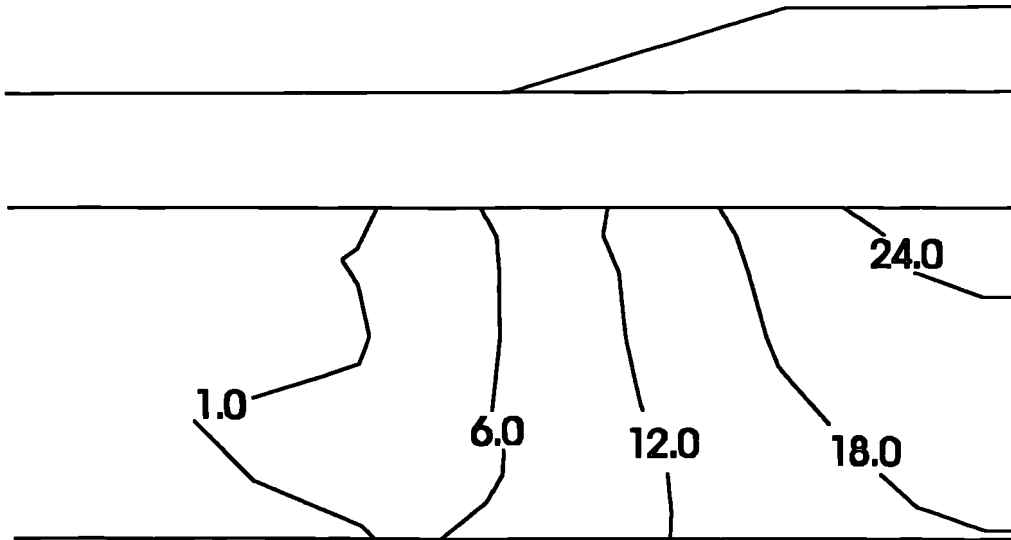
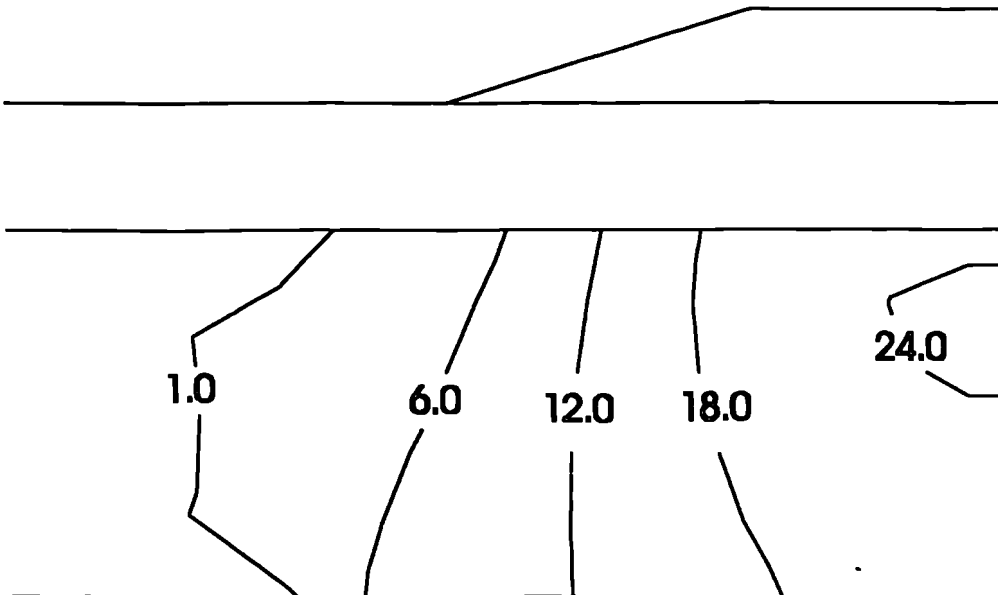


Figure 7.28b - Predicted absolute undrained shear strength.



**Figure 7.29a - Contours of the strength increase at the end of the consolidation stage predicted by the finite element analysis of Porto Tolle.**



**Figure 7.29b- Contours of the strength increase at the end of the consolidation stage predicted by the simplified method at Porto Tolle.**

maximum=14.1kPa  
minimum=-3.37kPa

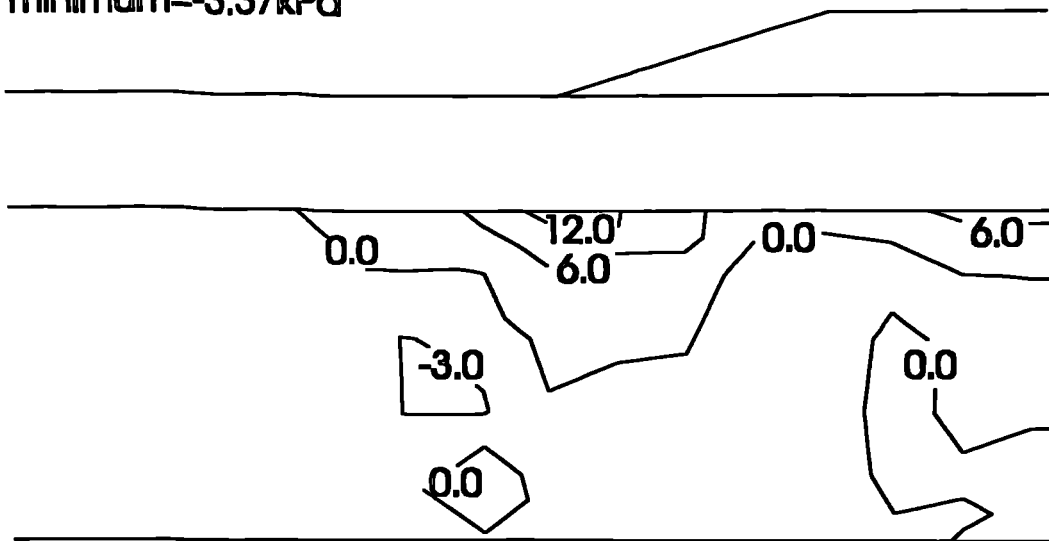


**Figure 7.30 - Contours of the strength difference predicted by the finite element analysis and the simplified method at the end of the consolidation stage at Porto Tolle.**

by the failure of the elastic solution to accurately predict the vertical stress increase. The unsafe error is relatively small and occurs only at a depth at which failure mechanisms are unlikely due to the increase of strength with depth.

## 7.5. Summary

The idealized study has provided information on the behaviour of a multi-stage construction of an embankment over a soft cohesive deposit. As expected analysis showed that multi-stage construction allows a significantly higher embankment to be constructed than would be possible in a single lift.

Comparison of limit equilibrium and finite element analysis has proved inconclusive. A higher factor of safety was found from the finite element

analysis. This was due, in part, to the consolidation which occurred during construction, in the finite element analysis, producing strength increases that were not allowed for in the (undrained) limit equilibrium analysis. Also the method by which the embankment was brought to failure in the finite element analysis was different from that used in the limit equilibrium analysis.

The undrained shear strength increases for the idealized multi-stage analysis have been calculated from the void ratios predicted by the finite element analysis. Simplified calculations of strength increases have also been made and comparisons of these methods with the finite element analysis have shown reasonable agreement. The simplified strength increase calculation procedures have also been applied to the Porto Tolle case history, Chapter 6. Agreement for this case was not as good, but the size of the error produced still indicates that the simple procedures for the prediction of undrained shear strength increase may be used.

The good agreement achieved despite a major assumption made in the simple methods regarding the generation of excess pore pressure during loading. The proposed procedure used a one-dimensional approach ignoring the pore pressures which would result from distortion. Such a method would underestimate the excess pore pressure generated and, therefore, would overestimate both the effective stress and the undrained shear strength. Further investigation of this aspect is needed.

## 8. Conclusions and Further Work

### 8.1. Objectives and Completed Work

The research reported in this thesis had several objectives;

- *To modify an existing finite element computer program so as to better model reinforced embankments constructed over soft clay subsoils involving vertical drains.* These modifications involved the incorporation of three additional elements to model: 1) the reinforcement, 2) the reinforcement/soil interface and 3) the vertical drains. A facility to model the variation of permeability with stress level has been incorporated for use with the modified Cam-clay constitutive model.
- *To benchmark the program by comparing finite element analyses with analytical solutions.* These comparisons were made for both the undrained failure of reinforced and unreinforced subsoils and for the consolidation of soil around a single vertical drain.
- *To compare the results of finite element analysis of well documented case histories with observed behaviour.* The case history analysed was a pre-loading embankment constructed over a soft normally consolidated clay improved using vertical drains.
- *To develop simplified design procedures for the effect of both reinforcement and vertical drains upon embankment stability.* This was divided into two parts. Firstly, a design method for single stage embankments, built with a constant side slope, based on published plasticity solutions was developed. Secondly, for the design of multi-stage constructed embankments a design philosophy was proposed in which undrained shear strengths were calculated at the start of each loading stage. These strengths were then used in a total

stress limit equilibrium analysis to assess the factor of safety of the embankment. Methods of estimating the undrained strength increases were investigated.

## **8.2. Conclusions**

The following conclusions have been drawn from the results presented in the previous chapters.

### **8.2.1. Undrained Collapse of Cohesive Soils**

Plasticity solutions for the undrained collapse of rigid strip footings on cohesive subsoils have been compared with a series of finite element analyses so as to confirm the ability to numerically model such problems. Once confidence in the finite element program was established, it was then used to model similar embankment problems for which analytical solutions were not available. Two relevant idealized subsoils were considered: firstly, a subsoil with strength increasing linearly and indefinitely with depth and, secondly, a subsoil with constant strength over a limited depth overlying a rough rigid layer.

- The displacement controlled finite element analysis has been shown to be in good agreement with the plasticity solutions. Analyses were carried out using both elastic-perfectly plastic (with a Tresca yield criterion) and modified Cam-clay constitutive models.
- Load controlled finite element analysis of the same idealized subsoils has shown that the surface settlement profile does not significantly affect the ultimate surface stress distribution. This conclusion is relevant to the application of plasticity solutions, which assume a rigid footing, to the design of embankments which are not rigid.
- The interface element has been shown to significantly improve the quality of the solution when analysing problems of this type containing

rough boundaries. The improvement in the solution cannot be matched by using a mesh with additional two dimensional elements with a similar number of degrees of freedom.

- The displacements predicted from the finite element analyses have been shown to be in good agreement with those predicted from plasticity solutions for a subsoil of uniform strength and limited depth.
- The mechanism of failure in the two types of subsoil considered has been shown to agree with the mechanisms predicted by plasticity theory. For a uniform strength and limited depth subsoil the failure is predominantly translational, and for a subsoil with strength increasing with unlimited depth the mechanism is rotational.
- A design procedure has been validated, using finite element *analyses*, in which the plasticity solutions can be used to predict the safe uniform side slope length for a single lift embankment under undrained conditions.

### **8.2.2. Consolidation of Soil Around Single Vertical Drains**

The behaviour of the soil around a single vertical drain has been studied and compared with analytical solutions.

- Comparisons between analytical and finite element results show that the drainage element implemented in CRISP correctly models a single vertical drain in an axisymmetric analysis.
- The predicted analytical trends for drains with well resistance and soil smear, caused by drain installation, have been correctly reproduced.
- A procedure for analysing a soil containing vertical drains in a plane strain finite element analyses has been developed. This matching procedure has been shown to produce good results for an elastic soil in a variety of conditions, which include the effects of smear, well resistance and vertical pore water flow in the soil.

### **8.2.3. Porto Tolle Case History Analysis**

A case history of an embankment constructed over a normally consolidated clay in northern Italy has been used as a case history for which finite element analyses could be carried out and compared with observed behaviour. All material parameters chosen for the analysis were obtained from published data at the outset and no attempt was made to revise the parameters subsequently.

- A series of matching analyses was performed in which the rates of consolidation of axisymmetric and plane strain unit cells were compared. In all cases the rate of consolidation of both unit cells was in good agreement. These analyses indicated that the matching procedure is suitable for more realistic soil conditions, in which material properties vary with depth and plastic deformations occur.
- A full plane strain analysis of the Porto Tolle subsoil was carried out. The vertical drains were installed at a spacing derived from the matching procedure. Comparisons of finite element and observed displacements were in good agreement. The predicted and observed excess pore pressures near the embankment centreline were in reasonable agreement during construction of the embankment. However, during the consolidation stage differences in the observed and predicted behaviour occurred with the finite element excess pore pressures almost completely dissipating whilst the observed values showed little dissipation. Jamiolkowski and Lancellotta (1984) suggested that the observed piezometer data were in error due to the presence of organic gas in the subsoil. This would explain the discrepancy between observed and predicted behaviour but it is also important to note that other phenomenon, such as destructuring of the subsoil, may have contributed to this difference.

#### **8.2.4. Idealized Two-Stage Construction**

In order to assess the finite element modelling of multi-stage embankment construction an idealized two-stage reinforced embankment was analysed. The material parameters and geometry were chosen to give a situation which is typical of such embankments in practice.

- The analysis confirmed that the height of an embankment could be increased above its single stage height by using a multi-stage construction approach, making use of the increase of undrained shear strength during consolidation stages.
- Comparisons of the finite element predicted factors of safety and limit equilibrium factors of safety were inconclusive. The difference in the assumptions for the two analyses made comparison difficult as consolidation occurred during the finite element construction stages and the method by which the embankment was made to fail was not the same in each case.
- The predicted lower interface shear stress distribution indicated that slip occurred along the entire underside of the reinforcement at failure. Reinforcement strains of over 8% were predicted at failure.
- Stress paths at various positions in the subsoil reflected expected behaviour and agreed with results of previous research.
- A simplified procedure for the prediction of the increases in undrained shear strength during stage construction has been proposed. The result of applying this procedure agreed well with the finite element predicted strength increases for the idealized subsoil. The procedure was also used to predict the strength increases for the Porto Tolle case history and the agreement with the finite element predictions was reasonably good considering the simplifications made.

## 8.3. Suggestions for Further Work

### 8.3.1. Further Modifications to CRISP

- The interface element has been implemented as a total stress element. This limits use of the element as it cannot be used to represent an drained frictional interface correctly and cannot predict strength increases for consolidating soils. An effective stress modification to the present element would allow more accurate predictions of collapse after consolidation of soft clay subsoils.
- Several aspects of the behaviour of soft clays are neglected in the current constitutive models in CRISP; their inclusion would lead to better modelling of these materials and improved predictions of embankment behaviour. Such aspects include strength anisotropy and the present model could be modified to better represent the variation of strength along a failure surface in an embankment analysis. A second problem with the modified Cam-clay model is the high value for the coefficient of earth pressure,  $K_0$ , which must be used to accurately model one-dimensional conditions. Also, many soft clays exhibit brittle behaviour and strain softening; this aspect is not modelled in CRISP but is likely to be important in the practice. No attempt has been made to model the creep behaviour of the soft clays; creep deformations can be significant but are not considered in the current version of the program.
- CRISP uses an incremental solution procedure. The size of the loading increments is hard to assess before analysis. A suitable increment size can only be found by performing several analyses, with increasing numbers of increments, and monitoring the displacements predicted. Iterative techniques can provide more efficient solutions and

eliminate the need to perform sensitivity studies on the number of increments.

### **8.3.2. Matching Procedure**

- The matching procedure has not been fully tested for all soil conditions. Additional analyses of over-consolidated soils and situations where the lateral displacements of the soil are larger should be carried out.
- The matching of the undrained strength increases in plane strain and axisymmetry have not been fully investigated. Analyses in which the increase in shear strength and comparisons of failure loads of unit cells could be carried out to verify the procedure.

### **8.3.3. Simplified Design Procedures**

- Comparison of finite element, limit equilibrium and plasticity analyses for single stage construction are in good agreement and indicate that any of the three methods is suitable for design. However, further research is required before similar simplified design methods for multi-stage embankments can be recommended. Comparisons of finite element and limit equilibrium analyses of loading stages must be performed to ensure that limit equilibrium analyses produce realistic results. Further investigation into the simple prediction of undrained shear strength is required including the generation of pore pressures during loading, the applicability of analytical solutions, such as Hansbo (1981), for elasto-plastic soils and calculations of the increase in stresses due to embankment loading.

## Appendix A - Strength of Modified Cam-clay

In this Appendix equations for the undrained shear strength, in both plane strain and axisymmetry, are developed within the modified Cam-clay framework (Roscoe and Burland, 1968).

### A.1. Relationship Between the Stress Invariant $q$ and the Undrained Shear Strength $s_u$

Definitions of the generalised stress invariant,  $q$ , used in critical state and the maximum shear stress at failure must be found and related in order to derive definitions for the undrained shear strength of modified Cam-clay.

The generalised deviator stress is defined in terms of the principal stresses as

$$q = \frac{1}{\sqrt{2}} \left[ (\sigma'_1 - \sigma'_2)^2 + (\sigma'_2 - \sigma'_3)^2 + (\sigma'_3 - \sigma'_1)^2 \right]^{\frac{1}{2}} \dots\dots\dots(A1)$$

where  $\sigma'_1 > \sigma'_2 > \sigma'_3$ .

The undrained shear strength is defined as

$$s_u = \frac{1}{2} (\sigma'_1 - \sigma'_3) \dots\dots\dots(A2)$$

#### Triaxial Conditions

In a triaxial test  $\sigma'_2 = \sigma'_3$ , therefore from Equations A1 and A2

$$s_{uTX} = \frac{q}{2} \dots\dots\dots(A3)$$

where the subscript TX represents triaxial conditions.

**Plane Strain Conditions**

Bishop (1966) introduced the parameter

$$b = \frac{\sigma'_2 - \sigma'_3}{\sigma'_1 - \sigma'_3} \dots\dots\dots(A4)$$

For plane strain conditions a value of  $b=1/2$  is often used, based on perfect plasticity, the intermediate principal stress is therefore

$$\sigma'_2 = \frac{1}{2}(\sigma'_1 + \sigma'_3) \dots\dots\dots(A5)$$

substituting for Equation A5 in Equation A1 and relating to Equation A2

$$s_{UPL} = \frac{q}{\sqrt{3}} \dots\dots\dots(A6)$$

where the subscript PL represents plane strain conditions.

**A.2. Relationship Between the Gradient of the Critical State Line M and the Angle of Shearing Resistance  $\phi'$**

For a cohesive deposit the angle of shearing resistance is defined as shown in Figure A1, from which the relationship between the angle of shearing resistance and the principal stresses at failure can be shown to be

$$\frac{\sigma'_1}{\sigma'_3} = \frac{1 + \sin \phi'}{1 - \sin \phi'} \dots\dots\dots(A7)$$

The definition of the gradient of the critical state line is

$$M = \left( \frac{q}{p'} \right) \dots\dots\dots(A8)$$

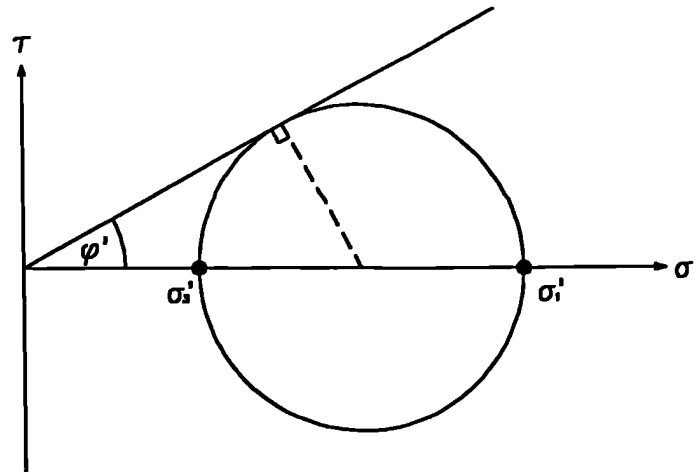


Figure A1 - Definition of Mohr Coulomb Yield surface for a cohesive material.

**Triaxial Conditions**

In a triaxial test the stress invariants are  $p'=(\sigma_1'+2\sigma_3')/3$  and  $q=(\sigma_1'-\sigma_3')$ , so that

$$M_{TX} = \frac{3(\sigma'_1 - \sigma'_3)}{(\sigma'_1 + 2\sigma'_3)} \dots\dots\dots(A9)$$

rearranging Equation A9 and combining with Equation A7

$$M_{TX} = \frac{6 \sin \phi'_{TX}}{3 - \sin \phi'_{TX}} \dots\dots\dots(A10)$$

**Plane Strain**

Using the definition of the stress invariant q from Equation A1 and  $p'=(\sigma_1'+\sigma_2'+\sigma_3')/3$  and substituting for the intermediate principal stress defined in Equation A5 it can be shown that

$$M_{PL} = \frac{\sqrt{3}(\sigma'_1 - \sigma'_3)}{(\sigma'_1 + \sigma'_3)} \dots\dots\dots(A11)$$

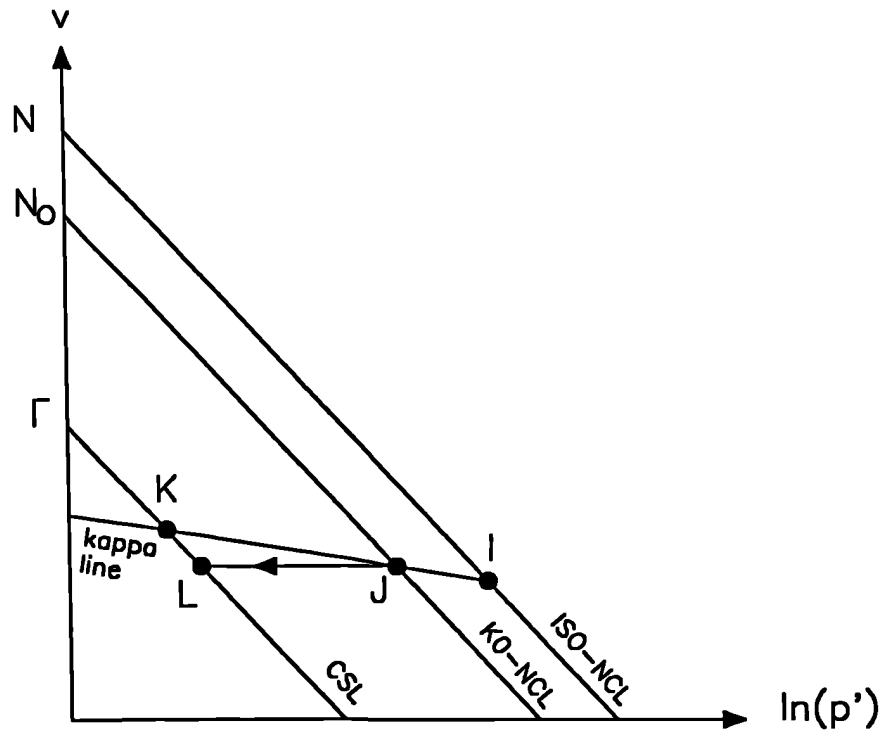


Figure A2 - Undrained stress path for a normally consolidated modified Cam-clay sample.

combining with Equation A7

$$M_{pL} = \sqrt{3} \sin \phi'_{pL} \dots\dots\dots(A12)$$

### A.3. Undrained Shear Strength of a Normally Consolidated Modified Cam-clay

Figure A2 shows a sample of  $K_0$  normally consolidated clay at position J the sample is then sheared undrained until failure at L. As the sample is normally consolidated at J it must lie on the yield surface

$$q_J^2 + M^2 p_J'^2 = 2M^2 p_K' p_J' \dots\dots\dots(A13)$$

rearranging and substituting  $\tau_J = q_J/p_J'$

$$\left(\frac{p'_K}{p'_J}\right) = \left(\frac{\eta_J^2 + M^2}{2M^2}\right) \dots\dots\dots(A14)$$

From geometry and using the critical state gradient for the normal consolidation lines and critical state lines of  $\lambda$  and the gradient of the swelling line  $\kappa$

$$\left(\frac{p'_L}{p'_J}\right) = \left(\frac{p'_K}{p'_J}\right)^\Lambda \dots\dots\dots(A15)$$

where  $\Lambda=(\lambda-\kappa)/\lambda$

Combining Equation A14 and A15

$$p'_L = p'_J \left(\frac{\eta_J^2 + M^2}{2M^2}\right)^\Lambda \dots\dots\dots(A16)$$

Point L is at the critical state, therefore  $q_L = Mp'_L$ , so that

$$q_L = Mp'_J \left(\frac{\eta_J^2 + M^2}{2M^2}\right)^\Lambda \dots\dots\dots(A17)$$

Equation A17 defines the deviator stress at failure in terms of the initial stresses for any normally consolidated modified Cam-clay sample subject to undrained loading.

### Triaxial Conditions

Substituting Equation A3 into Equation A17

$$s_{UTX} = M_{TX} \frac{p'_J}{2} \left(\frac{\eta_J^2 + M_{TX}^2}{2M_{TX}^2}\right)^\Lambda \dots\dots\dots(A18)$$

As the sample is  $K_0$  normally consolidated at J, the initial stress invariants are  $p'_J = \sigma'_{vc}(1+2K_{ONC})/3$  and  $q_J = \sigma'_{vc}(1-K_{ONC})$ , where  $K_{ONC}$  is the coefficient of earth pressure at rest for the normally consolidated sample and  $\sigma'_{vc}$  is the vertical preconsolidation pressure, therefore Equation A18 becomes

$$\frac{S_{UTX}}{\sigma'_{vc}} = M_{TX} \frac{(1+2K_{0NC})}{6} \left( \left( \frac{1-K_{0NC}}{1+2K_{0NC}} \right)^2 \frac{9}{2M_{TX}^2} + \frac{1}{2} \right)^\lambda \dots\dots\dots(A19)$$

**Plane Strain Conditions**

Combining Equation A6 with Equation A17

$$S_{UPL} = M_{PL} \frac{p'_J}{\sqrt{3}} \left( \frac{\eta_J^2 + M_{PL}^2}{2M_{PL}^2} \right)^\lambda \dots\dots\dots(A20)$$

again substituting for initial conditions

$$\frac{S_{UPL}}{\sigma'_{vc}} = M_{PL} \frac{(1+2K_{0NC})}{3\sqrt{3}} \left( \left( \frac{1-K_{0NC}}{1+2K_{0NC}} \right)^2 \frac{9}{2M_{PL}^2} + \frac{1}{2} \right)^\lambda \dots\dots\dots(A21)$$

**A.4. Undrained Shear Strength of an Over-Consolidated Modified Cam-clay**

Figure A3 shows a  $K_0$  normally consolidated sample at A and a lightly over-consolidated sample at B. If the sample undergo undrained shearing they would reach the critical state line at A\* and B\*.

From the defined geometry and gradients of the swelling and compression lines

$$\left( \frac{p_{B^*}}{p_{A^*}} \right) = \left( \frac{p_B}{p_A} \right)^\frac{\lambda}{\lambda} \dots\dots\dots(A22)$$

The over consolidation ratio in terms of mean effective stresses is defined as

$$R = \frac{p'_A}{p'_B} \dots\dots\dots(A23)$$

and at the critical state  $q_{A^*}=Mp'_{A^*}$  and  $q_{B^*}=Mp'_{B^*}$ , Equation A22 can be rewritten as

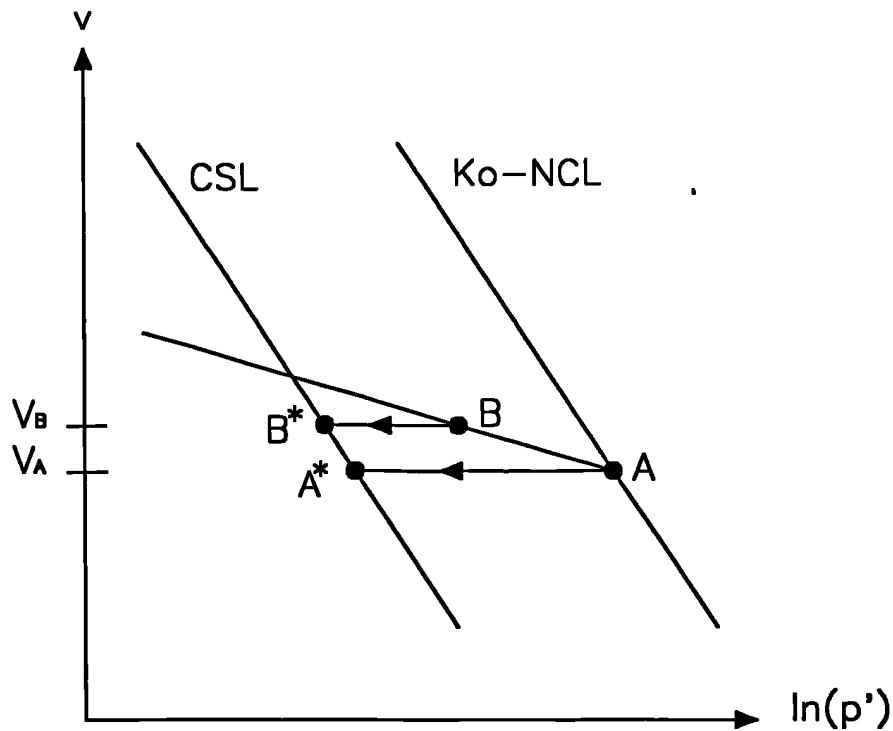


Figure A3 - Undrained stress paths for normally consolidated and lightly over-consolidated modified Cam-clay samples.

$$\left(\frac{q_{B^*}}{p_B'}\right) = \left(\frac{q_{A^*}}{p_A'}\right) R^{\lambda} \dots\dots\dots(A24)$$

The coefficient of earth pressure for the normally consolidated and over-consolidated samples,  $K_{0NC}$  and  $K_0$  respectively, can be substituted into Equation A24

$$\left(\frac{3q_{B^*}}{(1+2K_0)\sigma_{vB}'}\right) = \left(\frac{3q_{A^*}}{(1+2K_{0NC})\sigma_{vA}'}\right) \left(\frac{(1+2K_{0NC})\sigma_{vA}'}{(1+2K_0)\sigma_{vB}'}\right)^{\lambda} \dots\dots\dots(A25)$$

now the overconsolidation ratio, OCR, is defined as

$$OCR = \frac{\sigma_{vA}'}{\sigma_{vB}'} \dots\dots\dots(A26)$$

Substituting Equation A26 into Equation A25 and rearranging

$$\left(\frac{q_{B^*}}{\sigma'_{vB}}\right) = \left(\frac{q_{A^*}}{\sigma'_{vA}}\right) \left(\frac{(1+2K_0)}{(1+2K_{0NC})}\right) \left(\frac{OCR(1+2K_{0NC})}{(1+2K_0)}\right) \dots\dots\dots(A27)$$

An identical equation to Equation A27 can be derived for heavily over-consolidated samples where the initial state is on the dry side of the critical state line.

**Triaxial Conditions**

Point A in Figure A3 is normally consolidated and substituting Equation A3 into Equation A27

$$\left(\frac{S_{UTX}}{\sigma'_v}\right)_{OC} = \left(\frac{S_{UTX}}{\sigma'_{vc}}\right)_{NC} \left(\frac{(1+2K_0)}{(1+2K_{0NC})}\right) \left(\frac{OCR(1+2K_{0NC})}{(1+2K_0)}\right) \dots\dots\dots(A28)$$

where the subscripts OC and NC represent over-consolidated and normally consolidated states respectively

**Plane Strain Conditions**

Similarly for plane strain conditions substituting Equation A6 into Equation A27

$$\left(\frac{S_{UPL}}{\sigma'_v}\right)_{OC} = \left(\frac{S_{UPL}}{\sigma'_{vc}}\right)_{NC} \left(\frac{(1+2K_0)}{(1+2K_{0NC})}\right) \left(\frac{OCR(1+2K_{0NC})}{(1+2K_0)}\right) \dots\dots\dots(A29)$$

**A.5. Calculation of the Undrained Shear Strength of Modified Cam-clay From Void Ratio Data**

The finite element analysis produces values for the void ratio during a modified Cam-clay analysis. From this data the undrained shear strength can be derived as follows.

For any stress state if the specific volume,  $v$ , is known then at the critical state

$$v = \Gamma - \lambda \ln(p'_{cs}) \dots\dots\dots(A30)$$

where the subscript cs represents critical state conditions.

Rearranging Equation A30

$$p'_{cs} = \exp\left[\frac{\Gamma - v}{\lambda}\right] \dots\dots\dots(A31)$$

At the critical state  $q_{cs} = Mp'_{cs}$ , therefore Equation A31 becomes

$$q_{cs} = M \exp\left[\frac{\Gamma - v}{\lambda}\right] \dots\dots\dots(A32)$$

Substituting for triaxial conditions, from Equation A3, Equation A32 becomes

$$s_{UTX} = \frac{M_{TX}}{2} \exp\left[\frac{\Gamma - v}{\lambda}\right] \dots\dots\dots(A33)$$

Substituting for plane strain conditions, from Equation A6, Equation A32 becomes

$$s_{UPL} = \frac{M_{PL}}{\sqrt{3}} \exp\left[\frac{\Gamma - v}{\lambda}\right] \dots\dots\dots(A34)$$

### **A.5. Calculation of the Coefficient of the Earth Pressure at Rest**

Calculation of the undrained shear strength, Equations A19, A21, A28 and A29, requires the calculation of the coefficient of earth pressure at rest. Calculations are outlined below for both normally and over consolidated soils.

#### **Coefficient of Earth Pressure at Rest for a Normally Consolidated Soil ( $K_{0NC}$ )**

Empirical relationships for the coefficient of earth pressure at rest have been proposed for normally consolidated clays. For example Jaky (1944)

$$K_{0NC} = 1 - \sin \phi' \dots\dots\dots(A35)$$

From critical state theory it is also possible to derive an equation which ensures zero strains in the horizontal directions for an increment of vertical load, as

$$K_{0NC} = \frac{3 - \eta_{0NC}}{3 + 2\eta_{0NC}} \dots\dots\dots (A36)$$

where

$$\frac{\eta_{0NC}(1 + \nu') (1 - \Lambda)}{3(1 - 2\nu')} + \frac{3\eta_{0NC}\Lambda}{M^2 - \eta_{0NC}^2} = 1 \dots\dots\dots (A36a)$$

In the current research a value of  $G = \infty$  has been used so that Equation A36a becomes

$$\eta_{0NC} = \frac{-3\Lambda + \sqrt{9\Lambda^2 + 4M^2}}{2} \dots\dots\dots (A37)$$

Equations A35 and A36 can be applied for the Porto Tolle case history (Chapter 6) where  $\phi_{PL}' = 32^\circ$ ,  $M_{PL} = 0.92$  and  $\Lambda = 0.8$ . The coefficients of earth pressure at rest for the normally consolidated soil are 0.47 and 0.74 for the empirical and theoretical relationships respectively.

In all analyses presented in this Thesis the theoretical relationship, Equation A36 has been used to calculate  $K_{0NC}$ . Analyses of unit cells with insitu stresses defined using this relationship and loaded one-dimensionally produced correct stress paths. However, comparative analyses using the empirical relationship produced unrealistic stress paths.

**Coefficient Of Earth Pressure at Rest for an Over-Consolidated Soil ( $K_0$ )**

Several empirical relationships have been suggested for the coefficient of earth pressure at rest for over-consolidated soils, for example Schmitt (1966)

$$K_0 = K_{0NC} (OCR)^\alpha \dots\dots\dots (A38)$$

where OCR is the over-consolidation ratio and  $\alpha$  is an empirical constant.

Wroth (1975) proposed a theoretically correct relationship based on the assumption of elastic unloading

$$K_0 = (OCR) K_{0NC} - \frac{\nu'}{1-\nu'} (OCR - 1) \dots\dots\dots(A39)$$

In which  $\nu'$  is the Poissons ratio.

For the lightly overconsolidated soils, considered in this Thesis, Equation A39 has been used to calculate the coefficient of earth pressure at rest. However, it is noted that as the over-consolidation ratio (OCR) becomes higher the predicted coefficient, using this relationship, overestimates the observed value which are better represented by Equation A38.

### **A.6. Triaxial Versus Axisymmetric Conditions**

The equation derived in this Appendix for triaxial conditions have assumed  $\sigma_2' = \sigma_3'$ . The equation have been applied to axisymmetric conditions where in general  $\sigma_2'$  is not equal to  $\sigma_3'$ . However in the analyses presented this difference has been negligible.

## Appendix B - Consolidation of a Plane Strain

### Unit Cell

#### Average Degree Of Consolidation

A plane strain unit cell of width B, shown in Figure B1, has a central vertical drain of zero thickness and a vertical discharge capacity  $Q_w$ . Hansbo's (1981) Theory can be adapted for such a cell as follows.

If  $v_x$  represents the rate of pore water flow towards the drain and  $i_x$  is the hydraulic gradient at distance x from the drain then from Darcy's law

$$v_x = ki_x \dots\dots\dots(B1)$$

where k is the horizontal soil permeability.

Equation B1 may be rewritten as

$$v_x = \frac{k}{\gamma_w} \frac{\partial u}{\partial x} \dots\dots\dots(B2)$$

where  $\gamma_w$  is the unit weight of water and u the excess pore pressure.

Consider a horizontal slice of soil of thickness dz. The flow in the slice at distance x from the drain is equal to the change in volume within a block of soil of width (B-x), so that

$$v_x = \frac{\partial \epsilon}{\partial t} (B-x) dz \dots\dots\dots(B3)$$

where  $\epsilon$  is the strain in the z direction

Substituting Equation B3 into Equation B2 and rearranging

$$\frac{\partial u}{\partial x} = \frac{\gamma_w}{k} \frac{\partial \epsilon}{\partial t} (B-x) \dots\dots\dots(B4)$$

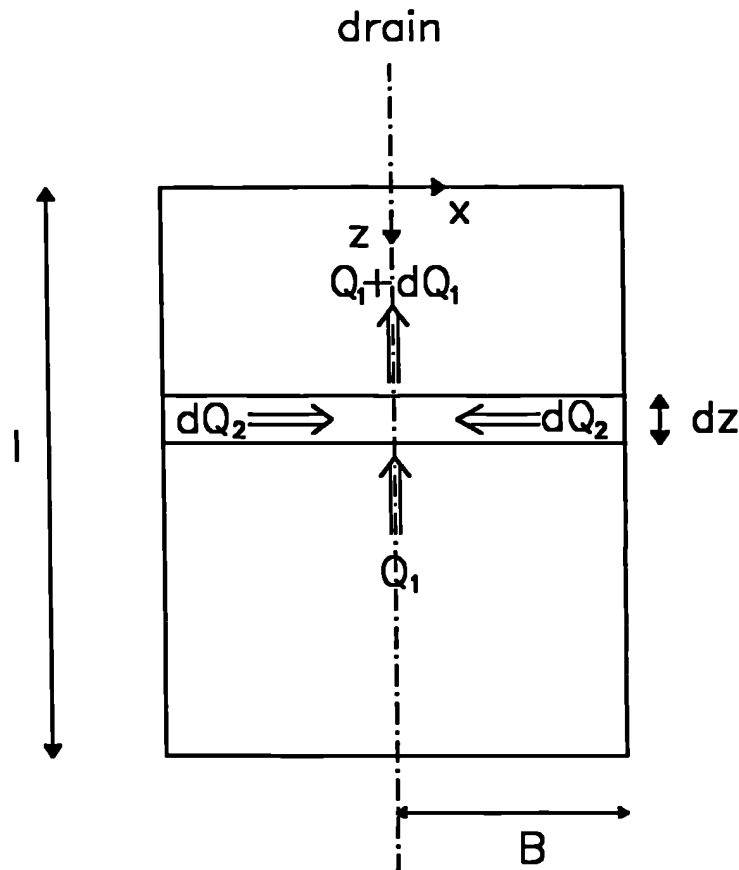


Figure B1 - Plane strain unit cell.

Consider next the corresponding slice of drain. As only vertical flow occurs in the drain, the change of flow from the entrance to the exit of the slice,  $dQ_1$ , is

$$dQ_1 = \frac{Q_w}{\gamma_w} \left( \frac{\partial^2 u}{\partial z^2} \right)_{x=0} dz dt \dots\dots\dots(B5)$$

The horizontal inflow to the slice from each side,  $dQ_2$ , is

$$dQ_2 = \frac{k}{\gamma_w} \left( \frac{\partial u}{\partial x} \right)_{x=0} dz dt \dots\dots\dots(B6)$$

For continuity

$$dQ_1 + 2dQ_2 = 0 \dots\dots\dots(B7)$$

Substituting for  $dQ_1$  and  $dQ_2$  into Equation B7

$$\frac{Q_w}{\gamma_w} \left( \frac{\partial^2 u}{\partial z^2} \right)_{x=0} dzdt + \frac{2k}{\gamma_w} \left( \frac{\partial u}{\partial x} \right)_{x=0} dzdt = 0 \dots\dots\dots(B8)$$

Rearranging

$$\left( \frac{\partial u}{\partial x} \right)_{x=0} + \frac{Q_w}{2k} \left( \frac{\partial^2 u}{\partial z^2} \right)_{x=0} = 0 \dots\dots\dots(B9)$$

Substituting Equation B4 into Equation B9

$$\frac{B\gamma_w}{k} \frac{\partial \epsilon}{\partial t} + \frac{Q_w}{2k} \left( \frac{\partial^2 u}{\partial z^2} \right)_{x=0} = 0 \dots\dots\dots(B10)$$

Rearranging

$$\left( \frac{\partial^2 u}{\partial z^2} \right)_{x=0} = -\frac{2B\gamma_w}{Q_w} \frac{\partial \epsilon}{\partial t} \dots\dots\dots(B11)$$

Integrating Equation B11 with depth and introducing the boundary conditions that at  $z=0, u=0$  and at  $z=L, \frac{\partial u}{\partial z} = 0$

$$(u)_{x=0} = \frac{2B\gamma_w}{Q_w} \frac{\partial \epsilon}{\partial t} \left( Lz - \frac{z^2}{2} \right) \dots\dots\dots(B12)$$

Integrating Equation B4 and introducing the boundary conditions defined by Equation B12.

$$u = \frac{\gamma_w}{2} \frac{\partial \epsilon}{\partial t} \left[ \frac{1}{k} (2Bx - x^2) + \frac{2B}{Q_w} (2Lz - z^2) \right] \dots\dots\dots(B13)$$

Let  $\bar{u}$  be the average excess pore pressure across the section at depth  $z$ , so that

$$\bar{u}B = \int_0^B u dx \dots\dots\dots(B14)$$

Substituting  $u$  from Equation B13 into Equation B14 and integrating

$$\bar{u} = \frac{B^2 \gamma_w}{2k} \frac{\partial \bar{\epsilon}}{\partial t} \left[ \frac{2}{3} + \frac{2k}{BQ_w} (2Lz - z^2) \right] \dots\dots\dots(B15)$$

Now

$$\frac{\partial \bar{\epsilon}}{\partial t} = m_v \frac{\partial \bar{\sigma}'}{\partial t} = -m_v \frac{\partial \bar{u}}{\partial t} \dots\dots\dots(B16)$$

where  $m_v$  is the coefficient of volume change

Substituting Equation B16 into Equation B15

$$\frac{\partial \bar{u}}{\partial t} = -\frac{B^2 \gamma_w m_v}{2k} \left[ \frac{2}{3} + \frac{2k}{BQ_w} (2Lz - z^2) \right] \frac{1}{\bar{u}} \dots\dots\dots(B17)$$

Integrating Equation B17 and applying the boundary condition that at  $t=0$ ,  $\bar{u} = \bar{u}_0$ .

$$t = -\frac{B^2 \gamma_w m_v}{2k} \left[ \frac{2}{3} + \frac{2k}{BQ_w} (2Lz - z^2) \right] \ln \left( \frac{\bar{u}}{\bar{u}_0} \right) \dots\dots\dots(B18)$$

Rearranging

$$t = -\frac{B^2 \gamma_w m_v}{2k} \mu \ln \left( \frac{\bar{u}}{\bar{u}_0} \right) \dots\dots\dots(B19)$$

where

$$\mu = \left[ \frac{2}{3} + \frac{2k}{BQ_w} (2Lz - z^2) \right] \dots\dots\dots(B20)$$

Introducing expressions for the time factor

$$T_h = \frac{C_h t}{4B^2} \dots\dots\dots(B21)$$

and the coefficient of consolidation

$$C_h = \frac{k}{m_v \gamma_w} \dots\dots\dots(B22)$$

Equation B19 can be rearranged as

$$u = u_o \exp\left[\frac{-8T_h}{\mu}\right] \dots\dots\dots(B23)$$

Therefore, the average degree of consolidation at depth z is given by

$$\bar{U}_h = \frac{u_o - u}{u_o} = 1 - \exp\left[\frac{-8T_h}{\mu}\right] \dots\dots\dots(B24)$$

**Ratio of Excess Pore Pressure in Axisymmetric and Plane Strain Unit Cells**

Consider a drain without well resistance or smear. It can be shown (Hansbo, 1981) that the excess pore pressure at a distance r from the centreline in an axisymmetric unit cell of radius R is

$$u_{ax} = \frac{\gamma_w}{2k_{ax}} \frac{\partial \varepsilon}{\partial t} \left[ R^2 \ln\left(\frac{r}{r_w}\right) - \left(\frac{r^2 - r_w^2}{2}\right) \right] \dots\dots\dots(B25)$$

Similarly, for a plane strain unit cell of half width B the excess pore pressure at a distance x from the centreline is given by Equation B13 which for a drain with no well resistance ( $Q_w \rightarrow \infty$ ) becomes

$$u_{pl} = \frac{\gamma_w}{k_{pl}} \frac{\partial \varepsilon}{\partial t} \left[ Bx - \frac{x^2}{2} \right] \dots\dots\dots(B26)$$

Expressing Equation B25 and Equation B26 as a ratio

$$\frac{u_{ax}}{u_{pl}} = \frac{k_{pl}}{k_{ax}} \frac{R^2}{2B^2} \left[ \frac{\left( \ln\left(\frac{r}{r_w}\right) - \frac{r^2}{2R^2} + \frac{r_w^2}{2R^2} \right)}{\left( \frac{x}{B} - \frac{x^2}{2B^2} \right)} \right] \dots\dots\dots(B27)$$

If the axisymmetric and plane strain unit cells are matched using geometry matching (Section 5.3) then

$$B = R \sqrt{\frac{3}{2} \left( \ln(n) - \frac{3}{4} \right)} \dots\dots\dots(B28)$$

and

$$k_{pl} = k_{ax} \dots\dots\dots(B29)$$

Substituting Equation B28 and Equation B29 into Equation B26

$$\frac{U_{ax}}{U_{pl}} = \frac{\left[ \ln\left(\frac{r}{r_w}\right) - \frac{r^2}{2R^2} + \frac{r_w^2}{2R^2} \right]}{\left[ 3\left(\ln(n) - \frac{3}{4}\right) \right] \left[ \frac{x}{B^2} - \frac{x^2}{2B^2} \right]} \dots\dots\dots(B30)$$

Substituting  $n=R/r_w$  and introducing the geometric ratio,  $\alpha$ , where

$$\alpha = \frac{r}{R} = \frac{x}{B} \dots\dots\dots(B31)$$

Equation B30 becomes

$$\frac{U_{ax}}{U_{pl}} = \frac{\left[ 2 \ln(n\alpha) - \alpha^2 + \frac{1}{n^2} \right]}{\left[ 3\left(\ln(n) - \frac{3}{4}\right) \right] \left[ 2\alpha - \alpha^2 \right]} \dots\dots\dots(B32)$$

At the periphery of the unit cells  $\alpha=1$  and ignoring the small term  $(1/n^2)$

$$\frac{U_{ax}}{U_{pl}} = \frac{2 \ln(n) - 1}{3\left(\ln(n) - \frac{3}{4}\right)} \dots\dots\dots(B33)$$

## Appendix C - Development of Pore Pressures due to Ramped Loading

Hansbo (1981) developed an analytical solution for the consolidation of a soil cylinder by radial flow towards a central vertical drain.

$$\bar{U}_h = u_0 e^{(-8T_h/\mu)} \dots\dots\dots(C1)$$

where  $u_0$  is the initial excess pore pressure throughout the soil cylinder,  $T_h$  is the time factor for radial consolidation and  $\mu$  is a parameter dependent on the radius of the drain and soil cylinder, the well resistance and the amount of smear which has taken place on installation.

A similar equation for plane strain conditions was derived in Appendix B, Equation B24. Both equations assume that a load has been applied instantaneously to the top of the unit cell so that no dissipation of pore pressure has taken place.

In practice loads cannot be applied instantaneously and a certain period for application must be allowed. In this Appendix Hansbo's analytical solution is modified to allow for the effect of a load applied at a constant rate, i.e. ramp loading.

Figure C1 shows a load applied at a constant rate over of a time  $T$  so that the final load is  $Q$ . At any time,  $t$ , the applied load,  $q$ , can be defined as

$$q = \frac{Q}{T}t \dots\dots\dots(C2)$$

During application of the load it is necessary to calculate the excess pore pressure developed, at say time  $t_1$ .

Consider an infinitely small time increment from  $t$  to  $t+dt$ , during this time the load has increased from  $q$  to  $q+dq$ , as this is an infinitely small time the loading is undrained. So that from Equation C2 the increase in excess pore pressure is

$$du = dq = \frac{Q}{T}dt \dots\dots\dots(C3)$$

The excess pore pressure can then dissipate for a time  $t_1-t$ .

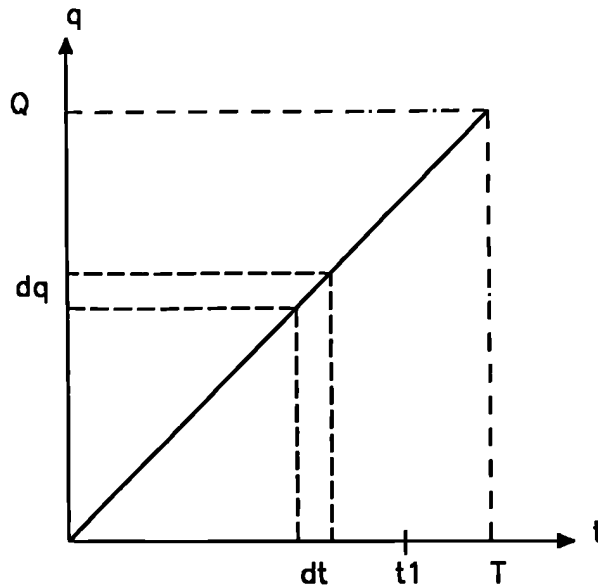


Figure C1 - Ramp loading scheme.

From Equation C1 and substituting  $\alpha=8c_v/D^2\mu$  and considering the increment of load we have

$$d\bar{U}_h = (du) e^{-\alpha(t_1-\theta)} \dots\dots\dots(C4)$$

Substituting for du from Equation C3 into Equation C4

$$d\bar{U}_h = \frac{Q}{T} e^{-\alpha(t_1-\theta)} dt \dots\dots\dots(C5)$$

The excess pore pressure developed at time  $t_1$  can be found by integrating Equation C5 from  $t=0$  to  $t=t_1$

$$\bar{U}_h = \frac{Q}{T} \int_{\theta=0}^{t=t_1} e^{-\alpha(t_1-\theta)} dt \dots\dots\dots(C6)$$

therefore

$$\bar{U}_h = \frac{Q}{\alpha T} (1 - e^{-\alpha t_1}) \dots\dots\dots(C7)$$

Equation C7 defines the excess pore pressure developed by a ramp loading. If a series of ramp loadings and consolidation periods are used the Equation C7 and Equation C1 can be alternated using the calculated values for the average excess pore pressure as input to the next stage.

# References

- 1 Abid, M.M. (1980). *The consolidation behaviour of laminated clays using the finite element method*. PhD Thesis, Sheffield University.
- 2 Abid, M.M. and Pyrah, I.C.(1990). *The consolidation behaviour of finely laminated clays*. Computers and Geotechnics, Vol. 10, pp. 307-323.
- 3 Almeida, M.S.S. (1984). *Stage constructed embankments on soft clays*. PhD Thesis, University of Cambridge.
- 4 Almeida, M.S.S, Britto, A.M, and Parry, R.H.G. (1985). *Centrifuged embankments on strengthened and unstrengthened clay foundations*. Géotechnique, Vol. 35, pp. 425-441.
- 5 Almeida, M.S.S, Britto, A.M and Parry, R.H.G. (1986). *Numerical modelling of a centrifuged embankment on soft clay*. Canadian Geotechnical Journal, Vol. 23, pp. 103-114.
- 6 Atkinson, J.H. and Bransby, P.L (1981). *The mechanics of soils - An introduction to critical state soil mechanics*. Pub: McGraw Hill.
- 7 Atkinson, J.H. (1981). *Foundations and slopes*. Pub: McGraw Hill.
- 8 Barron, R.A. (1948). *Consolidation of fine-grained soils by drain wells*. Trans. ASCE, 113, pp. 718-742.
- 9 Bassett, R.H. (1987). *Original design of the trial embankment*. Prediction Symposium on a Reinforced Embankment, King's College, London.
- 10 Bassett, R.H. and Guest D.R. (1990). *Model and analytical comparisons of the behaviour of reinforced embankments on soft foundations*. Proc. Int Reinforced Soil Conf., Glasgow, pp. 461-467.
- 11 Biot, M.A. (1941). *General theory of three dimensional consolidation*. J. Appl. Phs. Vol. 12, pp. 155-164.
- 12 Bishop, A.W. (1955). *The use of slip circle in the stability analysis of slopes*. Géotechnique No. 5, pp. 7-17.
- 13 Bishop, A.W. (1966). *The strength of soils as geotechnical materials*. Géotechnique, Vol. 10, pp. 91-128.

- 14 Bishop, A.W. and Bjerrum L. (1960). *The relevance of triaxial the test to the solution of stability problems*. Proc. Research Conf. on Shear Strength of Cohesive Soils, ASCE, pp. 437-501.
- 15 Bonaparte, R. and Christopher, B.R. (1987). *Design and Construction of reinforced embankments over weak foundations*. Transportation Research Record 1153, pp. 26-39.
- 16 Bond, A. (1984). *The behaviour of embankments on soft clay*. MSc Dissertation, Imperial College, London.
- 17 Booker, J.R. and Small, J.C. (1975). *An investigation of the stability of numerical solutions of Biot's equations of consolidation*. Int. J. Solids and Structures. Vol. 11, pp. 907-911.
- 18 Boultrap, E. and Holtz, R.D. (1983). *Analysis of embankments on soft ground reinforced with geotextiles*. Proc. 8<sup>th</sup> ECSMFE. Vol. 1, pp. 469-472.
- 19 Britto, A.M and Gunn, M.J. (1987). *Critical state soil mechanics via finite elements*. Pub: Ellis Horwood.
- 20 Brown, C.B. and King, I.P. (1966). *Automatic embankment analysis: equilibrium and instability conditions*. Géotechnique, Vol. 16, No. 3, pp. 209-219.
- 21 Burland, J.B. (1972). *A method of estimating the pore pressures and displacements beneath embankments on soft, natural clay deposits*. Proceedings of the Roscoe Memorial lecture, pp. 505-536, Pub: G.T. Foulis and Co.
- 22 Burland, J.B. (1990). *On the compressibility and shear strength of natural clays*. Géotechnique Vol. 40, pp. 329-378.
- 23 Clough, R.W. and Woodward, R.J. (1967). *Analysis of embankment stresses and deformations* Journal of Soil Mechanics and Foundations Division ASCE , Vol. 9, SM4, pp. 529-549.
- 24 Cook, R.D. (1981). *Concepts and applications of finite element analysis*. Pub: Wiley.
- 25 Croce, A., Calabresi, G. and Viglianni, C. (1973). *In situ investigation on pore pressures in soft clay*. Proceedings of the 8<sup>th</sup> ICSMFE, Moscow, Vol. 2.2, pp. 53-60.
- 26 Davis, E.H. and Booker, J.R. (1973). *Effect of increasing strength with depth on bearing capacity of clays*. Géotechnique Vol. 23, pp. 551-563.

- 27 Delmas, P., Magnan, J.P. and Soyez, B. (1987). *New techniques for building embankments on soft soils*. Embankments on Soft Clays, Chapter 6, Bulletin of the Public Works Research Centre, Athens, Greece.
- 28 Dluzewski, J.M. and Termaat, R.J. (1990). *Consolidation by finite element method in engineering problems*. 2<sup>nd</sup> European Speciality Conference on Numerical Methods in Geotechnical Engineering, pp. 213-222.
- 29 Duncan, J.M. and Chang, C.Y. (1970). *Non-linear analysis of stress and strain in soils*. J. Soil Mech. Fdns. Div., ASCE, Vol. 96, SM 5, pp. 1629-1653.
- 30 Duncan, J.M., Schafer, V.R., Franks, L.W. and Collins, S.A. (1987). *Design and performance of a reinforced embankment for mohicanville dike No. 2 in Ohio*. Transportation Research Record 1153, pp. 15-25.
- 31 Fellenius, W. (1927). *Erdstatische berechnungen mit reibung and kohaesion*, Ernst, Berlin.
- 32 Fowler, J. (1982). *Theoretical design considerations for fabric-reinforced embankments*. Proc 2<sup>nd</sup> Int. Conf. Geotextiles, Vol. 3, Las Vegas, pp. 665-670.
- 33 Garassino, A., Jamiolkowski, M., Lancellotta, R. and Tonghini, M. (1979). *Behaviour of pre-loading embankments on different vertical drains with reference to soil consolidation characteristics*. Proc. 7<sup>th</sup> European Conf. Soil Mech. Brighton Vol. 3, pp. 213-218.
- 34 Goodman, R.E., Taylor, R.L. and Brekke, T.L. (1968). *A model for the mechanics of jointed rock*. J. Soil Mechanics and Foundation Div. ASCE, Vol 94, pp. 637-659.
- 35 Gray, H. (1936). *Stress distribution in elastic solids*. Proc. 1<sup>st</sup> Int. Conf. Soil Mech. and Found. Eng., Vol. 2, p. 157.
- 36 Griffiths, D.V. (1985). *The effect of pore fluid compressibility on failure loads in elasto plastic soils*. Int. J. Numerical and Analytical Methods in Geomechanics, Vol 9, pp. 253-259.
- 37 Gunn, M.J. and Britto, A.M. (1982). *CRISP: users' and programmers' guide*. Engineering Department, Cambridge University.
- 38 Gunn, M.J. and Britto, A.M. (1984). *CRISP84-users and programmers guide*. Engineering Department, Cambridge University.

- 39 Hight, D.W., Jardine, R.J. and Gens, A.(1987). *The behaviour of soft clays*. Embankments on Soft Clays, Chapter 2, Bulletin of the Public Works Research Centre, Athens, Greece.
- 40 Hansbo, S. (1981). *Consolidation of fine-grained soils by prefabricated drains*. Proc. 10<sup>th</sup> ICSMFE, Stockholm, Vol. 3, pp. 677-682.
- 41 Hansbo, S., Jamiolkowski, M. and Kok, L. (1981). *Consolidation by vertical drains*. Géotechnique, Vol 31, No. 1, pp. 45-66.
- 42 Hardin, B.O. and Black, W.L. (1966). *Sand stiffness under various triaxial stresses*. Journal of Soil Mechanics and Foundation Engineering, ASCE, Vol. 92, SM2.
- 43 Hinton, B. and Campbell, J.S. (1974). *Local global smooting of discontinuous finite element functions using a least squares method*. International Journal of Numerical Methods in Engineering, Vol. 8, pp. 461-480.
- 44 Hird, C.C and Kwok, C.M. (1986). *Predictions for the Stanstead Abbots trial Embankment*. Prediction Symposium on a Reinforced Embankment, King's College, London.
- 45 Hird, C.C and Kwok, C.M. (1990a). *Finite element studies of interface behaviour in reinforced embankments on soft ground*. Computer and Geotechnics, Vol. 8, pp. 111-131.
- 46 Hird, C.C and Kwok, C.M. (1990b). *Parametric studies of the behaviour of a reinforced embankment*. Proceedings of the 4<sup>th</sup> International Conference on Geotextiles, Geomembranes and Related Products, The Hauge, Netherlands.
- 47 Hird, C.C and Russell, D. (1990). *A benchmark for soil-structure interface elements*. Computer and Geotechnics, Vol. 10, pp. 139-147.
- 48 Hird, C.C, Pyrah, I.C. and Russell, D. (1990). *Finite element analysis of the collapse of reinforced embankments on soft ground*. Vol. 40, No. 4, pp. 633-640.
- 49 Hird, C.C. and Pyrah; I.C. (1990). *Predictions of the behaviour of a reinforced embankment on soft ground*, Performance of reinforced soil structures, British Geotechnical Society.
- 50 Hird, C.C and Jewell, R.A. (1990). *Theory of reinforced embankments Reinforced Embankments: Theory and Practice in the British Isles*. pp. 115-139. Pub: Thomas Telford.

- 51 Hohberg, J.M. (1990). *A note on spurious oscillations in FEM joint elements*. Earthquake Engineering and Structural Dynamics, Vol. 19, pp. 773-779.
- 52 Holtz, R.D., Jamiolkowski, M., Lancellotta, R. and Pedroni, S. (1987). *Performance of band-shaped drains*. CIRIA Report 364.
- 53 Holtz, R.D., Jamiolkowski, M., Lancellotta, R. and Pedroni, S. (1991). *Prefabricated vertical drains - design and performance*. CIRIA, Pub: Butterworth Heinemann.
- 54 Horne, M.R. (1964). *The consolidation of stratified soil with vertical and horizontal drainage*. Int. J. of Mech. Sc., Vol. 6, pp. 187-197.
- 55 Houlsby, G.T. and Jewell, R.A. (1988). *Analysis of unreinforced and reinforced embankments on soft clays by plasticity theory*. Proc. 6th Int. Conf. on Numerical Methods in Geomechanics, Innsbruck, Vol. 2, pp. 1443-1448.
- 56 Jacky J. (1944). *The coefficient of earth pressure at rest*. Magyar Mernok es Epitesz Egylet Kozloyne.
- 57 Jamiolkowski, M., Lancellotta, R. and Tordelle, M.L. (1980). *Geotechnical properties of Porto Tolle NC silty clay*. 6<sup>th</sup> ECSMFE, Varna, Bulgaria, pp. 151-179.
- 58 Jamiolkowski, M., Lancellotta, R. and Wolski W. (1983). *Precompression and speeding up consolidation*. General report, 8<sup>th</sup> ECSMFE, Helsinki, Vol. 3, pp. 1201-1226.
- 59 Jamiolkowski, M. and Lancellotta, R. (1984). *Embankment on vertical drains - pore pressures during construction*. Proc. Int. Conf. Case Histories in Geotechnical Engineering, St Louis, MO, USA, Vol. 1, pp. 275-278.
- 60 Jardine R.J. and Hight D.W. (1987). *The behaviour and analysis of embankments on soft clay*. Embankments on Soft Clays, Chapter 3, Bulletin of the Public Works Research Centre, Athens, Greece.
- 61 Jewell, R.A. (1982). *A limit equilibrium design method for embankment on soft soils*. Proc. 2<sup>nd</sup> Int. Conf. on Geotextiles, Las Vegas, Vol. 3, pp. 671-676.
- 62 Jewell, R.A. (1988). *The mechanics of a reinforced embankment on soft soils*. Geotextiles and Geomembranes, Vol. 7, pp. 237-273.

- 63 Jewell, R.A. (1990). *Strength and deformation in reinforced soil design*. Proceedings of the 4<sup>th</sup> International Conference on Geotextiles, Geomembranes and Related Products, The Hague, Netherlands.
- 64 Johnson, S.J. (1970a). *Precompression for improving foundation soils*. J. Soil Mech. Fnds. Div., ASCE, Vol. 96, SM1, pp. 111-144.
- 65 Johnson, S.J. (1970b). *Foundation precompression with vertical sand drains*. J. Soil Mech. Fnds. Div., ASCE, Vol. 96, SM1, pp. 145-175.
- 66 Kjellman, M. (1948). *Accelerating consolidation of fine-grained soils by means of cardboard wicks*. Proc. 11<sup>th</sup> Conf. Soil Mech., Rotterdam, Vol. 2, pp. 302-305.
- 67 Kulhawy, F.H. and Duncan, J.M. (1972). *Stresses and movements in Oroville Dam*. Journal of Soil Mechanics and Foundations Division ASCE. Vol. 98, SM7, pp. 653-665.
- 68 Kumamoto, N., Sumioka, N., Moriwaki, T. and Yoshikuni, H. (1988). *Settlement behaviour of improved ground with a vertical drain system*. Soils and Foundations. Vol. 28, No. 1, pp. 77-88.
- 69 Kwok, C.M. (1987). *Reinforced embankments on soft ground*. PhD Thesis, University of Sheffield.
- 70 Ladd, C.C. (1991). *Stability evaluation during staged construction*. J. Geotechnical Engineering, ASCE, Vol. 117, No. 4, pp. 540-615.
- 71 Lade, P.V. (1977). *Elasto-plastic stress-strain theory for cohesionless soils with curved yield surfaces*. Int. Jnl Solids and Structures, Vol. 13, pp. 1019-1035.
- 72 Leroueil, S., Bouclin, G., Tavenas F., Bergeron, L. and La Rochelle, P. (1990). *Permeability anisotropy as a function of strain*. Canadian Geotechnical Journal, Vol. 27, pp. 568-579.
- 73 Leroueil, S., Magnan, J. and Tavenas, F. (1991). *Embankments on soft clays*. Published: Ellis Horwood.
- 74 Mandel, J. and Salençon, J. (1972). *Force portante d'un soil sur assise rigide (etude theoretique)*. Géotechnique, Vol. 22, pp. 79-93.
- 75 Mongilardi, E. and Tortensson, B. (1977). *8000,000 metres of Geodrain in the Porto Tolle thermoelectric power plant*. Goetechnical report from Terrafigo, Stockholm.

- 76 Morgenstern, N.R. and Price, V.E. (1965). *The analysis of stability of general slip surfaces*. Géotechnique, Vol. 15, pp. 79-93.
- 77 Murray, R.T. and Symons, I.F. (1974). *Embankments on soft foundations: settlement and stability study at Tickton in Yorkshire*. TRRL Laboratory Report 643.
- 78 Mylleville, B.L.J. and Rowe, R.K. (1991). *On the design of reinforced embankments on soft brittle clays*. Geosynthetics 91 Conference, Atlanta, USA, pp. 395-408.
- 79 Newmark, N.M. (1948). *Influence charts for the computation of stresses in elastic foundation*. University of Illinois Eng. Exp. Sta. Bul., 378.
- 80 Onoue, A. (1988). *Consolidation by vertical drains taking well resistance and smear into consideration*. Soils and Foundations, Vol. 28, No. 4, pp. 165-174.
- 81 Owen, D.R.J. and Hinton, E. (1980). *Finite elements in plasticity: theory and practice*. Pub: pineridge press, Swansea.
- 82 Parry, R.H.G. (1970). *Overconsolidation in soft clay deposits*. Géotechnique, Vol. 20, pp. 442-446.
- 83 Parry, R.H.G. (1972). *Stability analysis for low embankments*. Proceedings of the Roscoe Memorial lecture, pp. 643-668, Pub: G.T. Foulis and Co.
- 84 Pilot, G., Chaput, D. and Queyroi, D. (1987). *Improvement of clay properties - Usual methods*. Embankments on Soft Clays, Chapter 5, Bulletin of the Public Works Research Centre, Athens, Greece.
- 85 Potts, D.M., Ganendra, D. and Day, R.A. (1990). *Increment size and solution accuracy in finite element analysis*. 4<sup>th</sup> CRISP Users workshop, Surrey University.
- 86 Potts, D.M. and Ganendra, D. (1991). *Finite element analysis of the collapse of reinforced embankments on soft ground*. Discussion: Géotechnique, Vol. 41, No. 4, pp 627-630.
- 87 Poran, C.J., Kaliakin, V.N., Herrmenn, L.R., Romstadd, K.M., Lee, D.F. and Shen, C.K. (1986). *Prediction of trial embankment behaviour Hertfordshire county council - Stanstead Abbots*. Prediction Symposium on a Reinforced Embankment, King's College, London.

- 88 Poulos, H.G. and Davis, E.H. (1974). *Elastic solutions for soil and rocks*. Wiley, New York.
- 89 Roscoe, K.H. and Burland, J.B. (1968). *On the generalised stress-strain behaviour of "wet" clay*. In: *Engineering Plasticity*, Ed. J. Heyman and F.A. Leckie, Cambridge University Press, pp. 535-609.
- 90 Rowe, P.W. (1972). *The relevance of soil fabric to site investigation practice*. *Géotechnique*, Vol. 22, No. 2, pp. 199-300.
- 91 Rowe, R.K. (1982). *The analysis of an embankment constructed on a geotextile*. Proc. 2<sup>nd</sup> Int. conf. on Geotextiles, Las Vegas, Vol. 2, pp. 677-682.
- 92 Rowe, R.K. (1984). *Reinforced embankments: Analysis and design*. *Journal of Geotechnical Engineering Division, ASCE*. Vol. 110, GT2, pp. 231-246.
- 93 Rowe, R.K., Maclean, M.P. and Soderman, K.L. (1984). *Analysis of a geotextile reinforced embankment constructed on peat*. *Canadian Geotechnical Journal*. Vol. 21, pp. 563-576.
- 94 Rowe, R.K. and Soderman, K.L. (1985). *An approximate method for estimating the stability of geotextile-reinforced embankments*. *Canadian Geotechnical Journal*, Vol. 22, No. 3, pp. 392-398.
- 95 Rowe, R.K. and Soderman, K.L. (1987). *Stabilization of very soft soils using high strength geosynthetics: the role of finite element analyses*. *Geotextiles and Geomembranes*, Vol. 6, pp. 53-80.
- 96 Rowe, R.K. and Mylleville, B.L.J. (1988). *The analysis of steel-reinforced embankments on soft clay foundations*. Proc. 6<sup>th</sup> Int. conf. on Numerical Methods in Geomechanics, Innsbruck, pp. 1273-1278.
- 97 Rowe, R.K. and Mylleville, B.L.J. (1989). *Consideration of strain in the design of reinforced embankments*. *Geosynthetics '89 Conference*, San Diego, USA, pp. 124-135.
- 98 Rowe, R.K. and Mylleville, B.L.J. (1990). *Implications of adopting an allowable geosynthetic strain in estimating stability*. *Proceedings of the 4<sup>th</sup> International Conference on Geotextiles, Geomembranes and Related Products*, The Hague, Netherlands, pp. 131-136.
- 99 Russell, D. (1988). *A comparison of CRISP84 and CRISP81*. University of Sheffield, Internal Report.

## References

- 100 Russell, D. (1990). *An element to model thin, highly permeable materials in two dimensional finite element consolidation analyses*. 2<sup>nd</sup> European Speciality Conference on Numerical Methods in Geotechnical Engineering, pp. 303-310.
- 101 Russell, D. (1992). *DRCRISP User's manual*. Internal report, University of Sheffield.
- 102 Sanchez, J.M. and Sagaseta, C. (1990). *Analysis of stage construction of embankments on soft soil*. 2<sup>nd</sup> European Speciality Conference on Numerical Methods in Geotechnical Engineering, pp. 303-310.
- 103 Schmidt, B. (1966). *Discussion of earth pressures at rest related to stress history*. Canadian Geotechnical Journal, Vol 3, pp. 239-242.
- 104 Schafer, V.R. (1987). *Analysis of reinforced embankments and foundations overlying soft soils*. PhD Thesis, Virginia Polytechnic Institute and State University.
- 105 Schofield, A.N. and Wroth, C.P. (1968). *Critical state soil mechanics*. London: Mcgraw-Hill.
- 106 Shinsha et al (1982). *Consolidation settlement and lateral displacements of soft soil ground improved by sand drains*. Soils and Foundations, May, pp. 7-12 (in Japanese).
- 107 Skempton, A.W. (1954). *The pore pressure coefficients A and B*. Géotechnique, Vol. 4, No. 4, pp. 143-147.
- 108 Sloan, S.W. and Randolph, M.F. (1982). *Numerical prediction of collapse loads using finite element methods*. International Journal of Numerical and Analytical Methods in Geomechanics, Vol. 6, pp. 47-48.
- 109 Smith, I.M. and Hobbs R. (1974). *Finite element analysis of centrifuged and built-up slopes*. Géotechnique, Vol. 24, pp. 531-559.
- 110 Smith, I.M. and Hobbs R. (1976). *Biot analysis of consolidation beneath embankments*. Géotechnique, Vol. 26, pp. 149-171.
- 111 Smith, I.M. (1982). *Programming the finite element method - with application to geomechanics*. Wiley, London.
- 112 Smith, P.R. (1984). *The construction of multistage embankments on soft clay*, MSc Dissertation, Imperial College, London.

## References

- 113 Tavenas, F., Jean, P., Leblond, P. and Leroueil, S. (1983). *The permeability of natural soft clays. part II: Permeability characteristics*. Canadian Geotechnical Journal, Vol. 20, pp. 645-659.
- 114 Tavenas, F. and Leroueil, S. (1980). *The behaviour of embankments on clay foundations*. Canadian Geotechnical J., Vol. 17, No. 2, pp. 236-260.
- 115 Taylor, D.W. (1937). *Stability of earth slopes*. Journal of the Boston Society of Civil Engineers, Vol. 24, pp. 197.
- 116 Taylor, D.W. (1948). *Fundamentals of soil mechanics*. Pub: McGraw-Hill, New York.
- 117 Terzaghi, K. and Peck, R.B. (1967). *Soil mechanics in engineering practice*. Pub: Wiley, London.
- 118 Tomlinson, M.J. (1987). *Foundation design and construction*. Fifth Edition, Pub: Longman.
- 119 Van Langen, H. and Vermeer, P.A. (1991). *Interface elements for singular plasticity points*. Int. J. Num. Meth in Geomech, Vol. 15, pp. 301-315.
- 120 Watson, H., Crooks, J.H.A., Williams, R.S. and Yam, C.C. (1984). *Performance of preloaded and stage loaded structures on soft soils in Trinidad*. Géotechnique, No. 34, pp. 239-259.
- 121 Wroth, C.P. and Simpson, B. (1972). *An induced failure at a trial embankment. Part II - finite element computations*. Proc. Spec. Conf. on Performance of Earth and Earth-Supported Structures, ASCE, Lafayette, Vol. 1, pp. 65-79.
- 122 Wroth, C.P. (1975). *In-situ measurement of initial stresses and deformation characteristics*. Proc. Spec. Conf. in In-situ Measurement of Soil Properties. ASCE, Raleigh, North Caroline, pp. 181-230.
- 123 Wroth, C.P. (1977). *The predicted performance of soft clay under a trial embankment loading based on the Cam-clay model*. Finite Elements in Geomechanics, Willey, Chapter 6. (ed. Gudehus).
- 124 Wroth, C.P. (1984). *The interpretation of in-situ soil tests*. Geotechnique, Vol. 34, No. 4, pp. 449-489.
- 125 Yoshikuni, H. and Nakanodo, H. (1974). *Consolidation of soils by vertical drain wells with finite permeability*. Soils and Foundations. Vol. 14, No. 2, pp. 35-46.

## References

126 Yudbir, C. and Wood, D.M. (1989). *Recent developments in laboratory strength and deformation testing*. General report. Proc. 12<sup>th</sup> Int. Conf. Soil Mech., Rio de Janeiro.

127 Zeng G.X., Xie, K.H. and Shi,Z.Y. (1987). Consolidation analysis of sand-drained ground by F.E.M. Proc. 8<sup>th</sup> Regional Conf Soil Mech., Kyoto. Vol. 1, pp. 139-142.

128 Zeng G.X. and Xie, K.H. (1989). *New development of vertical drain theories*. Proc. 12<sup>th</sup> Int. Conf. Soil Mech., Rio de Janeiro. Vol. 2, pp. 1433-1438.

129 Zienkiewicz, O.C. (1977). *Finite Element Method*. McGraw-Hill, London.